Determination of the induction machine Parameters from Starting Transient Measurements

Hengameh Kojooyan Jafari

Barcelona, June 2013

Determination of the induction machine Parameters from Starting Transient Measurements

Hengameh Kojooyan Jafari

Thesis presented to obtain the qualification of Doctor from Polytechnic University of Catalunya

Director

Dr. Joaquin Pedra Duran

Barcelona, June 2013

Departament d'Enginyeria Elèctrica

UNIVERSITAT POLITÈCNICA DE CATALUNYA

Determination of the induction machine Parameters from Starting Transient Measurements

Projecte d´investigacio: Ministerio de Ciencia e Innovacion ENE2009-10274

Impres a Barcelona

June 2013

UNIVERSITAT POLITECNICA DE CATALUNYA (UPC)

Grup de Recerca

Qualitat del subministrament electric (QSE)

Av. Diagonal, 647

08028 Barcelona

Telefon: 0034 - 934016728

Fax:0034 - 934017433

Web: http://www.dee.upc.edu

UNIVERSITAT POLITÈCNICA DE CATALUNYA
BARCELONATECH
Escola de Doctorat

Acta de qualificació de tesi doctoral

Curs acadèmic:

Nom i cognoms

Programa de doctorat

Unitat estructural responsable del programa

Resolució del Tribunal

Reunit el Tribunal designat a l'efecte, el doctorand / la doctoranda exposa el tema de la seva tesi doctoral titulada _____
_____.
Acabada la lectura i després de donar resposta a les qüestions formulades pels membres titulars del tribunal, aquest atorga la qualificació:

APTA/E ☐ NO APTA/E ☐

(Nom, cognoms i signatura) President/a	(Nom, cognoms i signatura) Secretari/ària	
(Nom, cognoms i signatura) Vocal	(Nom, cognoms i signatura) Vocal	(Nom, cognoms i signatura) Vocal

_____, _____ d'/de _____ de _____

El resultat de l'escrutini dels vots emesos pels membres titulars del tribunal, efectuat per l'Escola de Doctorat, a instància de la Comissió de Doctorat de la UPC, atorga la MENCIÓ CUM LAUDE:

SÍ ☐ NO ☐

(Nom, cognoms i signatura) Presidenta de la Comissió de Doctorat	(Nom, cognoms i signatura) Secretària de la Comissió de Doctorat

Barcelona, _____ d'/de _____ de _____

Acknowledgement

The research presented in this thesis was performed at the Polytechnic University of Catalunya.

I would like to thank to my supervisor, Dr. Joaquin Pedra Duran, Professor of Electrical Engineering Department for his valuable ideas, comments and discussions and Lluis Monjo, Assistant Professor of Electrical Engineering Department for his comments and suggestions.

Thanks to Islamic Azad university for fund of this research.

I appreciate my family for their unlimited support.

Summary

This Thesis study the parameters estimation of the induction machine with the single-cage and double-cage models, using the stator currents, voltages and mechanical speed from a starting transient. The dynamic equations of the induction machine are expressed in the synchronous reference frame because in this reference the values of the direct and quadrature currents have a slower variation than those in the other reference frames. This reference frame is important to facilitate the data filtering. The proposed method for the single-cage parameters estimation introduces an approximation of the rotor flux using the stator currents and voltages. It has been demonstrated in the thesis that this approximation improves the accuracy of the calculated parameters significantly. Two different methods to calculate the parameters have been developed. The first is based on the linear least-square method and the second on the resolving of a nonlinear system of equations. A detailed error study of the parameters and predicted behavior have been made in the thesis. An interesting result of the error study is that it is very important that the speed of the points be used in the calculations. It is very important to use the points with the maximum torque speed and points near the synchronous speed. The thesis presents the two first methods developed for parameters estimation of the induction machine with double-cage model using data from a starting transient. The other methods known in the literature use steady state data. Both methods use data from the point of maximum torque to the synchronous speed to calculate the parameters of a single-cage model, because the torque- and current-speed curves of this single-cage fit very well with the torque- and current-speed curves of the double-cage. Later, the first method uses a point with a speed near to zero speed and a point in the synchronous speed and other single-cage is calculated. With these two single-cages the impedances of three points are calculated and they are used to estimate the six parameters of the double-cage model solving a nonlinear system of equations. The second method, called instantaneous power method, uses the fact that the averaged transient torque has similar values to the steady-state torque in the mechanical transient region. Then, several impedance values are calculated for points with different speeds in this region, where the effects of the double-cage are more important. Finally, with impedance values in the synchronous speed and the maximum torque speed obtained with the regression method and impedance values obtained with the instantaneous power method, a set of non linear equations are defined. Their solution is the estimated parameters of the induction machine double-cage model.

Table of contents

a Introduction

Background and motivation

Induction motor parameters estimation is an important topic as is evidenced by the fact that there are standards published about this matter by the IEEE: Standard test procedure for poly phase induction motors and generators, IEEE Std. 112-2004 [1] and the IEC: Rotating electrical machines-Part 28: Test methods for determining quantities of equivalent circuit diagrams for three-phase low-voltage cage (single- and double-cage) induction motors, IEC 60034-28 [2].

In power system analysis, induction motor parameters are necessary for the study of the transient behavior of the induction motors and their contribution to short-circuit currents and power system stability.

Another important area where the induction motor parameters are necessary is the tuning of the controllers of drives, e.g. current, flux and speed controllers, and for the correct tuning of the employed flux and torque models.

Nowadays there are a lot of papers about the single-cage model parameters, but the estimation of the double-cage induction motor parameters is a topic that has been poorly studied in the literature.

It is important to say that the study of the induction motor parameters estimation in this thesis report does not take in account the motor saturation. A recent work in this area is the reference [3].

The motivation of this work is the development of a method to estimate the parameters of the single-cage and double-cage induction motor model from transient measurements that can be easily obtained in an industrial situation. This goal can be achieved with a starting transient, from standstill to steady-state speed, recording voltages, currents and speed.

b Literature study

There are many publications aimed at the estimation of parameters for control applications, as evidenced by bibliographic reviews [4]. In this case the methods are focused to determine only the significant parameters of rotor for the control application, and usually do not determine all the parameters of the steady-state equivalent circuit.

Despite the large number of studies on induction motor parameters estimation, it is not a well solved problem. Since the majority of the works use the single-cage model, and it can be seen in [5], the motor measurements only can be properly adjusted with the double-cage model.

The main techniques for estimate the single-cage induction motor parameters from experimental measurements are based on,

- Steady-state measurements [6]-[7]
- Variable frequency measurements [8]-[11]
- Transient measurements [12]-[22]

In steady-state measurements methods the reference [6] is one of the last studies. This method uses steady-state data like the starting torque and current, maximum torque, nominal torque and current, etc. These methods are the most employed and there are two published standards, the IEEE [1] and IEC [2]. The main drawback of these methods is that it is very difficult to test an induction motor when it has been installed in a factory, because the measurement of the torque is not trivial. A simple introduction of the typical steady-state test to identify the equivalent circuit parameters is in reference [7].

There are the references [8]-[11] in variable frequency measurement methods. In these methods there are two different methodologies. The former has the motor powered by voltage of variable frequency, and the later is the use of a voltage with different frequencies, like the case of a PWM voltage waveform.

Transient methods can be classified in three categories.

- Kalman filter methods [12]-[14]
- Linear Least-square methods [15]-[18]
- Non-Linear Least-square methods [19]-[22]

The extended Kalman filter is an algorithm for optimal state estimation of non linear systems in the presence of noise. An example of the use of an extended Kalman filter to estimate the parameters of the induction motor are references [12]-[14].

In linear least-square methods the electric machine differential equations are manipulated to eliminate the non-measurable magnitudes of the rotor (rotor currents or rotor fluxes). In references [15] to [18] there are different works that use this technique. The linear least-square method is the methodology chosen to develop estimation method by rotor flux approximation in this thesis.

In the non-linear least-square methods, an error function is calculated with the measured currents and the simulated currents. This method is computationally worthy because each error function evaluation requires a transient simulation. The use of this error function in a minimization algorithm defines an estimation parameters method that has been applied with different modifications in references [19]-[22].

There are other interesting papers like reference [23] where the torque is measured in an instantaneous process that has resemblances with the instantaneous power method proposed in this thesis. In reference [24] the instantaneous measurements has been also used like variables that are rms values.

As has been commented before, an important problem in the literature of the estimation of the induction motor parameters is that the single-cage model is mostly used. For low power induction motors the double-cage effect is not significant, but in medium power and high power induction motors the double-cage effect is necessary to justify the experimental values of starting torque and current, which are bigger than the values predicted by the single-cage model.

The estimation of double-cage parameters has been only studied using steady-state data [25] and [26]. The authors do not know any reference about the double-cage estimation using transient data.

Reference [27] has a detailed study of the minimum number of parameters that characterize the double-cage model. The estimation of the double-cage induction motor model has been included the function: “power_AsynchronousMachineParams” in SimPowerSystems of Matlab [28]. This function is based on the estimation method developed in [25] and [26]. Finally, reference [29] has a mention to the double-cage parameters estimation, but it does not give a clear methodology of how to realize their estimation.

1 Single cage induction motor theory

1.1 Dynamic equations of single cage induction motor

The induction machine rotor and stator windings are shown in Fig. 1.1 and the induction machine voltage-current equations in *abc* variables are

$$\begin{pmatrix} v_s \\ v_r \end{pmatrix} = \begin{pmatrix} R_s & 0 \\ 0 & R_r \end{pmatrix} \begin{pmatrix} i_s \\ i_r \end{pmatrix} + \frac{d}{dt}\left[\begin{pmatrix} M_{ss} & M_{sr} \\ M_{rs} & M_{rr} \end{pmatrix} \begin{pmatrix} i_s \\ i_r \end{pmatrix} \right] \tag{1}$$

For simplifying the electric machine equation, the equations in *abc* variables are transformed to *0dq* variables using Park transformation, that is

$$(f_{abc}) = P(\theta).(f_{0dq}) \tag{2}$$

where the vector f_{abc} can be stator or rotor voltages and currents.

The Park transformation and its inverse is defined according to the literature [30] as

$$P(\theta) = \sqrt{\frac{2}{3}} \begin{pmatrix} \frac{1}{\sqrt{2}} & \cos(\theta) & -\sin(\theta) \\ \frac{1}{\sqrt{2}} & \cos\left(\theta - \frac{2\pi}{3}\right) & -\sin\left(\theta - \frac{2\pi}{3}\right) \\ \frac{1}{\sqrt{2}} & \cos\left(\theta + \frac{2\pi}{3}\right) & -\sin\left(\theta + \frac{2\pi}{3}\right) \end{pmatrix} \quad ; \quad P^{-1}(\theta) = \sqrt{\frac{2}{3}} \begin{pmatrix} \frac{1}{\sqrt{2}} & \frac{1}{\sqrt{2}} & \frac{1}{\sqrt{2}} \\ \cos(\theta) & \cos\left(\theta - \frac{2\pi}{3}\right) & \cos\left(\theta + \frac{2\pi}{3}\right) \\ -\sin(\theta) & -\sin\left(\theta - \frac{2\pi}{3}\right) & -\sin\left(\theta + \frac{2\pi}{3}\right) \end{pmatrix} \tag{3}$$

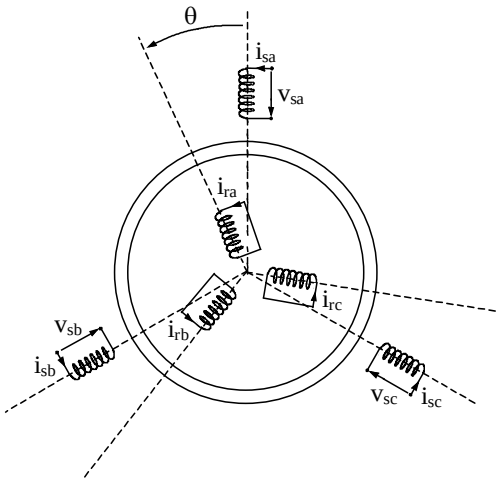

Fig. 1.1. Stator and rotor windings of Single-cage induction motor model

and the stator and rotor magnetizing matrix of induction machine in Fig. 1.1 is

$$M(\theta) = \begin{bmatrix} L_s^p & M_s^p\cos\left(\frac{2\pi}{3}\right) & M_s^p\cos\left(-\frac{2\pi}{3}\right) & M^p\cos(\theta) & M^p\cos\left(\theta+\frac{2\pi}{3}\right) & M^p\cos\left(\theta-\frac{2\pi}{3}\right) \\ M_s^p\cos\left(-\frac{2\pi}{3}\right) & L_s^p & M_s^p\cos\left(\frac{2\pi}{3}\right) & M^p\cos\left(\theta-\frac{2\pi}{3}\right) & M^p\cos(\theta) & M^p\cos\left(\theta+\frac{2\pi}{3}\right) \\ M_s^p\cos\left(\frac{2\pi}{3}\right) & M_s^p\cos\left(-\frac{2\pi}{3}\right) & L_s^p & M^p\cos\left(\theta+\frac{2\pi}{3}\right) & M^p\cos\left(\theta-\frac{2\pi}{3}\right) & M^p\cos(\theta) \\ M^p\cos(\theta) & M^p\cos\left(\theta-\frac{2\pi}{3}\right) & M^p\cos\left(\theta+\frac{2\pi}{3}\right) & L_r^p & M_r^p\cos\left(\frac{2\pi}{3}\right) & M_r^p\cos\left(-\frac{2\pi}{3}\right) \\ M^p\cos\left(\theta+\frac{2\pi}{3}\right) & M^p\cos(\theta) & M^p\cos\left(\theta-\frac{2\pi}{3}\right) & M_r^p\cos\left(-\frac{2\pi}{3}\right) & L_r^p & M_r^p\cos\left(\frac{2\pi}{3}\right) \\ M^p\cos\left(\theta-\frac{2\pi}{3}\right) & M^p\cos\left(\theta+\frac{2\pi}{3}\right) & M^p\cos(\theta) & M_r^p\cos\left(\frac{2\pi}{3}\right) & M_r^p\cos\left(-\frac{2\pi}{3}\right) & L_r^p \end{bmatrix} \quad (4)$$

where M^p, M_s^p, M_r^p are the physical mutual inductance between stator and rotor windings, the physical mutual inductance between stator windings and the physical mutual inductance between rotor windings, respectively. θ is the relative angular position between rotor and stator (Fig. 1.1) and L_s^p, L_r^p are physical stator and rotor self inductances. Normally the rotor voltages and currents are reduced by transforming rotor to the stator side. Then the physical mutual inductances are equal; $M^p = M_s^p = M_r^p$. Therefore in all of the next equations the rotor magnitudes are reduced to the stator.

The Park transformation for variable voltages and currents is

$$\left(v_{abc}\right)_{s,r} = P(\theta_s,\theta_r).\left(v_{0dq}\right)_{s,r} \quad ; \quad \left(i_{abc}\right)_{s,r} = P(\theta_s,\theta_r).\left(i_{0dq}\right)_{s,r} \quad (5)$$

$$P(\theta_s,\theta_r)=\sqrt{\frac{2}{3}}\begin{pmatrix}\frac{1}{\sqrt{2}} & \cos(\theta_s) & -\sin(\theta_s) & 0 & 0 & 0\\ \frac{1}{\sqrt{2}} & \cos\left(\theta_s-\frac{2\pi}{3}\right) & -\sin\left(\theta_s-\frac{2\pi}{3}\right) & 0 & 0 & 0\\ \frac{1}{\sqrt{2}} & \cos\left(\theta_s+\frac{2\pi}{3}\right) & -\sin\left(\theta_s+\frac{2\pi}{3}\right) & 0 & 0 & 0\\ 0 & 0 & 0 & \frac{1}{\sqrt{2}} & \cos(\theta_r) & -\sin(\theta_r)\\ 0 & 0 & 0 & \frac{1}{\sqrt{2}} & \cos\left(\theta_r-\frac{2\pi}{3}\right) & -\sin\left(\theta_r-\frac{2\pi}{3}\right)\\ 0 & 0 & 0 & \frac{1}{\sqrt{2}} & \cos\left(\theta_r+\frac{2\pi}{3}\right) & -\sin\left(\theta_r+\frac{2\pi}{3}\right)\end{pmatrix} \tag{6}$$

and the inverse Park transformation is

$$P^{-1}(\theta_s,\theta_r)=\sqrt{\frac{2}{3}}\begin{pmatrix}\frac{1}{\sqrt{2}} & \frac{1}{\sqrt{2}} & \frac{1}{\sqrt{2}} & 0 & 0 & 0\\ \cos(\theta_s) & \cos\left(\theta_s-\frac{2\pi}{3}\right) & \cos\left(\theta_s+\frac{2\pi}{3}\right) & 0 & 0 & 0\\ -\sin(\theta_s) & -\sin\left(\theta_s-\frac{2\pi}{3}\right) & -\sin\left(\theta_s+\frac{2\pi}{3}\right) & 0 & 0 & 0\\ 0 & 0 & 0 & \frac{1}{\sqrt{2}} & \frac{1}{\sqrt{2}} & \frac{1}{\sqrt{2}}\\ 0 & 0 & 0 & \cos(\theta_r) & \cos\left(\theta_r-\frac{2\pi}{3}\right) & \cos\left(\theta_r+\frac{2\pi}{3}\right)\\ 0 & 0 & 0 & -\sin(\theta_r) & -\sin\left(\theta_r-\frac{2\pi}{3}\right) & -\sin\left(\theta_r+\frac{2\pi}{3}\right)\end{pmatrix} \tag{7}$$

Multiplying equation (1) by the inverse of Park matrix, $P^{-1}(\theta_s,\theta_r)$, it can be written as

$$\left[P^{-1}\right].[v]=\left[P^{-1}\right].[R][P].\left[P^{-1}\right].[i]+\left[P^{-1}\right].\frac{d}{dt}\left[\left[M(\theta)\right][P].\left[P^{-1}\right].[i]\right] \tag{8}$$

and operating the previous equations gives

$$\begin{pmatrix}v_{ps}\\ v_{pr}\end{pmatrix}=\begin{pmatrix}R_s & 0\\ 0 & R_r\end{pmatrix}\begin{pmatrix}i_{ps}\\ i_{pr}\end{pmatrix}+\begin{pmatrix}P(\theta_s)^{-1}M_{ss}P(\theta_s) & P(\theta_s)^{-1}M_{sr}P(\theta_r)\\ P(\theta_r)^{-1}M_{rs}P(\theta_s) & P(\theta_r)^{-1}M_{rr}P(\theta_r)\end{pmatrix}\frac{d}{dt}\left[\begin{pmatrix}i_{ps}\\ i_{pr}\end{pmatrix}\right]+$$
$$\begin{pmatrix}P(\theta_s)^{-1}M_{ss}\frac{dP(\theta_s)}{dt} & P(\theta_s)^{-1}\frac{dM_{sr}}{dt}P(\theta_r)+P(\theta_s)^{-1}M_{sr}\frac{dP(\theta_r)}{dt}\\ P(\theta_r)^{-1}\frac{dM_{rs}}{dt}P(\theta_s)+P(\theta_r)^{-1}M_{rs}\frac{dP(\theta_s)}{dt} & P(\theta_r)^{-1}M_{rr}\frac{dP(\theta_r)}{dt}\end{pmatrix}\begin{pmatrix}i_{ps}\\ i_{pr}\end{pmatrix} \tag{9}$$

The stator and rotor *abc* variables (v_s , v_r , i_s , i_r) and Park variables (v_{ps} , v_{pr} , i_{ps} , i_{pr}) are

$$\begin{aligned} &[v_s]=[v_{sa},v_{sb},v_{sc}] \;\; ; \;\; [v_r]=[v_{ra},v_{rb},v_{rc}] \;\; ; \;\; [i_s]=[i_{sa},i_{sb},i_{sc}] \;\; ; \;\; [i_r]=[i_{ra},i_{rb},i_{rc}] \\ &[v_{ps}]=[v_{s0},v_{sd},v_{sq}] \;\; ; \;\; [v_{pr}]=[v_{r0},v_{rd},v_{rq}] \;\; ; \;\; [i_{ps}]=[i_{s0},i_{sd},i_{sq}] \;\; ; \;\; [i_{pr}]=[i_{r0},i_{rd},i_{rq}] \end{aligned} \tag{10}$$

and the relation between Park variables and *abc* variables are

$$\begin{aligned} &[v_{pr}]=[P^{-1}(\theta_r)][v_r] \;\; ; \;\; [v_{ps}]=[P^{-1}(\theta_s)][v_s] \\ &[i_{pr}]=[P^{-1}(\theta_r)][i_r] \;\; ; \;\; [i_{ps}]=[P^{-1}(\theta_s)][i_s] \end{aligned} \tag{11}$$

Imposing that $\theta_s = \theta_m + \theta_r$, the equation (9) is rewritten as

$$\begin{pmatrix} v_{s0} \\ v_{sd} \\ v_{sq} \\ v_{r0} \\ v_{rd} \\ v_{rq} \end{pmatrix} = \begin{pmatrix} R_s + L_{s0}p & 0 & 0 & 0 & 0 & 0 \\ 0 & R_s + L_s p & -L_s \dfrac{d\theta_s}{dt} & 0 & M.p & -M\left(\dfrac{d\theta_r}{dt}+\omega_m\right) \\ 0 & L_s \dfrac{d\theta_s}{dt} & R_s + L_s p & 0 & M\left(\dfrac{d\theta_r}{dt}+\omega_m\right) & M.p \\ 0 & 0 & 0 & R_r + L_{r0}p & 0 & 0 \\ 0 & M.p & -M\left(\dfrac{d\theta_s}{dt}-\omega_m\right) & 0 & R_r + L_r p & -L_r \dfrac{d\theta_r}{dt} \\ 0 & M\left(\dfrac{d\theta_s}{dt}-\omega_m\right) & M.p & 0 & L_r \dfrac{d\theta_r}{dt} & R_r + L_r p \end{pmatrix} \begin{pmatrix} i_{s0} \\ i_{sd} \\ i_{sq} \\ i_{r0} \\ i_{rd} \\ i_{rq} \end{pmatrix} \tag{12}$$

and the parameters are defined as

$$L_{s0} = L_{ls} = L_s^p - M^p \;\; ; \;\; L_{r0} = L_{lr} = L_r^p - M^p \;\; ; \;\; L_s = L_s^p + \frac{M^p}{2} \;\; ; \;\; L_r = L_r^p + \frac{M^p}{2} \;\; ; \;\; M = \frac{3M^p}{2} \tag{13}$$

where L_{s0} is the zero leakage Park inductance, L_s and L_r are the *d*, *q* self stator and rotor Park inductances, respectively and *M* is magnetizing Park inductance between stator and rotor. In Park transformation function of the values of the angles, the motor dynamic equations can be expressed in three reference frames; the rotor, the stator and the synchronous reference frames.

In rotor reference frame, the angles of Park transformation are $\theta_r = 0$ and $\theta_s = \theta_m = \int \omega_m dt$. The transformed equations are

$$\begin{pmatrix} v_{s0} \\ v_{sd} \\ v_{sq} \\ v_{r0} \\ v_{rd} \\ v_{rq} \end{pmatrix} = \begin{pmatrix} R_s + L_{s0}p & 0 & 0 & 0 & 0 & 0 \\ 0 & R_s + L_s p & -L_s \omega_m & 0 & M.p & -M(\omega_m) \\ 0 & L_s \omega_m & R_s + L_s p & 0 & M(\omega_m) & M.p \\ 0 & 0 & 0 & R_r + L_{r0}p & 0 & 0 \\ 0 & M.p & 0 & 0 & R_r + L_r p & 0 \\ 0 & 0 & M.p & 0 & 0 & R_r + L_r p \end{pmatrix} \begin{pmatrix} i_{s0} \\ i_{sd} \\ i_{sq} \\ i_{r0} \\ i_{rd} \\ i_{rq} \end{pmatrix} \quad (14)$$

and the torque equation is

$$\Gamma(t) = \wp M (i_{rd} i_{sq} - i_{rq} i_{sd}) \quad (15)$$

where $\wp$ is the number of pole pairs.

In stator reference frame, the angles of Park transformation are $\theta_r = -\theta_m$ and $\theta_s = 0$. The transformed equations are

$$\begin{pmatrix} v_{s0} \\ v_{sd} \\ v_{sq} \\ v_{r0} \\ v_{rd} \\ v_{rq} \end{pmatrix} = \begin{pmatrix} R_s + L_{s0}p & 0 & 0 & 0 & 0 & 0 \\ 0 & R_s + L_s p & 0 & 0 & M.p & 0 \\ 0 & 0 & R_s + L_s p & 0 & 0 & M.p \\ 0 & 0 & 0 & R_r + L_{r0}p & 0 & 0 \\ 0 & M.p & -M(-\omega_m) & 0 & R_r + L_r p & L_r \omega_m \\ 0 & M(-\omega_m) & M.p & 0 & -L_r \omega_m & R_r + L_r p \end{pmatrix} \begin{pmatrix} i_{s0} \\ i_{sd} \\ i_{sq} \\ i_{r0} \\ i_{rd} \\ i_{rq} \end{pmatrix} \quad (16)$$

and the torque equation is

$$\Gamma(t) = \wp M (i_{rd} i_{sq} - i_{rq} i_{sd}) \quad (17)$$

In synchronous reference frame the angles of Park transformation are $\theta_r = s.\omega_s t$ and $\theta_s = \omega_s t$, where the slip, *s*, is defined as

$$s = \frac{\omega_s - \wp \omega_m}{\omega_s} \quad (18)$$

where $\wp$ is the number of pole pairs and ω_s is the synchronous speed, defined as

$$\omega_s = 2.\pi.f \quad (19)$$

The transformed equations in the synchronous reference frame are

$$\begin{pmatrix} v_{s0} \\ v_{sd} \\ v_{sq} \\ v_{r0} \\ v_{rd} \\ v_{rq} \end{pmatrix} = \begin{pmatrix} R_s + L_{s0}p & 0 & 0 & 0 & 0 & 0 \\ 0 & R_s + L_s p & -L_s \omega_s & 0 & M.p & -M(\omega_s) \\ 0 & L_s \omega_s & R_s + L_s p & 0 & M(\omega_s) & M.p \\ 0 & 0 & 0 & R_r + L_{r0}p & 0 & 0 \\ 0 & M.p & -M(s\omega_s) & 0 & R_r + L_r p & -L_r s\omega_s \\ 0 & Ms\omega_s & M.p & 0 & L_r s\omega_s & R_r + L_r p \end{pmatrix} \begin{pmatrix} i_{s0} \\ i_{sd} \\ i_{sq} \\ i_{r0} \\ i_{rd} \\ i_{rq} \end{pmatrix} \quad (20)$$

and the torque equation is

$$\Gamma(t) = \wp M (i_{rd} i_{sq} - i_{rq} i_{sd}) \quad (21)$$

1.2 Ku transformation of the single-cage induction motor equations

The Ku transformation is defined as

$$K(\theta)=\frac{1}{\sqrt{3}}\begin{pmatrix}1 & e^{j\theta} & e^{-j\theta}\\ 1 & a^2.e^{j\theta} & a.e^{-j\theta}\\ 1 & a.e^{j\theta} & a^2.e^{-j\theta}\end{pmatrix} \quad ; \quad K^{-1}(\theta)=\frac{1}{\sqrt{3}}\begin{pmatrix}1 & 1 & 1\\ e^{-j\theta} & a.e^{-j\theta} & a^2.e^{-j\theta}\\ e^{j\theta} & a^2.e^{j\theta} & a.e^{j\theta}\end{pmatrix} \tag{22}$$

where the operator *a* is defined as $a=1\underline{120^\circ}$ and $e^{j\theta}=\cos(\theta)+j\sin(\theta)$. The transformed stator and rotor voltages are

$$[v_{ks}]=\left[K^{-1}(\theta_s)\right][v_s] \quad ; \quad [v_{kr}]=\left[K^{-1}(\theta_r)\right][v_r] \tag{23}$$

and the transformed stator and rotor currents are

$$[i_{ks}]=\left[K^{-1}(\theta_s)\right][i_s] \quad ; \quad [i_{kr}]=\left[K^{-1}(\theta_r)\right][i_r] \tag{24}$$

being the variables in the *abc* variables

$$[v_s]=[v_{sa},v_{sb},v_{sc}] \;;\; [v_r]=[v_{ra},v_{rb},v_{rc}] \;;\; [i_s]=[i_{sa},i_{sb},i_{sc}] \;;\; [i_r]=[i_{ra},i_{rb},i_{rc}] \tag{25}$$

and the variables in Ku coordinates; forward, backward and homopolar variables, *0fb*, are

$$[v_{ks}]=\left[v_{s0},v_{sf},v_{sb}\right] \;;\; [v_{kr}]=\left[v_{r0},v_{rf},v_{rb}\right] \;;\; [i_{ks}]=\left[i_{s0},i_{sf},i_{sb}\right] \;;\; [i_{kr}]=\left[i_{r0},i_{rf},i_{rb}\right] \tag{26}$$

The electric machine equations expressed in Ku variables, are

$$\begin{pmatrix}v_{s0}\\ v_{sf}\\ v_{sb}\\ v_{r0}\\ v_{rf}\\ v_{rb}\end{pmatrix}=\begin{pmatrix}R_s+L_{s0}p & 0 & 0 & 0 & 0 & 0\\ 0 & R_s+L_s\left(p+j\frac{d\theta_s}{dt}\right) & 0 & 0 & M\left(p+j\left(\omega_m+\frac{d\theta_r}{dt}\right)\right) & 0\\ 0 & 0 & R_s+L_s\left(p-j\frac{d\theta_s}{dt}\right) & 0 & 0 & M\left(p-j\left(\omega_m+\frac{d\theta_r}{dt}\right)\right)\\ 0 & 0 & 0 & R_r+L_{r0}p & 0 & 0\\ 0 & M\left(p+j\left(\frac{d\theta_s}{dt}-\omega_m\right)\right) & 0 & 0 & R_r+L_r\left(p+j\frac{d\theta_r}{dt}\right) & 0\\ 0 & 0 & M\left(p-j\left(\frac{d\theta_s}{dt}-\omega_m\right)\right) & 0 & 0 & R_r+L_r\left(p-j\frac{d\theta_r}{dt}\right)\end{pmatrix}\begin{pmatrix}i_{s0}\\ i_{sf}\\ i_{sb}\\ i_{r0}\\ i_{rf}\\ i_{rb}\end{pmatrix} \tag{27}$$

The Ku transformation of the voltage-current equations in synchronous reference frame with the angles $\theta_r=s\omega_s t$ and $\theta_s=\omega_s t$ produces a system of differential equations in homopolar, forward and backward, *0fb*, variables

$$\begin{pmatrix} v_{s0} \\ v_{sf} \\ v_{sb} \\ v_{r0} \\ v_{rf} \\ v_{rb} \end{pmatrix} = \begin{pmatrix} R_s + L_{s0}p & 0 & 0 & 0 & 0 & 0 \\ 0 & R_s + L_s(p + j\omega_s) & 0 & 0 & M.(p + j\omega_s) & 0 \\ 0 & 0 & R_s + L_s(p - j\omega_s) & 0 & 0 & M.(p - j\omega_s) \\ 0 & 0 & 0 & R_r + L_{r0}p & 0 & 0 \\ 0 & M(p + js\omega_s) & 0 & 0 & R_r + L_r(p + js\omega_s) & 0 \\ 0 & 0 & M(p - js\omega_s) & 0 & 0 & R_r + L_r(p - js\omega_s) \end{pmatrix} \begin{pmatrix} i_{s0} \\ i_{sf} \\ i_{sb} \\ i_{r0} \\ i_{rf} \\ i_{rb} \end{pmatrix} \tag{28}$$

In equations (28) first and fourth rows are decoupled. They are the homopolar components. The second and fifth rows are independent of other equations and are only function of the forward variables (stator and rotor). These equations can be written as

$$\begin{aligned} v_s &= (R_s + L_s(p + j\omega_s))i_s + M(p + j\omega_s)i_r \\ 0 &= M(p + js\omega_s)i_s + (R_r + L_r(p + js\omega_s))i_r \end{aligned} \tag{29}$$

and torque equation is

$$\Gamma(t) = 2\wp M \ \mathrm{Im}(i_s i_r^*) \tag{30}$$

We can work only with the forward variables because the backward variables are complex conjugated of the forward variables.

In the stator reference frame ($\theta_s = 0, \theta_r = -\theta_m$) the voltage-current equations in *0fb* variables are

$$\begin{pmatrix} v_{s0} \\ v_{sf} \\ v_{sb} \\ v_{r0} \\ v_{rf} \\ v_{rb} \end{pmatrix} = \begin{pmatrix} R_s + L_{s0}p & 0 & 0 & 0 & 0 & 0 \\ 0 & R_s + L_s p & 0 & 0 & M.p & 0 \\ 0 & 0 & R_s + L_s p & 0 & 0 & M.p \\ 0 & 0 & 0 & R_r + L_{r0}p & 0 & 0 \\ 0 & M(p - j\omega_m) & 0 & 0 & R_r + L_r(p - j\omega_m) & 0 \\ 0 & 0 & M(p + j\omega_m) & 0 & 0 & R_r + L_r(p + j\omega_m) \end{pmatrix} \begin{pmatrix} i_{s0} \\ i_{sf} \\ i_{sb} \\ i_{r0} \\ i_{rf} \\ i_{rb} \end{pmatrix} \tag{31}$$

In this case, the second and fifth equations are also decoupled of the other equations and rotor voltage is zero then the equation can be rewritten as

$$\begin{aligned} v_s &= (R_s + L_s p)i_s + Mpi_r \\ 0 &= M(p - j\omega_m)i_s + (R_r + L_r(p - j\omega_m))i_r \end{aligned} \tag{32}$$

and torque equation is

$$\Gamma(t) = 2\wp M \operatorname{Im}(i_s i_r^*) \tag{33}$$

Then *0fb* variables in rotor reference frame ($\theta_s = \theta_m$, $\theta_r = 0$) are

$$\begin{pmatrix} v_{s0} \\ v_{sf} \\ v_{sb} \\ v_{r0} \\ v_{rf} \\ v_{rb} \end{pmatrix} = \begin{pmatrix} R_s + L_{s0}p & 0 & 0 & 0 & 0 & 0 \\ 0 & R_s + L_s(p + j\omega_m) & 0 & 0 & M.(p + j\omega_m) & 0 \\ 0 & 0 & R_s + L_s(p - j\omega_m) & 0 & 0 & M.(p - j\omega_m) \\ 0 & 0 & 0 & R_r + L_{r0}p & 0 & 0 \\ 0 & Mp & 0 & 0 & R_r + L_r p & 0 \\ 0 & 0 & Mp & 0 & 0 & R_r + L_r p \end{pmatrix} \begin{pmatrix} i_{s0} \\ i_{sf} \\ i_{sb} \\ i_{r0} \\ i_{rf} \\ i_{rb} \end{pmatrix} \tag{34}$$

where the forward variables also are decoupled in the equations

$$\begin{aligned} v_s &= \left(R_s + L_s(p + j\omega_m)\right) i_s + M(p + j\omega_m) i_r \\ v_r &= 0 = Mp i_s + (R_r + L_r p) i_r \end{aligned} \tag{35}$$

and torque equation is

$$\Gamma(t) = 2\wp M \operatorname{Im}(i_s i_r^*) \tag{36}$$

1.3 Ku- Park Relation of the single-cage induction motor equations

The Ku transformation of the voltage variables are

$$[v_{ks}]=\left[K^{-1}(\theta_s)\right][v_s] \quad ; \quad [v_s]=[v_{sa},v_{sb},v_{sc}] \quad ; \quad [v_{ks}]=\left[v_{s0},v_{sf},v_{sb}\right] \tag{37}$$

and the forward and backward stator voltages are

$$\begin{aligned} v_{sf} &= \sqrt{\frac{1}{3}}\left(v_{sa}e^{-j\theta}+ae^{-j\theta}v_{sb}+a^2e^{-j\theta}v_{sc}\right) \\ v_{sb} &= \sqrt{\frac{1}{3}}\left(v_{sa}e^{j\theta}+a^2e^{j\theta}v_{sb}+ae^{j\theta}v_{sc}\right) \end{aligned} \tag{38}$$

that results in

$$\begin{aligned} v_{sf} &= \sqrt{\frac{1}{3}}\left(\left(\cos\theta-j\sin\theta\right)v_{sa}+\left(\cos\left(-\theta+\frac{2\pi}{3}\right)+j\sin\left(-\theta+\frac{2\pi}{3}\right)\right)v_{sb}+\left(\cos\left(-\theta-\frac{2\pi}{3}\right)+j\sin\left(-\theta-\frac{2\pi}{3}\right)\right)v_{sc}\right) \\ v_{sb} &= \sqrt{\frac{1}{3}}\left(\left(\cos\theta+j\sin\theta\right)v_{sa}+\left(\cos\left(\theta-\frac{2\pi}{3}\right)+j\sin\left(\theta-\frac{2\pi}{3}\right)\right)v_{sb}+\left(\cos\left(\theta+\frac{2\pi}{3}\right)+j\sin\left(\theta+\frac{2\pi}{3}\right)\right)v_{sc}\right) \end{aligned} \tag{39}$$

where the angle depends on the reference frame.

The Park transformation of the voltages are

$$\left[v_{ps}\right]=\left[P^{-1}(\theta_s)\right][v_s] \quad ; \quad [v_s]=[v_{sa},v_{sb},v_{sc}] \quad ; \quad \left[v_{ps}\right]=\left[v_{s0},v_{sd},v_{sq}\right] \tag{40}$$

then the direct and quadrature voltages are derived

$$\begin{aligned} v_{sd} &= \sqrt{\frac{2}{3}}\left(v_{sa}\cos\left(\theta_{s,r}\right)+v_{sb}\cos\left(\theta_{s,r}-\frac{2\pi}{3}\right)+v_{sc}\cos\left(\theta_{s,r}+\frac{2\pi}{3}\right)\right) \\ v_{sq} &= \sqrt{\frac{2}{3}}\left(-v_{sa}\sin\left(\theta_{s,r}\right)-v_{sb}\sin\left(\theta_{s,r}-\frac{2\pi}{3}\right)-v_{sc}\sin\left(\theta_{s,r}+\frac{2\pi}{3}\right)\right) \end{aligned} \tag{41}$$

The relation between the Ku transformation and the Park transformation is

$$v_{s,rf}=\sqrt{\frac{1}{2}}\left(v_{s,rd}+jv_{s,rq}\right) \quad ; \quad v_{s,rb}=\sqrt{\frac{1}{2}}\left(v_{s,rd}-jv_{s,rq}\right) \tag{42}$$

$$v_{s,rd}=\sqrt{2}.\mathrm{Re}\left(v_{s,rf}\right) \quad ; \quad v_{s,rq}=\sqrt{2}.\mathrm{Im}\left(v_{s,rf}\right) \tag{43}$$

1.4 Steady-State Equivalent Circuit of the single-cage induction motor

Using the Ku equations (29) in synchronous reference frame

$$\begin{aligned} v_s &= \left(R_s + L_s\left(p + j\omega_s\right)\right)i_s + M\left(p + j\omega_s\right)i_r \\ 0 &= M\left(p + js\omega_s\right)i_s + \left(R_r + L_r\left(p + js\omega_s\right)\right)i_r \end{aligned} \tag{44}$$

and taking in account that a system of symmetrical voltages has a constant forward voltage in this reference frame. The steady state current will be also constant, and the steady state conditions in the synchronous reference frame are

$$pi_s = 0 \qquad ; \qquad pi_r = 0 \tag{45}$$

Thus the induction machine equations in synchronous reference frame in steady-state are

$$\begin{aligned} v_s &= \left(R_s + L_s\left(j\omega_s\right)\right)i_s + M\left(j\omega_s\right)i_r \\ 0 &= M\left(js\omega_s\right)i_s + \left(R_r + L_r\left(js\omega_s\right)\right)i_r \end{aligned} \tag{46}$$

where the slip s is defined as

$$s = \frac{\omega_s - \wp\,\omega_m}{\omega_s} \tag{47}$$

Then the equations can be rewritten as

$$\begin{aligned} v_s &= \left(R_s + L_s\left(j\omega_s\right)\right)i_s + M\left(j\omega_s\right)i_r \\ 0 &= M\left(j\omega_s\right)i_s + \left(\frac{R_r}{s} + L_r\left(j\omega_s\right)\right)i_r \end{aligned} \tag{48}$$

Adding $\left(M - M\right)\left(j\omega_s\right)i_s$ and $\left(M - M\right)\left(j\omega_s\right)i_r$ in the first and the second equation of (44) respectively

$$\begin{aligned} v_s &= \left(R_s + \left(L_s - M\right)\left(j\omega_s\right)\right)i_s + M\left(j\omega_s\right)\left(i_s + i_r\right) \\ 0 &= M\left(j\omega_s\right)\left(i_s + i_r\right) + \left(\frac{R_r}{s} + \left(L_r - M\right)\left(j\omega_s\right)\right)i_r \end{aligned} \tag{49}$$

where the steady-state circuit parameters are defined as

$$L_{sd} = L_s - M \qquad ; \qquad L_{rd} = L_r - M \tag{50}$$

and the equations finally result as

$$
\begin{aligned}
v_s &= \left(R_s + L_{sd}\left(j\omega_s\right)\right) i_s + \mathrm{M}\left(j\omega_s\right)\left(i_s + i_r\right) \\
0 &= \mathrm{M}\left(j\omega_s\right)\left(i_s + i_r\right) + \left(\frac{R_r}{s} + L_{rd}\left(j\omega_s\right)\right) i_r
\end{aligned}
\tag{51}
$$

These equations can be represented in the steady-state circuit in Fig. 1.2.

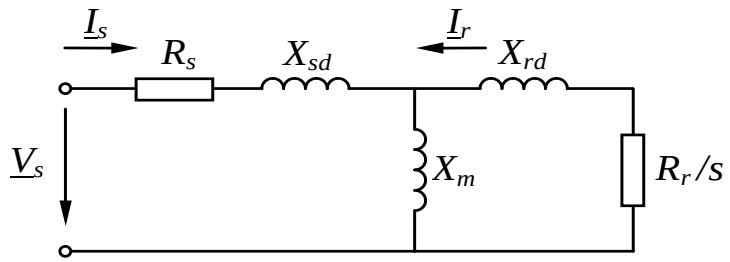

Fig. 1.2. Steady-state equivalent circuit for the single-cage model of the three-phase induction motor

1.5 Simulation of induction motor equations in different reference frames

In the study of the parameters determination from the transient measurements we must decide to work with *abc* variables and consequently with Park transformed variables in stator or rotor or synchronous reference frames.

In this part a comparison of different reference frame stator currents is presented for the induction machine of Table. 1.1. The transient data has been calculated using the program Simulink [31].

Table. 1.1. Induction machine data

$f_s(Hz)$	$V_{sph}(V)$	$R_s(\Omega)$	$L_s(H)$	$L_m(H)$	$L_r(H)$	$R_r(\Omega)$	*Pole pairs*	$S_n(VA)$	$J(kg.m^2)$
50	220	0.4	0.3246	0.3183	0.3246	0.4	1	4.5k	0.08

All the transient data are derived from free acceleration test where the mechanical torque (load) is zero.

Fig. 1.3 shows the voltages and currents of phases a, b, and c, that can be measured in the laboratory. Fig. 1.4 shows the mechanical speed.

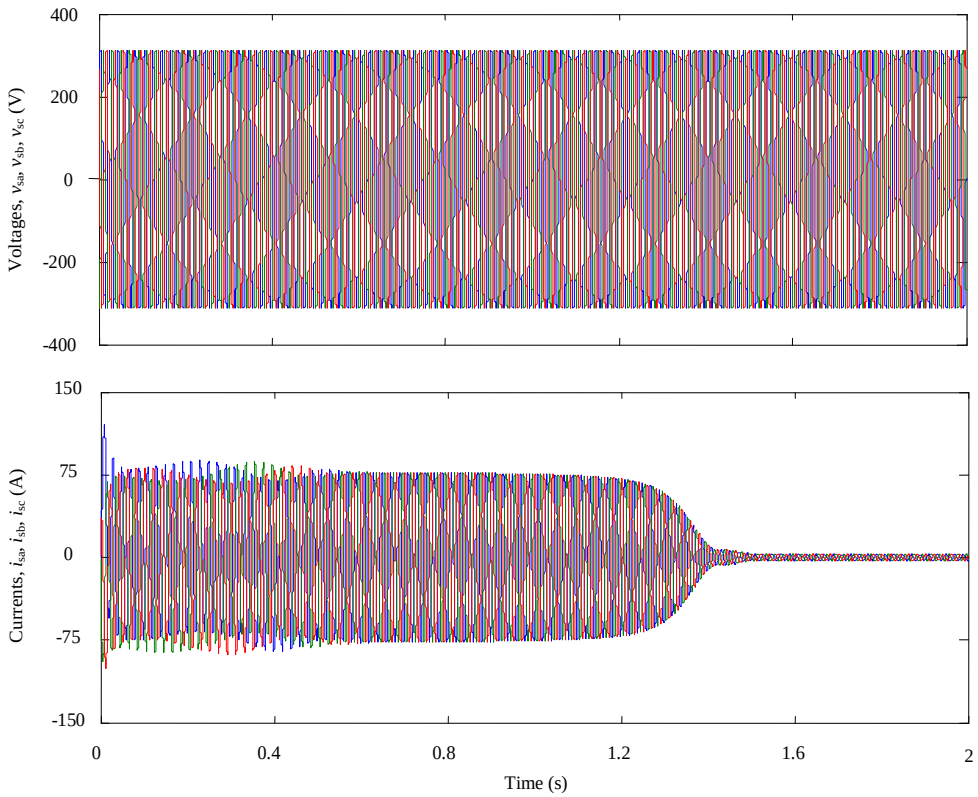

Fig. 1.3. Real values of stator *abc* voltages and currents in a starting transient

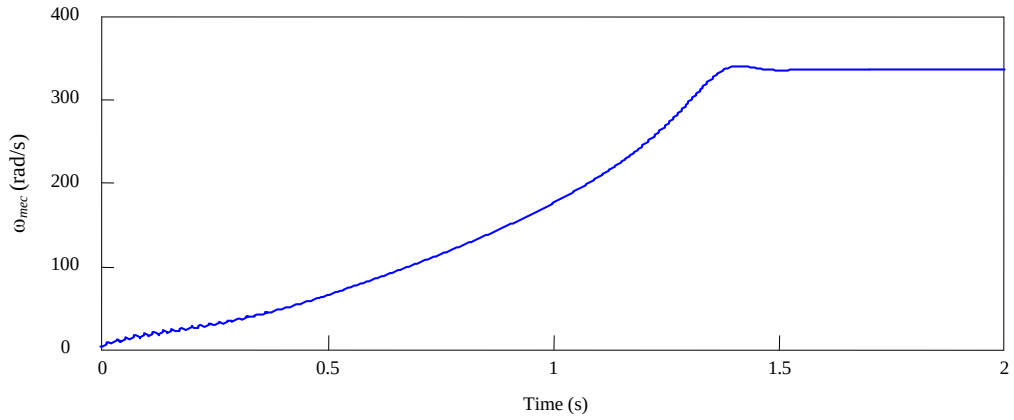

Fig. 1.4. Mechanical speed in a starting transient

In Fig. 1.5 the stator *d*, *q* voltages and currents can be observed in synchronous reference frame. The voltages are constant because in the synchronous reference frame symmetrical voltages result in constant values.

Fig. 1.5 shows the transformed direct and quadrature currents that are much smoother than those in the

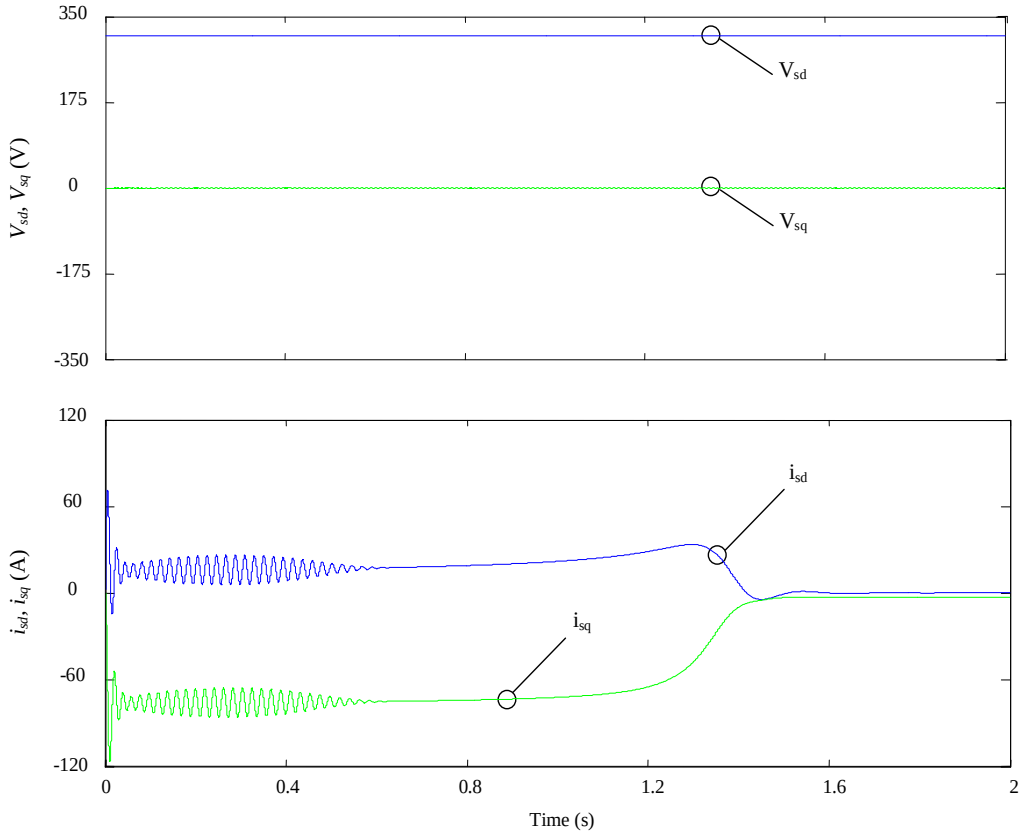

Fig. 1.5 Stator *d*, *q* voltages and currents in the synchronous reference frame

stator or rotor references (Figs. 1.6 and 1.7).

Direct and quadrature Park voltages and currents in synchronous reference frame are calculated from the *abc* variables (equation 11) as

$$\begin{aligned} v_{sd} &= \sqrt{\frac{2}{3}}\left(v_{sa}\cos(\theta_s) + v_{sb}\cos\left(\theta_s - \frac{2\pi}{3}\right) + v_{sc}\cos\left(\theta_s + \frac{2\pi}{3}\right)\right) \\ v_{sq} &= \sqrt{\frac{2}{3}}\left(-v_{sa}\sin(\theta_s) - v_{sb}\sin\left(\theta_s - \frac{2\pi}{3}\right) - v_{sc}\sin\left(\theta_s + \frac{2\pi}{3}\right)\right) \\ i_{sd} &= \sqrt{\frac{2}{3}}\left(i_{sa}\cos(\theta_s) + i_{sb}\cos\left(\theta_s - \frac{2\pi}{3}\right) + i_{sc}\cos\left(\theta_s + \frac{2\pi}{3}\right)\right) \\ i_{sq} &= \sqrt{\frac{2}{3}}\left(-i_{sa}\sin(\theta_s) - i_{sb}\sin\left(\theta_s - \frac{2\pi}{3}\right) - i_{sc}\sin\left(\theta_s + \frac{2\pi}{3}\right)\right) \end{aligned} \tag{52}$$

where the angle is calculated with

$$\theta_s = \omega_s t \tag{53}$$

Figure 1.6 shows direct and quadrature voltages and currents in rotor reference frame. It should be noted

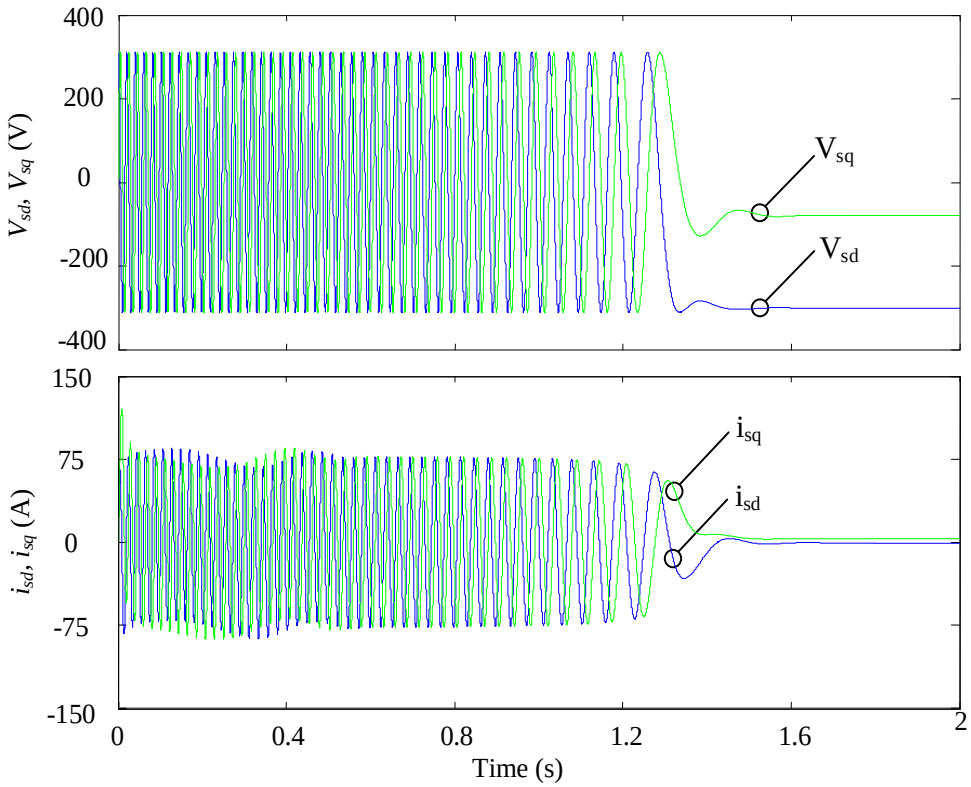

Fig. 1.6. Stator *d*, *q* voltages and currents in the rotor reference frame

that the voltage and the current have the big oscillations in the mechanical transient region. It is interesting to compare them with the synchronous reference frame results in Fig. 1.5, where the voltage is constant and the current has lower oscillations in the beginning of the transient region (electrical transient) and is very smooth in the last region of the transient (mechanical transient). These facts are of great interest because in the numerical process to determine the parameters of the induction machine, it is necessary to calculate the first and the second derivatives of the currents and the first derivative of voltages. Therefore, the synchronous reference frame allows having less numerical errors than those in the rotor reference frame.

Direct and quadrature Park voltages and currents in rotor reference frame are calculated from the laboratory data using the equations (52) and the angle

$$\theta_s = \theta_m = \int \wp\, \omega_m dt \tag{54}$$

where ω_m is the measured mechanical speed and $\wp$ is the number of pair of poles.

Fig. 1.7 shows *d*, *q* stator voltages and currents in the stator reference frame. In this case the voltage and

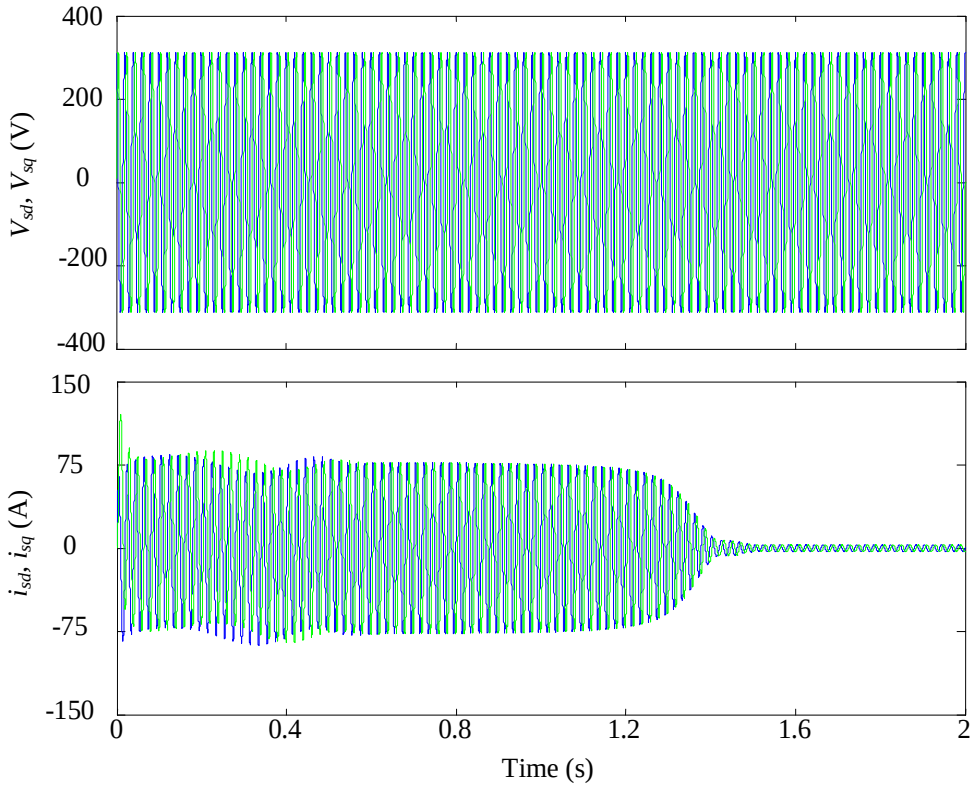

Fig. 1.7. Stator *d*, *q* voltages and currents in the stator reference frame, V_{sd}; dash line blue and V_{sq}; line green

currents present oscillations all the time. The use of this reference to develop the algorithm for parameter estimation is not adequate because it presents problems with the numerical derivatives.

The direct and quadrature voltage and currents in the stator reference frame are calculated with the equations of (52) and using the angle

$$\theta_s = 0 \tag{55}$$

In this case the expression of (52) is simplified to the equations

$$\begin{aligned} v_{sd} &= \sqrt{\frac{2}{3}}\left(v_{sa} - \frac{v_{sb}}{2} - \frac{v_{sc}}{2}\right) \quad ; \quad v_{sq} = \sqrt{2}\left(\frac{v_{sb}}{2} - \frac{v_{sc}}{2}\right) \\ i_{sd} &= \sqrt{\frac{2}{3}}\left(i_{sa} - \frac{i_{sb}}{2} - \frac{i_{sc}}{2}\right) \quad ; \quad i_{sq} = \sqrt{2}\left(\frac{i_{sb}}{2} - \frac{i_{sc}}{2}\right) \end{aligned} \tag{56}$$

As a summary of this presentation of the different reference frames, the synchronous reference frame is the best reference to work because the stator currents have oscillations of small magnitude during the electrical transient and in the zone of mechanical transient their variation is very smooth.

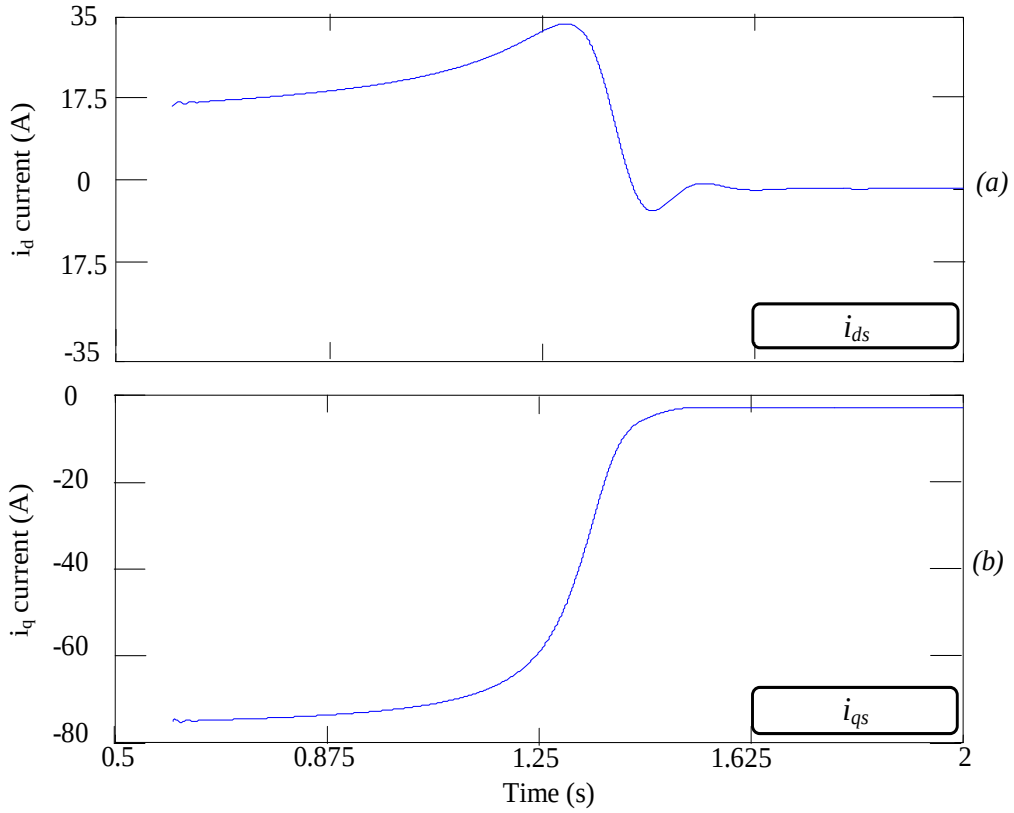

Fig. 1.8. a. Stator direct current in stator reference frame, b. Stator quadrature current

This is very important especially due to the noise effect over the laboratory measurements; however, the parameter estimation process is developed in the rotor reference frame in many papers [16],[17].

Fig. 1.8 shows the plot of different transient magnitudes of single-cage induction machine. The first part of the transient has been eliminated because it is a region with great oscillations and then great values of the derivatives. The magnitudes of interest which are used as data for estimation are $\frac{d\omega_m}{dt}$; derivative of rotor speed, $\frac{di_{sd}}{dt}$, $\frac{di_{sq}}{dt}$, $\frac{dv_{sd}}{dt}$, $\frac{dv_{sq}}{dt}$; derivative of *d*, *q* currents and voltages respectively and $\frac{d^2 i_{sd}}{dt^2}$, $\frac{d^2 i_{sq}}{dt^2}$; the second derivatives of *d*, *q* currents.

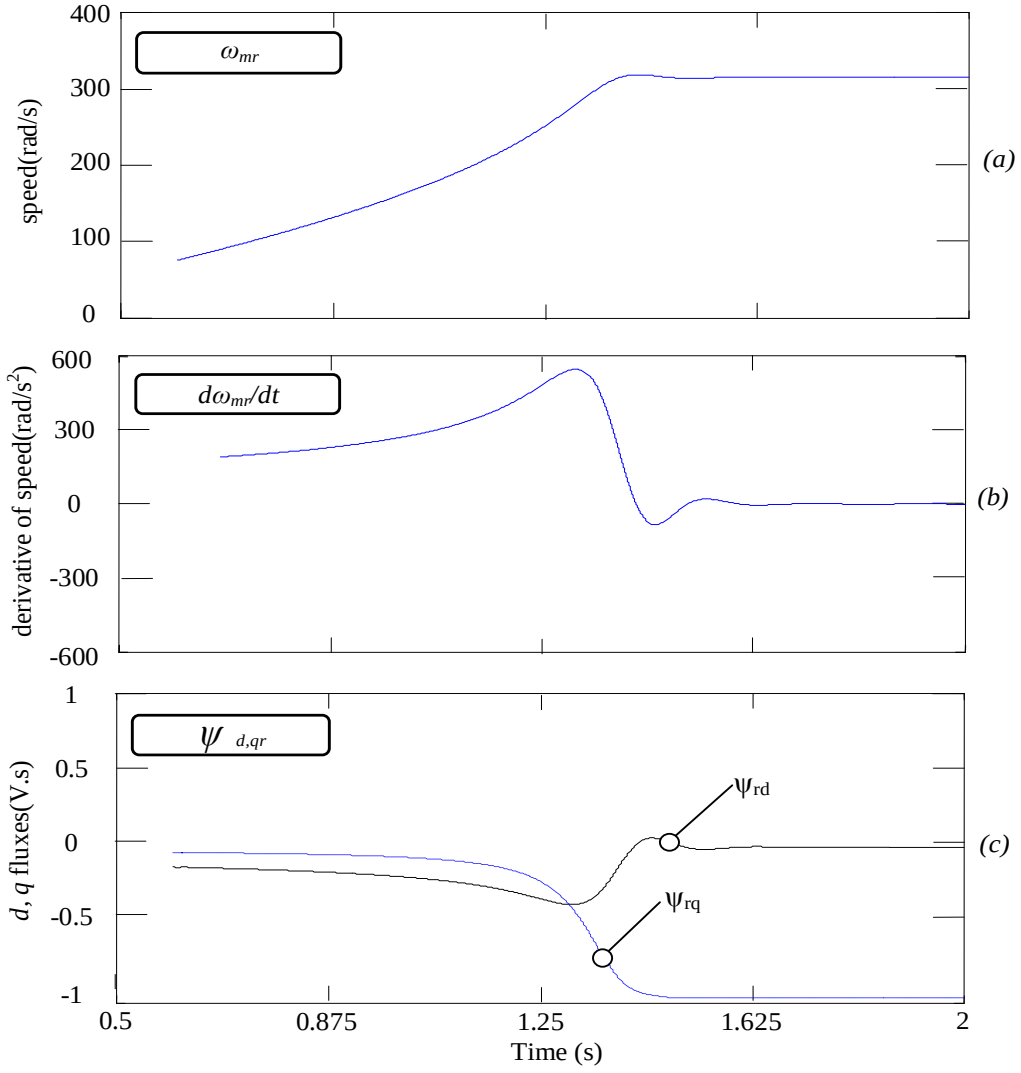

Fig. 1.9. a. mechanical rotor speed, b. derivative of mechanical rotor speed and c. rotor *d*, *q* fluxes in synchronous reference frame.

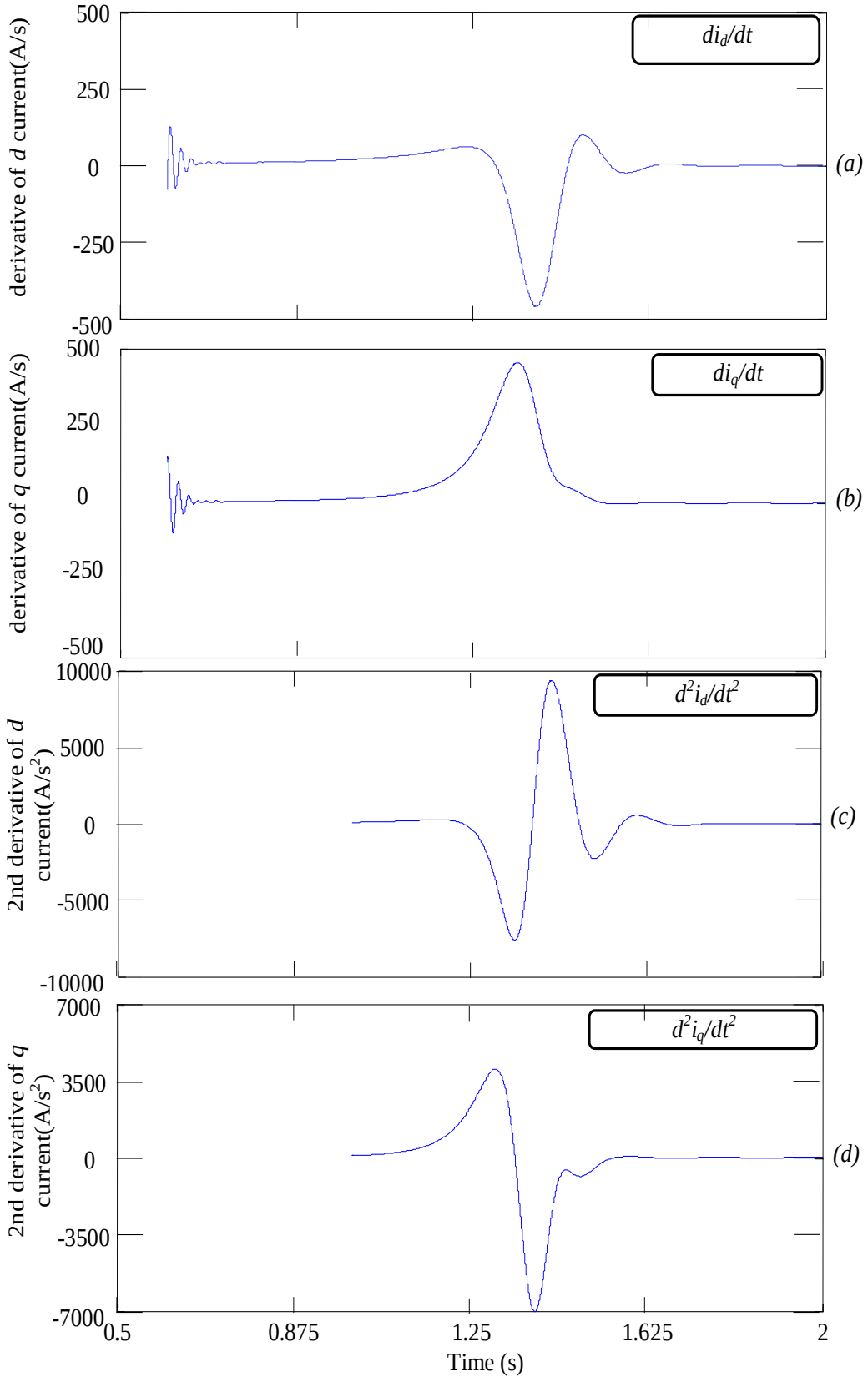

Fig. 1.10. a. Stator d current i_d derivative, b. Stator q current i_q derivative, c. Stator d current i_d second derivative and d. Stator q current i_q second derivative.

In Fig. 1.8 to 1.10 there are important machine magnitudes including *d, q* stator currents, mechanical rotor speed, rotor speed derivative, rotor *d, q* fluxes, the first and the second derivative of the stator *d, q* currents, respectively. The maximum value in speed derivative in Fig. 1.9b shows the point of maximum torque. In Fig. 1.8 and 1.9.a, the *d, q* currents and speed are respectively shown in synchronous reference frame that does not have oscillations after electrical transient region. Fig. 1.9.c shows the rotor fluxes. Fig.1.9.b and Fig. 1.10 shows first derivative of speed and also first and second derivative of the stator *d, q* currents in synchronous reference frame.

1.6 Single cage induction machine second order differential equations in synchronous reference frame

According to explanation of section 1.5, synchronous reference frame is the best reference frame for estimation of machine parameters. For machine parameters estimation in synchronous reference frame, stator currents and voltages and derivatives of them are calculated in *d*, *q* system. Dynamic voltage-current equations using Ku complex transformation in synchronous reference frame are

$$\begin{aligned} v_s &= \left(R_s + L_s\left(p + j\omega\right)\right)i_s + M\left(p + j\omega\right)i_r \\ 0 &= M\left(p + js\omega\right)i_s + \left(R_r + L_r\left(p + js\omega\right)\right)i_r \\ T\left(t\right) &= 2\wp M\ \mathrm{Im}\left(i_s i_r^*\right) \quad , \quad s = \left(\omega - \wp\,\omega_m\right)/\omega \end{aligned} \tag{57}$$

where $\wp$ is the pole pairs , p is the operator derivative $\frac{d}{dt}$, ω is the synchronous speed, ω_m is the mechanical rotor speed and s is the slip.

The main problem is that rotor magnitudes cannot be measured. Therefore, rotor currents must be substituted by other measurable magnitudes in above equations. These magnitudes are the first and second derivative of stator current and the first derivative of stator voltage. This process of substitution uses the rotor fluxes that are approximated by the stator fluxes. The development is made using Ku variables, because the analytical process is clearer. The rotor currents can be expressed as

$$\left.\begin{aligned} \psi_s &= L_s i_s + M i_r \\ \psi_r &= L_r i_r + M i_s \end{aligned}\right\} \quad \Rightarrow \quad i_r = \frac{1}{L_r}\left(\psi_r - M i_s\right) \tag{58}$$

Then voltage-flux equations of stator and rotor of induction machine are

$$v_s = \left(R_s + \left(L_s - \frac{M^2}{L_r}\right)\left(p + j\omega\right)\right)i_s + \frac{M}{L_r}\left(p + j\omega\right)\psi_r \tag{59}$$

Since the rotor voltage v_r is zero, the second equation of (57) and equation of (59) gives

$$0 = -\frac{R_r M}{L_r} i_s + \left(\frac{R_r}{L_r} + \left(p + j\left(\omega - \wp\,\omega_m\right)\right)\right)\psi_r \tag{60}$$

and the new machine equations are

$$\begin{pmatrix} \left(L_s - \frac{M^2}{L_r}\right) & \frac{M}{L_r} \\ 0 & 1 \end{pmatrix} p\begin{pmatrix} i_s \\ \psi_r \end{pmatrix} = \begin{pmatrix} -R_s - j\omega\left(L_s - \frac{M^2}{L_r}\right) & -j\omega\frac{M}{L_r} \\ \frac{R_r M}{L_r} & -\frac{R_r}{L_r} - j\left(\omega - \wp\,\omega_m\right) \end{pmatrix}\begin{pmatrix} i_s \\ \psi_r \end{pmatrix} + \begin{pmatrix} v_s \\ 0 \end{pmatrix} \tag{61}$$

Calculating the inverse matrix

$$\begin{pmatrix} \left(L_s - \frac{M^2}{L_r}\right) & \frac{M}{L_r} \\ 0 & 1 \end{pmatrix}^{-1} = \begin{pmatrix} \frac{L_r}{L_s L_r - M^2} & \frac{-M}{L_s L_r - M^2} \\ 0 & 1 \end{pmatrix} \tag{62}$$

The equation (61) can be rewritten as

$$p\begin{pmatrix} i_s \\ \psi_r \end{pmatrix} = \begin{pmatrix} A & B \\ C & D \end{pmatrix}\begin{pmatrix} i_s \\ \psi_r \end{pmatrix} + \begin{pmatrix} \frac{L_r}{L_s L_r - M^2} v_s \\ 0 \end{pmatrix} \tag{63}$$

where

$$\begin{aligned} A &= \left(\frac{L_r}{L_s L_r - M^2}\right)\left(-R_s - j\omega\left(L_s - \frac{M^2}{L_r}\right)\right) - \frac{M}{L_s L_r - M^2}\frac{R_r M}{L_r} \\ B &= \left(\frac{L_r}{L_s L_r - M^2}\right)\left(-j\omega\frac{M}{L_r}\right) + \frac{M}{L_s L_r - M^2}\left(\frac{R_r}{L_r} + j\left(\omega - \wp\,\omega_m\right)\right) \\ C &= \frac{R_r M}{L_r} \qquad ; \qquad D = -\frac{R_r}{L_r} - j\left(\omega - \wp\,\omega_m\right) \end{aligned} \tag{64}$$

Operating the expressions of A and B simplifies the equations to

$$\begin{aligned} A &= -\frac{R_s L_r^2 + R_r M^2}{L_r\left(L_s L_r - M^2\right)} - j\omega \qquad ; \qquad B = \frac{R_r M - j\wp\,\omega_m M L_r}{L_r\left(L_s L_r - M^2\right)} \\ C &= \frac{R_r M}{L_r} \qquad ; \qquad D = -\frac{R_r}{L_r} - j\left(\omega - \wp\,\omega_m\right) \end{aligned} \tag{65}$$

where

$$\sigma = 1 - \frac{M^2}{L_s L_r} \qquad ; \qquad \beta = \frac{M}{\sigma L_s L_r} \qquad ; \qquad T_r = \frac{L_r}{R_r} \qquad ; \qquad \gamma = \frac{R_s L_r^2 + R_r M^2}{L_r\left(L_s L_r - M^2\right)} \tag{66}$$

Then equations (65) can be rewritten as

$$A = -\gamma - j\omega \qquad ; \qquad B = \frac{R_r M - j\wp\,\omega_m M L_r}{L_r\left(L_s L_r - M^2\right)} = \frac{R_r M}{\sigma L_s L_r^2} - \frac{j\wp\,\omega_m M}{\sigma L_s L_r} = \frac{\beta}{T_r} - j\wp\,\omega_m \beta \tag{67}$$

$$C = \frac{R_r M}{L_r} = \frac{M}{T_r} \qquad ; \qquad D = -\frac{R_r}{L_r} - j\left(\omega - \wp\,\omega_m\right) = -\frac{1}{T_r} - j\left(\omega - \wp\,\omega_m\right)$$

where

$$\frac{L_r}{L_s L_r - M^2} = \frac{1}{\sigma L_s} \tag{68}$$

The stator current and rotor flux equations of single-cage the induction machine are

$$p\begin{pmatrix} i_s \\ \psi_r \end{pmatrix} = \begin{pmatrix} -\gamma - jw & \dfrac{\beta}{T_r} - j\wp\,\omega_m \beta \\ \dfrac{M}{T_r} & -\dfrac{1}{T_r} - j\left(\omega - \wp\,\omega_m\right) \end{pmatrix} \begin{pmatrix} i_s \\ \psi_r \end{pmatrix} + \begin{pmatrix} \dfrac{1}{\sigma L_s} v_s \\ 0 \end{pmatrix} \tag{69}$$

which can be rewritten as

$$\begin{aligned} \frac{di_s}{dt} &= \left(-\gamma - j\omega\right) i_s + \left(\frac{\beta}{T_r} - j\wp\,\omega_m \beta\right)\psi_r + \frac{1}{\sigma L_s} v_s \\ \frac{d\psi_r}{dt} &= \frac{M}{T_r} i_s - \left(\frac{1}{T_r} + j\left(\omega - \wp\,\omega_m\right)\right)\psi_r \end{aligned} \tag{70}$$

The stator current second derivative is

$$\frac{d^2 i_s}{dt^2} = \left(-\gamma - j\omega\right)\frac{di_s}{dt} + \left(\frac{\beta}{T_r} - j\wp\,\omega_m \beta\right)\frac{d\psi_r}{dt} - j\frac{d\omega_m}{dt}\wp\,\beta\psi_r + \frac{1}{\sigma L_s}\frac{dv_s}{dt} \tag{71}$$

Substituting the derivative of rotor flux (70) in the stator current equations (71) gives

$$\frac{d^2 i_s}{dt^2} = \left(-\gamma - jw\right)\frac{di_s}{dt} + \left(\frac{\beta}{T_r} - j\wp\,\omega_m \beta\right)\left(\frac{M}{T_r} i_s - \left(\frac{1}{T_r} + j\left(\omega - \wp\,\omega_m\right)\right)\psi_r\right) - j\frac{d\omega_m}{dt}\wp\,\beta\psi_r + \frac{1}{\sigma L_s}\frac{dv_s}{dt} \tag{72}$$

which can be rewritten as

$$\frac{d^2 i_s}{dt^2} = \left(-\gamma - j\omega\right)\frac{di_s}{dt} + \left(\frac{\beta}{T_r} - j\wp\,\omega_m \beta\right)\frac{M}{T_r} i_s - \left(\frac{\beta}{T_r} - j\wp\,\omega_m \beta\right)\left(\frac{1}{T_r} + j\left(\omega - \wp\,\omega_m\right)\right)\psi_r - j\frac{d\omega_m}{dt}\wp\,\beta\psi_r + \frac{1}{\sigma L_s}\frac{dv_s}{dt} \tag{73}$$

Multiplying both sides of (70) by

$$\left(\frac{1}{T_r}+j\left(\omega-\wp\,\omega_m\right)\right) \tag{74}$$

the following expression is obtained

$$\left(\frac{1}{T_r}+j\left(\omega-\wp\,\omega_m\right)\right)\frac{di_s}{dt}=\left\{\left(-\gamma-j\omega\right)i_s+\left(\frac{\beta}{T_r}-j\wp\,\omega_m\beta\right)\psi_r+\frac{1}{\sigma L_s}v_s\right\}.\left(\frac{1}{T_r}+j\left(\omega-\wp\,\omega_m\right)\right) \tag{75}$$

The equations (75) are rewritten as

$$\begin{aligned}&\left(\frac{\beta}{T_r}-j\wp\,\omega_m\beta\right)\left(\frac{1}{T_r}+j\left(\omega-\wp\,\omega_m\right)\right)\psi_r=\left(\frac{1}{T_r}+j\left(\omega-\wp\,\omega_m\right)\right)\frac{di_s}{dt}-\left(\frac{1}{T_r}+j\left(\omega-\wp\,\omega_m\right)\right)\left(-\gamma-j\omega\right)i_s-\\&-\left(\frac{1}{T_r}+j\left(\omega-\wp\,\omega_m\right)\right)\frac{1}{\sigma L_s}v_s\end{aligned} \tag{76}$$

Substituting rotor flux (76) from above equation to the second derivative of stator current (73) gives

$$\begin{aligned}&\frac{d^2i_s}{dt^2}=\left(-\gamma-j\omega\right)\frac{di_s}{dt}-\left(\frac{1}{T_r}+j\left(\omega-\wp\,\omega_m\right)\right)\frac{di_s}{dt}+\left(\frac{\beta}{T_r}-j\wp\,\omega_m\beta\right)\frac{M}{T_r}i_s+\left(\frac{1}{T_r}+j\left(\omega-\wp\,\omega_m\right)\right)\left(-\gamma-j\omega\right)i_s-\\&-j\frac{d\omega_m}{dt}\wp\,\beta\psi_r+\left(\frac{1}{T_r}+j\left(\omega-\wp\,\omega_m\right)\right)\frac{1}{\sigma L_s}v_s+\frac{1}{\sigma L_s}\frac{dv_s}{dt}\end{aligned} \tag{77}$$

which can be simplified as

$$\begin{aligned}&\frac{d^2i_s}{dt^2}+j\left(2\omega-\wp\,\omega_m\right)\frac{di_s}{dt}-\omega\left(\omega-\wp\,\omega_m\right)i_s+j\frac{d\omega_m}{dt}\wp\,\beta\psi_r=\\&-\left(\frac{1}{T_r}+\gamma\right)\frac{di_s}{dt}+\left(\frac{\beta}{T_r}-j\wp\,\omega_m\beta\right)\frac{M}{T_r}i_s-\left(\frac{1}{T_r}+j\left(\omega-\wp\,\omega_m\right)\right)\gamma i_s-\frac{j\omega}{T_r}i_s+\left(\frac{1}{T_r}+j\left(\omega-\wp\,\omega_m\right)\right)\frac{1}{\sigma L_s}v_s+\frac{1}{\sigma L_s}\frac{dv_s}{dt}\end{aligned} \tag{78}$$

Then, the coefficients K_i are defined as

$$\begin{aligned}&K_1=\frac{1}{T_r}+\gamma=\frac{R_s}{\sigma L_s}+\frac{1}{\sigma T_r}\quad;\quad K_2=\frac{\gamma}{T_r}-\frac{\beta M}{T_r^{\,2}}=\frac{R_s}{\sigma L_s T_r}\quad;\quad M_{31}=\gamma\quad;\quad M_{32}=\frac{\beta M}{T_r}\quad;\quad M_{33}=\frac{1}{T_r}\\&K_4=\frac{1}{\sigma L_s}\quad;\quad K_5=\frac{1}{\sigma L_s T_r}\quad;\quad K_{31}=M_{31}-M_{32}=\frac{1}{\sigma T_s}\quad;\quad K_{32}=M_{32}+M_{33}=\frac{1}{\sigma T_r}\end{aligned} \tag{79}$$

where

$$\sigma=1-\frac{M^2}{L_s L_r}\quad;\quad \beta=\frac{M}{\sigma L_s L_r}\quad;\quad T_r=\frac{L_r}{R_r}\quad;\quad T_s=\frac{L_s}{R_s}\quad;\quad \gamma=\frac{R_s L_r^2+R_r M^2}{L_r\left(L_s L_r-M^2\right)} \tag{80}$$

All the references [15 to 18] use the approximation of zero speed derivative; $\frac{d\omega_m}{dt}$ i.e. it can be neglected so that the rotor flux is eliminated in these equations. In this thesis this strategy is improved by a better approximation. This will be studied in section 1.9.

Using the coefficient K_i equation (78) can be rewritten as

$$\begin{aligned}&\frac{d^2 i_s}{dt^2}+j\left(2\omega-\wp\,\omega_m\right)\frac{di_s}{dt}-\omega\left(\omega-\wp\,\omega_m\right)i_s+j\frac{d\omega_m}{dt}\wp\,\beta\psi_r=\\&-K_1\frac{di_s}{dt}-K_2 i_s-\left(jM_{31}\left(\omega-\wp\,\omega_m\right)+j\wp\,\omega_m M_{32}+j\omega M_{33}\right)i_s+K_4\left(\frac{dv_s}{dt}+j\left(\omega-\wp\,\omega_m\right)v_s\right)+K_5 v_s\end{aligned} \tag{81}$$

and simplifying results

$$\begin{aligned}&\frac{d^2 i_s}{dt^2}+j\left(2\omega-\wp\,\omega_m\right)\frac{di_s}{dt}-\omega\left(\omega-\wp\,\omega_m\right)i_s+j\frac{d\wp\,\omega_m}{dt}\beta\psi_r=\\&-K_1\frac{di_s}{dt}-K_2 i_s-\left(jK_{31}\left(\omega-\wp\,\omega_m\right)+j\omega K_{32}\right)i_s+K_4\left(\frac{dv_s}{dt}+j\left(\omega-\wp\,\omega_m\right)v_s\right)+K_5 v_s\end{aligned} \tag{82}$$

and finally changing the sign of the equation gives

$$\begin{aligned}&-\frac{d^2 i_s}{dt^2}-j\left(2\omega-\wp\,\omega_m\right)\frac{di_s}{dt}+\omega\left(\omega-\wp\,\omega_m\right)i_s-j\frac{d\wp\,\omega_m}{dt}\beta\psi_r=\\&K_1\frac{di_s}{dt}+K_2 i_s+\left(jK_{31}\left(\omega-\wp\,\omega_m\right)+j\omega K_{32}\right)i_s-K_4\left(\frac{dv_s}{dt}+j\left(\omega-\wp\,\omega_m\right)v_s\right)-K_5 v_s\end{aligned} \tag{83}$$

This complex equation expressed in *d, q* variables results in two real equations. The real part is

$$\begin{aligned}&-\frac{d^2 i_{sd}}{dt^2}+\left(2\omega-\wp\,\omega_m\right)\frac{di_{sq}}{dt}+\omega\left(\omega-\wp\,\omega_m\right)i_{sd}+\frac{d\wp\,\omega_m}{dt}\beta\psi_{rq}=\\&K_1\frac{di_{sd}}{dt}+K_2 i_{sd}-K_{31}\left(\omega-\wp\,\omega_m\right)i_{sq}-K_{32}\omega i_{sq}-K_4\left(\frac{dv_{sd}}{dt}-\left(\omega-\wp\,\omega_m\right)v_{sq}\right)-K_5 v_{sd}\end{aligned} \tag{84}$$

and the imaginary part results

$$\begin{aligned}&-\frac{d^2 i_{sq}}{dt^2}-\left(2\omega-\wp\,\omega_m\right)\frac{di_{sd}}{dt}+\omega\left(\omega-\wp\,\omega_m\right)i_{sq}-\frac{d\wp\,\omega_m}{dt}\beta\psi_{rd}=\\&K_1\frac{di_{sq}}{dt}+K_2 i_{sq}+K_{31}\left(\omega-\wp\,\omega_m\right)i_{sd}+K_{32}\omega i_{sd}-K_4\left(\frac{dv_{sq}}{dt}+\left(\omega-\wp\,\omega_m\right)v_{sd}\right)-K_5 v_{sq}\end{aligned} \tag{85}$$

The equations (85) and (86) can be expressed in matrix notation as

$$\begin{pmatrix} \frac{di_{sd}}{dt} & i_{sd} & -(\omega-\wp\,\omega_m)i_{sq} & -\omega i_{sq} & -\frac{dv_{sd}}{dt}+(\omega-\wp\,\omega_m)v_{sq} & -v_{sd} \\ \frac{di_{sq}}{dt} & i_{sq} & (\omega-\wp\,\omega_m)i_{sd} & \omega i_{sd} & -\frac{dv_{sq}}{dt}-(\omega-\wp\,\omega_m)v_{sd} & -v_{sq} \end{pmatrix} \begin{pmatrix} K_1 \\ K_2 \\ K_{31} \\ K_{32} \\ K_4 \\ K_5 \end{pmatrix} = \tag{86}$$

$$= \begin{pmatrix} -\frac{d^2 i_{sd}}{dt^2}+(2\omega-\wp\,\omega_m)\frac{di_{sq}}{dt}+(\omega-\wp\,\omega_m)\omega i_{sd}+(\beta\psi_{rq}).\frac{d\wp\,\omega_m}{dt} \\ -\frac{d^2 i_{sq}}{dt^2}-(2\omega-\wp\,\omega_m)\frac{di_{sd}}{dt}+(\omega-\wp\,\omega_m)\omega i_{sq}-(\beta\psi_{rd}).\frac{d\wp\,\omega_m}{dt} \end{pmatrix}$$

and, it can be written in a more compact expression as

$$[\mathbf{A}][\mathbf{K}]=[\mathbf{B}] \quad \Rightarrow \quad \begin{pmatrix} a_{d1} & a_{d2} & a_{d3} & a_{d4} & a_{d5} & a_{d6} \\ a_{q1} & a_{q2} & a_{q3} & a_{q4} & a_{q5} & a_{q6} \end{pmatrix} \begin{pmatrix} K_1 \\ K_2 \\ K_{31} \\ K_{32} \\ K_4 \\ K_5 \end{pmatrix} = \begin{pmatrix} b_d \\ b_q \end{pmatrix} \tag{87}$$

where the coefficients are

$$\begin{aligned} &a_{d1}=\frac{di_{sd}}{dt} \;\; ; \;\; a_{d2}=i_{sd} \;\; ; \;\; a_{d3}=-(\omega-\wp\,\omega_m)i_{sq} \;\; ; \;\; a_{d4}=-\omega i_{sq} \\ &a_{d5}=-\left(\frac{dv_{sd}}{dt}-(\omega-\wp\,\omega_m)v_{sq}\right) \;\; ; \;\; a_{d6}=-v_{sd} \\ &b_d=-\frac{d^2 i_{sd}}{dt^2}+(2\omega-\wp\,\omega_m)\frac{di_{sq}}{dt}+\omega(\omega-\wp\,\omega_m)i_{sd}+(\beta\psi_{rq})\frac{d\wp\,\omega_m}{dt} \end{aligned} \tag{88}$$

$$\begin{aligned} &a_{q1}=\frac{di_{sq}}{dt} \;\; ; \;\; a_{q2}=i_{sq} \;\; ; \;\; a_{q3}=(\omega-\wp\,\omega_m)i_{sd} \;\; ; \;\; a_{q4}=\omega i_{sd} \\ &a_{q5}=-\left(\frac{dv_{sq}}{dt}+(\omega-\wp\,\omega_m)v_{sd}\right) \;\; ; \;\; a_{q6}=-v_{sq} \\ &b_q=-\frac{d^2 i_{sq}}{dt^2}-(2\omega-\wp\,\omega_m)\frac{di_{sd}}{dt}+\omega(\omega-\wp\,\omega_m)i_{sq}-(\beta\psi_{rd})\frac{d\wp\,\omega_m}{dt} \end{aligned} \tag{89}$$

From the K parameters

$$[\mathbf{K}]=\begin{bmatrix} K_1 & K_2 & K_{31} & K_{32} & K_4 & K_5 \end{bmatrix}^T \tag{90}$$

it can be estimated the induction machine parameters with the equations

$$R_s = \frac{K_1 - K_{32}}{K_4} \quad ; \quad L_s = \frac{K_{32}}{K_5} \quad ; \quad L_r = L_s$$

$$\sigma = \frac{1}{K_4 L_s} = 1 - \frac{M^2}{L_r^2} \quad ; \quad T_r = \frac{1}{\sigma K_{32}} \quad ; \quad R_r = \frac{L_r}{T_r} \quad ; \quad M = L_s \sqrt{1-\sigma} \tag{91}$$

1.7 Induction machine second order differential equations in the rotor reference frame

In the rotor reference frame, the induction machine second order differential equation can be obtained from the synchronous reference frame, imposing that $\omega = \wp\,\omega_m$, then the vector of K-parameters is

$$[\mathbf{K}] = \begin{bmatrix} K_1 & K_2 & K_3 & K_4 & K_5 \end{bmatrix}^T \tag{92}$$

and the equation $[\mathbf{A}][\mathbf{K}] = [\mathbf{B}]$ results

$$[\mathbf{A}] = \begin{pmatrix} \dfrac{di_{sd}}{dt} & i_{sd} & -\wp\,\omega_m i_{sq} & -\dfrac{dv_{sd}}{dt} & -v_{sd} \\ \dfrac{di_{sq}}{dt} & i_{sq} & \wp\,\omega_m i_{sd} & -\dfrac{dv_{sq}}{dt} & -v_{sq} \end{pmatrix} \tag{93}$$

$$[\mathbf{B}] = \begin{pmatrix} -\dfrac{d^2 i_{sd}}{dt^2} + \wp\,\omega_m \dfrac{di_{sq}}{dt} + \left(\beta\psi_{rq}\right)\dfrac{d\left(\wp\,\omega_m\right)}{dt} \\ -\dfrac{d^2 i_{sq}}{dt^2} - \wp\,\omega_m \dfrac{di_{sd}}{dt} - \left(\beta\psi_{rd}\right)\dfrac{d\left(\wp\,\omega_m\right)}{dt} \end{pmatrix} \tag{94}$$

The parameters K_i are determined from the induction machine parameters while K_3 in rotor reference frame is K_{31} of synchronous reference frame

$$\sigma = 1 - \frac{M^2}{L_s L_r} \quad ; \quad T_r = \frac{L_r}{R_r} \quad ; \quad T_s = \frac{L_s}{R_s} \quad ; \quad K_1 = \frac{R_s}{\sigma L_s} + \frac{1}{\sigma T_r} \tag{95}$$

$$K_2 = \frac{R_s}{\sigma L_s T_r} = \frac{1}{\sigma T_s T_r} \quad ; \quad K_3\left(rotor\right) = K_{31}\left(synchronous\right) = \frac{1}{\sigma T_s} \quad ; \quad K_4 = \frac{1}{\sigma L_s} \quad ; \quad K_5 = \frac{1}{\sigma L_s T_r} \tag{96}$$

and the equations to obtain the induction machine parameters from the K parameters are

$$\begin{gathered} R_s = \frac{K_1 - \dfrac{K_5}{\sigma K_4}}{K_4} = \frac{K_{31}}{K_4} \quad ; \quad L_s = \frac{1}{\sigma K_4} \quad ; \quad L_r = L_s \\ \sigma = \frac{1}{K_4 L_s} = 1 - \frac{M^2}{L_r^2} \quad ; \quad T_r = \frac{K_4}{K_5} \quad ; \quad R_r = \frac{L_r}{T_r} \quad ; \quad M = L_s\sqrt{1-\sigma} \end{gathered} \tag{97}$$

1.8 Induction machine second order differential equations in the stator reference frame

In stator reference frame, the induction machine second order differential equation can be obtained from the synchronous reference frame imposing that $\omega = 0$, then the vector of K-parameters is

$$[\mathbf{K}] = \begin{bmatrix} K_1 & K_2 & K_3 & K_4 & K_5 \end{bmatrix}^T \tag{98}$$

and the equation $[\mathbf{A}][\mathbf{K}] = [\mathbf{B}]$ results

$$[\mathbf{A}] = \begin{pmatrix} \dfrac{di_{sd}}{dt} & i_{sd} & \wp\,\omega_m i_{sq} & -\dfrac{dv_{sd}}{dt} - \wp\,\omega_m v_{sq} & -v_{sd} \\ \dfrac{di_{sq}}{dt} & i_{sq} & -\wp\,\omega_m i_{sd} & -\dfrac{dv_{sq}}{dt} + \wp\,\omega_m v_{sd} & -v_{sq} \end{pmatrix} \tag{99}$$

$$[\mathbf{B}] = \begin{pmatrix} -\dfrac{d^2 i_{sd}}{dt^2} - \wp\,\omega_m \dfrac{di_{sq}}{dt} + \left(\beta\psi_{rq}\right)\dfrac{d\left(\wp\,\omega_m\right)}{dt} \\ -\dfrac{d^2 i_{sq}}{dt^2} + \wp\,\omega_m \dfrac{di_{sd}}{dt} - \left(\beta\psi_{rd}\right)\dfrac{d\left(\wp\,\omega_m\right)}{dt} \end{pmatrix} \tag{100}$$

The parameters K_i are determinate from the coefficient of the induction machine while K_3 in stator reference frame is K_{32} of synchronous reference frame

$$\sigma = 1 - \frac{M^2}{L_s L_r} \quad ; \quad T_r = \frac{L_r}{R_r} \quad ; \quad T_s = \frac{L_s}{R_s} \quad ; \quad K_1 = \frac{R_S}{\sigma L_s} + \frac{1}{\sigma T_r} \tag{101}$$

$$K_2 = \frac{R_S}{\sigma L_s T_r} = \frac{1}{\sigma T_s T_r} \quad ; \quad K_3\,(stator) = K_{32}\,(synchronous) = \frac{1}{\sigma T_r} \quad ; \quad K_4 = \frac{1}{\sigma L_s} \quad ; \quad K_5 = \frac{1}{\sigma L_s T_r} \tag{102}$$

and the equations to obtain the induction machine parameters from the *K*-parameters are

$$\begin{gathered} R_s = \frac{K_1 - K_3}{K_4} \quad ; \quad L_s = \frac{K_3}{K_5} \quad ; \quad L_r = L_s \\ \sigma = \frac{1}{K_4 L_s} = 1 - \frac{M^2}{L_r^2} \quad ; \quad T_r = \frac{1}{\sigma K_3} \quad ; \quad R_r = \frac{L_r}{T_r} \quad ; \quad M = L_s\sqrt{1-\sigma} \end{gathered} \tag{103}$$

1.9 Flux approximation in synchronous reference frame

The rotor of the induction motor is not usually accessible. Consequently, rotor currents and fluxes cannot be measured. In synchronous reference frame an approximation for the rotor flux can be obtained using the relation

$$\beta\psi_r + i_s = \frac{M}{\sigma L_s L_r}\psi_r + i_s \tag{104}$$

and operating

$$\sigma L_s L_r \left(\beta\psi_r + i_s\right) = M\,\psi_r + \sigma L_s L_r i_s = M\left(L_r i_r + M i_s\right) + \left(L_s L_r - M^2\right) i_s = L_r\left(L_s i_s + M i_r\right) = L_r \psi_s \tag{105}$$

and finally the rotor flux is obtained from stator magnitudes as

$$\beta\psi_r + i_s = \frac{L_r}{\sigma L_s L_r}\psi_s \quad \Rightarrow \quad \beta\psi_r = \frac{1}{\sigma L_s}\psi_s - i_s \tag{106}$$

From the voltage-current equation (57) and (58) and approximation of the stator flux ψ_s can be obtained because the influence of R_s is negligible and ψ_s is approximately constant

$$v_s = R_s i_s + p\psi_s + j\omega\psi_s \tag{107}$$

The stator flux approximation is

$$\psi_s = \frac{v_s}{j\omega} \tag{108}$$

and inserting (108) in (106), the approximated equation of rotor flux in complex Ku transformation results

$$\beta\psi_r = \frac{v_s}{j\,\sigma\omega L_s} - i_s \tag{109}$$

The complex equation in direct and quadrature variables, *d*, *q*, results in two real equations

$$\beta\psi_{rd} = \frac{v_{sq}}{\sigma\omega L_s} - i_{sd} \quad ; \quad \beta\psi_{rq} = -\frac{v_{sd}}{\sigma\omega L_s} - i_{sq} \tag{110}$$

Fig.1.11a shows that ψ_{sd} and ψ_{sq} are nearly constant when the electrical transient is finished. This supports the approximation of equation (108). Fig.1.11b shows the variation of ψ_{rd} and ψ_{rq} that is important. Fig. 1.12 shows the mechanical speed.

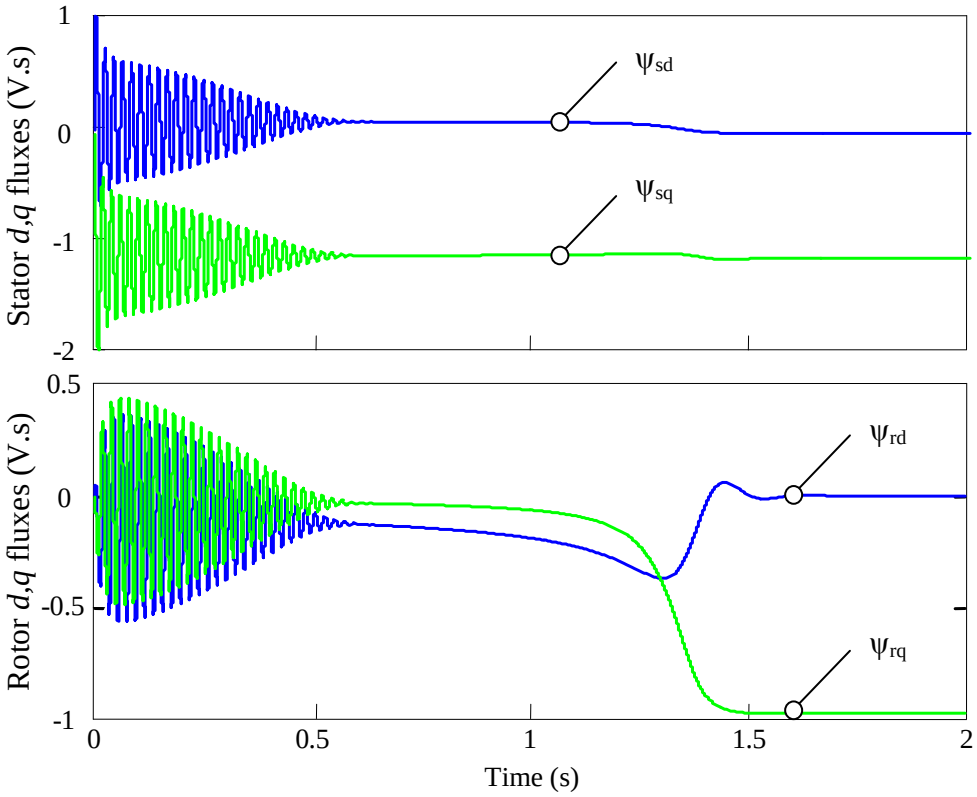

Fig. 1.11. Rotor *d*, *q* fluxes in synchronous reference frame

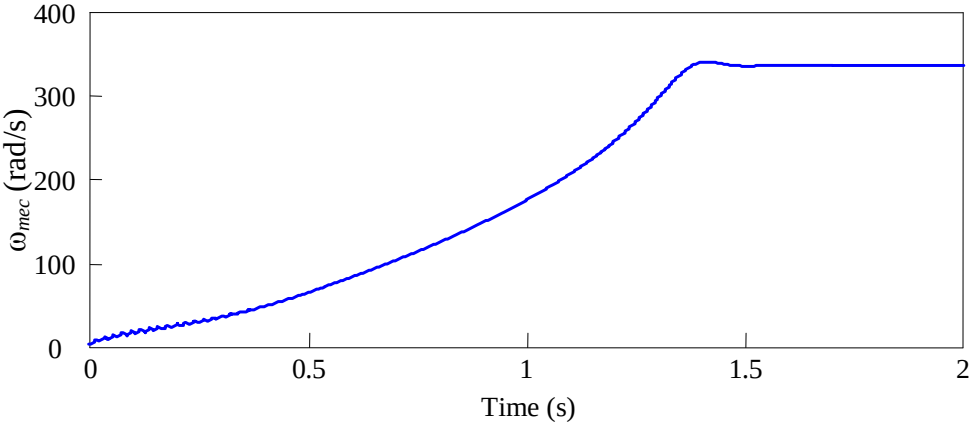

Fig. 1.12. Mechanical rotor speed in synchronous reference frame

Then using approximation of rotor fluxes equations in equation (86), gives

$$\begin{pmatrix} \frac{-di_{sd}}{dt} & -i_{sd} & (\omega-\wp\omega_m)i_{sq} & \omega i_{sq} & \frac{dv_{sd}}{dt}-(\omega-\wp\omega_m)v_{sq}-\frac{v_{sd}}{\omega}\frac{d(\wp\omega_m)}{dt} & v_{sd} \\ \frac{-di_{sq}}{dt} & -i_{sq} & -(\omega-\wp\omega_m)i_{sd} & -\omega i_{sd} & \frac{dv_{sq}}{dt}+(\omega-\wp\omega_m)v_{sd}-\frac{v_{sq}}{\omega}\frac{d(\wp\omega_m)}{dt} & v_{sq} \end{pmatrix} \begin{pmatrix} K_1 \\ K_2 \\ K_{31} \\ K_{32} \\ K_4 \\ K_5 \end{pmatrix} = \tag{111}$$

$$= \begin{pmatrix} \frac{d^2 i_{sd}}{dt^2}-(2\omega-\wp\omega_m)\frac{di_{sq}}{dt}-(\omega-\wp\omega_m)\omega i_{sd}+i_{sq}\frac{d\omega_m}{dt} \\ \frac{d^2 i_{sq}}{dt^2}+(2\omega-\wp\omega_m)\frac{di_{sd}}{dt}-(\omega-\wp\omega_m)\omega i_{sq}-i_{sd}\frac{d\omega_m}{dt} \end{pmatrix}$$

and in a more compact expression, it can be written as

$$[\mathbf{A}][\mathbf{K}]=[\mathbf{B}] \quad \Rightarrow \quad \begin{pmatrix} a_{d1} & a_{d2} & a_{d3} & a_{d4} & a_{d5} & a_{d6} \\ a_{q1} & a_{q2} & a_{q3} & a_{q4} & a_{q5} & a_{q6} \end{pmatrix} \begin{pmatrix} K_1 \\ K_2 \\ K_{31} \\ K_{32} \\ K_4 \\ K_5 \end{pmatrix} = \begin{pmatrix} b_d \\ b_q \end{pmatrix} \tag{112}$$

where the coefficients are

$$\begin{aligned} &a_{d1}=\frac{di_{sd}}{dt} \quad ; \quad a_{d2}=i_{sd} \quad ; \quad a_{d3}=-(\omega-\wp\omega_m)i_{sq} \quad ; \quad a_{d4}=-\omega i_{sq} \\ &a_{d5}=-\left(\frac{dv_{sd}}{dt}-(\omega-\wp\omega_m)v_{sq}-\frac{1}{\omega}\frac{d\wp\omega_m}{dt}v_{sd}\right) \quad ; \quad a_{d6}=-v_{sd} \\ &b_d=-\frac{d^2 i_{sd}}{dt^2}+(2\omega-\wp\omega_m)\frac{di_{sq}}{dt}+\omega(\omega-\wp\omega_m)i_{sd}-\frac{d\wp\omega_m}{dt}i_{sq} \end{aligned} \tag{113}$$

$$\begin{aligned} &a_{q1}=\frac{di_{sq}}{dt} \quad ; \quad a_{q2}=i_{sq} \quad ; \quad a_{q3}=(\omega-\wp\omega_m)i_{sd} \quad ; \quad a_{q4}=\omega i_{sd} \\ &a_{q5}=-\left(\frac{dv_{sq}}{dt}+(\omega-\wp\omega_m)v_{sd}-\frac{1}{\omega}\frac{d\wp\omega_m}{dt}v_{sq}\right) \quad ; \quad a_{q6}=-v_{sq} \\ &b_q=-\frac{d^2 i_{sq}}{dt^2}-(2\omega-\wp\omega_m)\frac{di_{sd}}{dt}+\omega(\omega-\wp\omega_m)i_{sq}+\frac{d\wp\omega_m}{dt}i_{sd} \end{aligned} \tag{114}$$

1.10 Error influence on B_D and B_Q coefficients

To analyze the influence of the error introduced by the derivatives of currents and voltages in synchronous reference frame in equations (113) and (114) terms $|b_d|$ and $|b_q|$ are defined as

$$\begin{aligned} |b_d| &= \left| -\frac{d^2 i_{sd}}{dt^2} + (2\omega - \wp\,\omega_m)\frac{di_{sq}}{dt} + \left(\omega(\omega - \wp\,\omega_m) i_{sd} - \frac{d\,\wp\,\omega_m}{dt} i_{sq} \right) \right| \\ |b_q| &= \left| -\frac{d^2 i_{sq}}{dt^2} - (2\omega - \wp\,\omega_m)\frac{di_{sd}}{dt} + \left(\omega(\omega - \wp\,\omega_m) i_{sq} + \frac{d\,\wp\,\omega_m}{dt} i_{sd} \right) \right| \end{aligned} \tag{115}$$

The quantities $|b_{2d}|$, $|b_{1d}|$, $|b_{0d}|$, $|b_{2q}|$, $|b_{1q}|$, $|b_{0q}|$ are defined as

$$\begin{aligned} |b_{2d}| &= \frac{\left| \frac{d^2 i_{sd}}{dt^2} \right|}{|b_d|} \quad ; \quad |b_{1d}| = \frac{\left| (2\omega - \wp\,\omega_m)\frac{di_{sq}}{dt} \right|}{|b_d|} \quad ; \quad |b_{0d}| = \frac{\left| \left(\omega(\omega - \wp\,\omega_m) i_{sd} - \frac{\wp\, d\,\omega_m}{dt} i_{sq} \right) \right|}{|b_d|} \\ |b_{2q}| &= \frac{\left| \frac{d^2 i_{sq}}{dt^2} \right|}{|b_q|} \quad ; \quad |b_{1q}| = \frac{\left| (2\omega - \wp\,\omega_m)\frac{di_{sd}}{dt} \right|}{|b_q|} \quad ; \quad |b_{0q}| = \frac{\left| \left(\omega(\omega - \wp\,\omega_m) i_{sq} + \frac{\wp\, d\,\omega_m}{dt} i_{sd} \right) \right|}{|b_q|} \end{aligned} \tag{116}$$

Fig. 1.13. shows the relative weight of each term in (116). From these results, it can be concluded that the terms that have a significant influence are those corresponding to the transformed currents, i.e., b_{0d} and b_{0q}. Less important terms are those including the first derivatives, and the terms with the second derivative are negligible. The most important result from this study is that the errors introduced by the second derivative hardly affect on the estimation procedure.

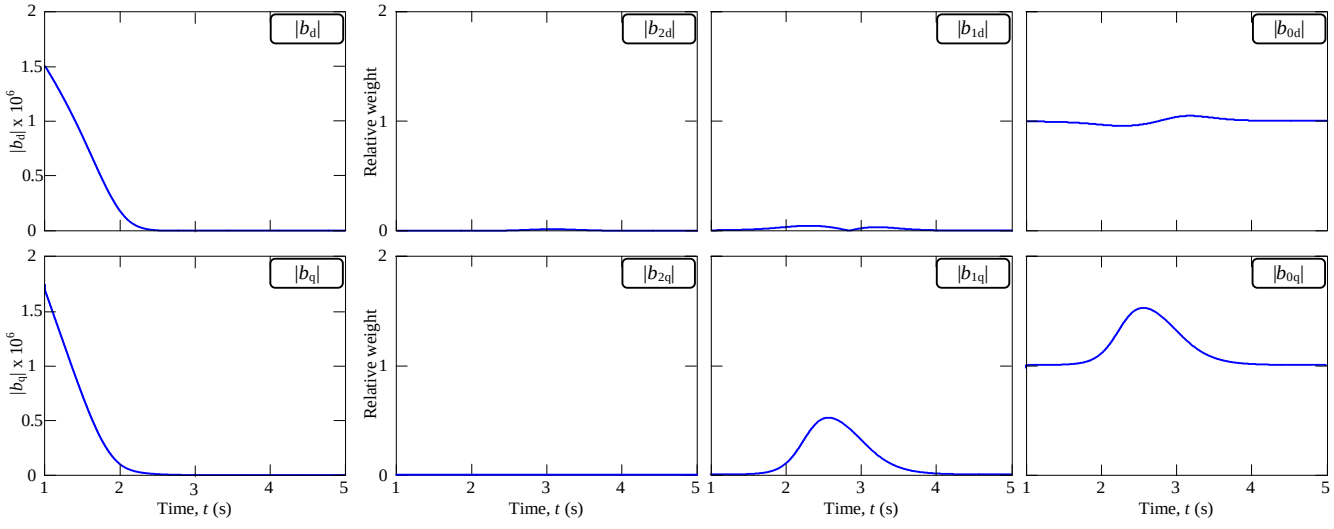

Fig. 1.13. Relative weights of the polynomial parts

2 Least-square regression method

2.1 Least-square theory

The Least-square method with two variables is the method of finding the best fit straight line for the observed (known) pairs (x_n, y_n), i.e. $y_n = ax_n + b$, where n is the number of pairs of data.

Thus, the problem is finding values of coefficients a, b in

$$y_n = a.x_n + b \tag{117}$$

that minimizes a quadratic error.

For simple explaining the method, in equation of $y = ax + b$ if there is the best fit, the errors equations should be minimum for n observed pairs

$$\begin{Bmatrix} \varepsilon_1 \\ . \\ . \\ . \\ \varepsilon_n \end{Bmatrix} = \begin{Bmatrix} y_1 - (ax_1 + b) \\ . \\ . \\ . \\ y_n - (ax_n + b) \end{Bmatrix} \tag{118}$$

For this reason, the variance ($\sigma^2_{y-(ax+b)}$) should be minimized. The variance shows how good a fit is. Also the importance of variance is more than that of mean value because in variance larger errors are weighted more than the errors in medium equation so that variance is used for least square method [33], then

$$\sigma^2_{y-(ax+b)} = \frac{1}{N}\sum_{n=1}^{N}\left(y_n - (ax_n + b)\right)^2 \tag{119}$$

To minimize the error, as a function of parameters a and b

$$\frac{\partial \sigma^2_{y-(ax+b)}}{\partial a} = 0 \quad ; \quad \frac{\partial \sigma^2_{y-(ax+b)}}{\partial b} = 0 \tag{120}$$

$$\frac{\partial}{\partial a}\left(\frac{1}{N}\sum_{n=1}^{N}\left(y_n - (ax_n + b)\right)^2\right) = 0 \quad ; \quad \frac{\partial}{\partial b}\left(\frac{1}{N}\sum_{n=1}^{N}\left(y_n - (ax_n + b)\right)^2\right) = 0 \tag{121}$$

$$\sum_{n=1}^{N} 2\left(y_n - (ax_n + b)\right)(-x_n) = 0 \quad ; \quad \sum_{n=1}^{N} 2\left(y_n - (ax_n + b)\right)(1) = 0 \tag{122}$$

then

$$\left(\sum_{n=1}^{N} x_n^{\,2}\right)a+\left(\sum_{n=1}^{N} x_n\right)b=\left(\sum_{n=1}^{N} x_n y_n\right) \quad ; \quad \left(\sum_{n=1}^{N} x_n\right)a+\left(\sum_{n=1}^{N} 1\right)b=\left(\sum_{n=1}^{N} y_n\right) \tag{123}$$

This equations can be rewritten as

$$\begin{pmatrix} a \\ b \end{pmatrix}=\begin{pmatrix} \sum_{n=1}^{N} x_n^2 & \sum_{n=1}^{N} x_n \\ \sum_{n=1}^{N} x_n & \sum_{n=1}^{N} 1 \end{pmatrix}^{-1}\begin{pmatrix} \sum_{n=1}^{N} x_n y_n \\ \sum_{n=1}^{N} y_n \end{pmatrix} \tag{124}$$

Defining the matrix X and vectors Y and K in Y=KX

$$\mathrm{X}=\begin{pmatrix} x_1 & 1 \\ . & . \\ . & . \\ . & . \\ x_n & 1 \end{pmatrix} \quad ; \quad \mathrm{Y}=\begin{pmatrix} y_1 \\ . \\ . \\ . \\ y_n \end{pmatrix} \quad ; \quad \mathrm{K}=\begin{pmatrix} a \\ b \end{pmatrix} \tag{125}$$

the estimated parameters can be derived from

$$K_{Estimated}=(X^T X)^{-1}\, X^T Y \tag{126}$$

In the general case with K variables ($x_n^{\,1}$, $x_n^{\,2}$, ..., $x_n^{\,k}$, y_n) the least-square method search the best (a^1, ..., a^k, b) parameters that satisfy the best fit according to equations

$$\begin{aligned} y_1 &= a^1 x_1^1+\ldots+a^k x_1^k+b \\ &\vdots \\ y_n &= a^1 x_n^1+\ldots+a^k x_n^k+b \end{aligned} \tag{127}$$

and errors to be minimized are defined as

$$\begin{Bmatrix} \varepsilon_1 \\ \vdots \\ \varepsilon_n \end{Bmatrix}=\begin{Bmatrix} y_1-\left(a^1 x_1^{\,1}+\ldots+a^k x_1^{\,k}+b\right) \\ \vdots \\ y_n-\left(a^1 x_n^{\,1}+\ldots+a^k x_n^{\,k}+b\right) \end{Bmatrix} \tag{128}$$

Then the matrix and vector are

$$\mathrm{X}=\begin{pmatrix} x_1^{\,1} & \cdots & x_1^{\,k} & 1 \\ \vdots & \vdots & \vdots & \vdots \\ x_n^{\,1} & \cdots & x_n^{\,k} & 1 \end{pmatrix} \quad ; \quad \mathrm{Y}=\begin{pmatrix} y_1 \\ \vdots \\ y_n \end{pmatrix} \quad ; \quad \mathrm{K}=\begin{pmatrix} a^1 \\ \vdots \\ a^k \\ b \end{pmatrix} \tag{129}$$

and the calculation of the coefficients K that minimizes the error can be made with

$$K_{Estimated} = (X^T X)^{-1} X^T Y \tag{130}$$

2.2 Application of the regression method to the single-cage induction machine parameters determination.

The single-cage induction motor second order differential equations with the rotor flux approximation gives for each experimental point two equations in (111) to obtain the K-parameters. This equation is repeated for clarity

$$[\mathbf{A}][\mathbf{K}]=[\mathbf{B}] \quad \Rightarrow \quad \begin{pmatrix} a_{d1} & a_{d2} & a_{d3} & a_{d4} & a_{d5} & a_{d6} \\ a_{q1} & a_{q2} & a_{q3} & a_{q4} & a_{q5} & a_{q6} \end{pmatrix} \begin{pmatrix} K_1 \\ K_2 \\ K_{31} \\ K_{32} \\ K_4 \\ K_5 \end{pmatrix} = \begin{pmatrix} b_d \\ b_q \end{pmatrix} \tag{131}$$

where the coefficients are

$$\begin{aligned} &a_{d1}=\frac{di_{sd}}{dt} \quad ; \quad a_{d2}=i_{sd} \quad ; \quad a_{d3}=-\left(\omega-\wp\,\omega_m\right)i_{sq} \quad ; \quad a_{d4}=-\omega i_{sq} \\ &a_{d5}=-\left(\frac{dv_{sd}}{dt}-\left(\omega-\wp\,\omega_m\right)v_{sq}+\frac{1}{\omega}\frac{d\wp\,\omega_m}{dt}v_{sd}\right) \quad ; \quad a_{d6}=-v_{sd} \\ &b_d=-\frac{d^2 i_{sd}}{dt^2}+\left(2\omega-\wp\,\omega_m\right)\frac{di_{sq}}{dt}+\omega\left(\omega-\wp\,\omega_m\right)i_{sd}-\frac{d\wp\,\omega_m}{dt}i_{sq} \end{aligned} \tag{132}$$

$$\begin{aligned} &a_{q1}=\frac{di_{sq}}{dt} \quad ; \quad a_{q2}=i_{sq} \quad ; \quad a_{q3}=\left(\omega-\wp\,\omega_m\right)i_{sd} \quad ; \quad a_{q4}=\omega i_{sd} \\ &a_{q5}=-\left(\frac{dv_{sq}}{dt}+\left(\omega-\wp\,\omega_m\right)v_{sd}-\frac{1}{\omega}\frac{d\wp\,\omega_m}{dt}v_{sq}\right) \quad ; \quad a_{q6}=-v_{sq} \\ &b_q=-\frac{d^2 i_{sq}}{dt^2}-\left(2\omega-\wp\,\omega_m\right)\frac{di_{sd}}{dt}+\omega\left(\omega-\wp\,\omega_m\right)i_{sq}+\frac{d\wp\,\omega_m}{dt}i_{sd} \end{aligned} \tag{133}$$

From the K-parameters

$$[\mathbf{K}]=\begin{bmatrix} K_1 & K_2 & K_{31} & K_{32} & K_4 & K_5 \end{bmatrix}^T \tag{134}$$

the induction machine parameters can be estimated with the equations

$$\begin{aligned} &R_s=\frac{K_1-K_{32}}{K_4} \quad ; \quad L_s=\frac{K_{32}}{K_5} \quad ; \quad L_r=L_s \\ &\sigma=\frac{1}{K_4 L_s}=1-\frac{M^2}{L_r^2} \quad ; \quad T_r=\frac{1}{\sigma K_{32}} \quad ; \quad R_r=\frac{L_r}{T_r} \quad ; \quad M=L_s\sqrt{1-\sigma} \end{aligned} \tag{135}$$

The minimum number of points to determine the induction machine parameters are three points. Then the minimum number of equations are six. In this case, the linear system of equations that must be solved is

$$\begin{pmatrix} a_{d1}^1 & a_{d2}^1 & a_{d3}^1 & a_{d4}^1 & a_{d5}^1 & a_{d6}^1 \\ a_{q1}^1 & a_{q2}^1 & a_{q3}^1 & a_{q4}^1 & a_{q5}^1 & a_{q6}^1 \\ a_{d1}^2 & a_{d2}^2 & a_{d3}^2 & a_{d4}^2 & a_{d5}^2 & a_{d6}^2 \\ a_{q1}^2 & a_{q2}^2 & a_{q3}^2 & a_{q4}^2 & a_{q5}^2 & a_{q6}^2 \\ a_{d1}^3 & a_{d2}^3 & a_{d3}^3 & a_{d4}^3 & a_{d5}^3 & a_{d6}^3 \\ a_{q1}^3 & a_{q2}^3 & a_{q3}^3 & a_{q4}^3 & a_{q5}^3 & a_{q6}^3 \end{pmatrix} \begin{pmatrix} K_1 \\ K_2 \\ K_{31} \\ K_{32} \\ K_4 \\ K_5 \end{pmatrix} = \begin{pmatrix} b_d^1 \\ b_q^1 \\ b_d^2 \\ b_q^2 \\ b_d^3 \\ b_q^3 \end{pmatrix} \tag{136}$$

The K-parameters are determined with

$$[\mathbf{K}] = [\mathbf{A}]^{-1} [\mathbf{B}] \tag{137}$$

In the case of using *n* points, the 2*n* equations produces an over determined linear system of equations

$$\begin{pmatrix} a_{d1}^1 & a_{d2}^1 & a_{d3}^1 & a_{d4}^1 & a_{d5}^1 & a_{d6}^1 \\ a_{q1}^1 & a_{q2}^1 & a_{q3}^1 & a_{q4}^1 & a_{q5}^1 & a_{q6}^1 \\ a_{d1}^2 & a_{d2}^2 & a_{d3}^2 & a_{d4}^2 & a_{d5}^2 & a_{d6}^2 \\ a_{q1}^2 & a_{q2}^2 & a_{q3}^2 & a_{q4}^2 & a_{q5}^2 & a_{q6}^2 \\ \vdots & \vdots & \vdots & \vdots & \vdots & \vdots \\ a_{d1}^n & a_{d2}^n & a_{d3}^n & a_{d4}^n & a_{d5}^n & a_{d6}^n \\ a_{q1}^n & a_{q2}^n & a_{q3}^n & a_{q4}^n & a_{q5}^n & a_{q6}^n \end{pmatrix} \begin{pmatrix} K_1 \\ K_2 \\ K_{31} \\ K_{32} \\ K_4 \\ K_5 \end{pmatrix} = \begin{pmatrix} b_d^1 \\ b_q^1 \\ b_d^2 \\ b_q^2 \\ \vdots \\ b_d^n \\ b_q^n \end{pmatrix} \tag{138}$$

that can be solved with the multidimensional regression method

$$[\mathbf{K}] = \left[[\mathbf{A}]^T [\mathbf{A}] \right]^{-1} [\mathbf{A}]^T [\mathbf{B}] \tag{139}$$

where $[\mathbf{K}] = \begin{bmatrix} K_1 & K_2 & K_{31} & K_{32} & K_4 & K_5 \end{bmatrix}^T$.

2.3 Error determination of the estimation method using T_m, T_s, I_s and I_n

Steady-state magnitudes for error determination are calculated from steady-state circuit of Fig. 2.1. The motor steady-state error magnitudes are maximum torque; T_m, starting torque; T_s, starting current; I_s and no-load current; I_n.

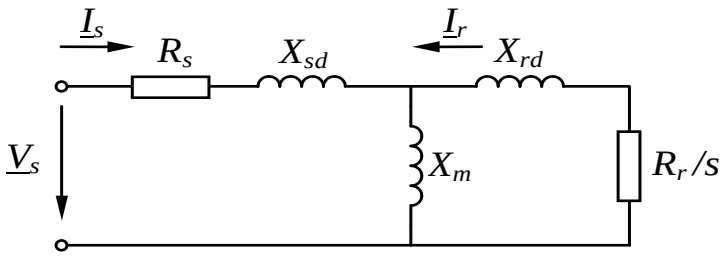

Fig. 2.1.Steady-state equivalent circuit for the single-cage model of the three-phase induction motor

Maximum torque and current in steady-state circuit are derived from below equations

$$T_m = \frac{3\wp}{\omega_s} I_{rm}^2 \frac{R_r}{s_m} \tag{140}$$

where $\wp$ is number of pairs of pole and I_{rm} is the rotor current

$$I_{rm} = abs\left(\frac{Z_m I_m}{\frac{R_r}{s_m} + j\,\omega L_{\mathrm{rd}}} \right) \tag{141}$$

where I_{m} is the stator current in maximum torque slip

$$I_m = \frac{V_{ph}}{\left(R_s + j\,\omega_s L_{\mathrm{sd}} + \underline{Z}_m\right)} \tag{142}$$

and

$$V_{ph} = \frac{U_{line-line}}{\sqrt{3}} \quad ; \quad \underline{Z}_m = \frac{1}{\frac{1}{j\,\omega_s M} + \frac{1}{\frac{R_r}{s_m} + j\,\omega_s L_{\mathrm{rd}}}} \tag{143}$$

considering s_m the slip of maximum torque

$$s_m = \frac{R_r}{\sqrt{R_t^2 + \left(\omega_s L_{\mathrm{rd}} + X_t\right)^2}} \tag{144}$$

and R_t is real part and X_t is imaginary part of

$$\underline{Z}_T = \frac{1}{\frac{1}{j\,\omega_s M} + \frac{1}{R_s + j\,\omega_s L_{\mathrm{sd}}}} \quad ; \quad R_t = real\,(\underline{Z}_T) \quad ; \quad X_t = \mathrm{Im}(\underline{Z}_T) \tag{145}$$

The starting torque and current in slip equal to 1 (starting slip) is calculated from equations

$$T_s = \frac{3\wp}{\omega_s} I_{rs}^2 R_r \tag{146}$$

where the rotor current in the starting; I_{rs} is

$$I_{rs} = abs\left(\frac{\underline{Z}_s\,\underline{I}_s}{R_r + j\,\omega L_{\mathrm{rd}}}\right) \tag{147}$$

and $\underline{I}_s$ is the stator current

$$\underline{I}_s = \frac{V_{ph}}{\left(R_s + j\,\omega_s L_{\mathrm{sd}} + \underline{Z}_s\right)} \quad ; \quad \underline{Z}_s = \frac{1}{\frac{1}{j\,\omega_s M} + \frac{1}{R_r + j\,\omega_s L_{\mathrm{rd}}}} \tag{148}$$

I_n is the stator current for $s = 0$ that coincide with the magnetizing current, $\underline{I}_{mag}$.

$$I_n = \underline{I}_{mag} = \frac{V_{ph}}{R_s + j\,\omega_s\left(L_{\mathrm{sd}} + M\right)} \tag{149}$$

Then the error of the method is quantified with the machine magnitudes

$$\begin{aligned} \varepsilon_{T_m} &= \frac{abs\left(T_{m,est} - T_{m,real}\right)}{T_{m,real}} \quad ; \quad \varepsilon_{T_s} = \frac{abs\left(T_{s,est} - T_{s,real}\right)}{T_{s,real}}; \\ \varepsilon_{I_s} &= \frac{abs\left(I_{s,est} - I_{s,real}\right)}{abs\left(I_{s,real}\right)} \quad ; \quad \varepsilon_{I_{NL}} = \frac{abs\left(I_{NL,est} - I_{NL,real}\right)}{I_{NL,real}} \end{aligned} \tag{150}$$

where the subscript real is for real magnitudes and subscript est is for estimated magnitudes.

The reason that these magnitudes are selected for error quantification is that these errors sensitivities to resistances and reactances of machine are better than other parameters. In reference [27] it is commented that the relative error $\left(\frac{\Delta R_s}{R_s}\right)$ has a low sensitivity, then it is a low quality indicator of the estimation errors.

3 Errors study of the regression method

In this chapter the errors in the single-cage parameters estimation using the least square method are studied. This method usually works with a lot of data, because it is an over determined problem, and the solution is optimal in the sense that optimizes a criteria of error that previously has been determined.

In the problem of the single-cage parameters estimation, there are other sources of errors, different of the experimental measurements. They are the different approximations of the numerical equations that are,

- Speed derivative term elimination
- Rotor flux approximation
- Numerical derivative approximation

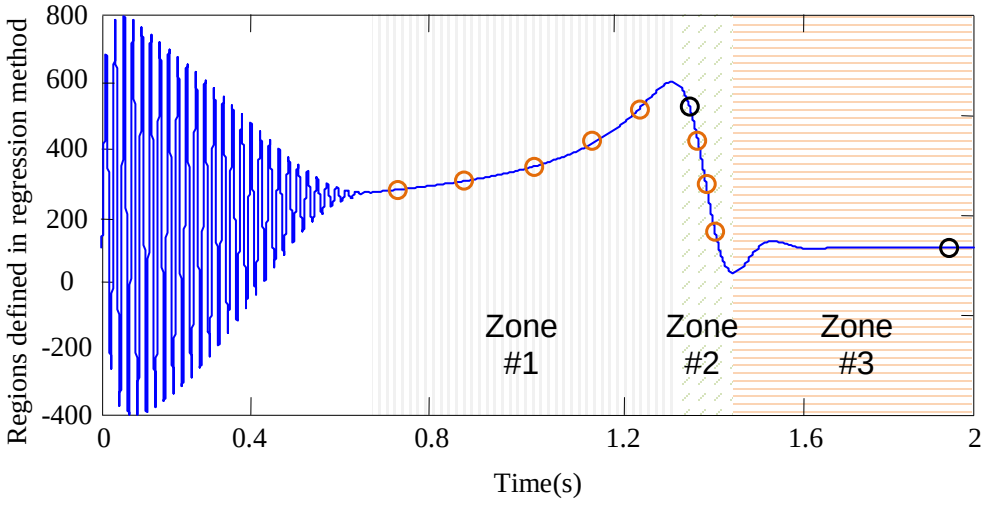

Fig.3.1. Change of the first point in region 1, 2 in Torque-Speed curve

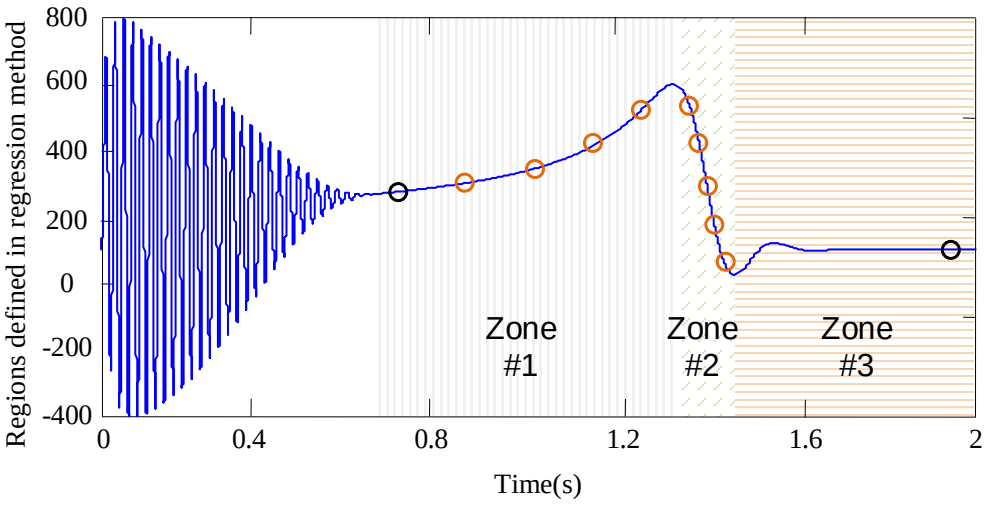

Fig.3.2. Change of the second point in region 1, 2 in Torque-Speed curve

To try to understand the significance of this kind of errors and the influence of the position of the points used in the estimation, the study use only three points, which are the minimum necessary data, that give six magnitudes to obtain the six parameters calculated in the regression method.

As it has been previously commented, the errors are defined as steady-state maximum torque; T_m, starting torque; T_s, starting currents; I_s and no load current; I_n from steady-state circuit equations (equation 150). The no load acceleration test data has been generated by simulation using the Power-System of Matlab program [31]. For this study three zones are considered. The first zone, between the mechanical transient (the end of electrical transient) and the maximum torque called zone ≠1.

The second zone between the maximum torque and the steady-state is zone≠2 and the third zone is the steady-state region called zone ≠3. The study of error estimation with 3-data points regression method is fixing two points in two regions and changing the third speed point position in special zone.

The Figs. 3.1 to 3.3 include the fixed points in black color and the moving point positions in orange color. In some results of estimation with regression method, it is needed to separate the second region of Fig. 3.2 for clarity of error study in another figure shown in Fig. 3.3.

These figures are the small torque speed figures that are shown inside of the error figures in next sections.

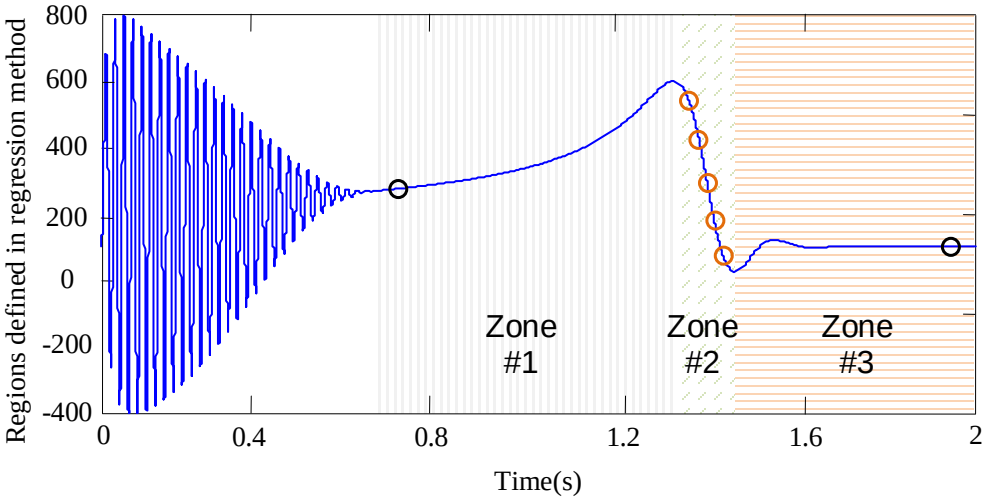

Fig.3.3. Change of the second point in region 2

3.1 Influence of flux approximation

In all the figures of this and next section the starting transient at no load of motor in Table 3.1 has been studied. In Figs. 3.4 to 3.9 the step size; 0.0001[s] is used to calculate the derivatives and an inertia of J= 0.08[kgm^2] is considered.

Table.3.1. Induction machine data

$f_s(Hz)$	$V_{sph}(V)$	$R_s(\Omega)$	$L_s(H)$	$L_m(H)$	$L_r(H)$	$R_r(\Omega)$	*Pole pairs*	$S_n(VA)$	$J(kg.m^2)$
50	220	0.4	0.3246	0.3183	0.3246	0.4	1	4.5k	0.08

Fig. 3.4 shows the maximum torque error in the different speed points for the case of the speed derivative term elimination with circles connected with a black line. Fig. 3.4 has two fixed points at ω_2=296[rad/s];

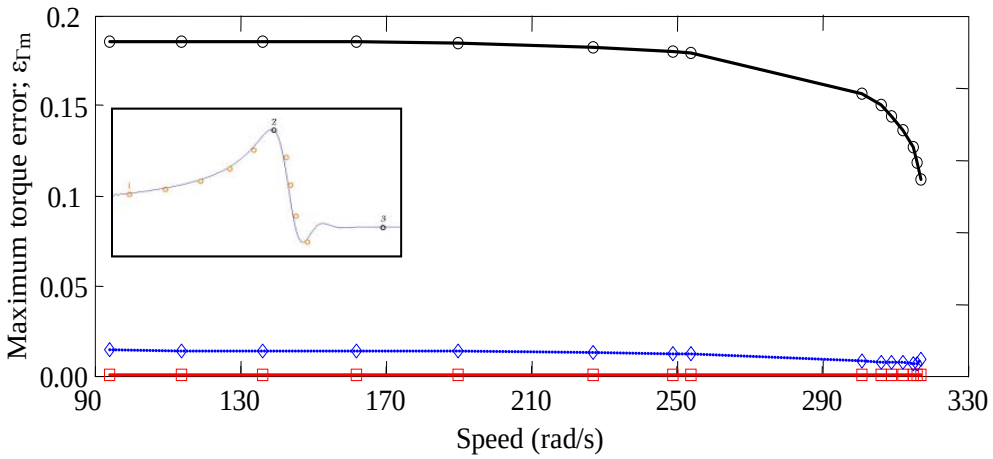

Fig. 3.4. Relative error of *Tm*-Speed for speed (ω_1 changes between 94 and 317; ω_2=296; ω_3=314.4) with regression method and *h*=0.0001 and *J*=0.08, with exact rotor flux; the line with square, with flux approximation; the line diamond, with zero rotor flux; the line with circle.

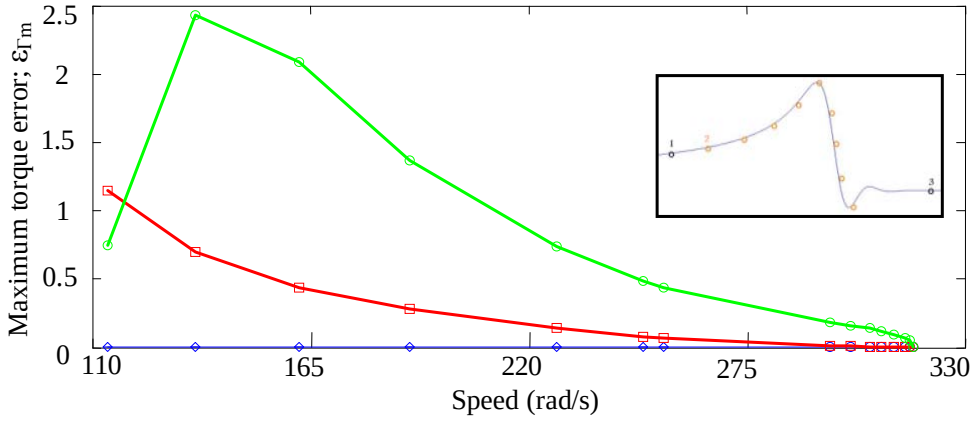

Fig. 3.5. Relative error of *Tm*-Speed for speed (ω_2 changes between 94 and 317; ω_1=94; ω_3=314.4) with regression method and *h*=0.0001 and *J*=0.08, with exact rotor flux; the line with diamond, with flux approximation; the line with square, with zero rotor flux; the line with circle.

ω_3=314.4[rad/s], that corresponds to a point near the maximum torque point and another in the steady-state speed, respectively. In this figure the point that moves has speeds between 94[rad/s] to 317[rad/s] (before steady-state the speed is more than synchronous speed). The influence of the speed derivative term is not negligible in contrary of the usual hypothesis in the literature that eliminates the term of the speed derivative. In the Fig. 3.4 the error in the maximum torque using the rotor flux approximation (equations 110) is represented with diamonds connected to a blue line. This error is very low and confirms that the rotor flux approximation is a significant improvement in comparison with speed derivative term elimination (zero flux approximation).

As this study of the errors is based on data obtained from simulation, the exact value of the rotor flux is accessible. For a validation of the process of calculation of the errors, the maximum torque error has been

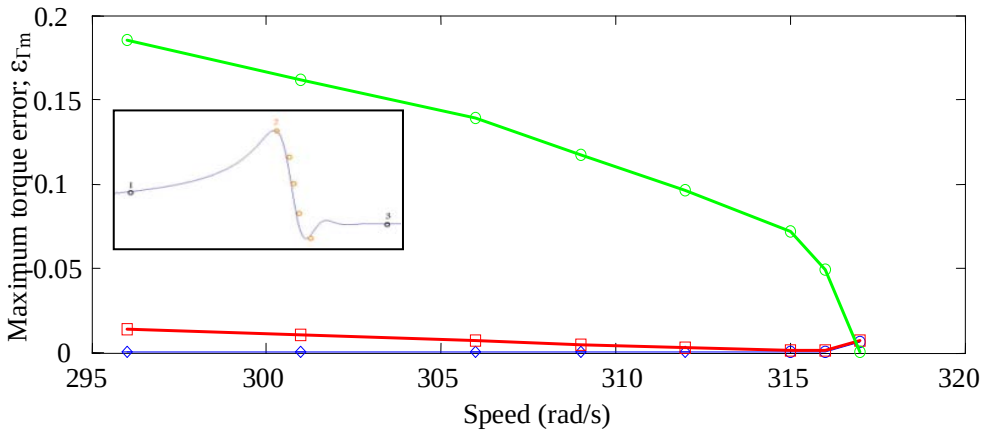

Fig. 3.6. Relative error of *Tm*-Speed for speed (ω_2 changes between 296 and 317; ω_1=94; ω_3=314.4) with regression method and *h*=0.0001 and *J*=0.08, with exact rotor flux; blue line with diamonds, with flux approximation; red line with squares, with zero rotor flux; green line with circles

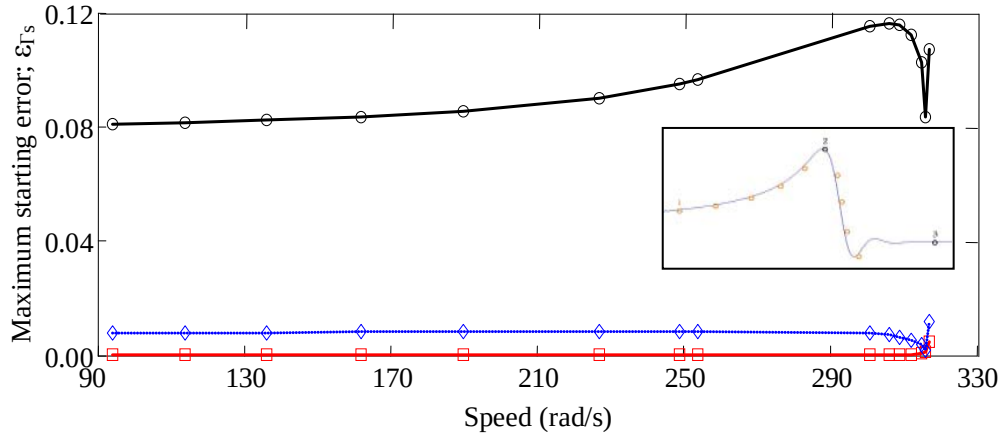

Fig. 3.7. Relative error of *Ts*-Speed for speed (ω_1 changes between 94 and 317; ω_2=296; ω_3=314.4) with regression method and *h*=0.0001 and *J*=0.08, with zero rotor flux; black line with circles, with flux approximation; blue line with diamonds, with exact rotor flux; red line with squares.

calculated using the exact value of the rotor flux (equations 86). Fig. 3.4 shows that error with squares connected to a red line, is always near to zero. This fact confirms that the main source of this error in the method is the rotor flux that can not be measured. Fig. 3.5 shows the maximum torque error study similar to Fig. 3.4, but in this case the two fixed points are ω_1=94[rad/s] and ω_3=314.4[rad/s] and the position of the second point changes between speeds 114[rad/s] to 317[rad/s].

The maximum torque error using the speed derivative elimination is represented with circles connected with a green line, and it can be observed that the errors are very high. The case with the rotor flux approximation is represented with square connected with a red line, and when the speed point is moved far from the maximum torque speed in zone 1, the maximum torque error also is very high. To validate the calculation process, the error has been calculated using the exact rotor flux, and this has been represented by diamonds connected with a blue line. In this case the error is not significant.

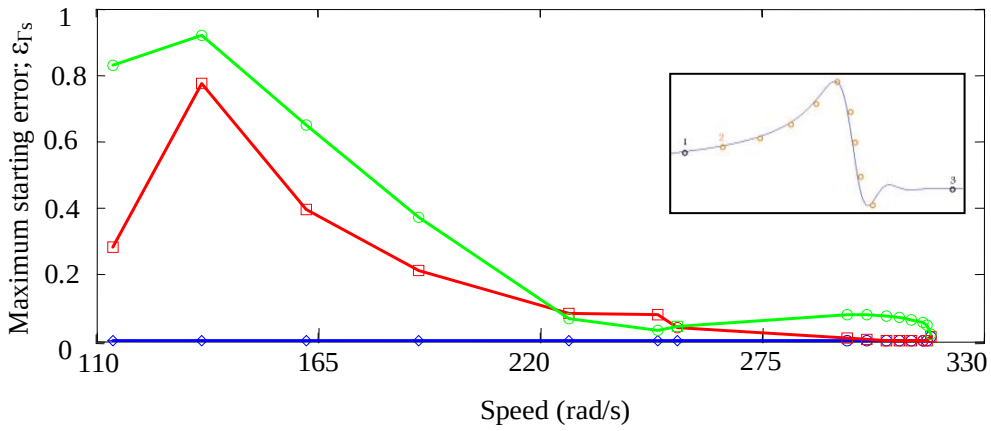

Fig. 3.8. Relative error of *Ts*-Speed for speed (ω_2 changes between 94 and 317; ω_1=94; ω_3=314.4) with regression method and *h*=0.0001 and *J*=0.08, with exact rotor flux; blue line with diamonds, with flux approximation; red line with squares, with zero rotor flux; green line with circles.

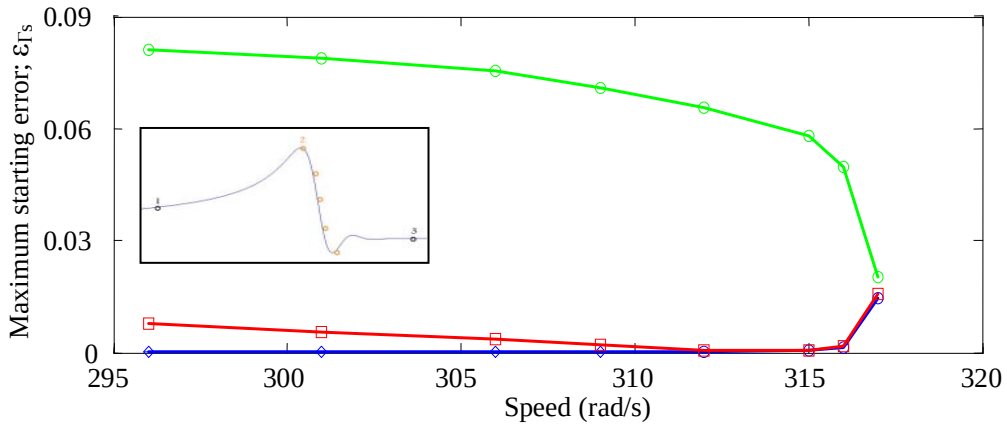

Fig. 3.9. Relative error of *Ts*-Speed for speed (ω_2 changes between 296 and 317; ω_1=94; ω_3=314.4) with regression method and *h*=0.0001 and *J*=0.08, with exact rotor flux; blue line with diamonds, with flux approximation; red line with squares, with zero rotor flux; green line with circles.

The main conclusion of this comparison is that the points used to calculate the induction motor parameters must include always a point at steady-state speed and another point near the maximum torque speed. This idea is confirmed in Fig. 3.5, because in the red line with squares when the moving point goes near the maximum torque speed, the errors are very low. Fig. 3.6 is a zoom of Fig. 3.5 to show that the rotor flux approximation has a low error when a point is in this region.

Fig. 3.7 to 3.9 show the relative error of the starting torque; T_s for exact rotor flux, rotor flux approximation and zero rotor flux (speed derivative term elimination). In Figs. 3.7 to 3.9, inertia=0.08[kgm^2] and step size for the derivative calculation is 0.0001[s]. In Fig. 3.7 just the first point changes and point 2 is fix at 296[rad/s] in zone 2 and point 3 is fix at 314.4[rad/s] in zone 3. In Fig.3.8 just the second point changes in region 1 and 2 between 94[rad/s] (sometimes 114 to avoid having 2 points on each other) to 317[rad/s] and point 2 is fix at 94[rad/s] and point 3 is fix at 314.4[rad/s]. In Fig. 3.7 red solid line with squares is starting torque relative error with exact rotor flux that is very low. Blue line with diamonds is T_s relative error with rotor flux approximation that is low. Black solid line with circles is this error with zero rotor flux that is high and it is the usual method in the literature [15]. In Fig. 3.8 green line with circles is T_s error with zero rotor flux. The red line with squares is error of T_s with rotor flux approximation and blue line with diamonds is the T_s error without approximation (with exact rotor flux).

Fig. 3.9 is a zoom of Fig. 3.8 in zone 2 that shows that the error in the starting torque with rotor flux approximation is less than 0.03.

The main conclusion of all figures in this chapter is that the errors are low in 2 cases with rotor flux approximation. One case is for two points in zone 2 that one of them is maximum torque point and the third point in zone 3. Another case is with three points in three different regions that one point is in the maximum torque point.

3.2 Influence of step size on the maximum and starting torque relative errors

In this study rotor flux approximation has been used. The inertia of the motor is 0.08[kgm^2]. The study has been executed with three step sizes for derivative calculation; h=0.0001[s], h=0.001[s] and h=0.01[s]. In Fig. 3.10- 3.15 relative error of maximum torque T_m and starting torque T_s are shown. In Figs. 3.10 and 3.13 that are T_m and T_s errors respectively, just the first point changes between regions 1 and 2 from 94[rad/s] to 317[rad/s]. In Figs. 3.11 and 3.14 that include T_m and T_s errors respectively, just the second point changes between region 1 and 2.

In Fig. 3.10 and 3.13 red solid lines with squares are T_m and T_s relative errors respectively for step size 0.01, blue lines with diamonds are these errors for step size 0.001 and black solid lines with circles are these errors for step size 0.0001. The errors in these figures are always low.

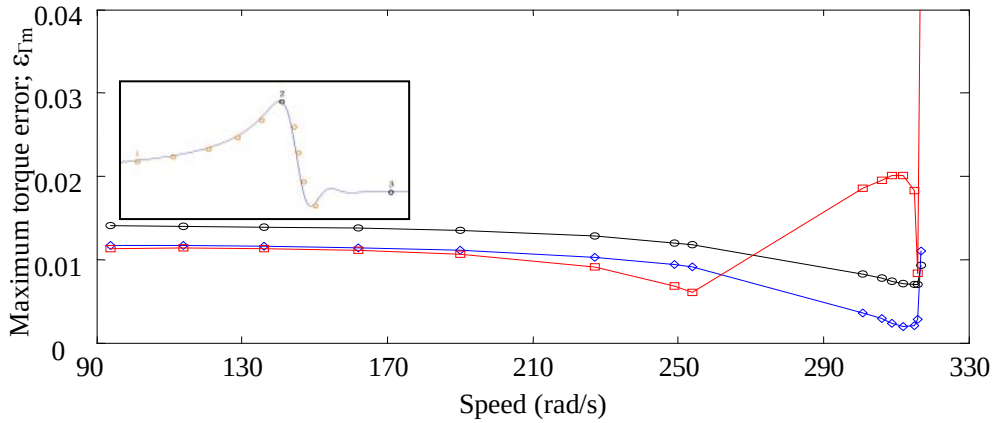

Fig. 3.10. Relative error of *Tm*-Speed (ω_1 changes between 94 and 317; ω_2=296; ω_3=314.4) with regression method and flux approximation and *J*=0.08, with *h*=0.01; red line with squares, with *h*=0.001; blue line with diamonds, with *h*=0.0001; black line with circles.

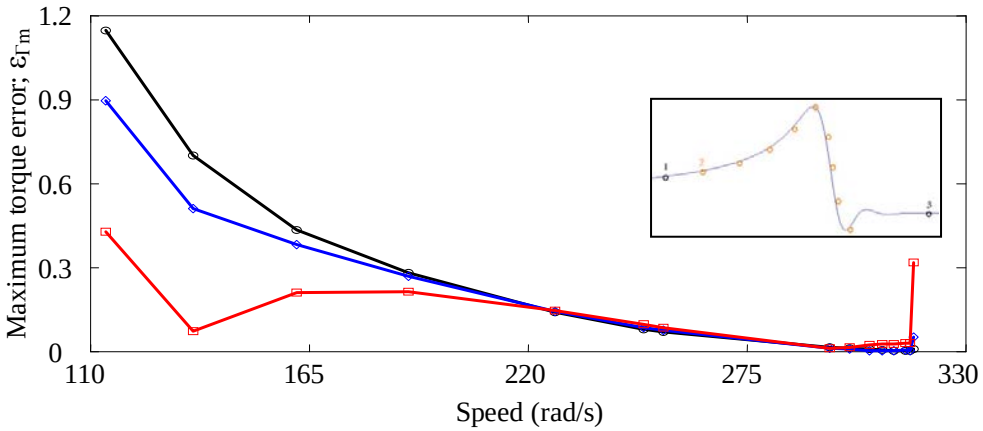

Fig. 3.11. Relative error of *Tm*-Speed (ω_2 changes between 94 and 317; ω_1=94; ω_3=314.4) with regression method and flux approximation and *J*=0.08, with *h*=0.01; red line with square, with *h*=0.001; blue line with diamond, with *h*=0.0001; black line with circles.

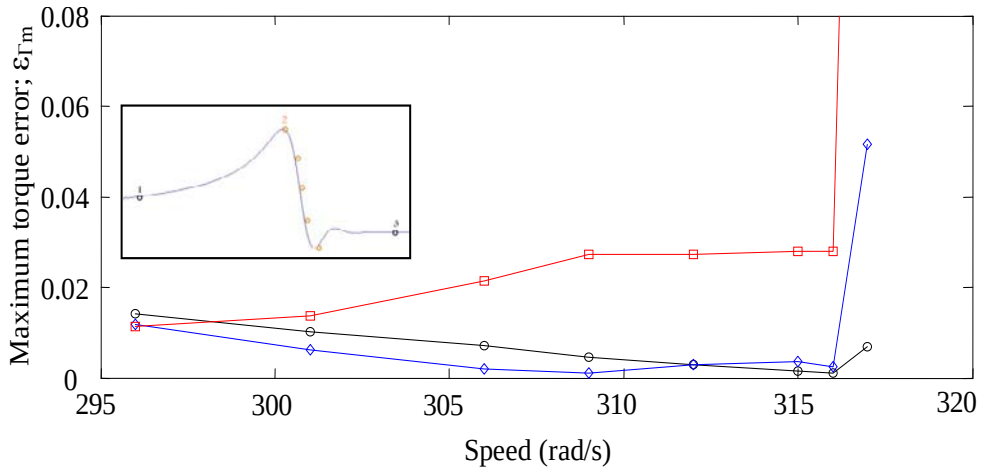

Fig. 3.12. Relative error of Tm-Speed (ω_2 changes between 296 and 317; ω_1=94; ω_3=314.4) with regression method and flux approximation and J=0.08, with h=0.01; red line with squares, with h=0.001; blue line with diamonds, with h=0.0001; black line with circles.

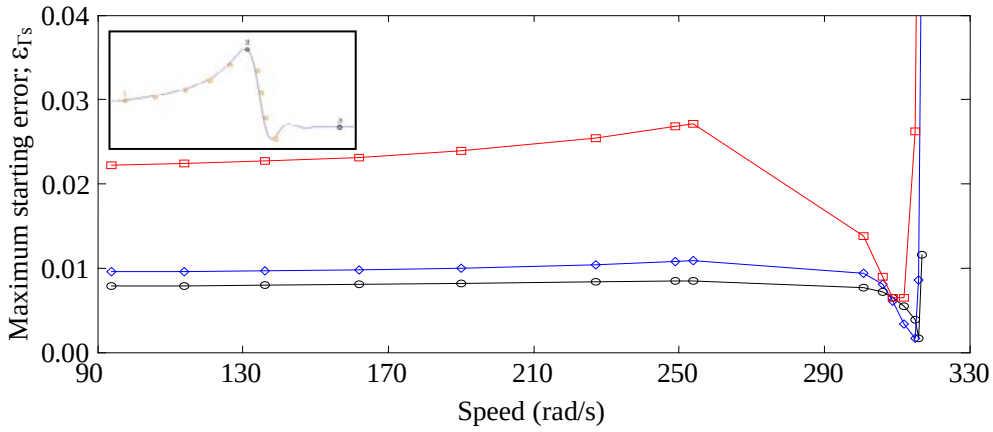

Fig. 3.13. Relative error of *Ts*-Speed (ω_1 changes between 94 and 317; ω_2=296; ω_3=314.4) with regression method and flux approximation and *J*=0.08, with *h*=0.01; red line with squares, with *h*=0.001; blue line with diamonds, with *h*=0.0001; black line with circles.

In Fig. 3.11 and 3.14 red solid lines with squares are T_m and T_s relative errors respectively for step size 0.01, blue lines with diamonds are these errors for step size 0.001 and black solid lines with circles are these errors for step size 0.0001. Figs. 3.12 and 3.15 are zoom of Figs. 3.11 and 3.14 respectively in zone 2 of moving point. The result of these figures is that good estimation is in zone 2.

This study shows the step size change is not important while two points are the maximum torque point and the steady-state point in the study.

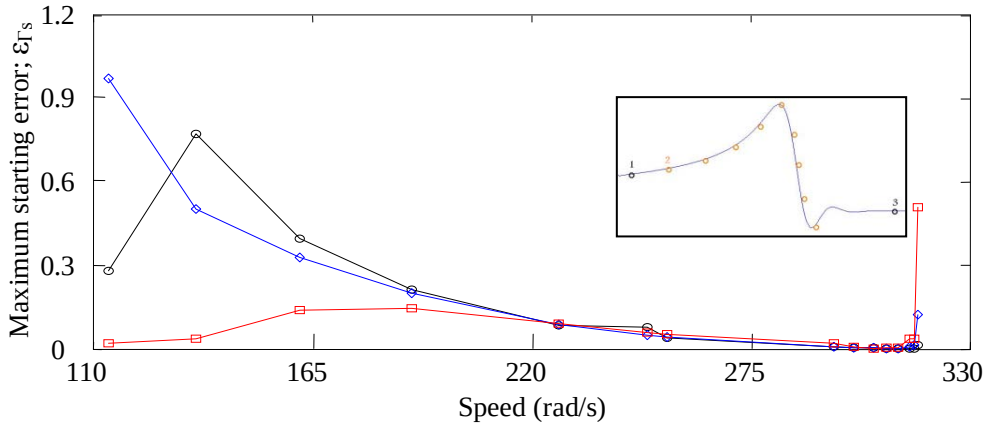

Fig. 3.14. Relative error of *Ts*-Speed (ω_2 changes between 94 and 317; ω_1=94; ω_3=314.4) with regression method and flux approximation and *J*=0.08, with *h*=0.01; red line with squares, with *h*=0.001; blue line with diamonds, with *h*=0.0001; black line with circles.

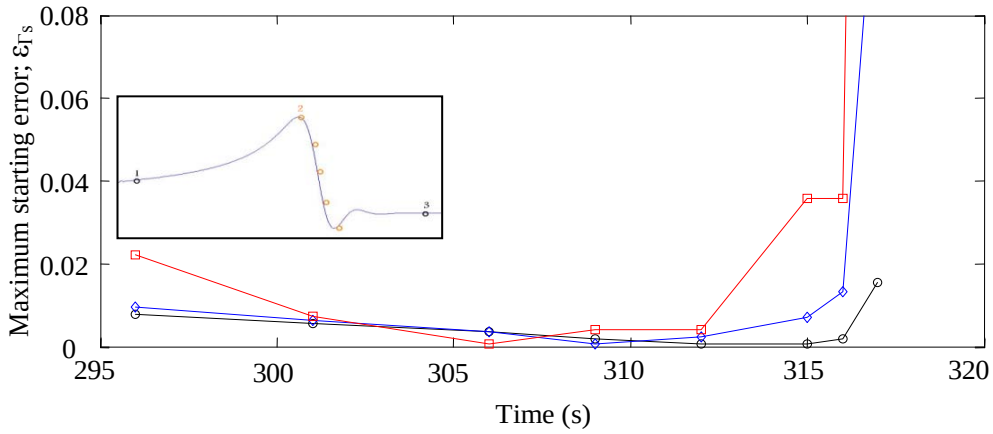

Fig. 3.15. Relative error of *Ts*-Speed (ω_2 changes between 296 and 317; ω_1=94; ω_3=314.4) with regression method and flux approximation and *J*=0.08, with *h*=0.01; red line with squares, with *h*=0.001; blue line with diamonds, with *h*=0.0001; black line with circles.

.

3.3 Study of inertia influence in the error

In this study the rotor flux approximation and step size for derivative calculation of 0.0001[s] are considered. The study is executed for different inertias; 0.08[kgm^2], 0.2[kgm^2] and 0.8[kgm^2] and the relative error of maximum torque as a typical error is shown.

In Fig. 3.16 to 3.18, square red lines are T_m relative error for inertia 0.2[kgm^2], diamond blue lines are T_m errors for inertia 0.8[kgm^2] and circle black solid line is this error for inertia 0.08[kgm^2].

In Fig. 3.16 the first point changes in zones 1 and 2 between 94[rad/s] to 317[rad/s]. In this figure two other points are fix at ω_2=296[rad/s] and ω_3=314.4[rad/s]. In this figure the maximum torque errors are always low.

In Figs. 3.17 the second point changes between zones 1 and 2 between 94[rad/s] to 317[rad/s]. In this

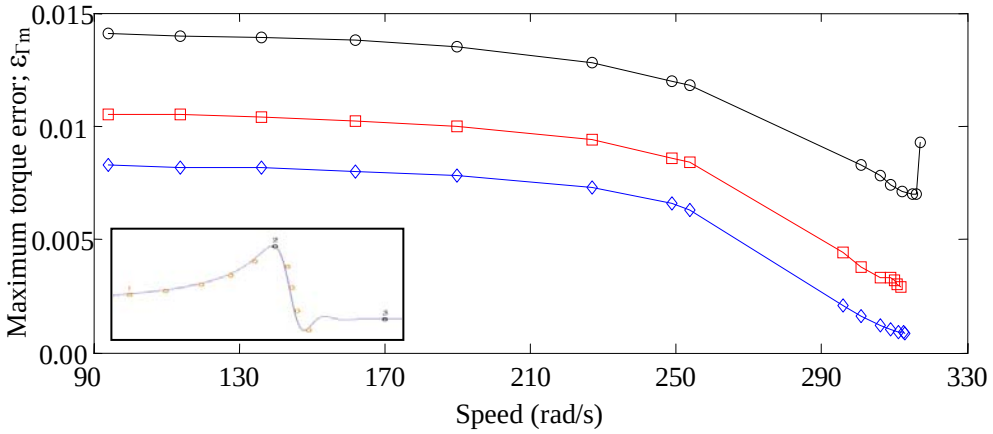

Fig. 3.16. Relative error of *Tm*-Speed (ω_1 changes between 94 and 317; ω_2=296; ω_3=314.4) with regression method with *h*=0.0001 and flux approximation and *J*=0.08; black line with circles , *J*=0.2; red line with squares, *J*=0.8; blue line with diamonds.

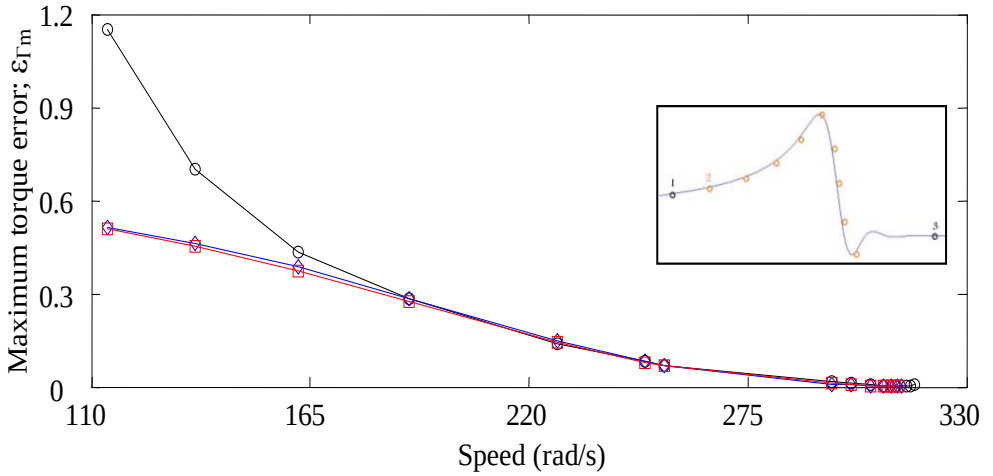

Fig. 3.17.Relative error of *Tm*-Speed (ω_2 changes between 94 and 317; ω_1=94; ω_3=314.4) with regression method with *h*=0.0001 and flux approximation and *J*=0.08 black line with circles, *J*=0.2; red line with squares, *J*=0.8; blue line with diamonds.

figure two other points are fix at ω_1=94[rad/s] and ω_3=314.4[rad/s]. Fig. 3.18 is a zoom of Fig. 3.17.The result is that the error in the second region of point 2 is low.

Finally these figures show the inertia influence has a low significance on the error estimation with maximum torque and steady-state points.

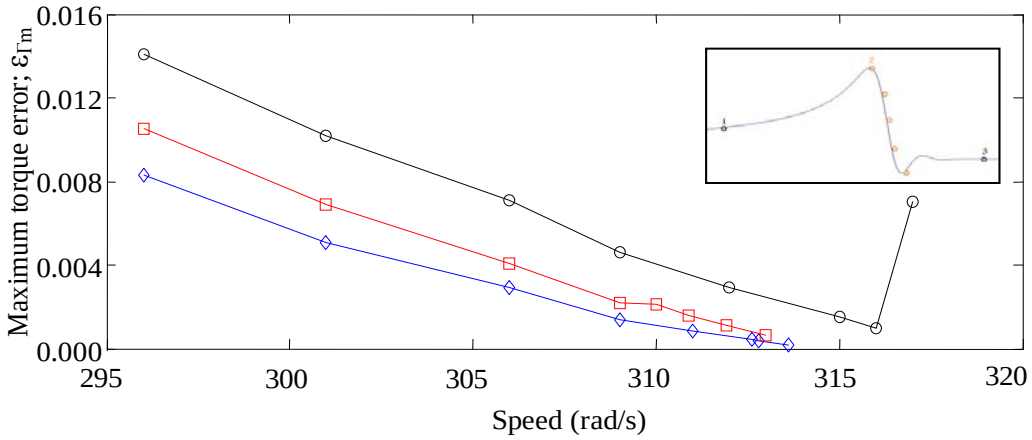

Fig. 3.18. Relative error of *Tm*-Speed (ω_2 changes between 296 and 318; ω_1=94; ω_3=314.4) with regression method with *h*=0.0001 and flux approximation and *J*=0.08; black line with circles, *J*=0.2; red line with squares, *J*=0.8; blue line with diamonds

3.4 Relation between estimated parameters and error

In this study the step size is 0.0001[s], the inertia is 0.08[kgm^2] and the rotor flux approximation is considered. In Figs. 3.19 and 3.20 black line with circles is estimated stator resistance; R_s, red line with squares is estimated rotor resistance; R_r, green line with triangles is estimated mutual inductance; M and the blue line with diamonds is the estimated stator inductance; L_s that is predefined to be equal to the rotor inductance L_r [25].

Fig. 3.19. shows estimated resistances and inductances while just the first point changes in zone 1 and 2 between 94[rad/s] to 317[rad/s] and two other points are fix at 296[rad/s] and 314.4[rad/s]. The figure shows in all of speeds of point 1 the parameters are well estimated except for R_s. This parameter has good estimation when 2 points are in the second region and the third point is in the third region. Fig. 3.20. shows estimated resistances and inductances while just the second point changes between zones 1 and 2 between 94[rad/s] to 317[rad/s] and two other points are fix at 94[rad/s] and 314.4[rad/s] according to the

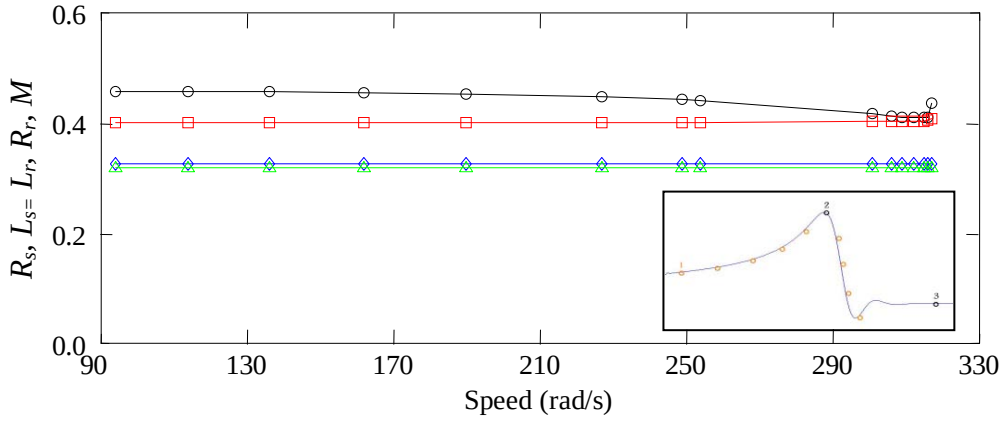

Fig. 3.19. Estimated machine 1 parameters for speed (ω_1 changes between 94 and 317; ω_2=296; ω_3=314.4) with regression method with h=0.0001 and rotor flux approximation R_s; black line with circles, R_r; red line with squares, L_s=L_r; blue line with diamonds, M; green line with triangles.

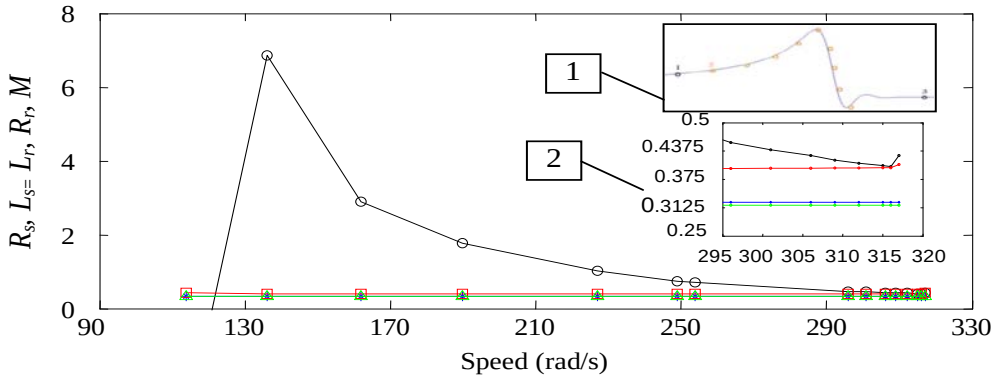

Fig. 3.20. Estimated machine parameters speed (ω_2 changes between 94 and 317; ω_1=94; ω_3=314.4) with regression method with h=0.0001 and rotor flux approximation R_s; black line with circles, L_s=L_r; red line with squares, R_r; blue line with stars, M; green line with triangles.

small Fig. 1 inside of Fig. 3.20. Fig. 3.20 shows in all of speeds of point 1 the parameters are well estimated except for R_s. Small figure 2 in Fig. 3.20 is zoom of Fig. 3.20 that shows the estimation of all parameters and R_s in the second zone of moving point, is good.

The main conclusion is that the good estimation is possible with the maximum torque point and the steady-state point.

3.5 Influence of increasing number of points in each zone

In this study the step size and inertia are 0.0001[s] and 0.08[kgm^2] respectively. The rotor flux approximation is considered. The minimum numbers of points are 3 points in 3 different zones. Fig. 3.21 shows the relative error of maximum torque; T_m in the regression-method.

In Fig. 3.21, 3 points in 3 different zones are considered then the number of points are added in zone 1 between 94[rad/s] to 296[rad/s] (the black line with circles), then in zone 2 between 296[rad/s] to 314.4[rad/s] (the blue line with diamonds) and then in both zones 1 and 2 (the red line with squares) to see the multiple points effects in estimation.

Finally Fig. 3.21 shows that the influence of the numbers of points is low because the error is always lower than 0.015 while the number of the points are more than three.

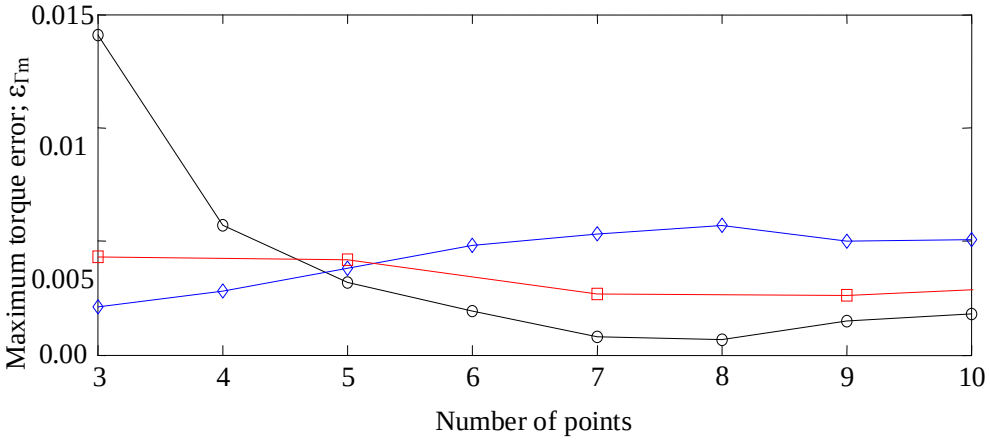

Fig. 3.21. Influence of multiple points in zone 1, multiple points in zone 2 and multiple points in both zones (1 and 2) with regression method with h=0.0001, J=0.08 and rotor flux approximation with more than 1 point in region 1, one fixed point in region 2 and one fixed point in region 3; black line with circles, with more than 1 point in region 2, one fixed point in region 1 and one fixed point in region 3; blue line with diamonds, with more than 1 point in region 1 and 2 and one fixed point in region 3; red line with squares

3.6 Comparison of estimation error for different machines

In this study three machines of Table 3.2 are tested. The step size for derivative calculation is 0.0001[s] and rotor flux approximation is used in the parameter estimation.

Table. 3.2. Parameters of three induction machine with f_s=50 [Hz]

$S_n(VA)$	$V_{s\,ph}(V)$	$R_s(\Omega)$	$L_s(H)$	$L_m(H)$	$L_r(H)$	$R_r(\Omega)$	$\wp$	$J(kg.m^2)$
4.5k	220	0.4	0.3246	0.3183	0.3246	0.4	1	0.08
7.460k	460/√3	0.6837	0.15275	0.1486	0.15275	0.451	1	0.1
160k	400/√3	0.01379	0.007842	0.00769	0.007842	0.007728	1	2.9

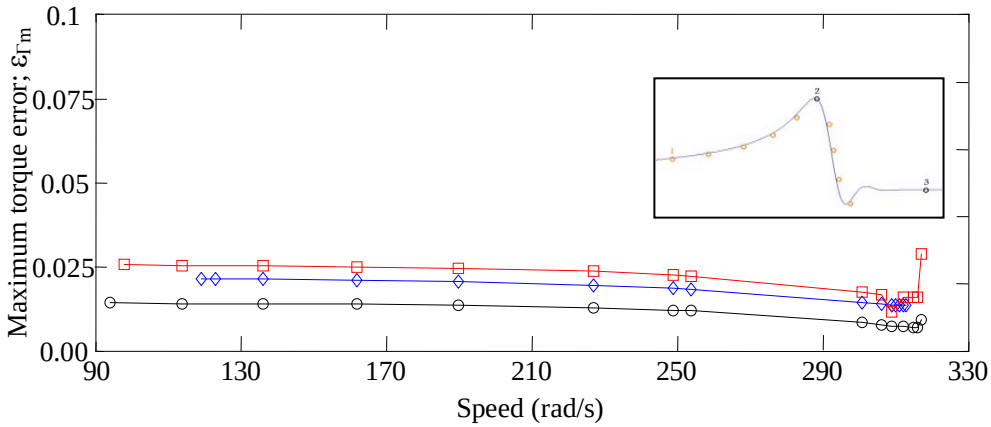

Fig. 3.22. Relative error of *Tm*-Speed (ω_1 changes between 94 and 317 (zone 1, 2); ω_2=296; ω_3=314.4) with regression method with h=0.0001 and rotor flux approximation for machine 1 (4.5kVA); black line with circles, for machine 2 (7.46kVA); blue line with diamonds, for machine 3 (160kVA); red line with squares

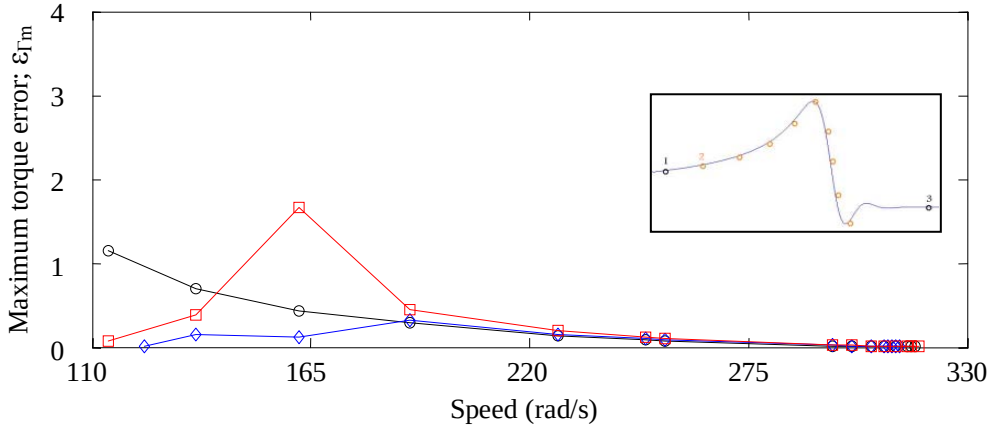

Fig. 3.23. Relative error of *Tm*-Speed (ω_2 changes between 94 and 317 (zone 1, 2); ω_1=94; ω_3=314.4) with regression method with *h*=0.0001 and rotor flux approximation for machine 1 (4.5kVA); black line with circles, for machine 2 (7.46kVA); blue line with diamonds, for machine 3 (160kVA); red line with squares

In Figs. 3.22 to 3.24 step size is 0.0001[s]. The inertia of machine 1 is 0.08[kgm^2], machine 2 is 0.2[kgm^2] and machine 3 is 2.9[kgm^2] in these figures and the relative error of T_m for 3 sample machines is studied.

In Fig. 3.22 to 3.24 red lines with squares are T_m relative errors for the third machine that is high power (160kVA) machine, the blue lines with diamonds are T_m relative error for the second machine (7.46kVA) and the black lines with circles are T_m relative error for machine 1 (4.5kVA).

In Fig. 3.22 just the first point changes between zone 1 and 2 from 94[rad/s] to 314.4[rad/s]. The two other points are fix at 296[rad/s] and 314.4[rad/s]. In this figure the errors are always low. In Fig. 3.23 just the second point changes between zone 1 and 2 from 94[rad/s] to 314.4[rad/s] and the two other points are fix at 94[rad/s] and 314.4[rad/s]. Fig. 3.24 is a zoom of Fig. 3.23. The results of Figs. 3.23 and 3.24 show good estimation is in the region 2. The error is not sensitive to the power of machine. The main conclusion is that the method works for high power and low power machines while one point is maximum torque point and another point is the steady-state point.

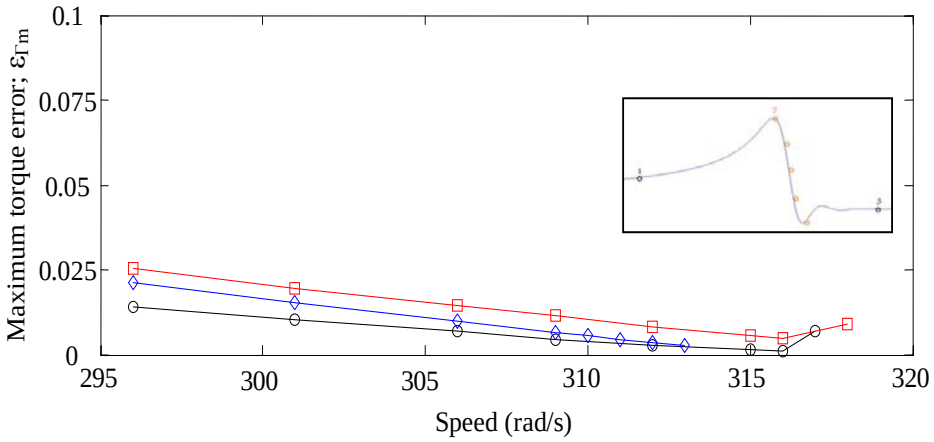

Fig. 3.24. Relative error of *Tm*-Speed (ω_2 changes between 296 and 317 (zone 2); ω_1=94; ω_3=314.4) with regression method with *h*=0.0001 and rotor flux approximation for machine 1 (4.5kVA); black line with circles, for machine 2 (7.46kVA); blue line with diamonds, for machine 3 (160kVA); red line with squares

3.7 Study of regression method omitting steady-state point

In this section the effect of the point in the steady-state zone on the estimation parameters errors is studied. In this study the step size for derivative calculation is 0.0001[s], inertia is 0.08[kgm^2] and rotor flux approximation has been used. In Fig. 3.25, relative error of T_m is shown in red line with squares while ω_1=94[rad/s], ω_2=296[rad/s] and the speed of the third point; ω_3, changes between ω_1 and steady-state speed according to the small Fig. 2 inside of Fig. 3.25. In this figure there is not any point in the steady-state zone. The blue line with stars is this T_m error while point 1 moves between 94[rad/s] and 317[rad/s]and two other fix points are maximum torque point at 296[rad/s] and the steady state point at 314.4[rad/s] shown in small Fig. 1 inside of Fig. 3.25. The conclusion is that error is not too much sensitive to the third point in the third zone.

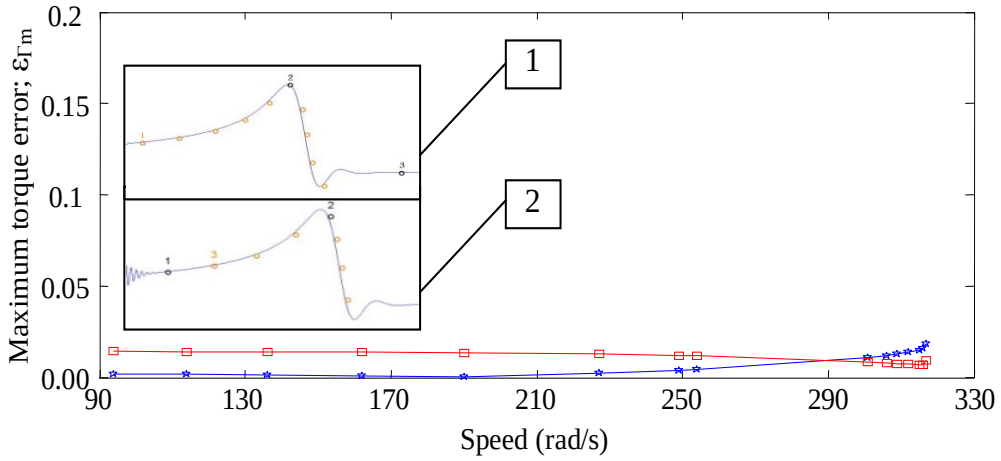

Fig. 3.25. Relative error of *Tm* while ω_2=296, ω_3=314.4 and ω_1 changes between 94 and 317 with *h*=0.0001 and *J*=0.08 with rotor flux approximation; blue line with stars, Relative error of *Tm* while ω_1=94, ω_2=296 and ω_3 is changed between zone 1 and 2 and there is not steady state point with the rotor flux approximation; red line with squares.

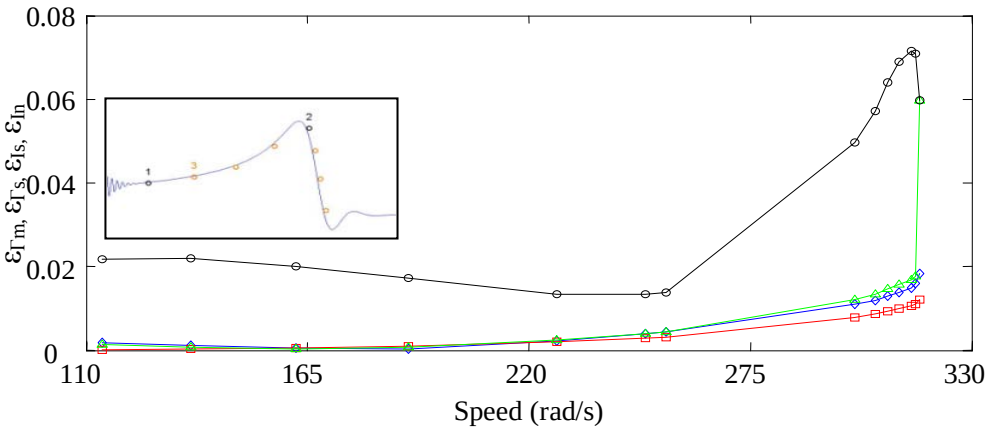

Fig. 3.26. Relative error of *Tm*, *Ts*, *Is*, *In* with flux approximation while ω_1=94, ω_2=296 and ω_3 changes between ω_1 and 317 with *h*=0.0001 and *J*=0.08 with rotor flux approximation for error of Tm; blue line with diamonds, error of *Ts*; red line with squares, error of *Is*; green line with triangles, error of *In*; black line with circles.

In Fig. 3.26 black line with circles is relative error of magnetizing current; I_n which is low. The green line with triangles is starting current relative error; I_s, blue line with diamonds is maximum torque relative error; T_m and red line with squares is starting torque relative error; T_s, while the third point moves between zones 1 and 2 between 94[rad/s] to 317[rad/s] and point 1 and 2 are fixed at 94[rad/s] and 296[rad/s] respectively. The main conclusion is that error is not too much sensitive to the third point in the steady-state region but the errors are greater than errors with the steady state point.

3.8 Study of starting and magnetizing currents errors

The maximum and starting torques errors were studied in previous sections. In this study starting and magnetizing currents errors are studied. The step size for derivative calculation and inertia are 0.0001[s] and 0.08[kgm^2] respectively and rotor flux approximation has been used.

Fig. 3.27. shows these calculated measurements of error currents, while the first point in region 1 changes in zone 1 and 2 between 94[rad/s] to 317[rad/s] and two other points are fixed at 296[rad/s] and 314.4[rad/s].Fig. 3.27. shows that the relative error of starting current (green line with squares) is always low. The error of magnetizing current is in black line with circles near to zero.

Fig. 3.28. demonstrates the relative error of currents while the second point changes between 114[rad/s] to 317[rad/s] and two fix points are at 94[rad/s] and 314.4[rad/s]. Fig. 3.29 is zoom of Fig. 3.28. Figs. 3.28 and 3.29 show the starting current error in green line with squares and the magnetizing current error in black line with circles.

These figures show that the errors are lower while the second point is moving in the second region between 296[rad/s] and 317[rad/s].

The main conclusion is that the errors are low while one point is maximum torque point and other point is the steady-state point.

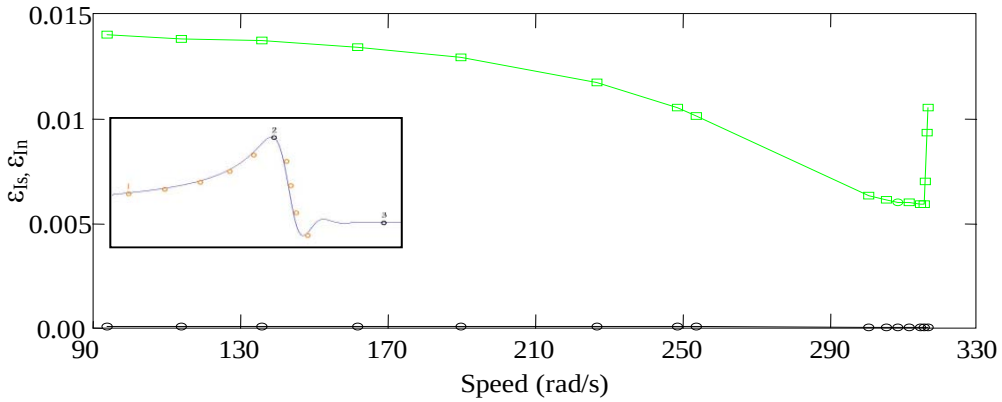

Fig. 3.27. Relative error of I_s-speed; green with squares, I_n-speed; black with circles for speeds ω_1 changes between 94 and 317; ω_2=296; ω_3=314.4 with h=0.0001, J=0.08 , rotor flux approximation and regression method.

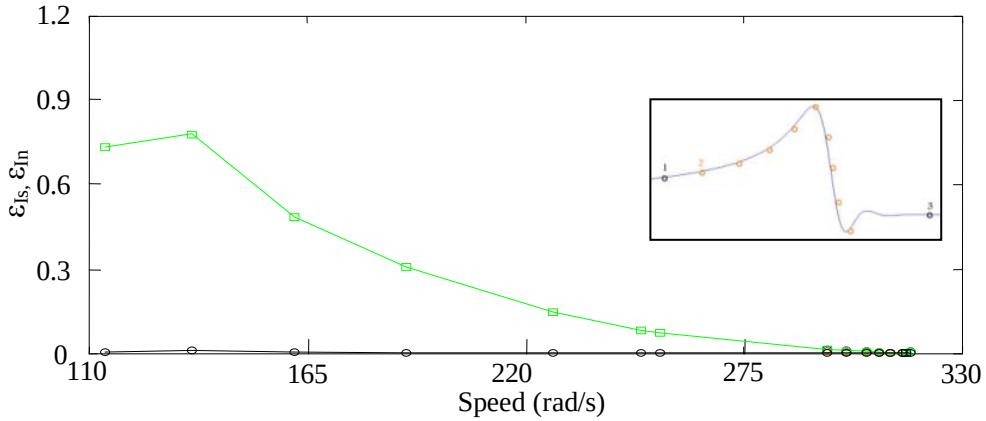

Fig. 3.28. Relative error of I_s-speed; green with squares, I_n-speed; black with circles for speeds ω_2 changes between 94 and 317 (region2); ω_1=94; ω_3=314.4 with h=0.0001, J=0.08 , rotor flux approximation and regression method.

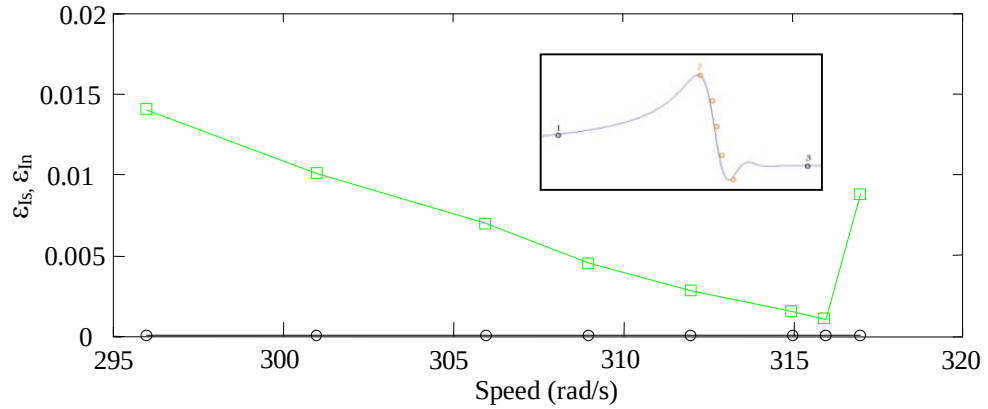

Fig. 3.29. Relative error of I_s-speed; green with squares, I_n-speed; black with circles for speeds ω_2 changes between 296 and 317; ω_1=94; ω_3=314.4) with h=0.0001, J=0.08 , rotor flux approximation and regression method.

4 Two-points method

4.1 Two-points method and single-cage induction machine equations

Another estimation method is based on the numerical relation of 4 nonlinear equations to find the values of 4 parameters of machine (Park or steady-state parameters); R_s, R_r, $L_s = L_r$, M. Then, two points satisfy 4 nonlinear *d*, *q* equations. This method is called two-points method. The resistances and inductances of machine are calculated from nonlinear current-flux *d*, *q* equations as function of six K_i coefficients

$$\begin{aligned}&\frac{d^2 i_{sd}}{dt^2} - \left(2\omega - \wp\,\omega_m\right)\frac{di_{sq}}{dt} - \omega\left(\omega - \wp\,\omega_m\right) i_{sd} - \frac{d\,\wp\,\omega_m}{dt}\beta\psi_{rq} = \\ &-K_1\frac{di_{sd}}{dt} - K_2 i_{sd} + K_{31}\left(\omega - \wp\,\omega_m\right) i_{sq} + K_{32}\omega i_{sq} + K_4\left(\frac{dv_{sd}}{dt} - \left(\omega - \wp\,\omega_m\right) v_{sq}\right) + K_5 v_{sd}\end{aligned} \tag{151}$$

$$\begin{aligned}&\frac{d^2 i_{sq}}{dt^2} + \left(2\omega - \wp\,\omega_m\right)\frac{di_{sd}}{dt} - \omega\left(\omega - \wp\,\omega_m\right) i_{sq} + \frac{d\,\wp\,\omega_m}{dt}\beta\psi_{rd} = \\ &-K_1\frac{di_{sq}}{dt} - K_2 i_{sq} - K_{31}\left(\omega - \wp\,\omega_m\right) i_{sd} - K_{32}\omega i_{sd} + K_4\left(\frac{dv_{sq}}{dt} + \left(\omega - \wp\,\omega_m\right) v_{sd}\right) + K_5 v_{sq}\end{aligned} \tag{152}$$

where six *K* parameters are determined from the coefficients of induction machine

$$\begin{aligned}&\sigma = 1 - \frac{M^2}{L_s L_r} \quad ; \quad T_r = \frac{L_r}{R_r} \quad ; \quad T_s = \frac{L_s}{R_s}; \quad K_1 = \frac{R_s}{\sigma L_s} + \frac{1}{T_r} \\ &K_2 = \frac{R_s}{\sigma L_s T_r} \quad ; \quad K_{31} = \frac{1}{\sigma T_s} \quad ; \quad K_{32} = \frac{1}{\sigma T_r} \quad ; \quad K_4 = \frac{1}{\sigma L_s} \quad ; \quad K_5 = \frac{1}{\sigma L_s T_r}\end{aligned} \tag{153}$$

and $L_s = L_r$ results

$$\begin{aligned}&K_1 = \frac{R_s + R_r}{\left[\left(1 - \frac{M^2}{L_s^2}\right) L_s\right]} \quad ; \quad K_2 = \frac{R_s}{\left[\left(1 - \frac{M^2}{L_s^2}\right)\frac{L_s^2}{R_r}\right]} \quad ; \quad K_{31} = \frac{1}{\left[\left(1 - \frac{M^2}{L_s^2}\right)\frac{L_s}{R_s}\right]} \\ &K_{32} = \frac{1}{\left[\left(1 - \frac{M^2}{L_s^2}\right)\frac{L_s}{R_r}\right]} \quad ; \quad K_4 = \frac{1}{\left[\left(1 - \frac{M^2}{L_s^2}\right) L_s\right]} \quad ; \quad K_5 = \frac{1}{\left[\left(1 - \frac{M^2}{L_s^2}\right)\frac{L_s^2}{R_r}\right]}\end{aligned} \tag{154}$$

Rewriting equations (151) and (152) results 4 nonlinear equations

$$F_{d,q}(k) = 0 \quad \Rightarrow \quad \begin{Bmatrix} f_d(\omega_{m1}) = 0 \\ f_q(\omega_{m1}) = 0 \\ f_d(\omega_{m2}) = 0 \\ f_q(\omega_{m2}) = 0 \end{Bmatrix} \tag{155}$$

where ω_1 and ω_2 are speeds of 2 data points and result the equations

$$\begin{pmatrix} \frac{di_{sd1}}{dt} & i_{sd1} & -(\omega-\wp\,\omega_{m1})i_{sq1} & -\omega i_{sq1} & -\frac{dv_{sd1}}{dt}+(\omega-\wp\,\omega_{m1})v_{sq1} & -v_{sd1} \\ \frac{di_{sq1}}{dt} & i_{sq1} & (\omega-\wp\,\omega_{m1})i_{sd1} & \omega i_{sd1} & -\frac{dv_{sq1}}{dt}-(\omega-\wp\,\omega_{m1})v_{sd1} & -v_{sq1} \\ \frac{di_{sd2}}{dt} & i_{sd2} & -(\omega-\wp\,\omega_{m2})i_{sq2} & -\omega i_{sq2} & -\frac{dv_{sd2}}{dt}+(\omega-\wp\,\omega_{m2})v_{sq2} & -v_{sd2} \\ \frac{di_{sq2}}{dt} & i_{sq2} & (\omega-\wp\,\omega_{m2})i_{sd2} & \omega i_{sd2} & -\frac{dv_{sq2}}{dt}-(\omega-\wp\,\omega_{m2})v_{sd2} & -v_{sq2} \end{pmatrix} \begin{pmatrix} \frac{R_s+R_r}{\left[\left(1-\frac{M^2}{L_s^2}\right)\frac{L_s^2}{R_r}\right]} \\ \frac{R_s}{\left[\left(1-\frac{M^2}{L_s^2}\right)\frac{L_s^2}{R_r}\right]} \\ \frac{1}{\left[\left(1-\frac{M^2}{L_s^2}\right)\frac{L_s}{R_s}\right]} \\ \frac{1}{\left[\left(1-\frac{M^2}{L_s^2}\right)\frac{L_s}{R_r}\right]} \\ \frac{1}{\left[\left(1-\frac{M^2}{L_s^2}\right)L_s\right]} \\ \frac{1}{\left[\left(1-\frac{M^2}{L_s^2}\right)\frac{L_s^2}{R_r}\right]} \end{pmatrix} -$$

$$-\begin{pmatrix} -\frac{d^2i_{sd1}}{dt^2}+(2\omega-\wp\,\omega_{m1})\frac{di_{sq1}}{dt}+(\omega-\wp\,\omega_{m1})\omega i_{sd1}+(\beta\psi_{rq1}).\frac{d\wp\,\omega_{m1}}{dt} \\ -\frac{d^2i_{sq1}}{dt^2}-(2\omega-\wp\,\omega_{m1})\frac{di_{sd1}}{dt}+(\omega-\wp\,\omega_{m1})\omega i_{sq1}-(\beta\psi_{rd1}).\frac{d\wp\,\omega_{m1}}{dt} \\ -\frac{d^2i_{sd2}}{dt^2}+(2\omega-\wp\,\omega_{m2})\frac{di_{sq2}}{dt}+(\omega-\wp\,\omega_{m2})\omega i_{sd2}+(\beta\psi_{rq2}).\frac{d\wp\,\omega_{m2}}{dt} \\ -\frac{d^2i_{sq2}}{dt^2}-(2\omega-\wp\,\omega_{m2})\frac{di_{sd2}}{dt}+(\omega-\wp\,\omega_{m2})\omega i_{sq2}-(\beta\psi_{rd2}).\frac{d\wp\,\omega_{m2}}{dt} \end{pmatrix} = \begin{pmatrix} 0 \\ 0 \\ 0 \\ 0 \end{pmatrix} \quad (156)$$

The vector of estimated parameters ([R_s L_s R_r M]) is determined by applying F-solve function of MATLAB , where L_s is inductance of stator that has the same value as the inductance of rotor [25]. After parameter estimation, the steady state induction circuit is used to calculate the four magnitudes of machine as maximum torque, starting torque, starting current and magnetizing or no-load current; T_m, T_s, I_s, I_n, respectively to calculate the error of machine parameters.

4.2 Rotor flux approximation

The same as regression method, the rotor flux value can not be measured. Then the rotor flux approximation (equation 111) must be used which is repeated here for clarity.

$$\beta\psi_{rd} = +\frac{v_{sq}}{\sigma\omega L_s} - i_{sd} \quad ; \quad \beta\psi_{rq} = -\frac{v_{sd}}{\sigma\omega L_s} - i_{sq} \tag{157}$$

Considering the approximation (157), the equation (156) can be rewritten

$$\begin{pmatrix} \frac{di_{sd1}}{dt} & i_{sd1} & -(\omega-\wp\omega_{m1})i_{sq1} & -\omega i_{sq1} & -\frac{dv_{sd1}}{dt}+(\omega-\wp\omega_{m1})v_{sq1}-\frac{1}{\omega}\frac{d\wp\omega_m}{dt}v_{sd1} & -v_{sd1} \\ \frac{di_{sq1}}{dt} & i_{sq1} & (\omega-\wp\omega_{m1})i_{sd1} & \omega i_{sd1} & -\frac{dv_{sq1}}{dt}-(\omega-\wp\omega_{m1})v_{sd1}-\frac{1}{\omega}\frac{d\wp\omega_m}{dt}v_{sq1} & -v_{sq1} \\ \frac{di_{sd2}}{dt} & i_{sd2} & -(\omega-\wp\omega_{m2})i_{sq2} & -\omega i_{sq2} & -\frac{dv_{sd2}}{dt}+(\omega-\wp\omega_{m2})v_{sq2}-\frac{1}{\omega}\frac{d\wp\omega_m}{dt}v_{sd2} & -v_{sd2} \\ \frac{di_{sq2}}{dt} & i_{sq2} & (\omega-\wp\omega_{m2})i_{sd2} & \omega i_{sd2} & -\frac{dv_{sq2}}{dt}-(\omega-\wp\omega_{m2})v_{sd2}-\frac{1}{\omega}\frac{d\wp\omega_m}{dt}v_{sq2} & -v_{sq2} \end{pmatrix} \begin{pmatrix} \frac{R_s+R_r}{\left[\left(1-\frac{M^2}{L_s^2}\right)\frac{L_s^2}{R_r}\right]} \\ \frac{R_s}{\left[\left(1-\frac{M^2}{L_s^2}\right)\frac{L_s^2}{R_r}\right]} \\ \frac{1}{\left[\left(1-\frac{M^2}{L_s^2}\right)\frac{L_s}{R_s}\right]} \\ \frac{1}{\left[\left(1-\frac{M^2}{L_s^2}\right)\frac{L_s}{R_r}\right]} \\ \frac{1}{\left[\left(1-\frac{M^2}{L_s^2}\right)L_s\right]} \\ \frac{1}{\left[\left(1-\frac{M^2}{L_s^2}\right)\frac{L_s^2}{R_r}\right]} \end{pmatrix} -$$

$$\begin{pmatrix} -\frac{d^2i_{sd1}}{dt^2}+(2\omega-\wp\omega_{m1})\frac{di_{sq1}}{dt}+(\omega-\wp\omega_{m1})\omega i_{sd1}-\frac{d\wp\omega_{m1}}{dt}i_{sq1} \\ -\frac{d^2i_{sq1}}{dt^2}-(2\omega-\wp\omega_{m1})\frac{di_{sd1}}{dt}+(\omega-\wp\omega_{m1})\omega i_{sq1}+\frac{d\wp\omega_{m1}}{dt}i_{sd1} \\ -\frac{d^2i_{sd2}}{dt^2}+(2\omega-\wp\omega_{m2})\frac{di_{sq2}}{dt}+(\omega-\wp\omega_{m2})\omega i_{sd2}-\frac{d\wp\omega_{m2}}{dt}i_{sq2} \\ -\frac{d^2i_{sq2}}{dt^2}-(2\omega-\wp\omega_{m2})\frac{di_{sd2}}{dt}+(\omega-\wp\omega_{m2})\omega i_{sq2}+\frac{d\wp\omega_{m2}}{dt}i_{sd2} \end{pmatrix} = \begin{pmatrix} 0 \\ 0 \\ 0 \\ 0 \end{pmatrix} \tag{158}$$

4.3 Errors study of the two points method

In this section, study of the errors of the two points method as function of the speed values of the points is presented. Parameters of single cage wound induction machines are according to Table 4.1.
In the simulation with MATLAB SIMULINK 2011, simulation stop time or run time is 2[s] and the total number of points is 20000 and the step size or precision in the quantifying method is 0.0001[s].

Table. 4.1. Parameters of three induction machines with f_s=50 [Hz]

$S_n(VA)$	$V_{s\,ph}(V)$	$R_s(\Omega)$	$L_s(H)$	$L_m(H)$	$L_r(H)$	$R_r(\Omega)$	$\wp$	$J(kg.m^2)$
4.5k	220	0.4	0.3246	0.3183	0.3246	0.4	1	0.08
7.460k	460/√3	0.6837	0.15275	0.1486	0.15275	0.451	1	0.1
160k	400/√3	0.01379	0.007842	0.00769	0.007842	0.007728	1	2.9

The simulation results of the chapter 3 showed that for good estimation one point in zone 2 (maximum torque point) and another point in zone 3 (steady-state point) are necessary. This chapter studies the effect of speed position in machine parameters estimation.
In this method just two points are used. For this study three regions are defined according to the Figs. 4.1 to 4.3. The first region or zone is between mechanical transient after starting oscillations (electrical transient region) and the maximum torque point. The second region is between maximum torque point and the steady-state zone. The third region is steady-state region. According to the Figs.4.1 to 4.3 the idea is working with the orange circle points in regions 1 and 2, while the second black circle point in zone 3 is always fixed at steady-state point.

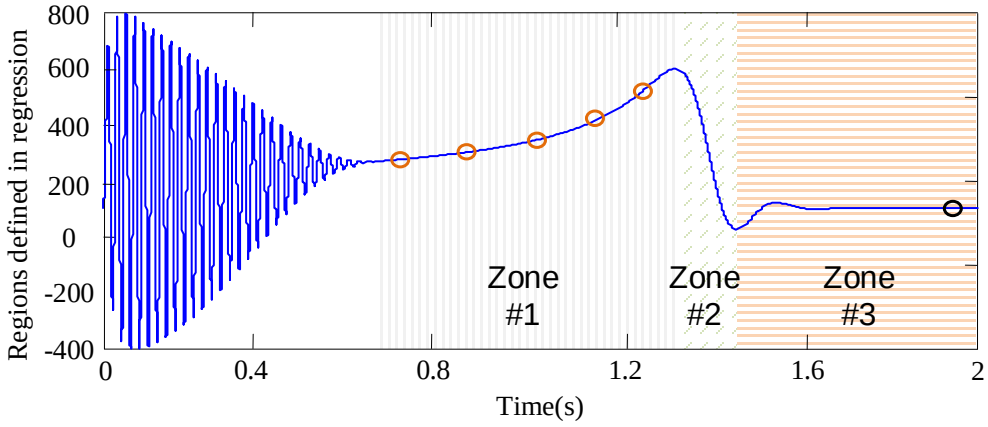

Fig. 4.1. Change of the first point in region 1

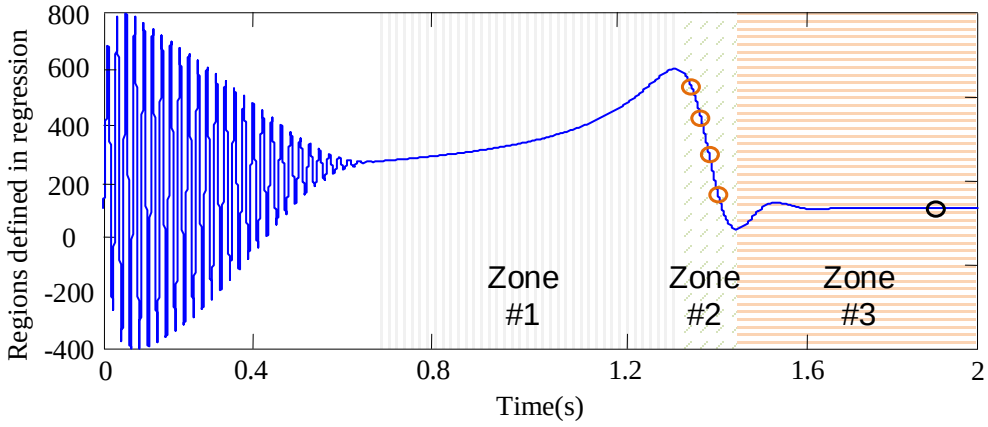

Fig. 4.2. Change of the first point in region 2

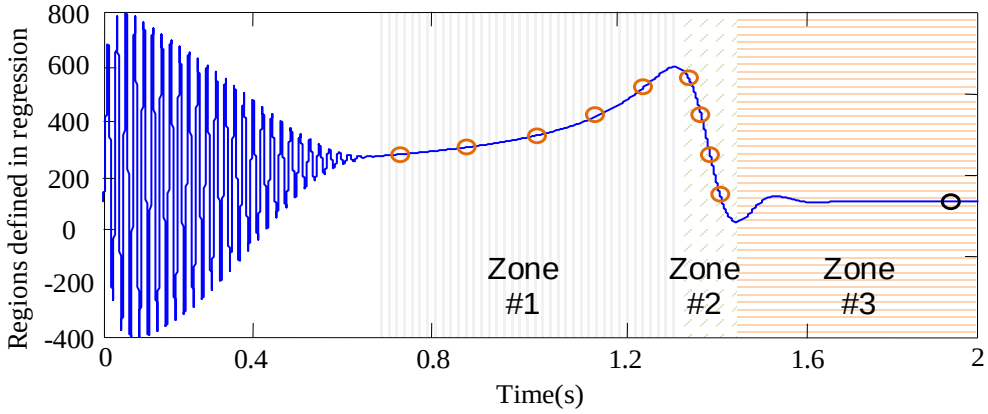

Fig. 4.3. Change of the first point in region 1, 2

4.3.1 Study of influence of rotor flux approximation

In this part constant inertia 0.08[kgm^2] and step size for derivative calculation; 0.0001[s] for machine 1 of Table 4.1, are considered in three states; zero rotor flux, exact rotor flux and rotor flux approximation. The maximum torque and starting torque relative errors are studied in Figs. 4.4 to 4.7. In Figs. 4.4 and 4.6 errors of T_m and T_s are shown while the first point changes in region 1 between 94[rad/s] to 254[rad/s] and the second point is fix at 314.4[rad/s]. In these figures, red lines with squares are errors with zero rotor flux, blue lines with diamonds are the errors with rotor flux approximation and black lines with circles are the errors with exact rotor flux. The figures show that the rotor flux approximation is better than zero rotor flux or zero speed derivative approximation (zero acceleration of the motor in literature [15]). In Figs. 4.5 and 4.7 the T_m and T_s errors are shown respectively for speeds of the first point from 94[rad/s] to

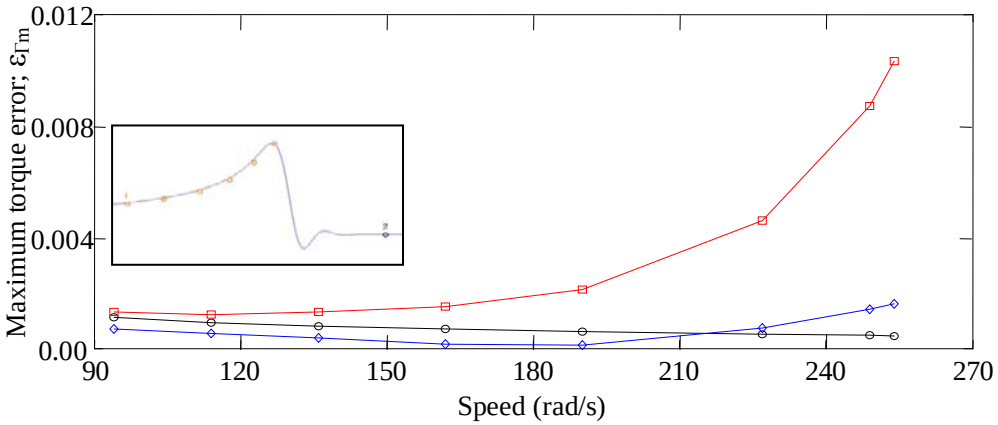

Fig. 4.4. Error of T_m for inertia 0.08 and h=0.0001 for machine 1 with exact rotor flux; black line with circles, with rotor flux approximation; blue line with diamonds, with zero rotor flux approximation; red line with squares.

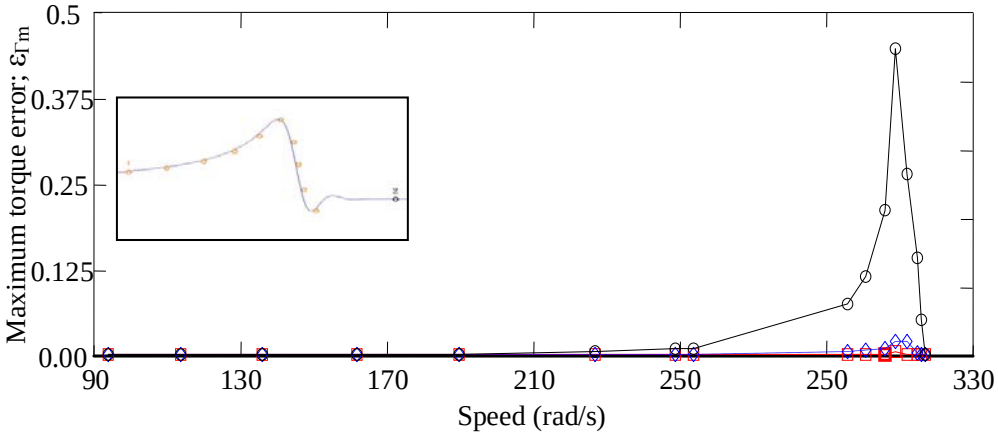

Fig. 4.5. Error of T_m for inertia 0.08 and h=0.0001 for machine 1 with exact rotor flux; red line with squares, with flux approximation; blue line with diamonds, with zero rotor flux; black line with circles.

317[rad/s]. The second point is fix at 314.4[rad/s]. In these figures, the red lines with squares are the errors for exact rotor flux or without approximation. The blue lines with diamonds are the errors for rotor flux approximation and the black lines with circles are the errors for zero rotor flux. These figures show that the rotor flux approximation is better than zero rotor flux approximation of literature [15].

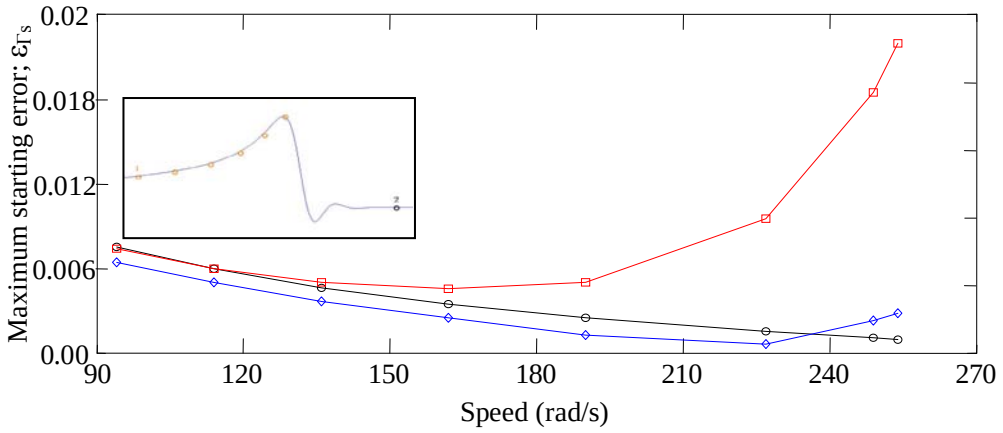

Fig. 4.6. Error of T_s for inertia 0.08 and h=0.0001 for machine 1 with exact rotor flux; black line with circles, with flux approximation; blue line with diamonds, with zero rotor flux; red line with squares.

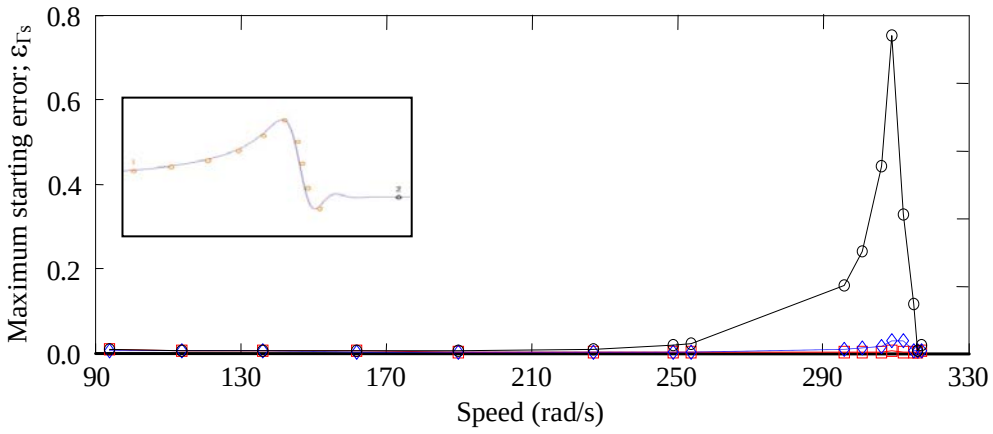

Fig. 4.7. Error of T_s for inertia 0.08 and h=0.0001 for machine 1 in region 1, 2 between mechanical transient point and steady state region with exact rotor flux; red line with squares, with flux approximation; blue line with diamonds, with zero rotor flux; black line with circles.

4.3.2 Study of influence of step size

The step size is the time between the data points in quantifying-two-points-method of estimation. In this study, step size is considered three amounts; 0.0001[s], 0.001[s] and 0.01[s]. Also the inertia is 0.08[kgm^2]. The rotor flux approximation is considered. In Fig. 4.8 the relative maximum torque error is shown while speed of first point changes in zone 1 between 94[rad/s] to 254[rad/s]. The second point is fix at steady-state point. The error for step size 0.0001[s] is in black line with circles, the error for step size 0.001[s] is in blue line with diamonds and the error with step size 0.01[s] is in red line with squares. The figure shows that the errors are always low.

In Fig.4.9 the maximum torque relative error is shown while speed of the first point changes in zone 1 and

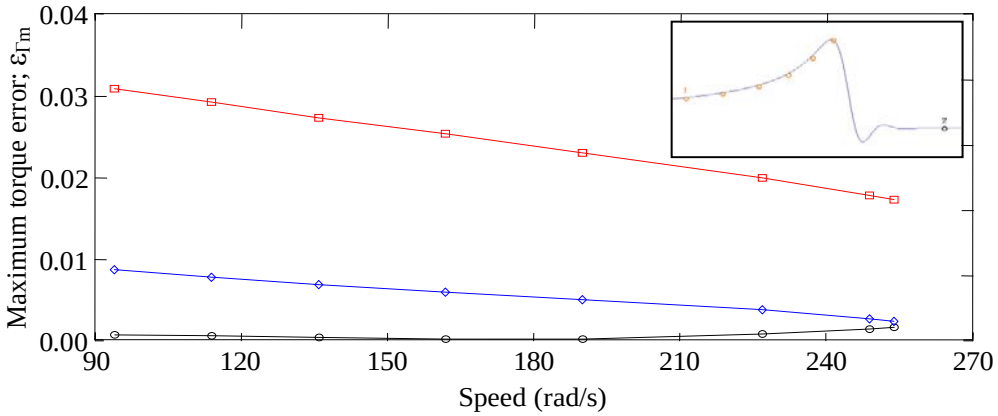

Fig. 4.8. Comparison of maximum torque error for different h in machine 1 for speeds between mechanical transient region and maximum speed in zone 1 with flux approximation and *J*=0.08, for *h*=0.0001; black line with circles, for *h*=0.001; blue line with diamonds and for *h*=0.01; red line with squares

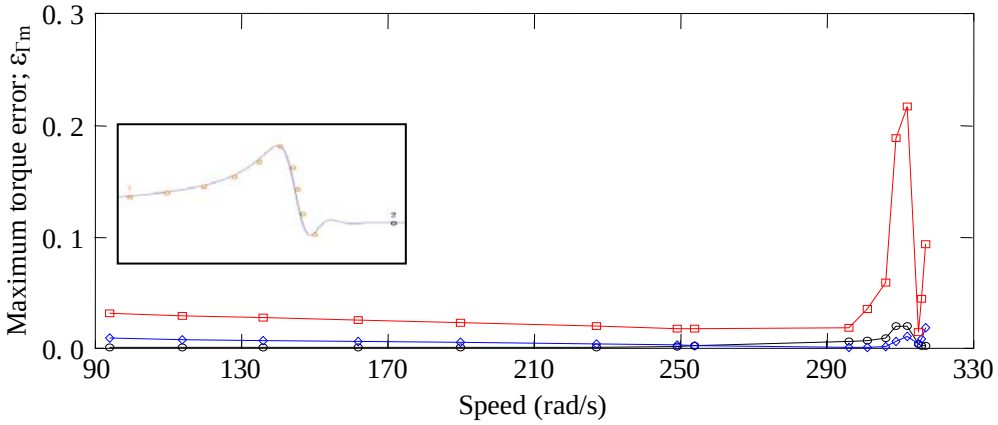

Fig. 4.9. Comparison of maximum torque error for different h in machine 1 for speeds between mechanical transient region and steady state in zone 1, 2 with flux approximation and *J*=0.08, for *h*=0.0001; black line with circles, for *h*=0.001; blue line with diamonds and for *h*=0.01; red line with squares

2 between 94[rad/s] to 317[rad/s]. The second point is fix at 314.4[rad/s]. The error for step size 0.0001[s] is in black line with circles, the error for step size 0.001[s]is in blue line with diamonds and error with step size 0.01[s] is in red line with squares. The figure shows the error is low except for the points near the steady-state (linear dependent phenomena). The main conclusion is that step size has a low influence on the errors.

4.3.3 Study of influence of inertia

In this part different inertias are considered. In this study the transient region speed in simulation or position of the first point in the first region is changed. Three inertias; 0.08, 0.2 and 0.8[kgm^2] in simulation with flux approximation and step size equal to 0.0001[s] are considered for machine 1 of Table 4.1. In Figs. 4.10 and 4.12 the maximum torque and starting torque errors are shown respectively. The speed of the first point changes from 94[rad/s] to 254[rad/s] and the second point speed is fix at 314.4[rad/s]; steady-state. In these figures the black lines with circles are the errors for inertia 0.08[kgm^2], the red lines with squares are for inertia 0.2[kgm^2] and the blue lines with diamonds are for inertia 0.8[kgm^2]. The figures show the errors are always low. In Figs. 4.11 and 4.13 the T_m and T_s errors are shown respectively. In these figures the first point moves in zones 1 and 2 between 94[rad/s] to 317[rad/s]

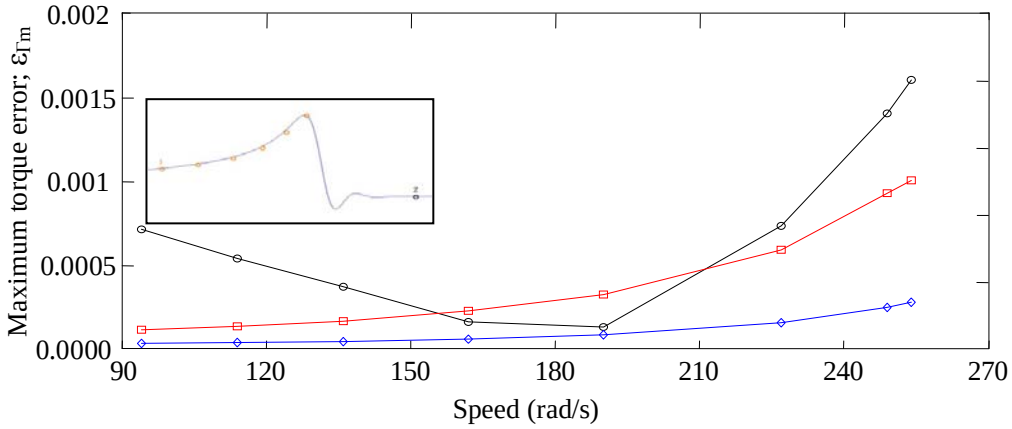

Fig. 4.10. Relative error of T_m for inertia 0.08, 0.8 and 0.2 and h=0.0001 for machine 1 for zone 1 before maximum torque point, with inertia 0.08; black line with circles, with inertia 0.2; red line with squares and with inertia 0.8; blue line with diamonds

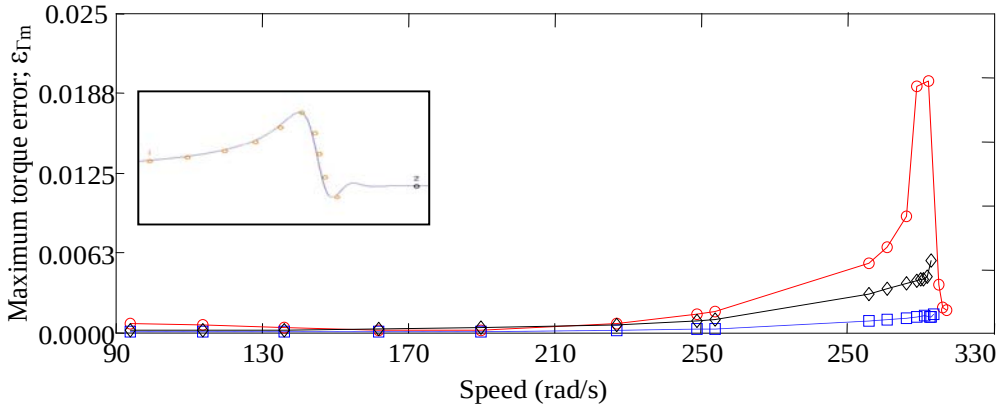

Fig. 4.11. Relative error of T_m with flux approximation and h=0.0001 for machine 1 for zones 1, 2 before steady state, with inertia 0.08; red line with circles with inertia 0.2; black line with diamonds, with inertia 0.8; blue line with squares

and the next point is fix at steady state speed; 314.4[rad/s]. The red lines with circles are the errors for inertia 0.08[kgm^2], the black lines with diamonds are the errors for inertia 0.2[kgm^2] and the blue lines with squares are the errors for inertia 0.8[kgm^2]. The main conclusion is that the inertia has a low influence on the errors.

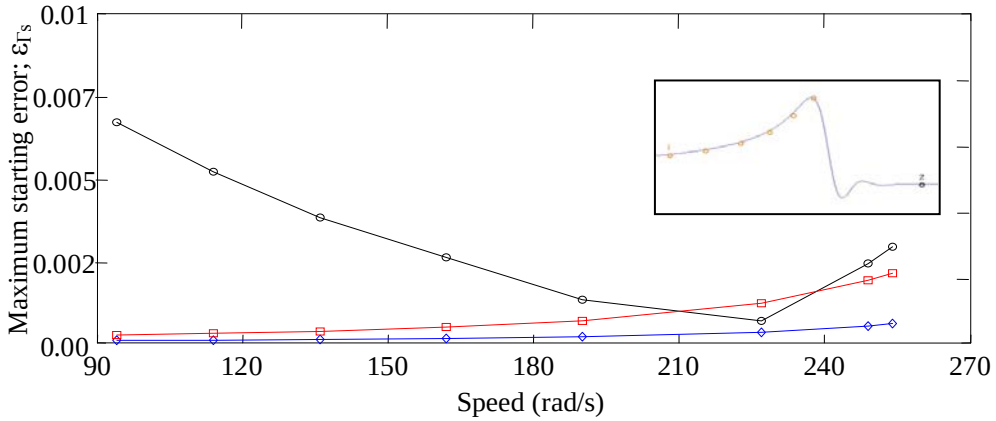

Fig. 4.12. Relative error of T_s for inertia 0.08, 0.8 and 0.2 and h=0.0001 for machine 1 for region 1 before maximum torque point, with inertia 0.08; black line with circles, with inertia 0.2; red line with squares, with inertia 0.8; blue line with diamonds

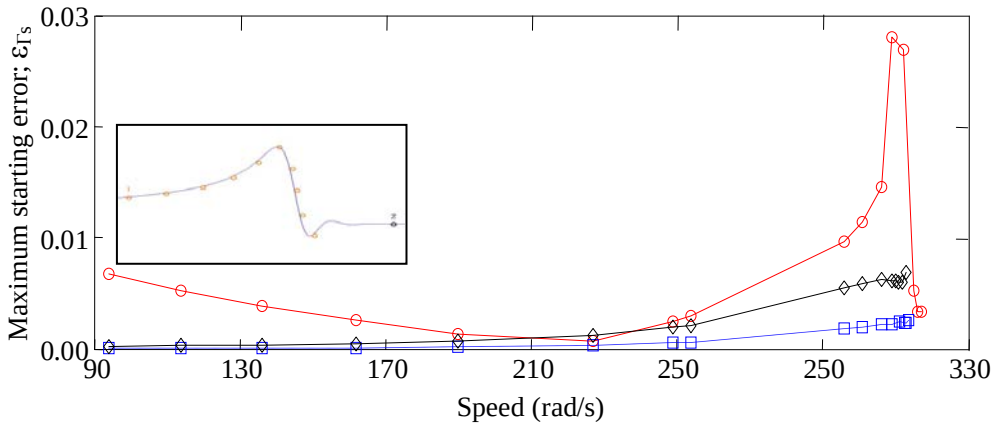

Fig. 4.13. Relative error of T_s with flux approximation and h=0.0001 for machine 1 for region1,2 before steady state, with inertia 0.08; red line with circles with inertia 0.2; black line with diamonds, with inertia 0.8; blue line with squares

4.3.4 Study of estimated parameters

This study is undertaken with step size, 0.0001[s], inertia, 0.08[kgm^2] and rotor flux approximation and 2 points method of estimation. In Fig. 4.14 estimated parameters of machine 1 of Table 4.1 are shown. In Fig. 4.14 stator resistance is in blue line with diamonds, rotor resistance in green line with triangles, stator and rotor inductances are the same in red line with squares and mutual inductance is in black line with circles. The figure shows that the parameters are well estimated in all speeds of zones 1 and 2 between 94[rad/s] to 317[rad/s]. The conclusion is that two points method is not too much sensitive to the position of point 1 in zones 1 and 2.

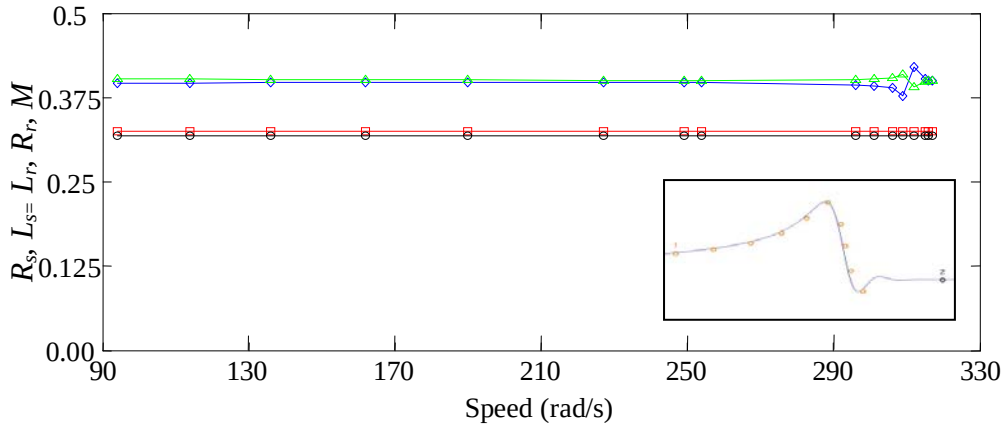

Fig. 4.14. Estimated parameters in machine 1 with rotor flux approx and h=0.0001, R_s; blue line with diamonds, L_s=L_r; red line with squares, R_r; green line with triangles, M; black line with circles.

4.3.5 Comparison of 3 different machines

In this study three different machines of Table 4.1 with powers 4.5[kW], 7.46[kW] and 160[kW] are selected with inertias 0.08[kgm^2], 0.2[kgm^2] and 2.9[kgm^2] respectively while step size is 0.0001[s] and rotor flux approximation is considered for all machines. The method is 2-points. In Fig. 4.15 the relative error of T_m is shown for speeds of the first point between 94[rad/s] to 317[rad/s]. The second point is fix at 314.4[rad/s] or steady-state speed. The blue line with diamonds is the error for machine 2, the red line with squares is the error for machine 3 and the black line with circles is the error for machine 1. The Fig. 4.15 shows the relative errors are lower than 0.025. The main conclusion is that the error is not sensitive to the power of machine.

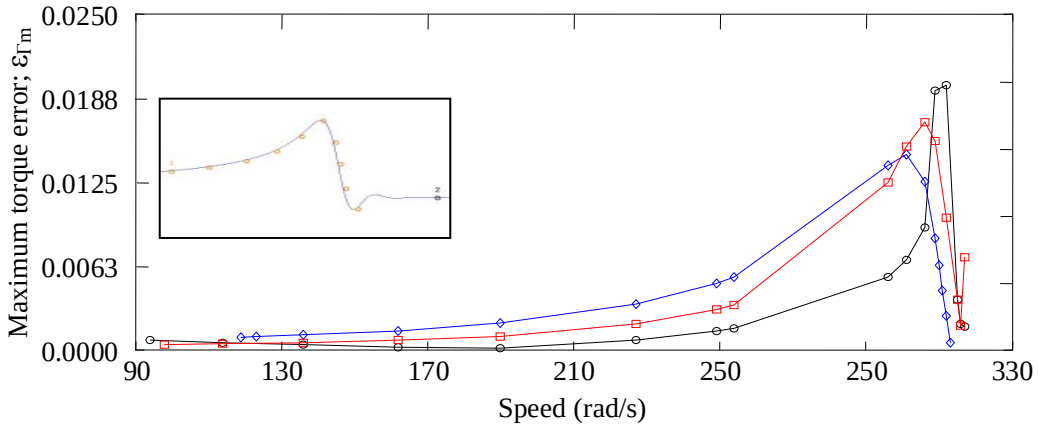

Fig. 4.15. Comparison of T_m relative error for 3 single cage machines with f_s=50 Hz and rotor flux approximation and h=0.0001, for machine 1; black line with circles, for machine 2; blue line with diamonds, for machine 3; red line with squares

4.3.6 Study of starting and magnetizing current errors:

In this part step size is 0.0001[s], inertia is 0.08[kgm^2] for machine of Table 4.1 and rotor flux approximation is considered. The method is 2 points method. The Fig. 4.16 shows relative errors of starting and magnetizing currents for speeds of zones 1 and 2 from 94[rad/s] to 317[rad/s] while the second point is at 314.4[rad/s]. The green line with triangles is the error of starting current. The black line with circles is the error of magnetizing current.

This figure shows the errors are always low, the same as studied maximum and starting torques errors.

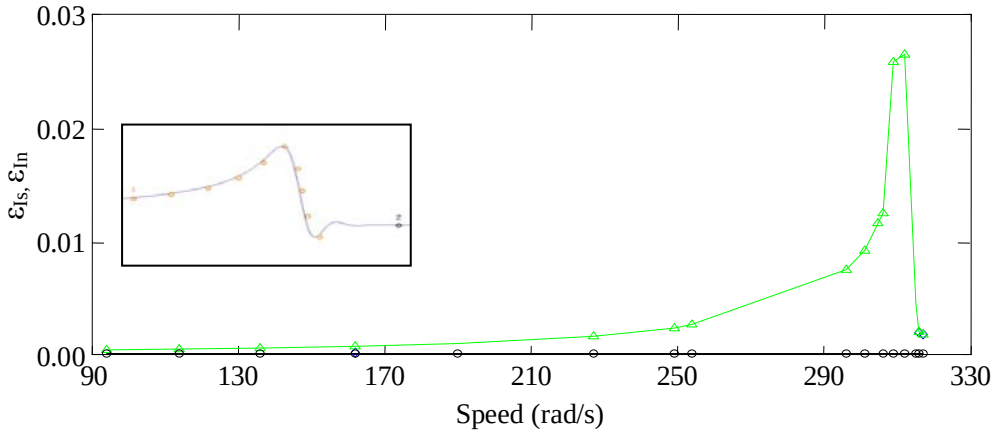

Fig. 4.16. Relative Error of I_s, I_n of machine 1 with rotor flux approximation in zone 1 (between mechanical transient and maximum torque point) and zone 2 (for speeds between maximum torque speed and steady state speed), error of Is; green line with triangles, error of In; black line with circles

5 Double-cage induction machine model

5.1 Dynamic equations

Double-cage machine model is shown in the steady-state circuit of Fig. 5.1. This model is the same as squirrel-single-cage machine model. All of real induction machine models are according to Fig. 5.1.

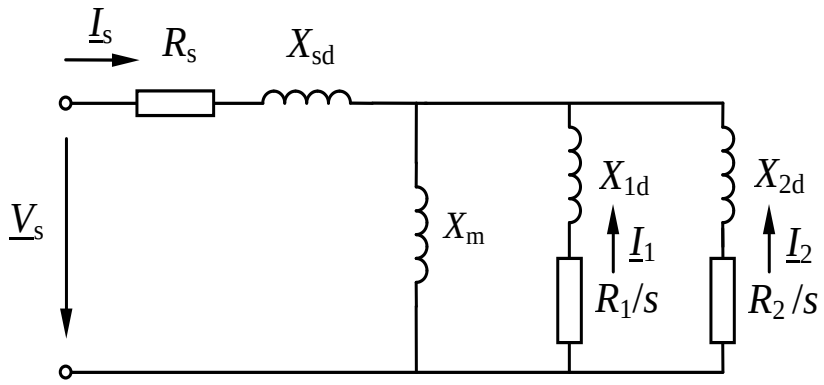

Fig. 5.1.Steady-state star equivalent circuits for the double-cage linear model of the squirrel-cage induction motor.

The double cage model of Fig. 5.1 using the Ku transformation in the synchronously rotating reference frame has the following transformed equations

$$\begin{aligned} v_s &= \left(R_s + L_s\left(p + j\omega\right)\right)i_s + M\left(p + j\omega\right)i_1 + M\left(p + j\omega\right)i_2 \\ 0 &= M\left(p + js\omega\right)i_s + \left(R_1 + L_1\left(p + js\omega\right)\right)i_1 + M\left(p + js\omega\right)i_2 \\ 0 &= M\left(p + js\omega\right)i_s + M\left(p + js\omega\right)i_1 + \left(R_2 + L_2\left(p + js\omega\right)\right)i_2 \\ T &= 2.\wp.M.\mathrm{Im}\left(i_s\left(i_1^* + i_2^*\right)\right) \quad , \quad s = \left(\omega - \wp\,\omega_m\right)/\omega, \end{aligned} \tag{159}$$

The relation between the coefficients in the dynamic equations (159) and the steady-state star equivalent circuit parameters in Fig. 5.1 is

$$\begin{aligned} M = X_m/\omega \quad ; \quad L_s &= \left(X_{sd} + X_m\right)/\omega \\ L_1 = \left(X_{1d} + X_m\right)/\omega \quad ; \quad L_2 &= \left(X_{2d} + X_m\right)/\omega \end{aligned} \tag{160}$$

the dynamic equations in Park variables

$$
\begin{aligned}
v_{sd} &= (R_s + L_s p) i_{sd} - L_s \omega i_{sq} + Mp i_{1d} - M \omega i_{1q} + Mp i_{2d} - M \omega i_{2q} \\
v_{sq} &= L_s \omega i_{sd} + (R_s + L_s p) i_{sq} + M \omega i_{1d} + Mp i_{1q} + M \omega i_{2d} + Mp i_{2q} \\
0 &= Mp i_{sd} - Ms \omega i_{sq} + (R_1 + L_1 p) i_{1d} - L_1 s \omega i_{1q} + Mp i_{2d} - Ms \omega i_{2q} \\
0 &= Ms \omega i_{sd} + Mp i_{sq} + L_1 s \omega i_{1d} + (R_1 + L_1 p) i_{1q} + Ms \omega i_{2d} + Mp i_{2q} \\
0 &= Mp i_{sd} - Ms \omega i_{sq} + Mp i_{1d} - Ms \omega i_{1q} + (R_2 + L_2 p) i_{2d} - L_2 s \omega i_{2q} \\
0 &= Ms \omega i_{sd} + Mp i_{sq} + Ms \omega i_{1d} + Mp i_{1q} + L_2 s \omega i_{2d} + (R_2 + L_2 p) i_{2q} \\
T(t) &= M \cdot \wp \left(i_{sq} (i_{1d} + i_{2d}) - i_{sd} (i_{1q} + i_{2q}) \right) \quad , \quad s = (\omega - \wp \omega_m) / \omega
\end{aligned}
\tag{161}
$$

The relations between the measured currents, i_{sa}, i_{sb}, i_{sc}, and the Park variables i_{sd}, i_{sq}, in the synchronous reference frame $(\theta = \omega t)$ are

$$
\begin{aligned}
i_{sd} &= \sqrt{\frac{2}{3}} \left\{ i_{sa} \cos\theta + i_{sb} \cos\left(\theta - \frac{2\pi}{3}\right) + i_{sc} \cos\left(\theta + \frac{2\pi}{3}\right) \right\} \\
i_{sq} &= -\sqrt{\frac{2}{3}} \left\{ i_{sa} \sin\theta + i_{sb} \sin\left(\theta - \frac{2\pi}{3}\right) + i_{sc} \sin\left(\theta + \frac{2\pi}{3}\right) \right\}
\end{aligned}
\tag{162}
$$

and for the voltages v_{sa}, v_{sb}, v_{sc}, the Park voltages v_{sd}, v_{sq}, are

$$
\begin{aligned}
v_{sd} &= \sqrt{\frac{2}{3}} \left\{ v_{sa} \cos\theta + v_{sb} \cos\left(\theta - \frac{2\pi}{3}\right) + v_{sc} \cos\left(\theta + \frac{2\pi}{3}\right) \right\} \\
v_{sq} &= -\sqrt{\frac{2}{3}} \left\{ v_{sa} \sin\theta + v_{sb} \sin\left(\theta - \frac{2\pi}{3}\right) + v_{sc} \sin\left(\theta + \frac{2\pi}{3}\right) \right\}
\end{aligned}
\tag{163}
$$

The main problem to estimate the double-cage induction motor parameters using the dynamic equations (161) and (162) is that the currents i_{1d}, i_{1q}, i_{2d} and i_{2q} are not measurable. The rotor flux approximation that was used for single-cage estimation can not be applied to the double-cage equations to eliminate four unknown *d*, *q* rotor currents of the double-cage machine.

Then two new methods for the parameter estimation of the double-cage induction machine are developed is this thesis. These methods are called:

- Two single-cage method
- Instantaneous power method

5.2 First proposed method: Two single-cage method.

This first method for the double-cage induction motor model parameters estimation is based on the idea of calculating the parameters of two different single cages that are estimated from the starting transient data of the double cage machine.

The main idea of the proposed method is

- Cage A: The torque-speed and current-speed curves of this single-cage fit well with the torque-speed and current-speed curves of the double-cage model in the range of speeds from the maximum torque speed until the steady-state speed.

- Cage D: This single-cage has the same values of torque and current as those of the double-cage machine in a point (point D) near the zero speed.

Fig. 5.2 shows that the first single-cage curve (red line) fits very well to the double-cage torque-speed

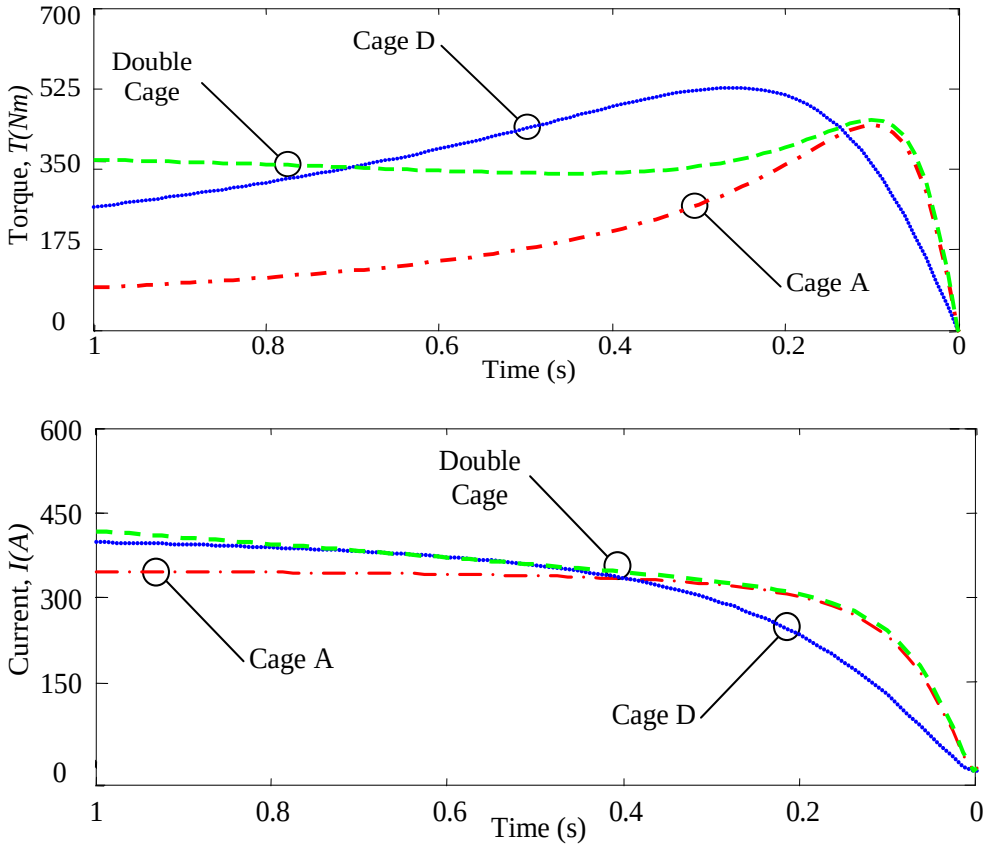

Fig. 5.2.a. Torque of single-cage A; red 1point dashed line, Torque of single-cage D; blue dot line and Torque of original double-cage; green dashed line.
5.2.b. Current of single-cage A; red 1point dashed line, Current of single-cage D; blue dot line and Current of original double-cage; green dashed line.

curve (green line) in the range between the maximum torque point and the synchronous speed.

The single-cage parameters of cage A can be obtained using starting transient data of the double-cage machine with speed values in the range from the maximum torque point until the steady-state speed. For the obtaining of the single-cage parameters the regression method or the two-points method can be used. The more adequate method is the regression method because it can use three or more points, that normally will produce a more reliable result.

The second single-cage D fits to a suitable starting point of double-cage. This starting point is as near as possible to the zero speed point for good estimation of this cage. The transient data near the zero speed has the problem of high oscillations as it can be observed in Fig. 5.3. The Fig. 5.3.a. shows *d, q* currents in black line and smoothed *d, q* currents in red dashed line. The Fig. 5.3.b. shows the speed in blue line and smoothed speed in red dashed line.

The important point is that after this starting area the oscillations are with lower domains and can be smoothed to create good data for estimation. Then the near starting smoothed points are used for estimation of starting single-cages called D_1, D_2 and D_3. These single-cages cross original double cage in

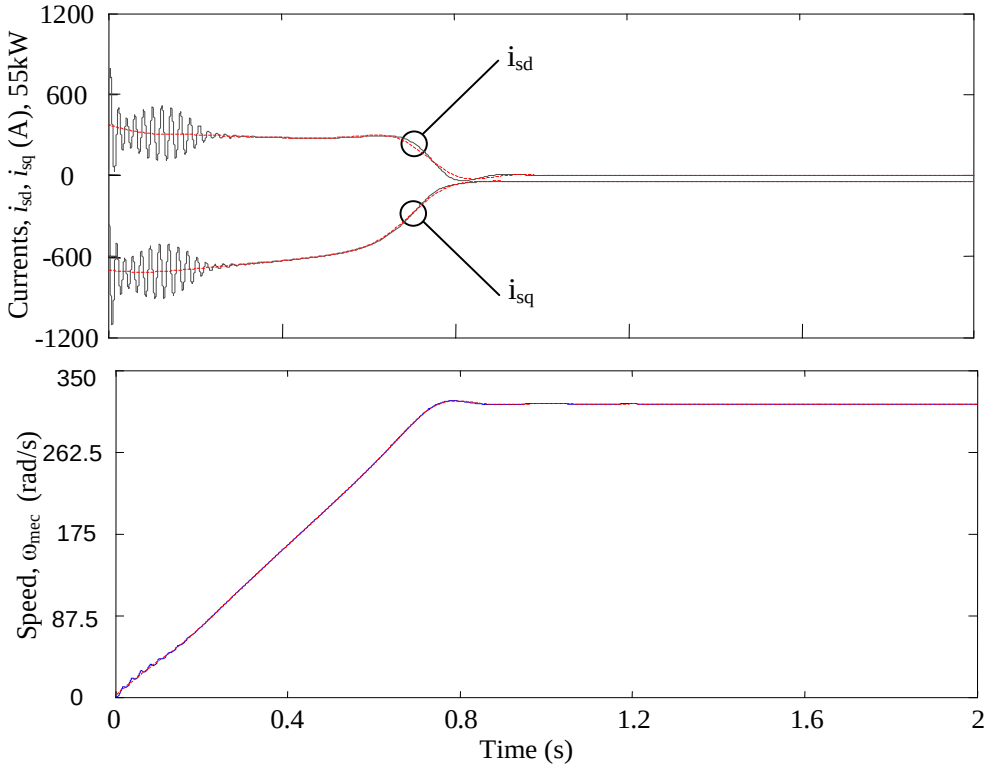

Fig. 5.3.a. *d, q* currents for machine 1; black line and smoothed *d, q* currents for machine 1; red dashed line. 5.3.b. Speed for machine 1; blue line and smoothed speed for machine 1; red dashed line.

slips; 0.7, 0.6 and 0.5 respectively.

The second single-cage (cage D) data fit the impedance value of a point near the starting point. In Fig. 5.2.a the dot blue line is torque of single cage D that intersects the dashed green line; the torque of double-cage in a starting torque point. In Fig. 5.2.b the dot blue line is current of single cage D that intersects the current of double-cage in dashed green line at starting current point.

With the parameters of the cage A and cage D, the necessary data to calculate the double-cage parameters can be obtained. These data are

- Cage A:This cage gives the impedance values in the no load point and the maximum torque point. Those are two complex numbers that result four nonlinear equations.
- Cage D: This cage gives the impedance value of the single-cage D in the speed of the point D that result two nonlinear equations.

The single-cage (cage A) data fit the impedance value of two points, one at the synchronous speed; Z_{nl} and the other at the maximum torque speed; Z_m.

The no-load impedance is calculated from the cage A data

$$\underline{Z}_{NL} = R_s^A + \left(\mathrm{X}_{sd}^A + \mathrm{X}_m^A\right) \tag{164}$$

The maximum torque impedance is obtained also from the cage A data in the maximum slip; s_m, (equation 144) using the single-cage A parameters

$$\underline{Z}_m^A = R_s^A + j\mathrm{X}_{sd}^A + \frac{1}{\frac{1}{j\mathrm{X}_m^A} + \frac{1}{R_r^A/s_m + j\mathrm{X}_{sd}^A}} \tag{165}$$

The impedance in the point of near starting region is obtained from the starting cage D parameters in a near starting slip; s_2 among 0.7, 0.6 and 0.5

$$\underline{Z}_2^D = R_s^D + j\mathrm{X}_{sd}^D + \frac{1}{\frac{1}{j\mathrm{X}_m^D} + \frac{1}{R_r^D/s_2 + j\mathrm{X}_{sd}^D}} \tag{166}$$

For the double-cage model the no load impedance equation in slip equal to zero is

$$\underline{Z}_{NL}^A = R_s + j\left(\mathrm{X}_{sd} + \mathrm{X}_m\right) \tag{167}$$

The impedance in the maximum torque point of double-cage, $\underline{Z}_m$, in maximum slip s_m the same as s_m of single-cage is

$$\underline{Z}_m^A = R_s + jX_{sd} + \frac{1}{\frac{1}{jX_m} + \frac{1}{R_1/s_m + jX_{1d}} + \frac{1}{R_2/s_m + jX_{2d}}} \tag{168}$$

and the impedance in the point of near starting region from double cage model in starting slip s_2 the same as s_2 of single-cage is

$$\underline{Z}_2^D = R_s + jX_{sd} + \frac{1}{\frac{1}{jX_m} + \frac{1}{R_1/s_2 + jX_{1d}} + \frac{1}{R_2/s_2 + jX_{2d}}} \tag{169}$$

The equality equations of single cage impedances and double cage impedances create a set of equations to estimate the double-cage parameters.

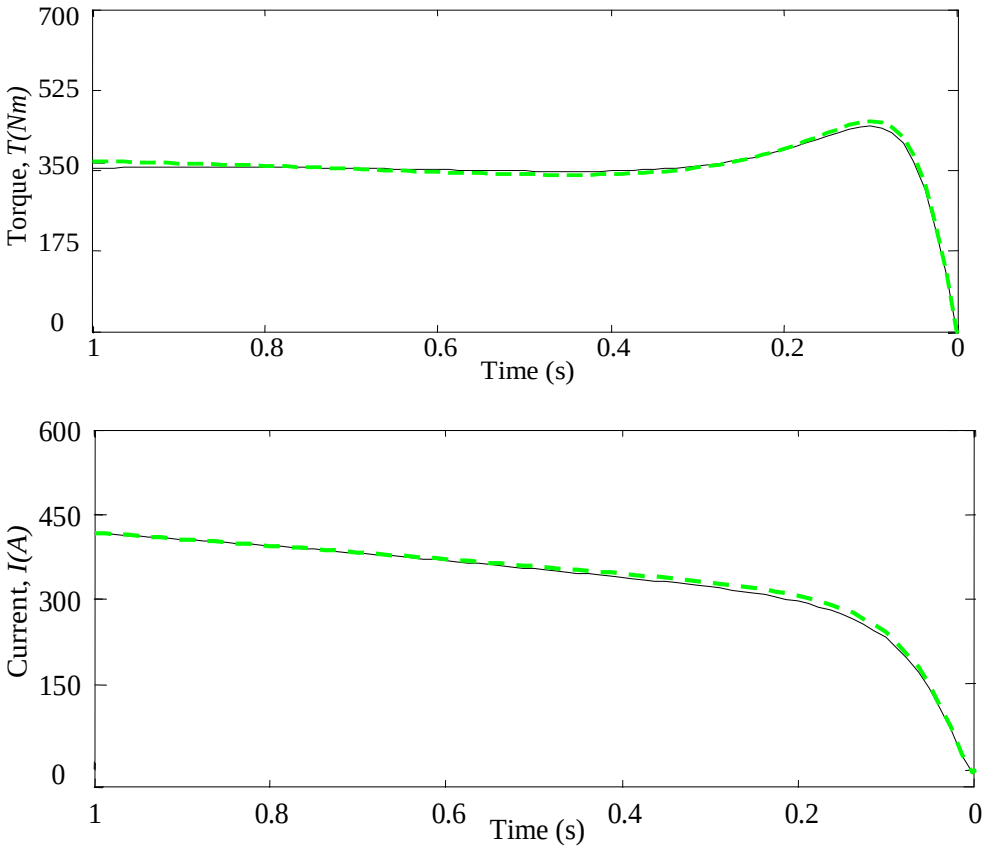

Fig. 5.4.a Torque of estimated double-cage; black solid line and Torque of original double-cage; green dashed line and 5.3.b Current of estimated double-cage; black solid line and Current of original double-cage; green dashed line.

The non-linear system includes Re($\underline{Z}_{NL}^{A}$), Im($\underline{Z}_{NL}^{A}$), Re($\underline{Z}_{m}^{A}$), Im($\underline{Z}_{m}^{A}$), Re($\underline{Z}_{2}^{D}$) and Im($\underline{Z}_{2}^{D}$) which are used to find double cage parameters $\mathbf{x} = (R_s, R_1, R_2, X_m, X_{sd}, X_{1d})$

$$
\begin{aligned}
f_1(\mathbf{x}) &= \left(\mathrm{Re}\left(\underline{Z}_{NL}\right) - R_{NL}(\mathbf{x})\right) \Big/ \left|\underline{Z}_{NL}^{A}\right| = 0 \\
f_2(\mathbf{x}) &= \left(\mathrm{Im}\left(\underline{Z}_{NL}\right) - X_{NL}(\mathbf{x})\right) \Big/ \left|\underline{Z}_{NL}^{A}\right| = 0 \\
f_3(\mathbf{x}) &= \left(\mathrm{Re}\left(\underline{Z}_{m}\right) - R_{m}(\mathbf{x})\right) \Big/ \left|\underline{Z}_{m}^{A}\right| = 0 \\
f_4(\mathbf{x}) &= \left(\mathrm{Im}\left(\underline{Z}_{m}\right) - X_{m}(\mathbf{x})\right) \Big/ \left|\underline{Z}_{m}^{A}\right| = 0 \\
f_5(\mathbf{x}) &= \left(\mathrm{Re}\left(\underline{Z}_{2}\right) - R_{2}(\mathbf{x})\right) \Big/ \left|\underline{Z}_{2}^{D}\right| = 0 \\
f_6(\mathbf{x}) &= \left(\mathrm{Im}\left(\underline{Z}_{2}\right) - X_{2}(\mathbf{x})\right) \Big/ \left|\underline{Z}_{2}^{D}\right| = 0
\end{aligned}
\qquad (170)
$$

where the equality restriction $X_{2d}=X_{sd}$ according to the literature [25], must be used.

Then the torque and current of estimated double-cage and original double-cage using this method are according to the Fig.5.4.a and b. In these figures the black lines are torque and current of estimated double cage and the dashed green lines are torque and current of original double-cage respectively. The figures show the method is suitable for good estimation.

In next part the proposed method is applied to three different machines of Table 5.1.

5.3 Double cage estimation of machine 1

In this study double-cage machine 1 of Table 5.1 is estimated by method of two single cages (A and D) estimation.

Table 5.1. Parameters of Double cage induction machines with V_{ph}=220(V), f_s=50(Hz) and $\wp$ =1

P(kW)	R_s	R_{r1}	R_{r2}	X_m	$X_{sd} = X_{r2}$	X_{r1}	*J*
55	0.0338Ω	0.0465	0.4074	7.3084	0.1698	0.3511	0.8
22	0.1300	0.1689	1.2269	14.977	0.5404	0.8503	0.3
500	0.00123	0.00245	0.04817	0.76736	0.01789	0.03911	13

Cage A is a single cage that passes from maximum point until steady state region of the double-cage and can be estimated by two-points method using F-solve function of MATLAB using transient stator data and mechanical rotor speed. Machine data have high frequency oscillations in dynamic transient region and these data are smoothed. After smoothing, a starting cage is estimated that passes from two points of double-cage torque and current curves; one point very near to this region, but not exactly in this region and the other in the steady-state region. Three starting-cages are estimated for slips 0.7, 0.6 and 0.5 which are called Cages D_1, D_2 and D_3 or C (half speed in the literature) respectively for comparison. The comparison between starting-cages shows that the best estimation is for slip equal to 0.7.

5.3.1 Estimation of cage A for machine 1

The two-points-method is used for estimation of single-cage A but this technique needs initial value parameters so that 3-points-regression-method is used for approximated initial values estimation. The three points of regression method for estimation of cage A are, maximum torque point, region 2 point between maximum torque and the steady-state region and finally the steady-state point. The two points of two-points method are maximum torque and steady state points.

The results of the initial and main estimated parameters of cage A are in Table 5.2.

Fig. 5.5.a shows machine 1 (55kW) starting transient *d*, *q* currents in red dashed line and its smoothing in

Table 5.2. Parameters of single cage A induction machine 1 (55kW) with f_s=50(Hz), V_{ph}=220V and J=0.8

Estimation	R_s	$X_{sd}=X_{rd}$	X_m	R_r
Initial regression	0.0499Ω	0.2302	7.2480	0.0417
Main Two points	0.0338	0.2303	7.2479	0.0450

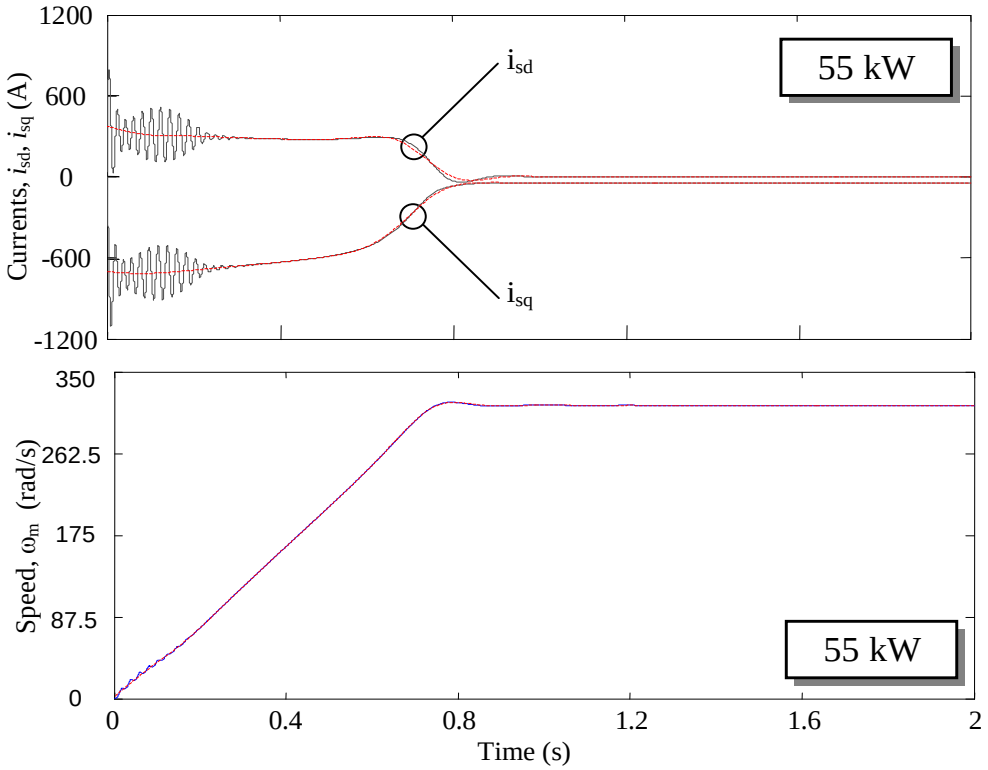

Fig. 5.5.a. *d, q* currents for machine 1; black line and smoothed *d, q* currents for machine 1; red dashed line and 5.5.b. Speed for machine 1; black line and smoothed speed for machine 1; red dashed line.

gray solid line. Fig. 5.5.b is the machine 1 (55kW) mechanical rotor speed in red point line and its smoothing in gray solid line. The estimation of near starting single-cage is done by smoothing of near starting point, because near to the starting region has lower magnitudes of oscillation than starting region. Then the initial starting cage D for initial value of two points method is estimated using 3-points-regression-method with near starting, near steady-state and steady-state points. Then with near starting and steady-state points by two points method, cage D parameters are estimated that are described in next section.

5.3.2 Estimation of cage D for machine 1

Three starting-cages D_1, D_2 and D_3 are estimated for machine 1 and slips of Table 5.3 while synchronous frequency is 50[Hz].

The method of estimation is two points that needs initial value. In this method two important points for estimation are the maximum torque and the steady-state points. The regression three points method is applied to approximate the initial value. The three important points in this method are the near starting point at the defined slip, the second region point very near to the third region that is a approximated point and the steady-state region point.

The two points method for estimation of cage D are near starting torque and steady state points.

Table 5.3 shows the results of initial parameters of single-cage D by regression estimation and real parameters estimation using two points method for three slips; 0.7, 0.6 and 0.5.

Table 5.3. Parameters of single cage D induction machine 1 (55kW) with f_s=50(Hz) and V_{ph}=220V J=0.8 S=0.7

Estimation	s	R_s	X_{sd}	X_m	R_r
Initial regression	0.7	0.0063Ω	0.1947	7.2835	0.0310
Main Two points	0.7	0.0338	0.1936	7.2846	0.1001
Initial regression	0.6	0.0077Ω	0.2006	7.2776	0.0291
Main Two points	0.6	0.0338	0.1995	7.2787	0.0896
Initial regression	0.5	0.0092Ω	0.2069	7.2713	0.0270
Main Two points	0.5	0.0338	0.2058	7.2724	0.0786

Then the steady-state impedance equations of double cage estimation using two points method are solved to produce double cage parameters according to the Table 5.4. The results of estimated parameters of double-cage are very near to the real data of machine 1 in Table 5.1.This Table shows good estimation, where the equality restriction X_{2d}=X_{sd} according to the literature [25], must be used.

Table 5.4. Parameters of double cage induction machine 1 (55kW) with f_s=50(Hz) and J=0.8

s	R_s	R_{r1}	R_{r2}	X_m	X_{sd} = X_{r2}	X_{r1}	V_{ph}	℘
0.7	0.0338Ω	0.0496	0.3468	7.2963	0.1819	0.3689	220	1
0.6	0.0338Ω	0.0498	0.3338	7.2918	0.1864	0.3662	220	1
0.5	0.0338Ω	0.0502	0.3152	7.2854	0.1928	0.3629	220	1

In Fig. 5.6 red 1point dashed line is torque of cage A, blue dot line is torque of cage D, black solid line is estimated torque of double-cage and green dashed line is original torque of double-cage from starting to synchronous slips. This figure shows cages D_1, D_2, D_3 torques and double-cage torque have intersection in slip 0.7, 0.6 and 0.5 respectively.

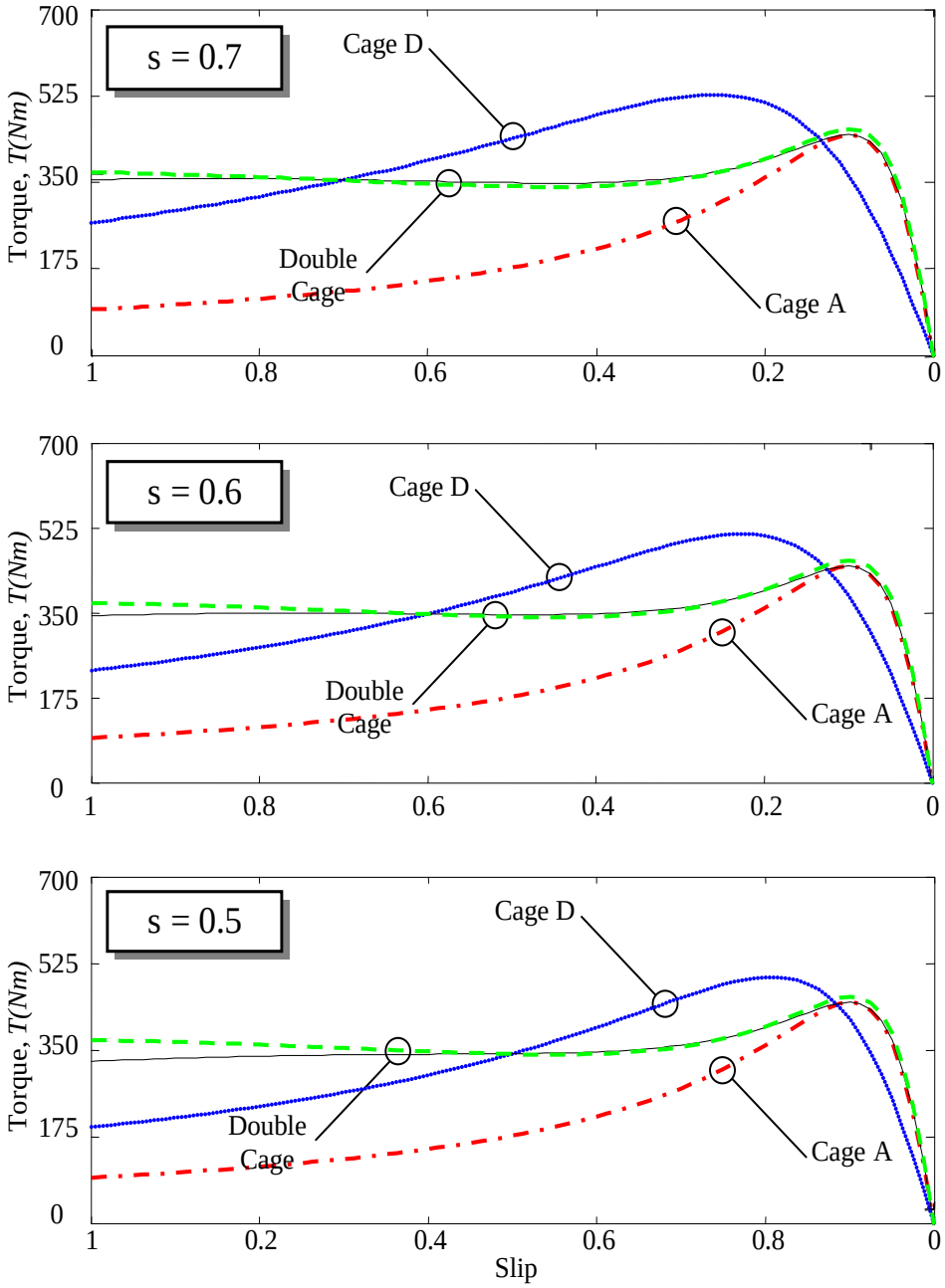

Fig. 5.6 Torque of single-cage A; red 1point dashed line, Torque of single-cage D; blue dot line, Torque of estimated double-cage; black solid line and Torque of original double-cage; green dashed line for three cross points slips; 0.7, 0.6 and 0.5.

In Fig. 5.7 red 1point dashed line is current of cage A, blue dot line is current of cage D, black solid line is estimated current of double-cage and green dashed line is original current of double-cage from starting to synchronous slips. In This figure cages D_1, D_2, D_3 currents and double-cage current have intersection in slip 0.7, 0.6 and 0.5 respectively.

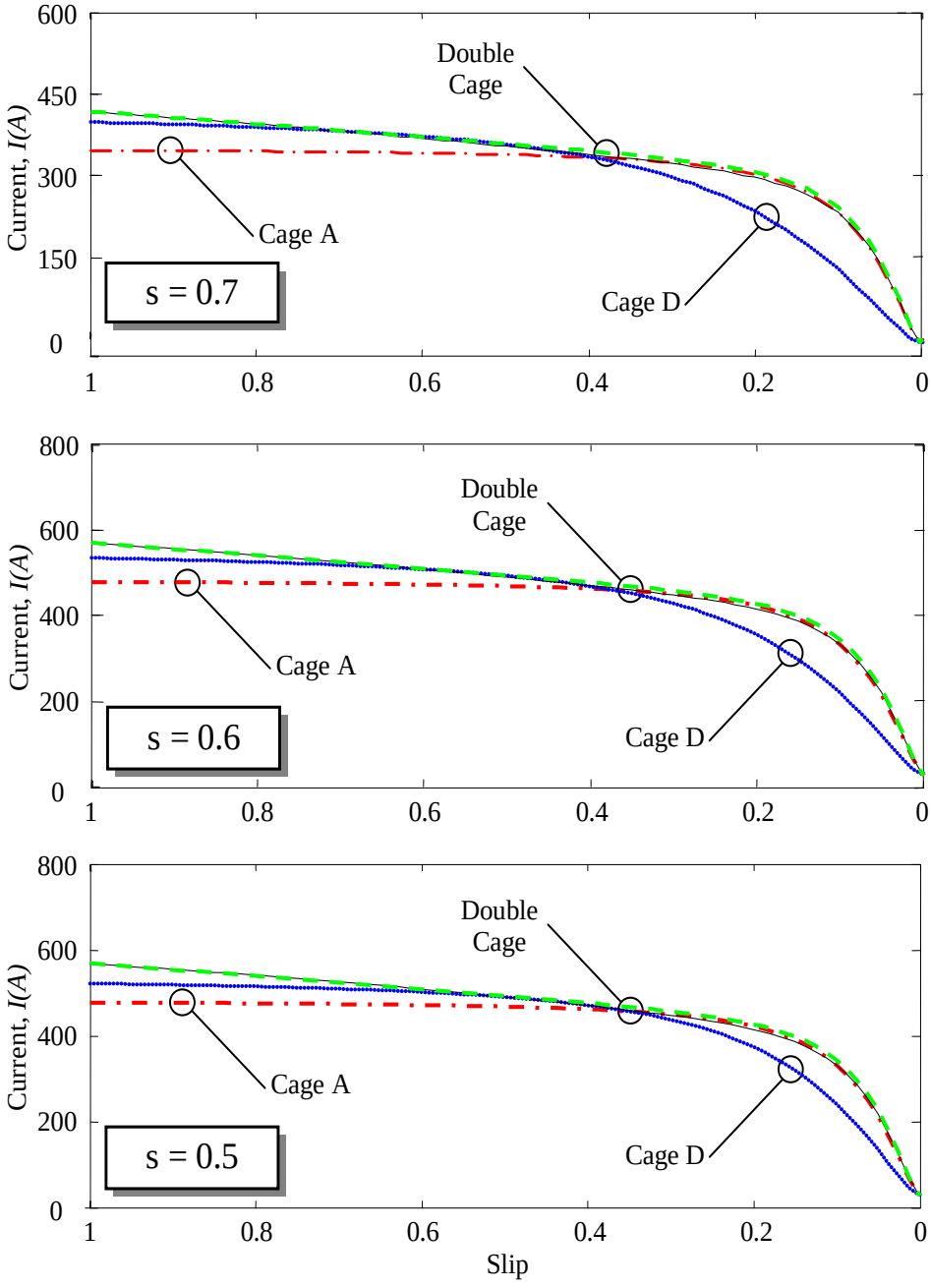

Fig. 5.7 Current of single-cage A; red 1point dashed line, Current of single-cage D; blue dot line, Current of estimated double-cage; black solid line and Current of original double-cage; green dashed line for three cross points slips; 0.7, 0.6 and 0.5.

The Table 5.5 shows the evolution of parameter estimation in different slips or speeds with smoothing.

The error of starting and no-load currents are not significant. The error of maximum torque is very low. It remains constant . The error of starting torque is sensitive to the distance of cross point (point that double cage torque and single cage D torque cross each other) from starting slip (zero speed).

Table 5.5. Calculated magnitudes for error determination with smoothing for machine 1 (55k)

Slip	D-cage	$T_m(Nm)$	$T_s(Nm)$	$I_s(A)$	$I_{NL}(A)$
0.7	Original	457.8	370.0	568.8	29.42
	Estimated	446.2	355.5	568.8	29.42
	Relative Error%	2.53	3.91	0	0
0.6	Original	457.8	370.0	568.8	29.42
	Estimated	446.2	344	568.8	29.42
	Relative Error%	2.53	7.02	0	0
0.5	Original	457.8	370.0	568.8	29.42
	Estimated	446.2	327.1	568.8	29.42
	Relative Error%	2.53	11.59	0	0

5.4 Double cage estimation of machine 2

In this study double-cage machine 2 of Table 5.1 is estimated by method of two single cages (A and D) estimation.

Cage A is a single cage that passes from maximum point until steady state region and can be estimated by two-points method using F-solve function of MATLAB using transient stator data and mechanical rotor speed. Starting region of machine has high frequency oscillations in dynamic transient region and after smoothing a starting cage is estimated that passes from two points of double-cage torque and current curves; one point very near to this region, but not exactly in this region and the other point in the steady-state region. Three starting - cages are estimated for slips 0.7, 0.6 and 0.5 which are called cages D_1, D_2 and D_3 or C (half speed) respectively for comparison. The comparison between starting-cages shows that the best estimation is for slip equal to 0.7.

5.4.1 Estimation of cage A for machine 2

The two-points-method is used for estimation of single-cage A but this technique needs initial value parameters so that 3-points-regression-method is used for approximated initial values estimation. The three points of regression method for estimation of cage A are, maximum torque point, region 2 point between maximum torque and the steady-state region and finally the steady-state point.

The two points of two-points method are maximum torque and steady state points. The results of the initial and main estimated parameters of cage A are in Table 5.6.

Table 5.6. Parameters of single cage A induction machine 2 (22kW) with f_s=50(Hz), V_{ph}=220V and J=0.3

Estimation	R_s	X_{sd}	X_m	R_r
Initial regression	0.1680	0.6083	14.9091	0.1471
Main Two points	0.1300	0.6077	14.9097	0.1567

Fig. 5.8.a shows machine 2 (22kW) starting transient *d, q* currents in red dashed line and its smoothing in gray solid line. Fig. 5.8.b is the machine 2 (22kW) mechanical rotor speed in red point line and its smoothing in gray solid line. The estimation of near starting single-cage is done by smoothing of near starting point, because near to the starting region has lower magnitudes of oscillation than starting region. Then the initial starting cage D for initial value of two points method is estimated by 3-points-regression-method using near starting point, near steady-state point and steady-state point. Then with near starting and steady-state points and two points method cage D parameters are estimated that are explained in next section.

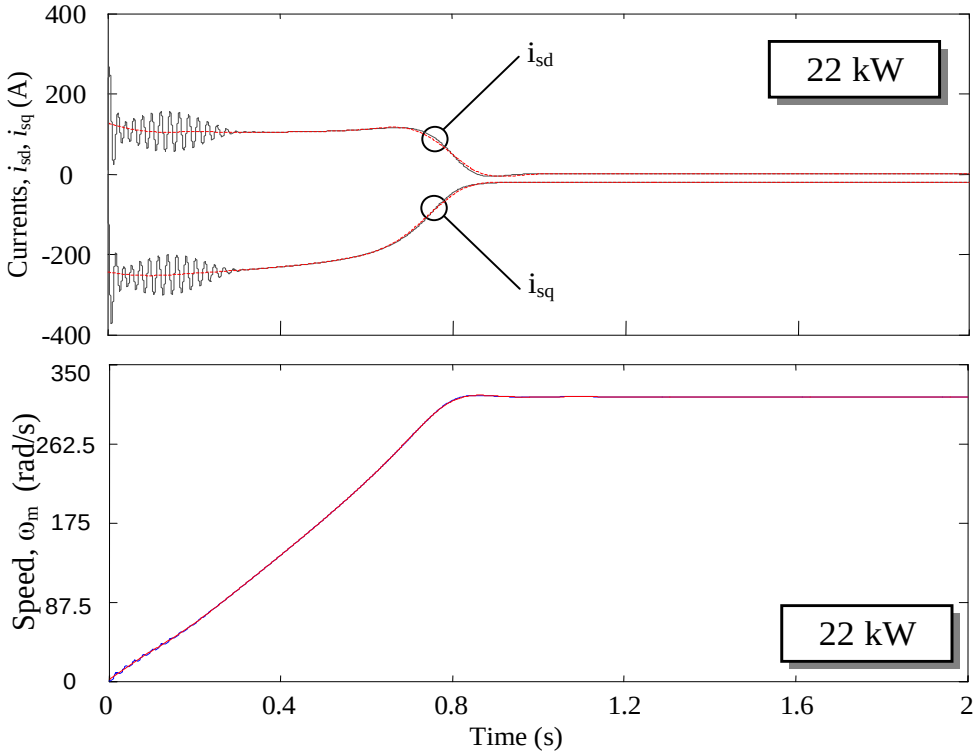

Fig. 5.8.a. *d, q* currents for machine 2; black line and smoothed *d, q* currents for machine 2; red dashed line and 5.8.b Speed for machine 2; black line and smoothed speed for machine 2; red dashed line.

5.4.2 Estimation of cage D for machine 2

Three starting-cages D_1, D_2 and D_3 are estimated for slips of Table 5.7 while synchronous frequency is 50[Hz].

The method of estimation is two-points that needs initial value. In this method two important points for estimation are the maximum torque and the steady-state points. The regression three points method is applied for approximated initial value estimation. The three important points in this method are the starting point at the defined slip, the second region point very near to the third region that is a approximated point and the steady-state region point.

The two points method for estimation of cage D are near starting torque and steady state points.

Table 5.7 shows the results of initial parameters estimation of single-cage D by regression method and real parameter estimation using two points method for three slips; 0.7, 0.6 and 0.5.

Table 5.7. Parameters of single cage D induction machine 2 (22kW) with f_s=50(Hz), V_{ph}=220V and J=0.3

Estimation	s	R_s	X_{sd}	X_m	R_r
Initial regression	0.7	0.1417Ω	0.5510	14.9664	0.1215
Main Two-points	0.7	0.1300	0.5494	14.9680	0.2596
Initial regression	0.6	0.1409Ω	0.5547	14.9627	0.1217
Main Two-points	0.6	0.1300	0.5522	14.9652	0.2521
Initial regression	0.5	0.1387Ω	0.5643	14.9531	0.1225
Main Two-points	0.5	0.1300	0.5618	14.9556	0.2324

Then the steady-state impedance equations of double cage estimation using two points method produces double cage parameters according to the Table 5.8. The results of estimated parameters of double-cage are very near to the real data of machine 2 in Table 5.1.

Table 5.8 shows good estimation, where the equality restriction X_{2d}=X_{sd} according to the literature [25] must be used.

Table 5.8. Parameters of double cage induction machine 2 (22kW) with f_s=50(Hz) and J=0.3

s	R_s	R_{r1}	R_{r2}	X_m	$X_{sd} = X_{r2}$	X_{r1}	V_{ph}	$\wp$
0.7	0.1300Ω	0.1779	1.0377	14.9496	0.5678	0.8859	220	1
0.6	0.1300Ω	0.1780	1.0236	14.9816	0.5358	0.9400	220	1
0.5	0.1300Ω	0.1787	0.9864	14.9890	0.5284	0.9634	220	1

In Fig. 5.9 red 1 point dashed line is torque of cage A, blue dot line is torque of cage D, black solid line is estimated torque of double-cage and green dashed line is original torque of double-cage from starting to synchronous slips. This figure shows that cages D_1, D_2, D_3 and double-cage torques have intersection in slips 0.7, 0.6 and 0.5 respectively. In Fig. 5.10 red 1point dashed line is current of cage A, blue dot line is current of cage D, black solid line is estimated current of double-cage and green dashed line is original

current of double-cage from starting to synchronous slips. In This figure cages D_1, D_2, D_3 currents and double-cage current have intersection in slip 0.7, 0.6 and 0.5 respectively.

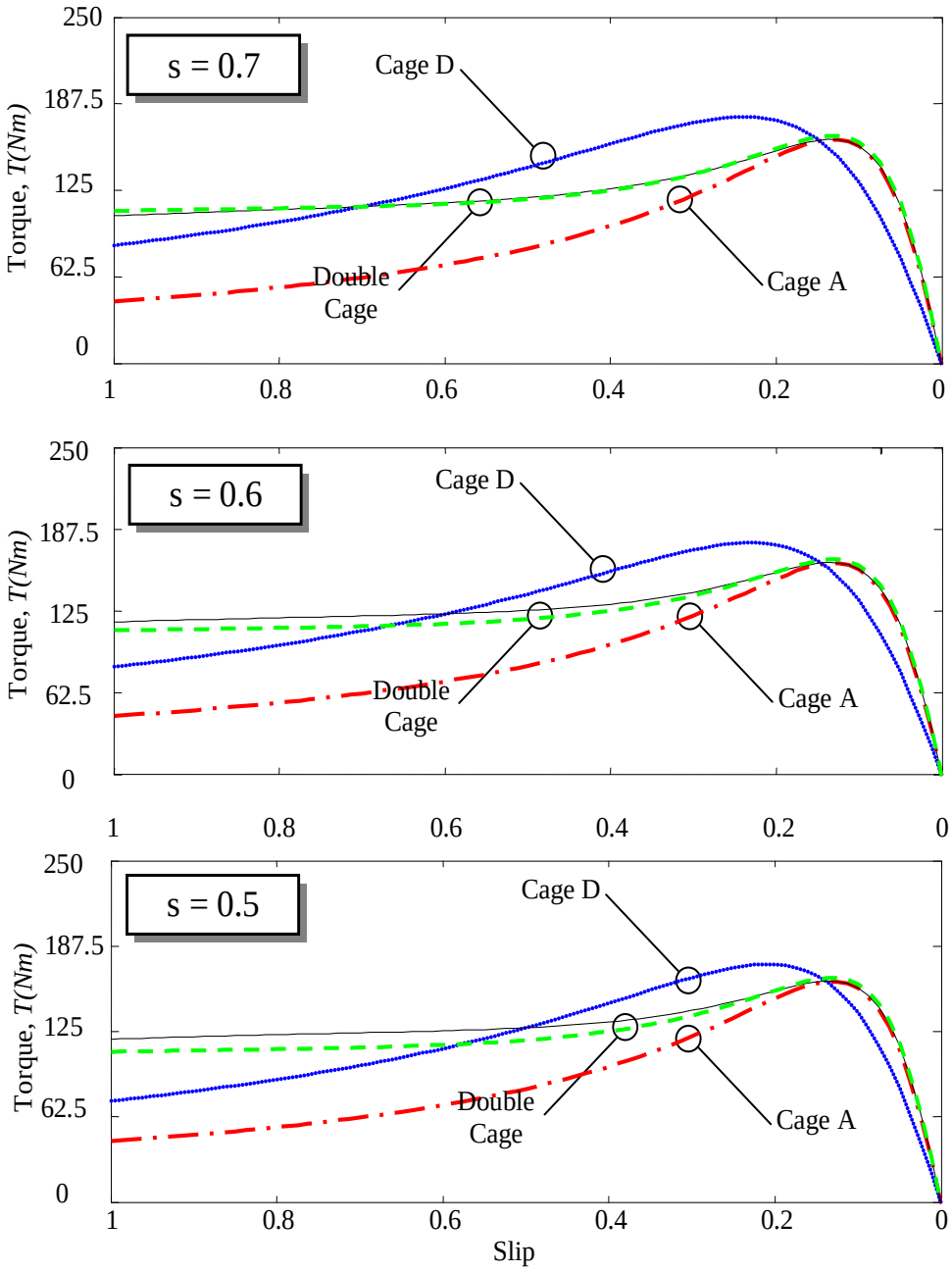

Fig. 5.9 Torque of single-cage A; red 1point dashed line, Torque of single-cage D; blue dot line, Torque of estimated double-cage; black solid line and Torque of original double-cage; green dashed line for three cross points slips; 0.7, 0.6 and 0.5.

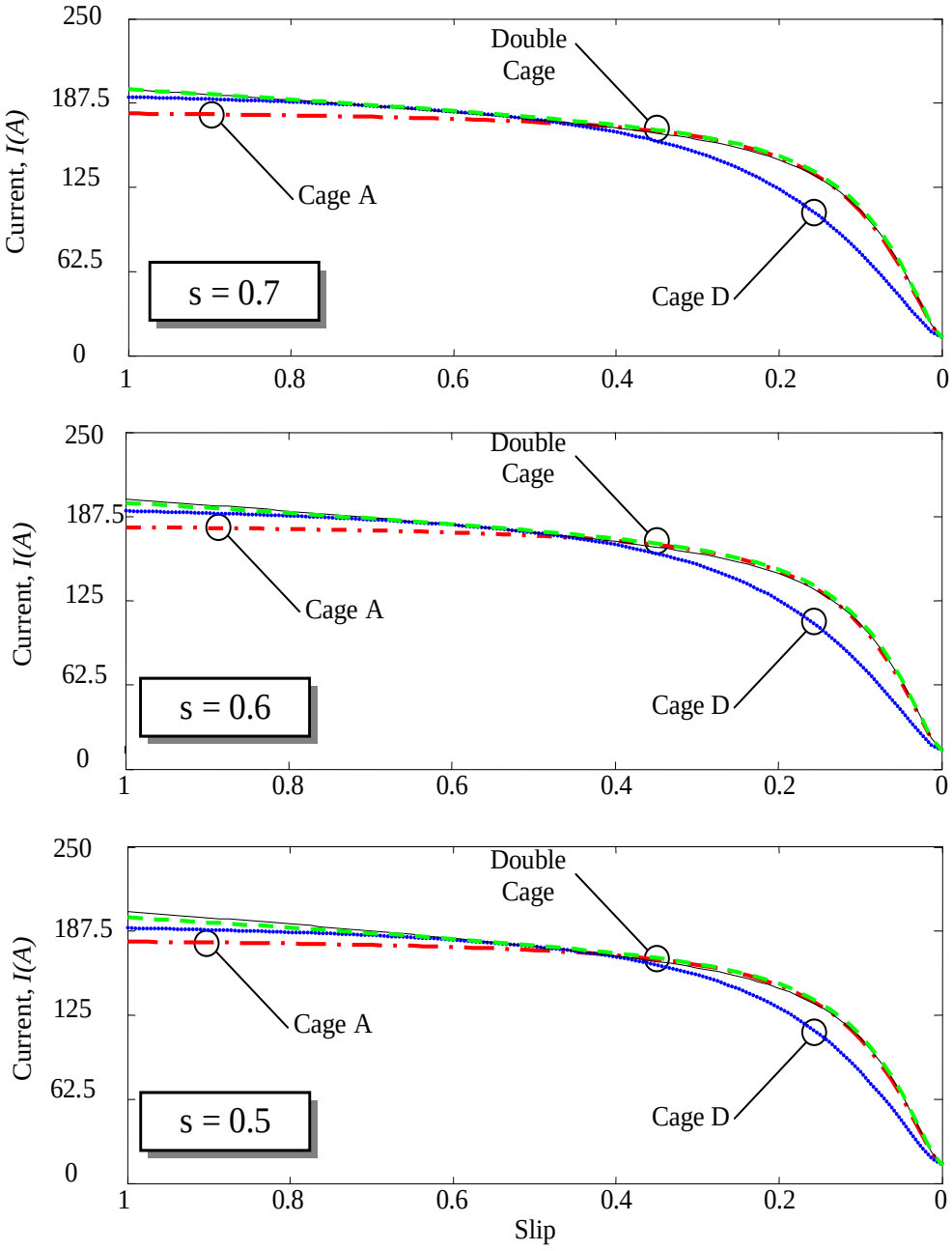

Fig. 5.10 Current of single-cage A; red 1point dashed line, current of single-cage D; blue dot line, current of estimated double-cage; black solid line and current of original double-cage; green dashed line for three cross points slips; 0.7, 0.6 and 0.5.

The Table 5.9 shows the evolution of parameter estimation in different slips or speeds with smoothing. The error of starting and no-load currents are not significant. The error of maximum torque is very low. It remains constant . The error of starting torque is sensitive to the distance of cross point (point that double cage torque and single cage D torque cross in it) from starting slip (zero speed).

Table 5.9. Calculated magnitudes for error determination with smoothing for machine 2 (22k)

Slip	*D-cage*	T_m*(Nm)*	T_s*(Nm)*	I_s*(A)*	I_{NL}*(A)*
0.7	Original	164.3	110.2	197.6	14.18
	Estimated	161.6	106.8	197.6	14.18
	Relative Error%	1.64	3.08	0	0
0.6	Original	164.3	110.2	197.6	14.18
	Estimated	161.6	116.5	200.3	14.18
	Relative Error%	1.64	5.71	1.36	0
0.5	Original	164.3	110.2	197.6	14.18
	Estimated	161.6	119.4	201.9	14.18
	Relative Error%	1.64	8.34	2.17	0

5.5 Double cage estimation of machine 3

In this study double-cage machine 3 of Table 5.1 is estimated by method of two single cages (A and D) estimation.

Cage A is a single cage that its torque and current pass from maximum torque point until steady state region of double-cage torque and current and can be estimated by two-points method using F-solve function of MATLAB using transient stator data and mechanical rotor speed. Starting region of machine has high frequency oscillations in dynamic transient region and after smoothing a starting cage is estimated that its torque and current pass from two points of torque and current of double-cage; one point is very near to this region, but not exactly in this region and the other is in the steady-state region. Three starting - cages are estimated for slips 0.7, 0.6 and 0.5 which are called Cages D_1, D_2 and D_3 or C (half speed) respectively for comparison. The comparison between starting-cages shows that the best estimation is for slip equal to 0.7.

5.5.1 Estimation of cage A for machine 3

The two-points-method is used for estimation of single-cage A but this technique needs initial value parameters so that 3-points-regression-method is used for approximated initial values estimation. The three points of regression method for estimation of initial cage A are, maximum torque point, region 2 point between maximum torque and the steady-state region and finally the steady-state point. The two-points method points are maximum torque and steady state points. The results of the initial and main estimated parameters of cage A are in Table 5.10.

Table 5.10. Parameters of single cage A induction machine 3 (500kW) with f_s=50(Hz) and V_{ph}=220V J=13

Estimation	R_s	X_{sd}	X_m	R'_r	T_m	T_s	I_s	I_n
Initial regression	0.0024Ω	0.0270	0.7583	0.0024	3896.3	362.0412	4132.5	280.1642
Main F-solve	0.0012	0.0271	0.7582	0.0024	3963.2	366.8746	4126	280.1652

Fig. 5.11.a shows machine 3 (500kW) starting transient *d, q* currents in red point line and its smoothing in gray solid line. Fig. 5.11.b is the machine 3 (500kW) mechanical rotor speed in red point line and its smoothing in gray solid line. The estimation of near starting single-cage is done by smoothing of near starting point because near to the starting region has lower magnitudes of oscillation than starting region. Then the initial starting cage D for initial value of two-points method is estimated using 3-points-regression-method and near starting, near steady-state and steady-state points. Then with near starting and

steady-state points and two points method, cage D parameters are estimated that are presented in next section.

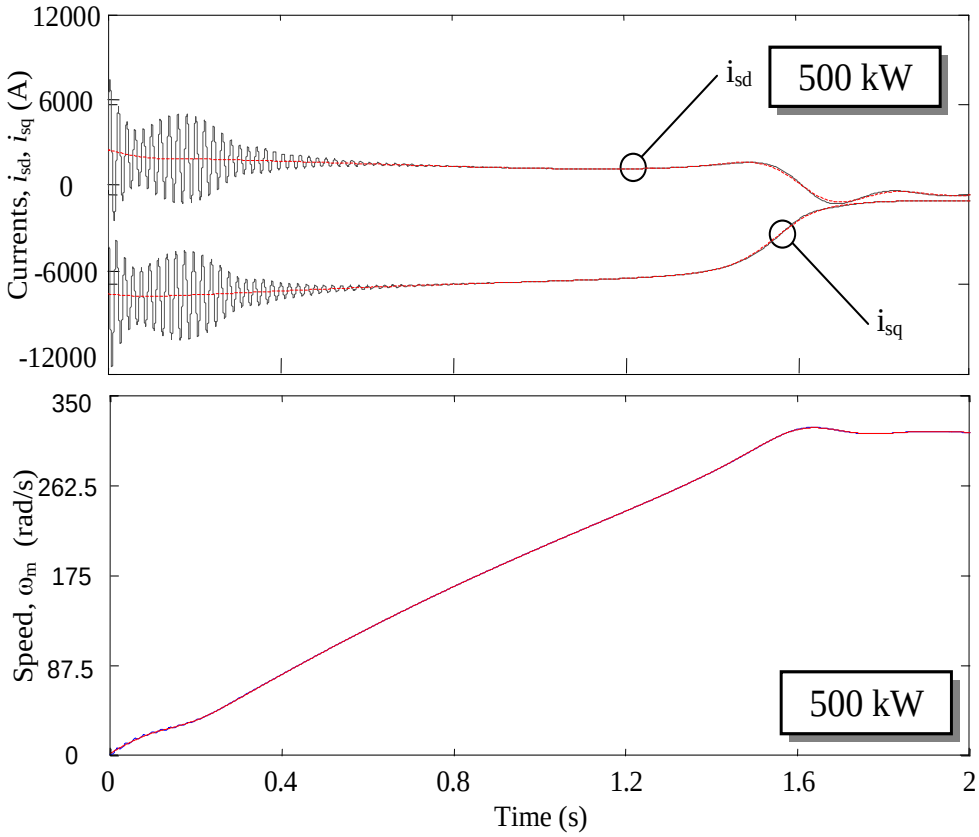

Fig. 5.11.a. *d, q* currents for machine 3; black line and smoothed *d, q* currents for machine 3; red dashed line and 5.11.b. Speed for machine 3; black line and smoothed speed for machine 3; red dashed line.

5.5.2 Estimation of cage D for machine 3

Three starting-cages D_1, D_2 and D_3 are estimated for slips of Table 5.11 while synchronous frequency is 50[Hz].

The method of estimation is two-points that needs initial value. In this method two important points for estimation are the maximum and the steady-state points. The regression three points method is applied for approximated cage D initial value estimation. The three important points in this method are the starting point at the defined slip, the second region point very near to the third region that is a approximated point and the steady-state region point.

The two points method for estimation of cage D are near starting torque and steady state points.

Table 5.11 shows the results of initial parameter estimation of single-cage D by regression method and real parameter estimation using two points method for three slips; 0.7, 0.6 and 0.5.

Then the steady-state impedance equations of double cage estimation using two points method are solved to produce double cage parameters according to the Table 5.12. The results of estimated parameters of double-cage are very near to the real data of machine 3 in Table 5.1.

This Table shows good estimation. The equality restriction $X_{2d}=X_{sd}$ according to the literature [25], must be used.

Table 5.12. Parameters of Double cage induction machine 3 (500kW) with *fs*=50(Hz) and *J*=13

s	R_s	R'_{r1}	R'_{r2}	X_m	$X_{sd} = X_{r2}$	X_{r1}	V_{ph}	$\wp$
0.7	0.0012	0.0025	0.0418	0.7660	0.0193	0.0400	220	1
0.6	0.0012	0.0025	0.0401	0.7653	0.0200	0.0394	220	1
0.5	0.0012	0.0025	0.0377	0.7645	0.0208	0.0386	220	1

Table 5.11. Parameters of single cage D induction machine 3 (500kW) with f_s=50(Hz), V_{ph}=220V and *J*=13

Estimation	s	R_s	X_{sd}	X_m	R'_r
Initial regression	0.7	0.0025	0.0222	0.7630	0.0015
Main Two points	0.7	0.0012	0.0221	0.7631	0.0102
Initial regression	0.6	0.0024	0.0230	0.7622	0.0016
Main Two points	0.6	0.0012	0.0229	0.7623	0.0087
Initial regression	0.5	0.0023	0.0238	0.7614	0.0017
Main Two points	0.5	0.0012	0.0237	0.7615	0.0072

In Fig. 5.12 red 1point dashed line is torque of cage A, blue dot line is torque of cage D, black solid line is estimated torque of double-cage and green dashed line is original torque of double-cage from starting to synchronous slips. This figure shows cages D_1, D_2, D_3 and double-cage torques have intersection in slip 0.7, 0.6 and 0.5 respectively for machine 3.

In Fig. 5.13 red 1point dashed line is current of cage A, blue dot line is current of cage D, black solid line is estimated current of double-cage and green dashed line is original current of double-cage from starting to synchronous slips. In This figure cages D_1, D_2 and D_3 currents and double-cage current have intersection in slips 0.7, 0.6 and 0.5 respectively for machine 3

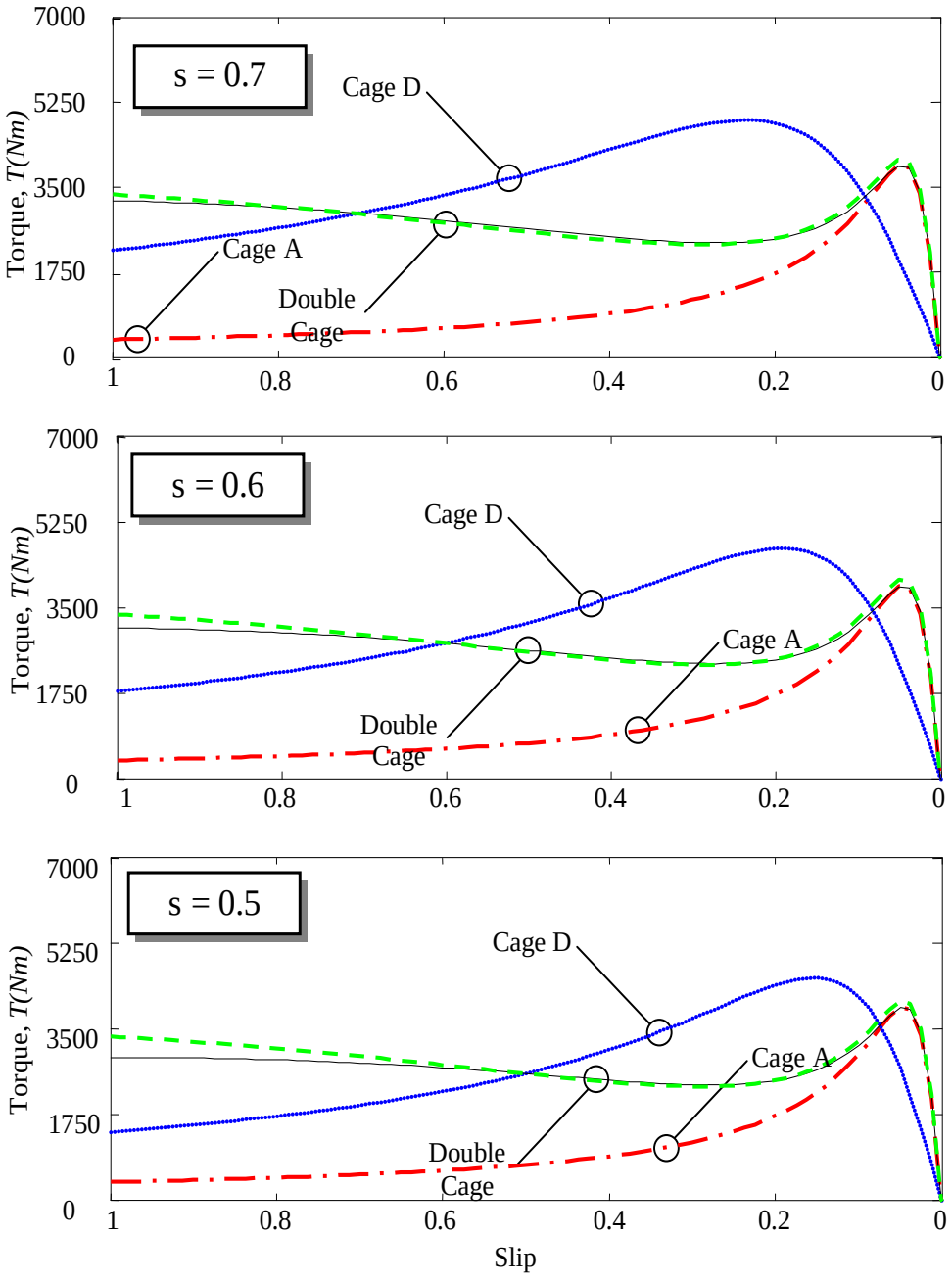

Fig. 5.12 Torque of single-cage A; red 1point dashed line, Torque of single-cage D; blue dot line, Torque of estimated double-cage; black solid line and Torque of original double-cage; green dashed line for three cross points slips; 0.7, 0.6 and 0.5.

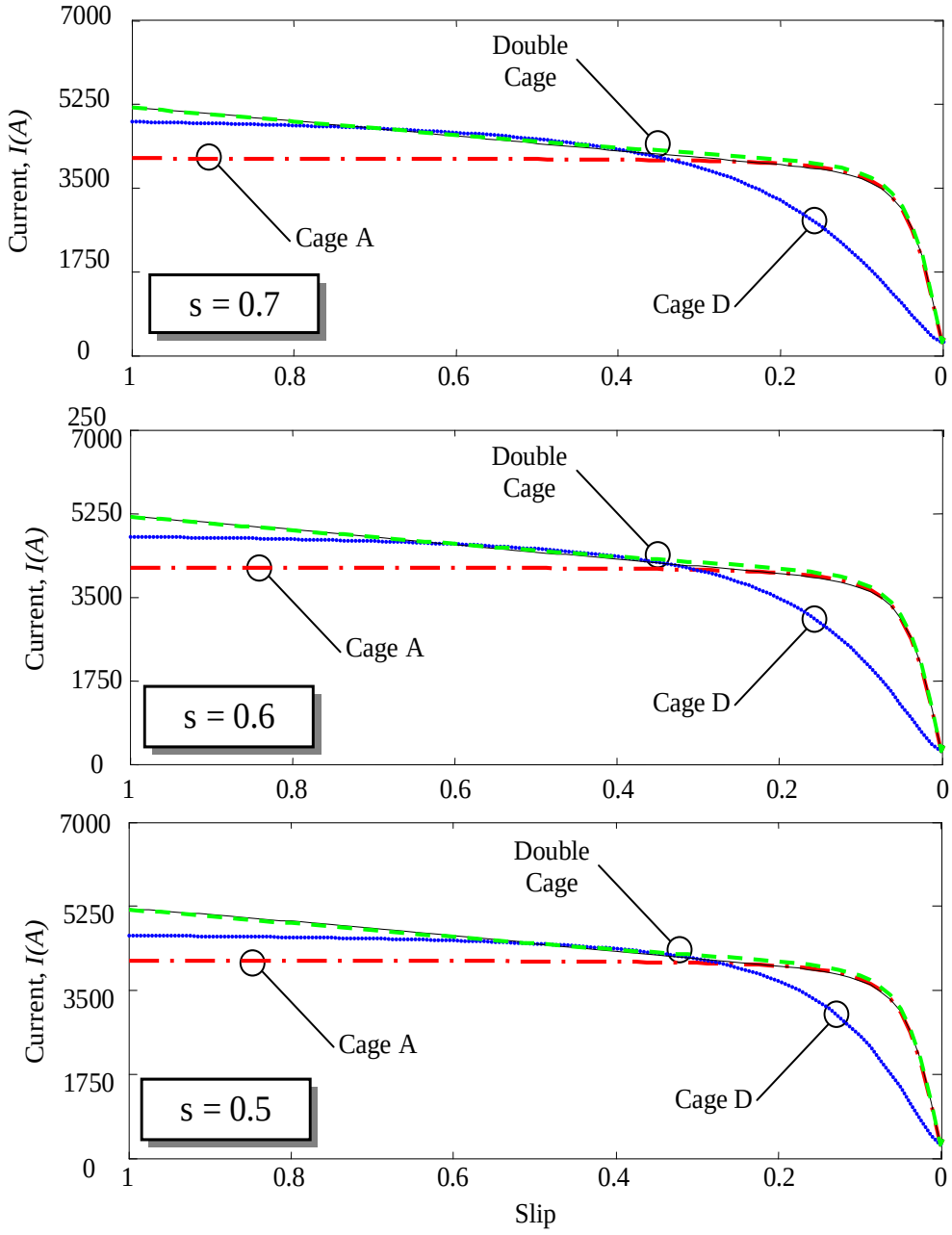

Fig. 5.13 Current of single-cage A; red 1point dashed line, Current of single-cage D; blue dot line, Current of estimated double-cage; black solid line and Current of original double-cage; green dashed line for three cross points slips; 0.7, 0.6 and 0.5.

The Table 5.13 shows the evolution of parameters estimation in different slips or speeds with smoothing.

The error of starting and no-load currents are not significant. The error of maximum torque is very low and remains constant . The error of starting torque is sensitive to the distance of cross point (point that double cage torque and single cage D torque cross) from starting slip (zero speed).

Table 5.13. Calculated magnitudes for error determination with smoothing for machine 3 (500k)

Slip	*D-cage*	T_m(Nm)	T_s(Nm)	I_s(A)	I_{NL}(A)
0.7	Original	4063	3349	5182	280.1
	Estimated	3934	3224	5182	280.1
	Relative Error%	3.175	3.7325	0	0
0.6	Original	4063	3349	5182	280.1
	Estimated	3929	3081	5182	280.1
	Relative Error%	3.2981	8.0024	0	0
0.5	Original	4063	3349	5182	280.1
	Estimated	3935	2910	5182	280.1
	Relative Error%	3.1504	13.1084	0	0

6. Method of double cage parameter estimation using instantaneous power, voltage and current

6.1 Relation between transient and steady-state magnitudes.

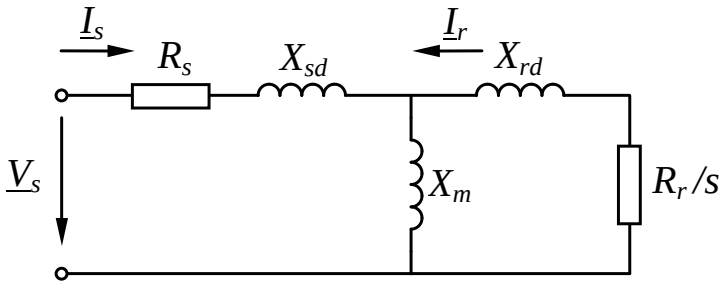

Fig. 6.1. Steady-state equivalent circuit for the single-cage model of the three-phase induction motor

The steady-state single-phase circuit of Fig. 6.1 shows that the active power consumed by the induction motor in steady-state is

$$P = 3.\mathrm{Re}\left[\underline{V}_s.\underline{I}_s^*\right] = 3.R_s.I_s^2 + 3\frac{R_r}{s}I_r{}^2 \tag{171}$$

The torque expression in steady-state results

$$\Gamma = \frac{3.\wp}{\omega_s}\frac{R_r}{s}I_r^2 \tag{172}$$

where the synchronous speed is $\omega_s = 2.\pi.f_s$ and the number of pair of poles is $\wp$. Then, the mechanical power and rotor loss are called synchronous power that is

$$\frac{\Gamma\omega_s}{\wp} = 3\frac{R_r}{s}I_r^2 \tag{173}$$

and the synchronous power and consequently the torque can be calculated in steady-state as

$$\frac{\Gamma\omega_s}{\wp} = 3\frac{R_r}{s}I_r^2 = P - 3.R_s.I_s^2 \tag{174}$$

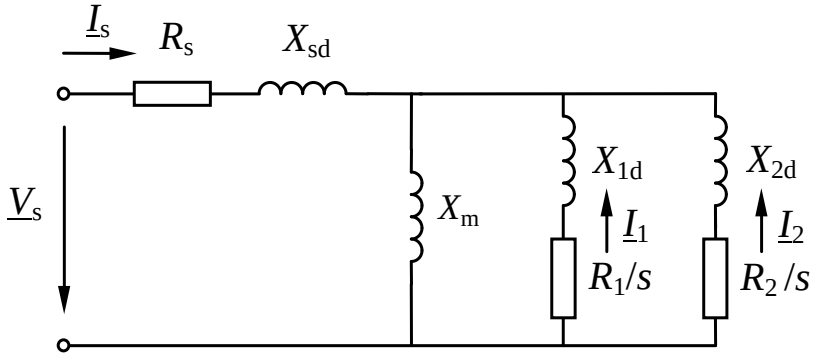

Fig. 6.2. Steady-state equivalent circuit for the double-cage model of the three-phase induction motor

The steady-state single-phase circuit of Fig. 6.2 shows the double-cage model where the active power consumed by the induction motor is

$$P = 3.\mathrm{Re}\left[\underline{V}_s.\underline{I}_s^*\right] = 3.R_s.I_s^2 + 3\frac{R_1}{s}I_1^2 + 3\frac{R_2}{s}I_2^2 \tag{175}$$

The torque expression in steady-state is

$$\Gamma = \frac{3.\wp}{\omega_s}\frac{R_1}{s}I_1^2 + \frac{3.\wp}{\omega_s}\frac{R_2}{s}I_2^2 \tag{176}$$

where the synchronous speed is $\omega_s = 2.\pi.f$ and the number of pair of poles is $\wp$. Then, the synchronous power in the double-cage model results

$$\frac{\Gamma\omega_s}{\wp} = 3\frac{R_1}{s}I_1^2 + 3\frac{R_2}{s}I_2^2 \tag{177}$$

and the steady-state torque Γ and consequently the synchronous power $\frac{\Gamma\omega_s}{\wp}$ can be calculated with

$$\frac{\Gamma\omega_s}{\wp} = 3\frac{R_1}{s}I_1^2 + 3\frac{R_2}{s}I_2^2 = P - 3.R_s.I_s^2 \tag{178}$$

It must be mentioned that the steady-state equivalent circuit is not exactly valid for transient phenomena, but an approximation of the synchronous power can be used from instantaneous values of starting transient data. Using the instantaneous values of voltage; $v_s(t)$ and current; $i_s(t)$, the instantaneous power; $P_{in}(t)$ is calculated with

$$P_{in}(t) = v_{sa}(t).i_{sa}(t) + v_{sb}(t).i_{sb}(t) + v_{sc}(t).i_{sc}(t) \tag{179}$$

and also the stator instantaneous loss can be calculated as

$$P_{stator}(t) = R_s\left(i_{sa}^2(t) + i_{sb}^2(t) + i_{sc}^2(t)\right) \tag{180}$$

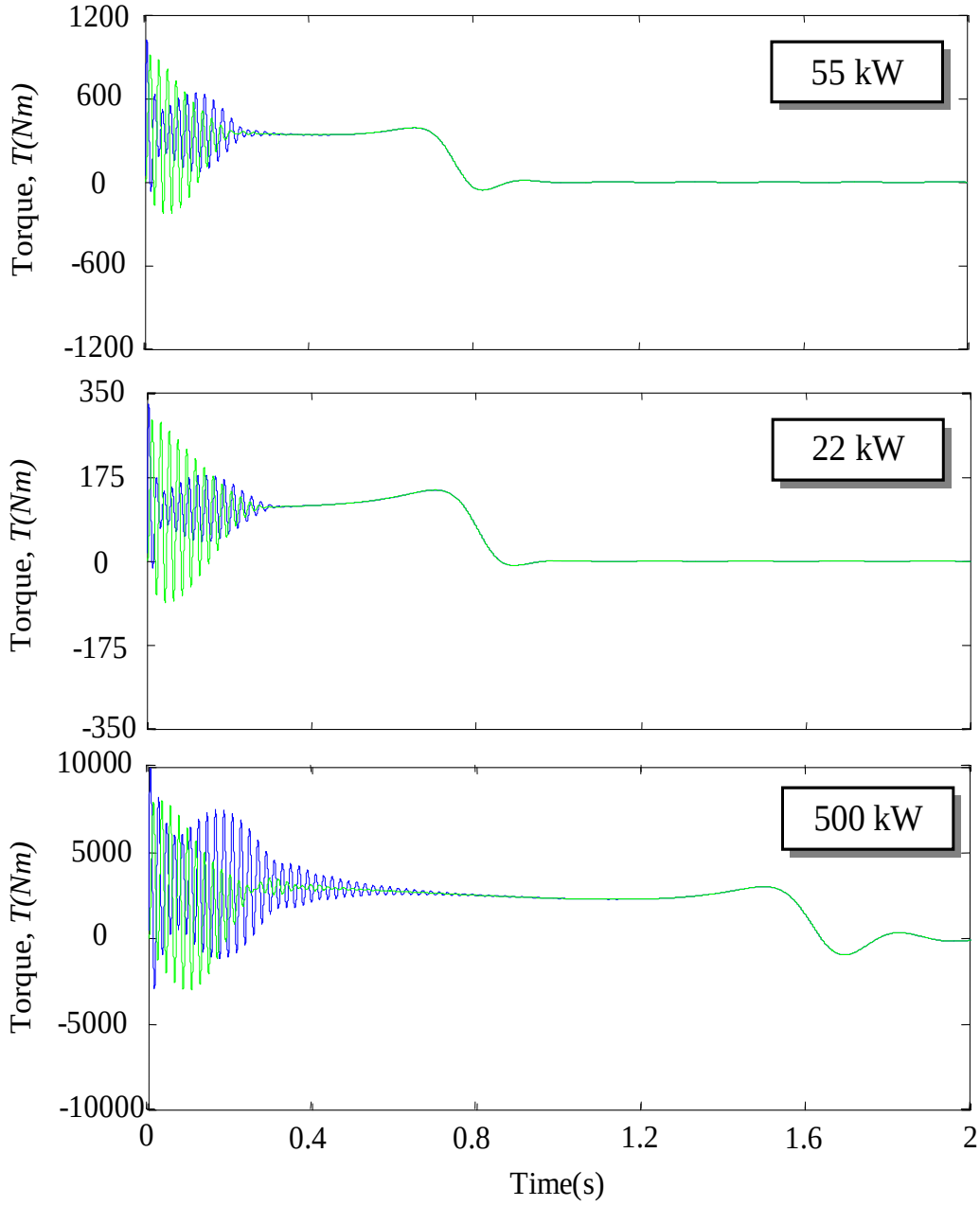

Fig. 6.3. Transient torque (green solid lines) and torque from instantaneous input power (blue solid lines) for three machines.

and an estimation of the instantaneous torque; $\Gamma_{in}(t)$ can be calculated with the expression

$$\Gamma_{in}(t)=\frac{\wp.\left[P_{in}(t)-P_{stator}(t)\right]}{\omega_s}=\frac{\wp}{\omega_s}\left[\left(v_{sa}(t).i_{sa}(t)+v_{sb}(t).i_{sb}(t)+v_{sc}(t).i_{sc}(t)\right)-R_s\left(i_{sa}^2(t)+i_{sb}^2(t)+i_{sc}^2(t)\right)\right] \quad (181)$$

Equation (181) is calculated with instantaneous data and equation (178) is justified with the steady-state-circuit. Equation (181) do not fit exactly the instantaneous torque from a transient because the steady-state circuit is not valid during the transient starting.

In Table 6.1, there are the data of three induction motors. With these parameters, the starting transient can be simulated with the software Power Systems Blockset of Matlab [31], and with the results of the

Table 6.1. Parameters of three double cage machines with f_s=50(Hz) and V_{ph}=220V

S_n	R_s	X_s=X_{2d}	X_m	R_{r1}	R_{r2}	X_{1d}	$\wp$	J
55 kVA	0.0338	0.1698	0.3084	0.0465	0.40747	0.3511	1	0.8
22kVA	0.13	0.5404	14.9770	0.1689	1.2269	0.8503	1	0.3
500kVA	0.0012	0.0179	0. 7674	0.0024H	0.0482	0.0391	1	13

simulation, the torque estimation proposed in equation (181) can be calculated and compared with the true simulated torque value in Fig. 6.3.

Fig. 6.3 shows the starting transients of these three motors. In these figures the transient torque (from simulation) and the estimated instantaneous torque proposed with the equation (181) are shown. In the first part of the starting transient, named the electromagnetic transient, there are important oscillations and a significant difference can be observed between the instantaneous torque and the approximation of it proposed in the equation (181). Although, Fig. 6.3 shows true and instantaneous torques, there are a surprising coincidence between the instantaneous torque and the estimated torque of equation (181) during the mechanical transient and steady-state regions.

Fig. 6.4 shows the torque slip curve of the steady-state torque and the estimation of the torque from equation (181) versus the slip. The comparison of the estimated torque- and steady state torque-speed curves shows a very good agreement between them when the oscillations of the electromagnetic transient are finished until the maximum torque zone. In Fig. 6.4 it can be observed the phenomena that the maximum instantaneous torque is always lower that the maximum steady-state torque.

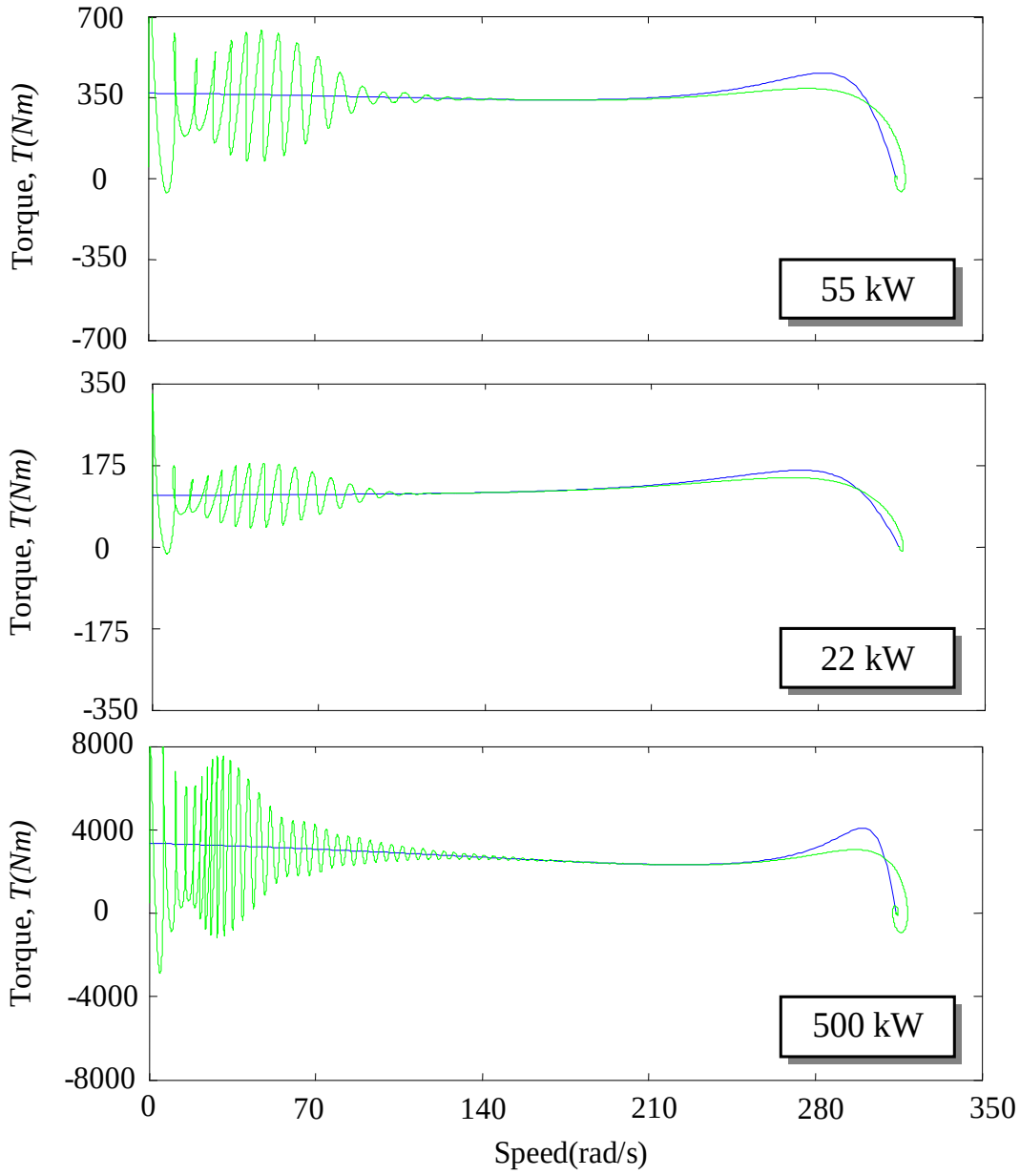

Fig. 6.4. Instantaneous torque (green solid lines) and the steady-state torque (blue solid lines) for three machines.

Fig. 6.5 shows the steady-state torque and the estimation of the torque versus the slip. The estimated torque is calculated with the instantaneous magnitudes defined in next section using equations (182) to (187). These equations average the magnitudes or eliminate the electromagnetic oscillations.

It can be observed in Fig. 6.5 that near to the zero speed, there are differences between the averaged estimated torque and the steady-state torque.

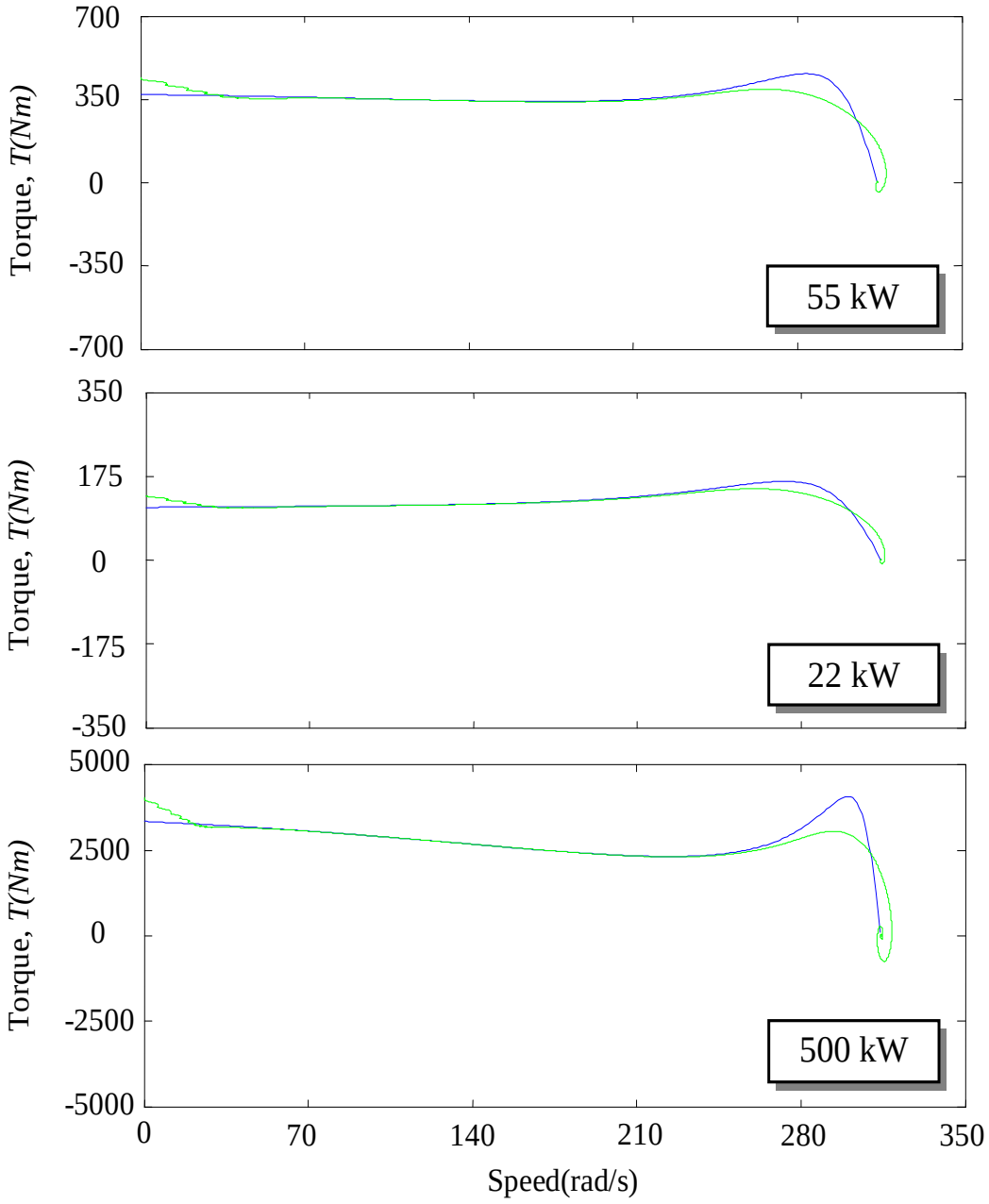

Fig. 6.5. Smoothed torque (green solid lines) and steady-state torque (blue solid lines) for three machines.

It is very important to use the averaged data near the zero speed for a good estimation of the starting torque. Despite the torque and power oscillate in the electromagnetic transient region, the application of the smoothing technique to the instantaneous power allows to use measured data near to the zero speed.

In Fig. 6.6 the averaging has been realized by deleting the points of the transient which are closer to the zero speed. The reason is that the averaging in the starting region has big error due to high oscillations.

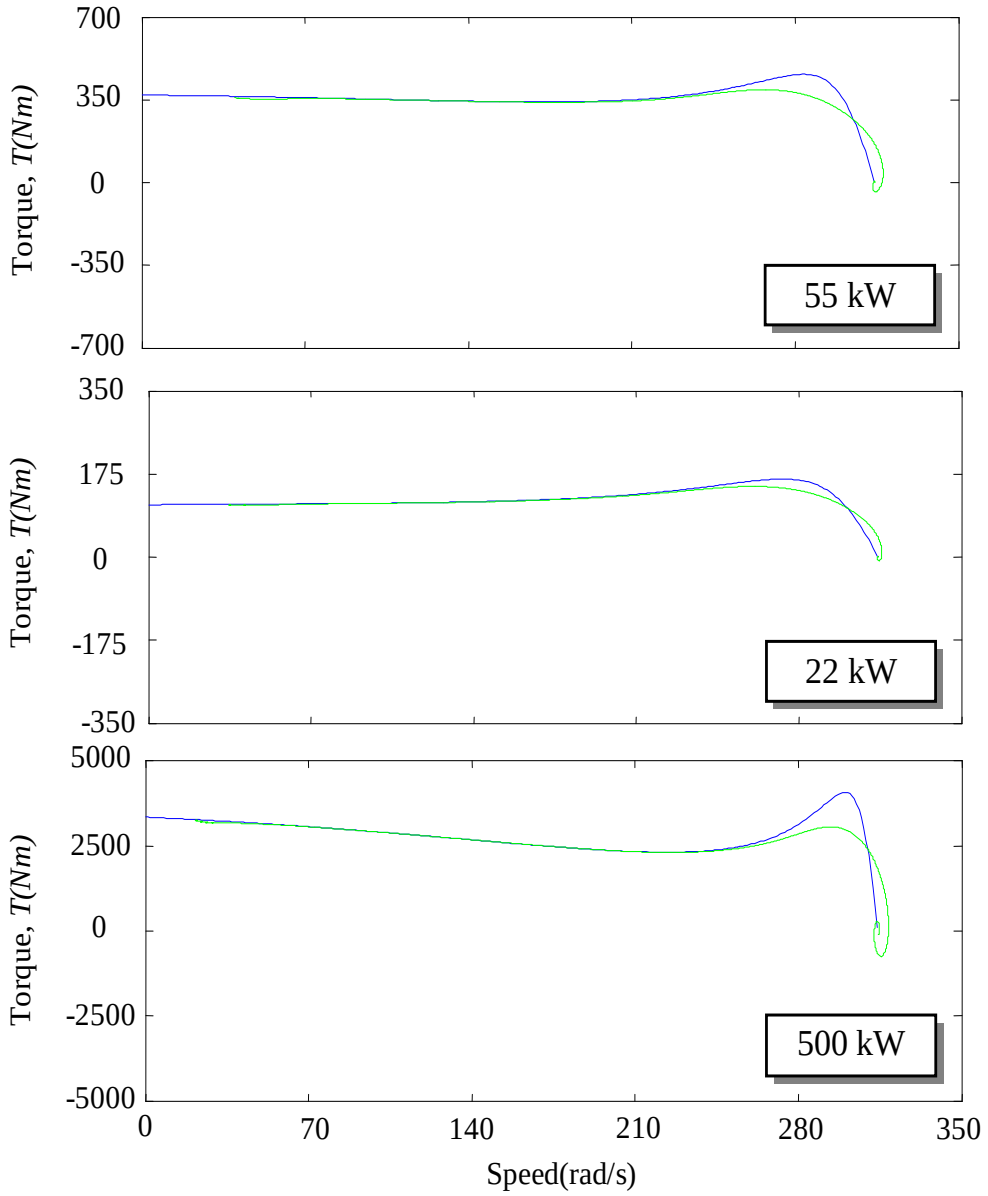

Fig. 6.6. Smoothed torque (green solid lines) with deleting starting region and steady-state torque (blue solid lines) for three machines.

Fig. 6.6 shows clearly that the proposed estimation of the instantaneous torque using the averaged magnitudes and the elimination of the points near to zero speed, has a good coincidence with steady-state torque before maximum torque point.

6.2 Averaged magnitudes

From the results shown in Figs. 6.3 to 6.5, it can be concluded that the instantaneous power can be used for parameters estimation of the double-cage induction motor. The used data is in the range from near zero speed until near the maximum torque zone. It is important to insist that the maximum torque value in a transient process is lower than the maximum torque value predicted by the steady-state model.

To avoid mixing instantaneous data and steady-state data, averaged magnitudes are defined for instantaneous data.

The instantaneous power is defined as

$$p_1(t) = v_{sa}(t) i_{sa}(t) + v_{sb}(t) i_{sb}(t) + v_{sc}(t) i_{sc}(t) \tag{182}$$

Then, the average instantaneous power function is defined as

$$P_{av}(t) = \frac{1}{T} \int_{t-\frac{T}{2}}^{t+\frac{T}{2}} p_1(t).dt \tag{183}$$

Also the averaged instantaneous current is

$$I_{av}(t) = \sqrt{\frac{1}{T} \int_{t-\frac{T}{2}}^{t+\frac{T}{2}} \left(\frac{i_{sa}^2(t) + i_{sb}^2(t) + i_{sc}^2(t)}{3} \right).dt} \tag{184}$$

and the averaged instantaneous voltage is derived from the equation

$$U_{av}(t) = \sqrt{\frac{1}{T} \int_{t-\frac{T}{2}}^{t+\frac{T}{2}} \left(\frac{v_{sa}^2(t) + v_{sb}^2(t) + v_{sc}^2(t)}{3} \right).dt} \tag{185}$$

The three phase averaged apparent power is

$$S_{av}(t) = 3 U_{av}(t).I_{av}(t) \tag{186}$$

The three phase averaged reactive power is according to

$$Q_{av}(t) = \sqrt{S_{av}^{\,2}(t) - P_{av}^{\,2}(t)} \qquad (187)$$

The star connected impedance in the steady-state is defined as

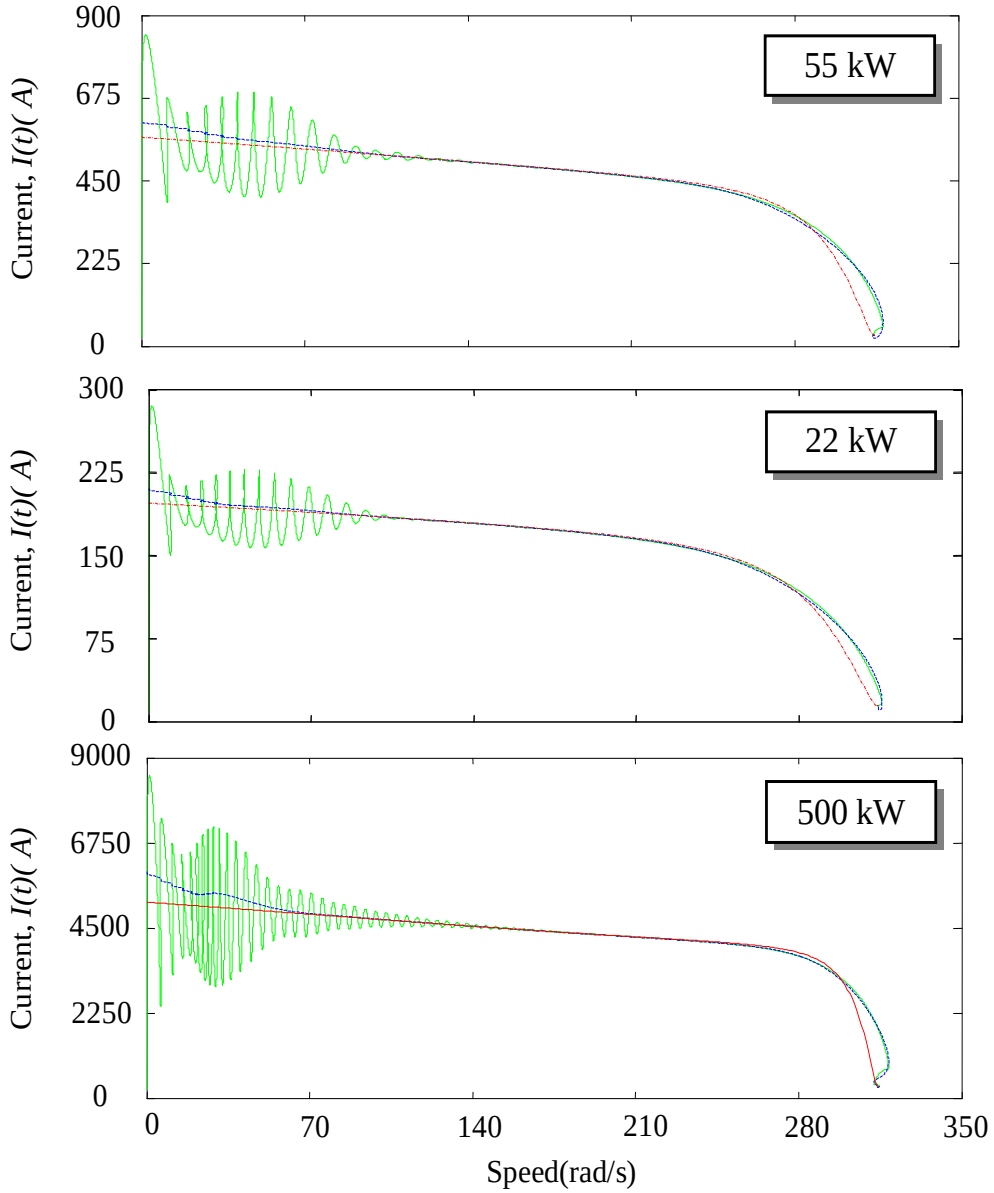

Fig. 6.7.a. Instantaneous current (green solid line) and averaged of that (blue dashed line) and steady-state stator current (red point dashed line) for machine 1,
6.7.b. Instantaneous current (green solid line) and averaged of that (blue dashed line) and steady-state stator current (red point dashed line) for machine 2
and 6.7.c. Instantaneous current (green solid line) and averaged of that (blue dashed line) and steady-state stator current (red point dashed line) for machine 3.

$$\underline{Z}(t) = \frac{3V_{ph}^{2}}{P(t) - jQ(t)} \tag{188}$$

In this method the averaged impedance is defined as

$$\underline{Z}_{av}\left(\omega_m(t)\right) = \frac{3\left(V_{ph}^{2}(t)\right)_{av}}{P_{av}(t) - jQ_{av}(t)} \tag{189}$$

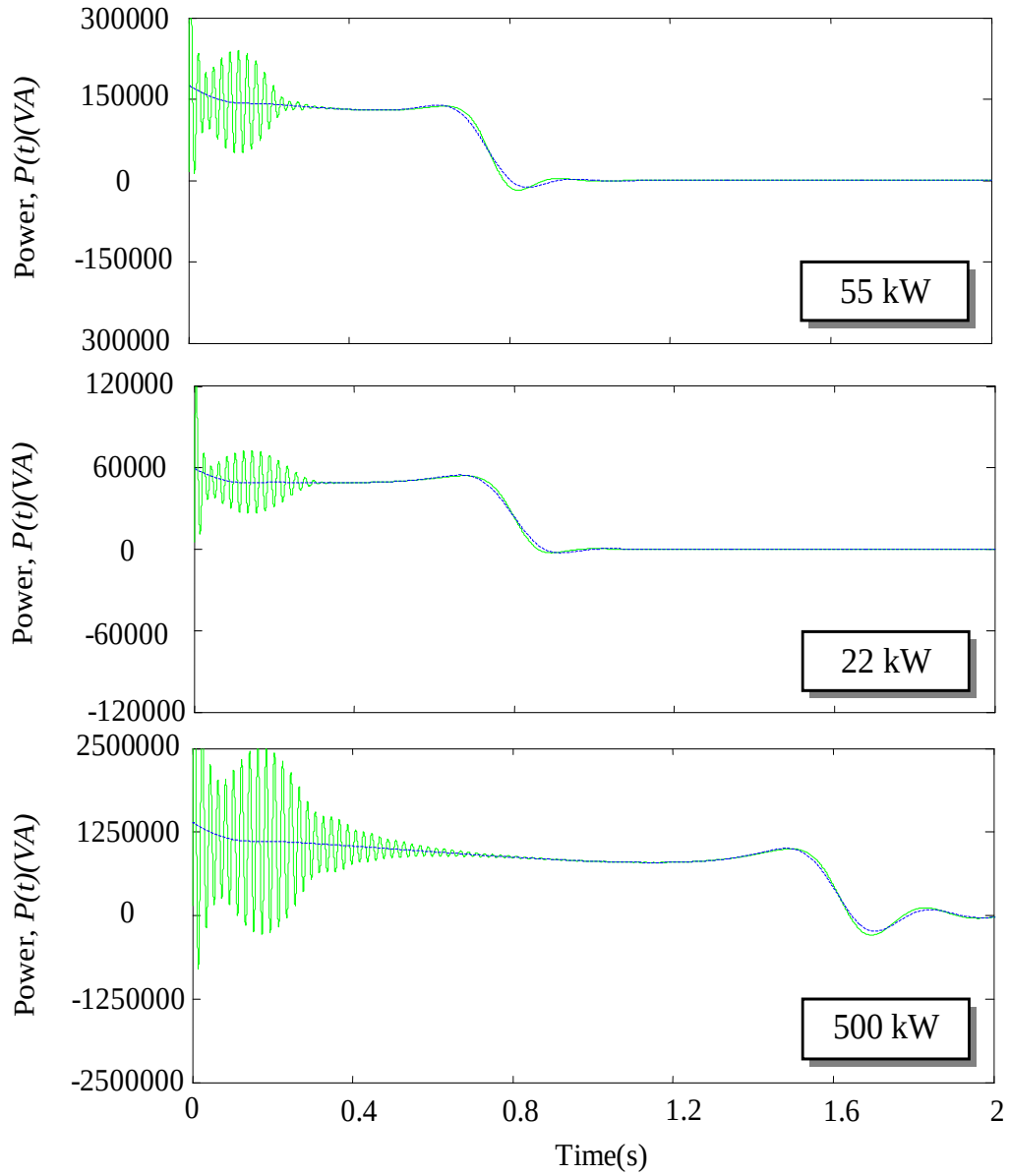

Fig. 6.8.a. Instantaneous power (green solid line) and averaged of that (blue dashed line) for machine 1, 6.8.b. Instantaneous power (green solid line) and averaged of that (blue dashed line) for machine 2 and 6.8.c. Instantaneous power (green solid line) and averaged of that (blue dashed line) for machine 3.

To clarify the above equations the averaging function of instantaneous current and power are shown in Fig. 6.7 and 6.8 respectively.

Fig. 6.7.a. shows the instantaneous current-speed (green solid line) and averaged instantaneous current-speed (blue dashed line) and steady-state stator current-speed (red point dashed line) for machine 1. In Fig. 6.7.b. and Fig. 6.7.c the similar curves are shown for machine 2 and machine 3 respectively.
Fig. 6.8.a. shows the instantaneous power-time (green solid line) and average of instantaneous power-time (blue dashed line) for machine 1. In Fig. 6.7.b. and Fig. 6.7.c the similar curves are shown for machine 2 and machine 3 respectively. These figures show that the instantaneous estimation method can give a good approximation of the torque and current after electrical transient zone until maximum power zone. This method is studied in next section by detail.

6.3 Second Proposed method: Instantaneous power method

The used starting transient data region for the estimation of the double-cage induction motor parameters with instantaneous power method is divided into two regions. One region is from the zero speed until the maximum torque point (region 1) and the other region is from the maximum torque point until the steady-state speed (region 2). The methods applied to these set of data are,

- Regression method (region 2)
- Instantaneous power method (region 1)

The regression method (equation 138) is used with data of region 2 for estimation of a single cage induction motor parameters called cage A. Fig. 6.9.a and b show the estimated single cage A torque and current in red point dashed line and torque and current of the double-cage in green dashed line respectively. Fig. 6.9.a and b show that double-cage and single-cage A have a good fitting in the region 2 from maximum torque speed to synchronous speed.

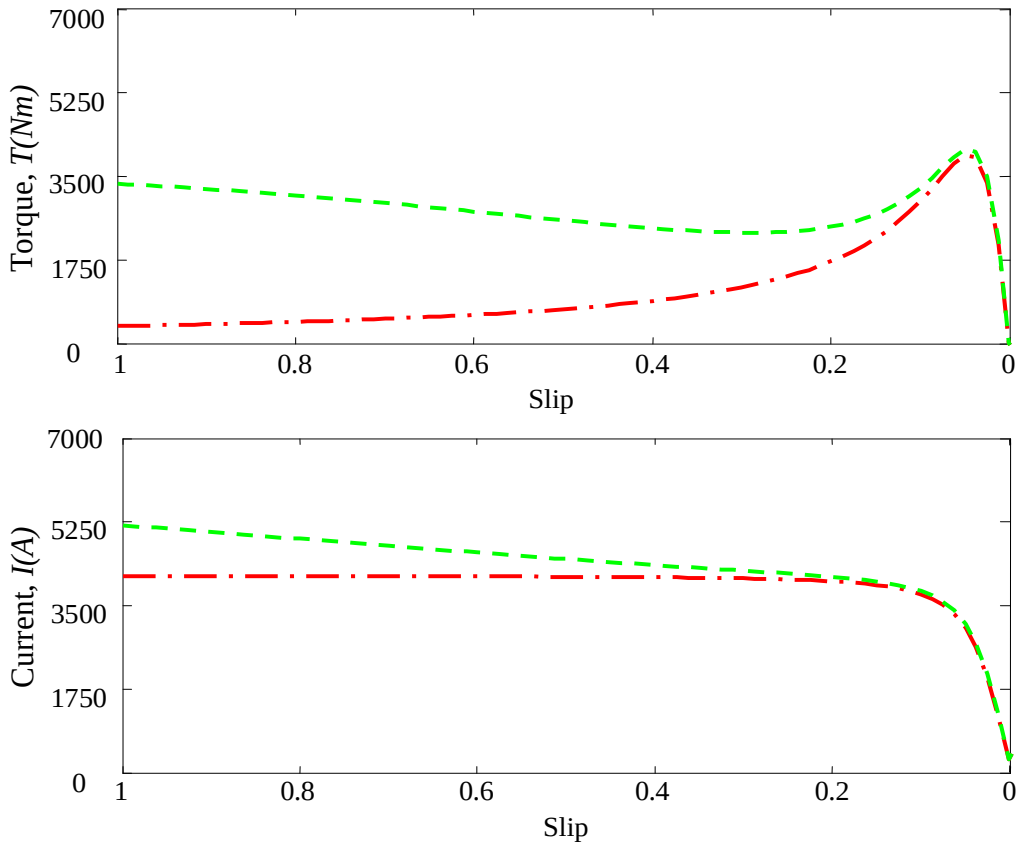

Fig. 6.9.a. Torque of single-cage A; red 1point dashed line, Torque of original double-cage; green dashed line and 6.9.b. current of single-cage A; red 1point dashed line, current of original double-cage; green dashed line

With the steady-state circuit parameters of single-cage A (estimated using the regression method), the impedance in the synchronous speed (s=0); $\underline{Z}_{NL}$ and the impedance in the maximum torque point; $\underline{Z}_{M}$ can be calculated. These two complex values of the impedances, which are equivalent to four real values (real and imaginary parts), are imposed as the values of the impedance of the steady-state double-cage circuit, in the points of no load, (s_{NL}=0) and maximum torque, (s_M). These equations are represented by

$$\begin{aligned} f_1(\mathbf{x}) &= \left(\mathrm{Re}\left(\underline{Z}_{NL}^{A}\right) - R_{NL}(\mathbf{x})\right) \Big/ \left|\underline{Z}_{NL}^{A}\right| = 0 \\ f_2(\mathbf{x}) &= \left(\mathrm{Im}\left(\underline{Z}_{NL}^{A}\right) - X_{NL}(\mathbf{x})\right) \Big/ \left|\underline{Z}_{NL}^{A}\right| = 0 \\ f_3(\mathbf{x}) &= \left(\mathrm{Re}\left(\underline{Z}_{m}^{A}\right) - R_{m}(\mathbf{x})\right) \Big/ \left|\underline{Z}_{m}^{A}\right| = 0 \\ f_4(\mathbf{x}) &= \left(\mathrm{Im}\left(\underline{Z}_{m}^{A}\right) - X_{m}(\mathbf{x})\right) \Big/ \left|\underline{Z}_{m}^{A}\right| = 0 \end{aligned} \tag{190}$$

The double-cage circuit has 6 independent parameters

$$x = (R_s,\ R_1,\ R_2,\ X_m,\ X_{sd},\ X_{1d}) \tag{191}$$

The steady state impedance of double-cage induction motor is calculated with

$$Z_{steady-state}^{dcage} = R_s + jX_s + \frac{1}{\dfrac{1}{jX_m} + \dfrac{1}{\dfrac{R_1}{s} + jX_1} + \dfrac{1}{\dfrac{R_2}{s} + jX_2}} \tag{192}$$

As equation (190) is not enough to determine parameters of (191), additional information is necessary. This is obtained from the zone where the instantaneous power fits well the steady-state synchronous torque.

The instantaneous power method uses transient data from region 1 to calculate the complex impedance value (equation 189) in one or more points in region 1.

In this method the minimum necessary data is one point data that satisfies two equations, but for a more reliable algorithm it is better to use n points that imposes 2n equations like

$$\begin{aligned} f_5(\mathbf{x}) &= w_p \left(\mathrm{Re}\left(\underline{Z}_{p,1}^{I}\right) - R_1(\mathbf{x})\right) \Big/ \left|\underline{Z}_{p,1}^{I}\right| = 0 \\ f_6(\mathbf{x}) &= w_p \left(\mathrm{Im}\left(\underline{Z}_{p,1}^{I}\right) - X_1(\mathbf{x})\right) \Big/ \left|\underline{Z}_{p,1}^{I}\right| = 0 \\ &\vdots \\ f_{2n+3}(\mathbf{x}) &= w_p \left(\mathrm{Re}\left(\underline{Z}_{p,n}^{I}\right) - R_n(\mathbf{x})\right) \Big/ \left|\underline{Z}_{p,n}^{I}\right| = 0 \\ f_{2n+4}(\mathbf{x}) &= w_p \left(\mathrm{Im}\left(\underline{Z}_{p,n}^{I}\right) - X_n(\mathbf{x})\right) \Big/ \left|\underline{Z}_{p,n}^{I}\right| = 0 \end{aligned} \tag{193}$$

where $\underline{Z}^{I}_{p,1},...,\underline{Z}^{I}_{p,n}$ are instantaneous impedances and $R_1(\mathbf{x})$, $X_1(\mathbf{x}),...,$ $R_n(\mathbf{x})$, $X_n(\mathbf{x})$ are real and imaginary parts of double-cage respectively. These 2n equations are coming from the instantaneous power algorithm that applies averaging process in the starting region to eliminate oscillations in the electrical transient region. The equations of (193) use weights w_p to reduce the influence of the points of the instantaneous power method in comparison with the influence of the points of the regression method.

6.4 Double-cage machine 1 estimation

The proposed method for double-cage parameters estimation using the instantaneous power method is applied to the machine 1 with power 55kW of Table 6.1. The starting transient has been simulated using the SimPowerSystems Blockset of Matlab [33].

First the regression method is applied to the transient data to the points in the region between the maximum torque point and the steady-state speed. Then single-cage A approximation is obtained. Estimation of cage A has been calculated with equation (138).

The results of cages A estimation for the machine 1 of Table 6.1 are presented in Tables 6.2.

Using parameters of Table 6.2, the impedances; Z_{nl} and Z_m for single-cage A have been calculated and their values are presented in Table 6.3.

Fig. 6.10 shows the good fitting of torque of cage A (in part a) and current of cage A (in part b)with the steady-state torque and current curves of the original double cage of machine 1 in the zone between the maximum torque speed and the synchronous speed (zone 2).

Table 6.2. Parameters of single cage A induction machine 1 (55kW) with f_s=50(Hz), V_{ph}=220V and J=0.8

Estimation	R_s	X_{sd}	X_m	R_r	T_m	T_s	I_s	I_n
Regression	0.0338	0.2303	7.2479	0.0450	446.1192	92.2838	478.0909	29.4185

Table 6.3. $\underline{Z}_{nl}$ and $\underline{Z}_m$ for single-cage A of machine 1 (55kW) with f_s=50(Hz), V_{ph}=220V and J=.8

Real($\underline{Z}_{nl}$)	*Imag*($\underline{Z}_{nl}$)	*Real*($\underline{Z}_m$)	*Imag*($\underline{Z}_m$)
0.0338	7.4782	0.4550	0.4789

Then instantaneous method that uses equation (189), estimates some impedances during mechanical transient region before maximum torque point. These impedances are presented in Table 6.4 for 5 points.

Then using maximum and no-load impedances of cage A and impedances of instantaneous method with a typical weight equal to 0.04 in equation (190) and (193) respectively, these set of equation are solved using F-solve function of MATLAB to estimate the double-cage parameters of machine 1. The estimated parameters are shown in Table 6.5. The steady-state torque-speed and current-speed curves with

Table 6.4. Instantaneous impedances of double cage machine1 with f_s=50(Hz) and V_{ph}=220V

Points	P_1	P_2	P_3	P_4	P_5
Rotor Speed	83.57	118.6	150.2	181.8	209.3
$Re(\underline{Z}_{approx})$	0.1654	0.1726	0.1791	0.1887	0.203
$Im\ (\underline{Z}_{approx})$	0.3789	0.3929	0.4052	0.4184	0.4306

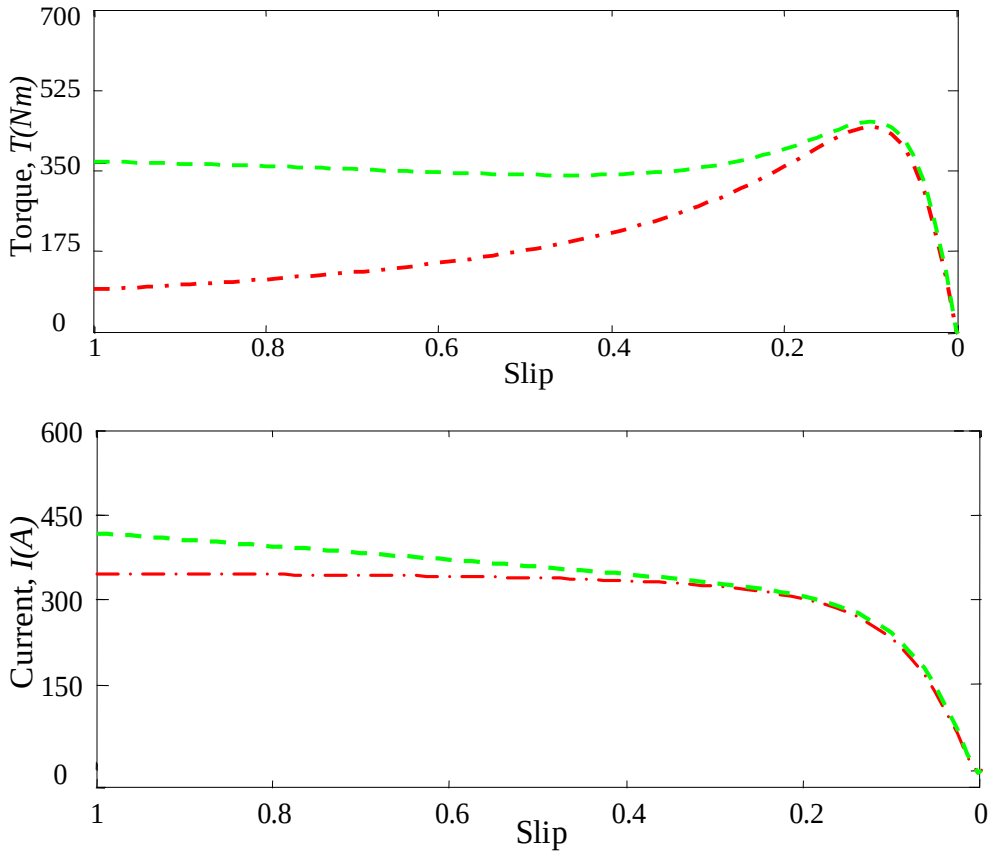

Fig. 6.10.a. Torque of single-cage A; red 1point dashed line and torque of original double-cage; green dashed line and 6.10.b. Current of single-cage A; red 1point dashed line and current of original double-cage; green dashed line.

parameters of Table 6.5 are seen in Fig. 6.11.

In the Fig. 6.11.a and b the red solid lines are original double cage torque and current and the black dashed lines are estimated double-cage torque and current respectively. The fitting between the original and estimated curves are very good.

Table 6.5. Parameters of double cage machine 1 with f_s=50(Hz), V_{ph}=220V and weight=0.04

Double-cage	R_s	$X_s=X_{2d}$	X_m	R_{r1}	R_{r2}	X_{1d}	$\wp$	J
Real	0.0338Ω	0.1698	7.2787	0.0465	0.40747	0.3511	1	0.8
Estimated	0.03206	0.1858	7.2922	0.0498	0.3482	0.3627	1	0.8

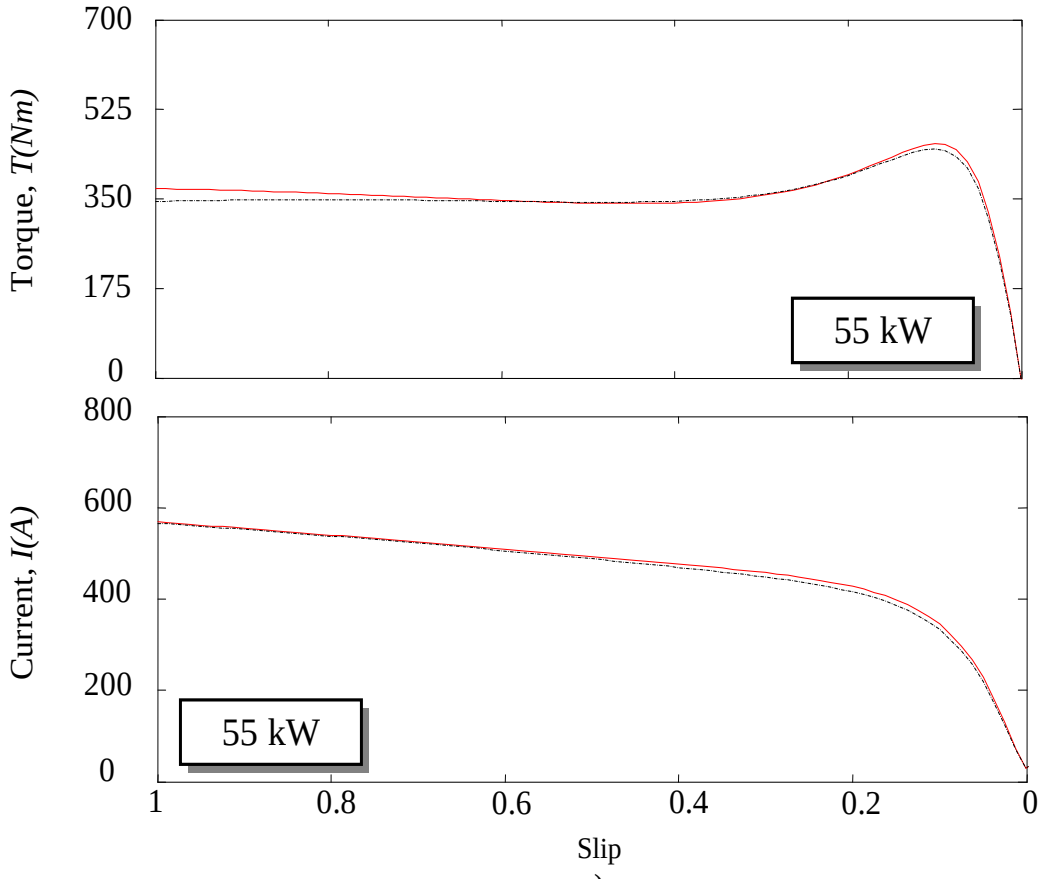

Fig. 6.11.a. Original torque(red solid line) and steady-state torque from estimated double cage parameters (black dashed line)for machine 55kW and 6.11.b. Original current (red solid line) and steady-state current from estimated double cage parameters (black dashed line)for machine 55kW for weight=0.04.

The relative errors of the estimation are presented in Table 6.6 that are 6.67% for starting torque, 2.14% for maximum torque and zero for starting and no-load currents respectively in machine 1.

Table 6.6. Calculated magnitudes for error determination for machine 1 (55k)

P(kW)	*D-cage*	T_m*(Nm)*	T_s*(Nm)*	I_s*(A)*	I_{NL}*(A)*
55	Original	457.8	370.0	568.8	29.42
	Estimated	448	345.3	568.8	29.42
	Real Error	0.0214	0.0667	0	0

6.5 Double-cage machine 2 estimation

The proposed method for double-cage parameters estimation using the instantaneous power method is applied to the machine 2 with power 22kW of Table 6.1. The starting transient has been simulated using the SimPowerSystems Blockset of Matlab [33].

First the regression method is applied to the transient data to the points in the region between the maximum torque point and the steady-state speed. Then single-cage A is estimated. Estimation of cage A has been calculated with equation (138).

The results of cages A parameters estimation for the machine 2 of Table 6.1 are presented in Tables 6.7.

Using parameters of Table 6.7, the impedances Z_{nl} and Z_m for single-cage A have been calculated and their values are presented in Table 6.8.

Fig. 6.12 shows the good fitting of cage A torque(in part a) and cage A current (in part b) with the steady-state torque and current curves of the original double cage of machine 2 in the zone between the maximum torque speed and the synchronous speed (zone 2).

Table 6.7. Parameters of single cage A induction machine 2 (22kW) with f_s=50(Hz), V_{ph}=220V and J=0.3

Estimation	R_s	X_{sd}	X_m	R_r	T_m	T_s	I_s	I_n
Regression	0.1300	0.6077	14.9097	0.1567	161.7923	44.6079	179.7107	14.1771

Table 6.8. Z_{nl} and Z_m for single-cage A of machine 2 (22kW) with f_s=50(Hz), V_{ph}=220V and J=0.3

Real($\underline{Z}_{nl}$)	*Imag*($\underline{Z}_{nl}$)	*Real*($\underline{Z}_m$)	*Imag*($\underline{Z}_m$)
0.1300	15.5174	1.2798	1.2845

Then instantaneous method that uses impedance equation (189), estimates some impedances during mechanical transient region before maximum torque point. These impedances are presented in Table 6.9 for 5 points.

Then using maximum and no-load impedances of cage A and impedances of instantaneous method with a typical weight equal to 0.04 in equation (190) and (193) respectively, these set of equation are solved using F-solve function of MATLAB to estimate the double-cage parameters of machine 2.

Table 6.9. Instantaneous impedances of double cage machine2 with f_s=50(Hz) and V_{ph}=220V

Points	P_1	P_2	P_3	P_4	P_5
Rotor Speed	83.57	118.6	150.2	181.8	209.3
$Re(Z_{approx})$	0.4645	0.4898	0.5191	0.5641	0.6278
$im(Z_{approx})$	1.076	1.101	1.124	1.149	1.175

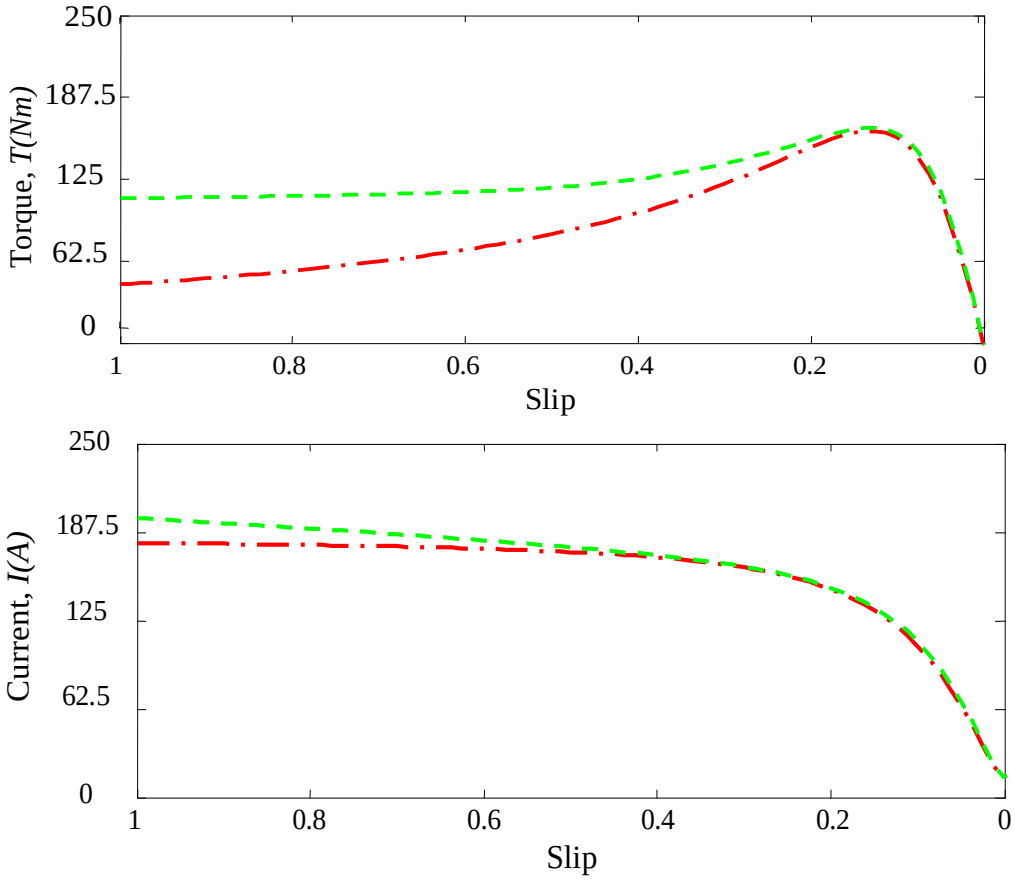

Fig. 6.12.a. Torque of single-cage A; red 1 point dashed line and torque of original double-cage; green dashed line and 6.12.b. Current of single-cage A; red 1 point dashed line and current of original double-cage; green dashed line

The estimated parameters are shown in Table 6.10. The steady-state torque-speed and current-speed curves with parameters of Table 6.10 are shown in Fig. 6.13.

Table 6.10. Parameters of double cage machine 2 with f_s=50(Hz), V_{ph}=220V and weight=0.04

Double-cage	R_s	X_s=X_{2d}	X_m	R_{r1}	R_{r2}	X_{1d}	$\wp$	J
Real	0.1300Ω	0.5404	14.977	0.1689	1.2269	0.8503	1	0.3
Estimated	0.1287	0.5773	14.9400	0.1777	1.0544	0.8666	1	0.3

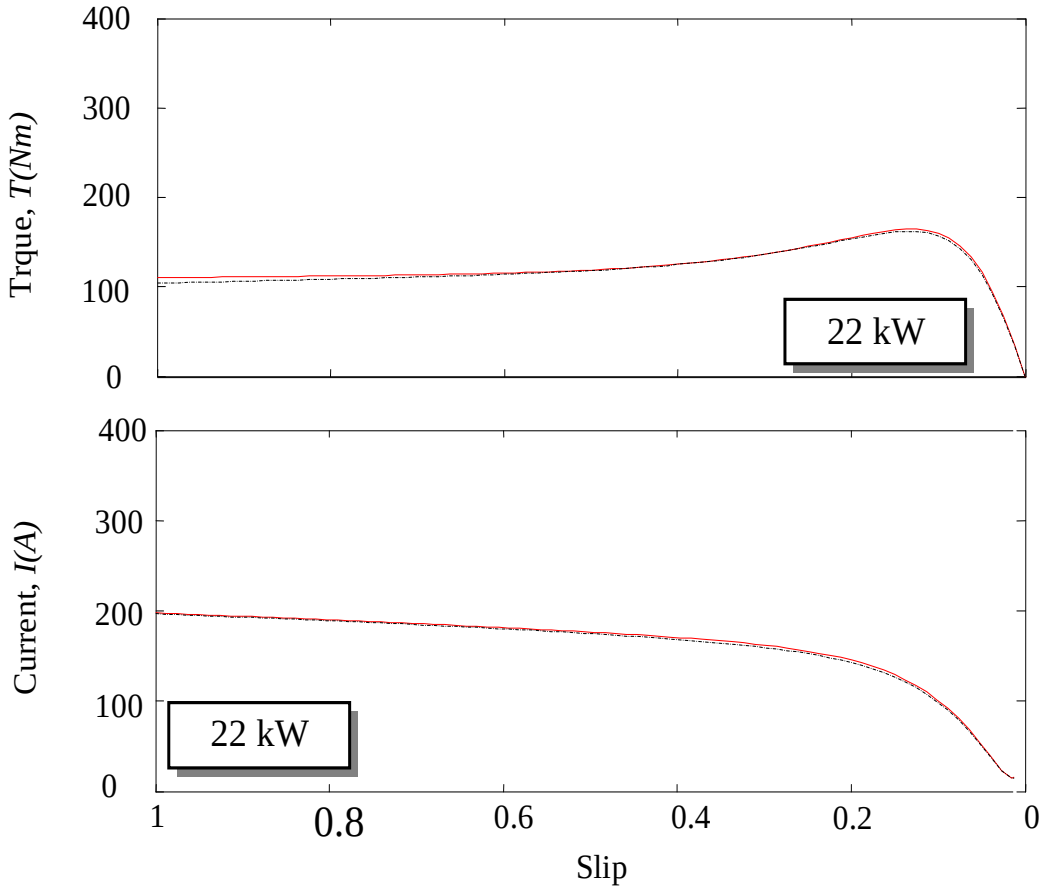

Fig. 6.13.a. Original torque(red solid line) and steady-state torque from estimated double cage parameters (black dashed line)for machine 22kW and 6.13.b. Original current (red solid line) and steady-state current from estimated double cage parameters (black dashed line) for machine 22kW for weight=0.04.

In the Fig. 6.13.a and b the red solid lines are original double cage torque and current and the black dashed lines are estimated double-cage torque and current respectively. The fitting between the original and estimated curves are very good.

The relative errors of the estimation are presented in Table 6.11 that are 5.62% for starting torque, 1.52% for maximum torque and zero for starting and no-load currents respectively in machine 2.

Table 6.11. Calculated magnitudes for error determination for machine 2 (22k)

P(kW)	*D-cage*	T_m*(Nm)*	T_s*(Nm)*	I_s*(A)*	I_{NL}*(A)*
22	Original	164.3	110.2	197.6	14.18
	Estimated	161.8	104	197.6	14.18
	Real Error	0.0152	0.0562	0	0

6.6 Double-cage machine 3 estimation

The proposed method for double-cage parameters estimation using the instantaneous power method is applied to the machine 3 with power 500kW of Table 6.1. The starting transient has been simulated using the SimPowerSystems Blockset of Matlab [31].

First the regression method is applied to the transient data to the points in the region between the maximum torque point and the steady-state point. Then single-cage A is estimated. Estimation of cage A has been calculated with equation (138).

The results of cages A estimation for the machine 3 of Table 6.1 are presented in Tables 6.12.

Using parameters of Table 6.12, no-load and maximum impedances; Z_{nl} and Z_m for single-cage A have been calculated and their values are presented in Table 6.13.

Fig. 6.14 shows the good fitting of cage A torque (in part a) and cage A current (in part b) with the steady-state torque and current curves of the original double cage of machine 3 in the zone between the maximum torque speed and the synchronous speed (zone 2).

Table 6.12. Parameters of single cage A induction machine 3 (500kW) with f_s=50(Hz), V_{ph}=220V and J=13

Estimation	R_s	X_{sd}	X_m	R_r	T_m	T_s	I_s	I_n
Regression	0.0012	0.0271	0.7582	0.0024	3963.2	366.8746	4126	280.1652

Table 6.13. Z_{nl} and Z_m for single-cage A of machine 3 (500kW) with f_s=50(Hz), V_{ph}=220V and J=13

$Real(\underline{Z}_{nl})$	$Imag(\underline{Z}_{nl})$	$Real(\underline{Z}_m)$	$Imag(\underline{Z}_m)$
0.0012	0.7853	0.0458	0.0560

Then instantaneous method that uses equation (189), estimates some impedances during mechanical transient region before maximum torque point. These impedances are presented in Table 6.14 for 5 points.

Table 6.14. Instantaneous impedances of double cage machine3 with f_s=50(Hz) and V_{ph}=220V

Points	P_1	P_2	P_3	P_4	P_5
Rotor Speed	83.57	118.6	150.2	181.8	209.3
$Re(Z_{approx})$	0.01476	0.01485	0.01477	0.01464	0.0147
$im(Z_{approx})$	0.04322	0.04497	0.04654	0.04813	0.04946

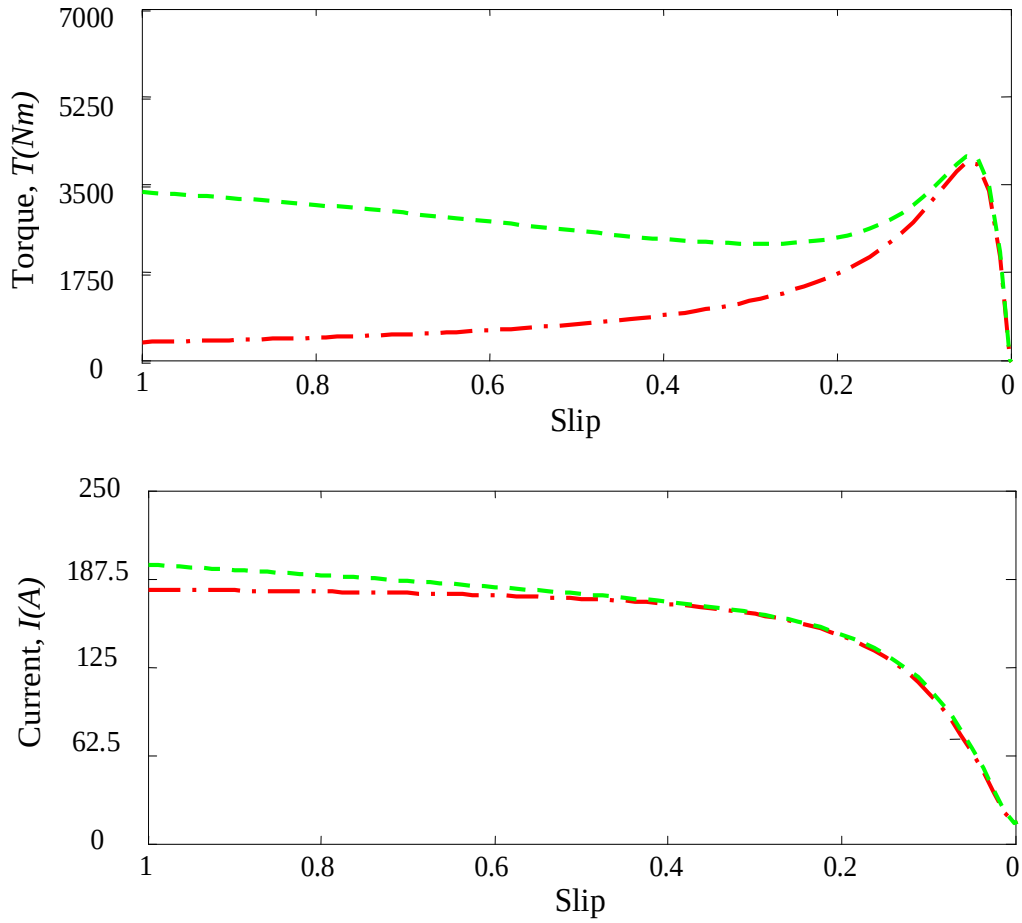

Fig. 6.14.a. Torque of single-cage A; red 1point dashed line and torque of original double-cage; green dashed line and 6.14.b. Current of single-cage A; red 1point dashed line and current of original double-cage; green dashed line.

Then using maximum and no-load impedances of cage A and impedances of instantaneous method with a typical weight equal to 0.04 in equation (190) and (193) respectively, these set of equations are solved using F-solve function of MATLAB to estimate the double-cage parameters of machine 3.

The steady-state torque-speed and current-speed curves with the estimated parameters of Table 6.15 are seen in Fig. 6.15.

Table 6.15. Parameters of double cage machine 3 with f_s=50(Hz) and V_{ph}=220V

Double-cage	R_s	$X_s=X_{2d}$	X_m	R_{r1}	R_{r2}	X_{1d}	$\wp$	J
Real	0.00123Ω	0.01789	0.76736	0.00245	0.03911	0.03911	1	13
Estimated	0.0011	0.0200	0.7653	0.0025	0.0411	0.0392	1	13

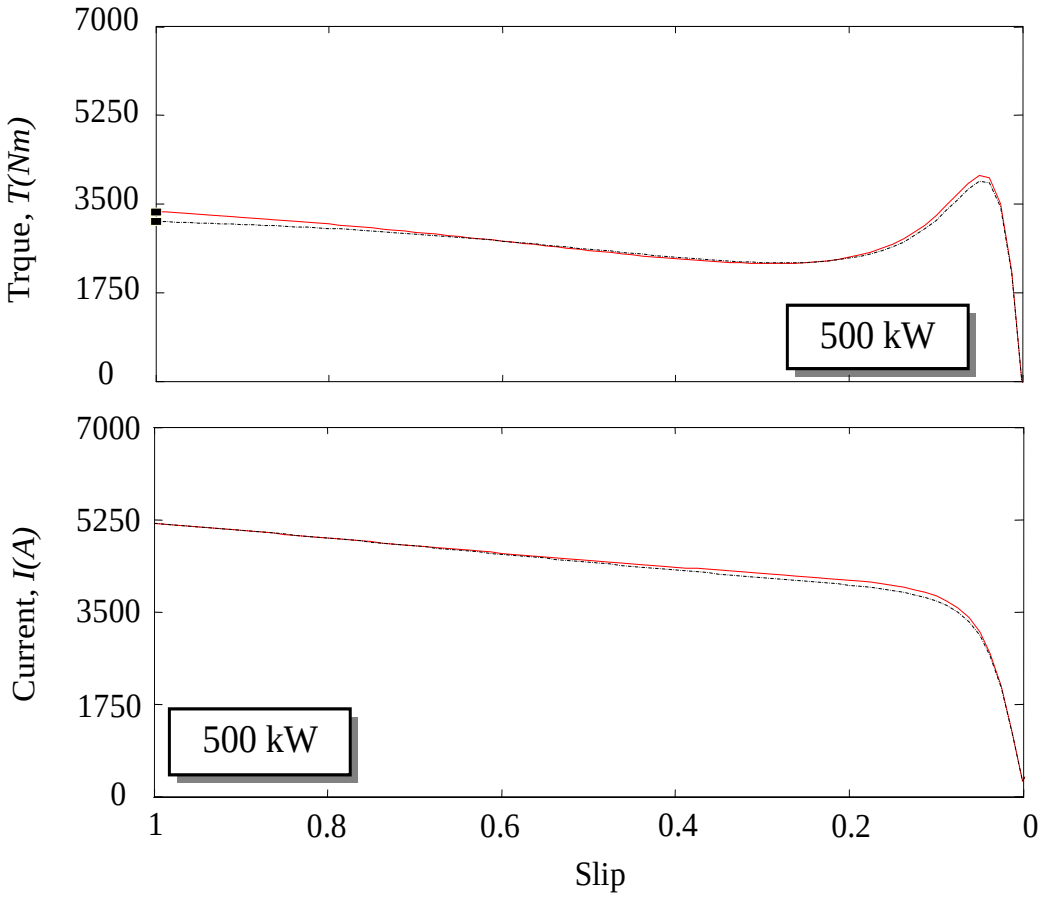

Fig. 6.15.a. Original torque(red solid line) and steady-state torque from estimated double cage parameters (black dashed line) for machine 500kW and 6.15.b. Original current (red solid line) and steady-state current from estimated double cage parameters (black dashed line) for machine 500kW for weight=0.04.

In the Fig. 6.15.a and b the red solid lines are original double cage torque and current and black dashed lines are estimated double-cage torque and current respectively. The fitting between the original and estimated curves are very good.

The relative errors of the estimation are presented in Table 6.16 that are 5.8% for starting torque, 2.6% for maximum torque and zero for starting and no-load currents respectively in machine 3.

Table 6.16. Calculated magnitudes for error determination for machine 3 (500k)

P(kW)	*D-cage*	T_m*(Nm)*	T_s*(Nm)*	I_s*(A)*	I_{NL}*(A)*
500	Original	4063	3349	5182	280.1
	Estimated	3956	3153	5182	280.1
	Real Error	0.026	0.058	0	0

7 Conclusions and contributions

The parameters estimation procedures of the single-cage induction model and the double-cage induction model developed in this project are based on the usual data that can be easily obtained from a starting transient; the three stator currents, the three stator voltages and the mechanical speed.

In this doctoral thesis, two new methods to estimate single-cage induction motor parameters and two new methods to estimate the double-cage induction motor parameters from transient measurements are presented.

Below the main conclusions and contributions of this thesis are summarized.

A) Single-cage model:

- It is demonstrated that the Park variables in the synchronous reference frame are used because they facilitate the data filtering. This reference frame is more reliable due to the slow variation of the direct and quadrature currents and voltages during mechanical transients and owing to the fact that these magnitudes have constant values in the steady state.

- A good improvement is the new approximation of the rotor flux as a function of the stator voltages and currents. It avoids the use of the speed derivative approximation, $d\omega/dt = 0$, used in the literature [15]. It has been demonstrated that the accuracy of the estimation procedure using rotor flux approximation is improved significantly.

- Two new different methods to estimate the single-cage induction machine model parameters have been proposed and studied: the regression method and the two points method. The first is based on the least-square method and the second is based on the resolving of a non-linear system of equations.

- In this thesis a detailed study of the errors as function of the speed of points used in the regression method and the two points method has been realized. This study reveals that for parameters estimation with low error, the use of points near maximum torque speed zone and points near the synchronous speed zone is very important.

- The errors study has shown that the influence of the rotor flux approximation is significant. On the other hand the influence of the step size in the derivative calculation, the inertia and other factors has low influence on the error estimation.

- The error study shows that the maximum torque value is usually the magnitude with the highest error, followed by the starting torque error value and the starting current error value. Finally the no load current, is the magnitude with the lowest error.

B) Double-cage model

One of the main purposes of this thesis is the study of the double-cage model. There are several papers about this topic in the literature. Practically all the literature review studies are about the single-cage model, in contrary of the reality that the most of the squirrel-cage motors behave according to the double-cage model.

- The first method of double-cage induction motor parameters determination is called two single-cage method. In this method the two points method has been used for obtaining single-cage parameters, valid in the range from the maximum torque speed to the synchronous speed. The other set of parameters can be obtained from data of two speeds; near zero speed and the synchronous speed.

- The second method of double-cage induction motor parameters determination is called the instantaneous power method. This method exploits the fact that in the mechanical transient region the averaged transient torque has a surprising coincidence with the steady-state torque. With this method an excellent estimation of motor impedances at different speeds has been obtained from averaged values of the instantaneous power obtained from the measured voltages and currents. This method has the advantage that it is very easy to obtain an approximation of the impedance values at different speeds in the region from mechanical transient point to the maximum torque point, where the effects of the double-cage are more important than effects of single-cage.

8 Future research

- Study of the mechanical parameters estimation with the electrical parameters estimation. Then it is possible to do an estimation of the mechanical parameters.
- Study of the effects of the saturation with the data of starting transients at different voltages. Therefore the influence of the saturation on the estimated parameters can be studied.
- Study of the very fast transients (mechanical time constant near the electrical time constant). As limitation of the proposed methods needs a slow mechanical transient zone, the development of new estimation methods for machines with very low inertia is an interesting study.

9 Bibliography

[1] IEEE Standard test procedure for polyphase induction motors and generators, IEEE Std. 112-2004, Nov. 2004.

[2] IEC Rotating electrical machines-Part 28: Test methods for determining quantities of equivalent circuit diagrams for three-phase low-voltage cage induction motors, IEC 60034-28 Ed. 2.0 (2012-12)

[3] Ll. Monjo, F. Corcoles, J. Pedra, "Saturation effects on torque- and current-slip curves of squirrel-cage induction motors" IEEE Trans. Energy Conversion, Vol. 28, No. 1, 2013, pp. 243-254

[4] H. A. Toliyat, E. Levi, M. Raina, "A review of RFO induction parameter estimation techniques", IEEE Trans. Energy Conversion, Vol. 18, No.2, June 2003, pp. 271-283.

[5] J. Pedra, L. Candela, L. Sainz, "Modeling of squirrel-cage induction motors for electromagnetic transient", IET Electric Power Applications, Vol. 3, No. 2, March 2009, pp. 111-122.

[6] E. Laroche, M. Boutayeb, "Identification of the induction motor in sinusoidal mode", IEEE Trans. Energy Conversion, Vol. 25, No.1, March 2010, pp. 11-19.

[7] S. Ayasun, C. O. Nwankpa, "Induction motor test using MATLAB/Simulink and their integration into undergraduate electric machinery courses", , IEEE Trans. Education, Vol. 48, No.1, Feb. 2005, pp. 37-46.

[8] I. Zubia, A. Zatarain, C. Alcalde, X. Ostolaza, "In situ electrical identification meted for induction wind generators", IET Electric Power Applications, Vol. 5, No. 7, 2011, pp. 549-557.

[9] M. O. Sonnaillon, G. Bisheimer, C. De Angelo, G. O. Garcia, "Automatic induction machine parameters measurements using standstill frequency-domain tests", IET Electric Power Applications, Vol. 1, No. 5, 2007, pp. 833-838.

[10] L. A. S. Ribeiro, C. B. Jacobina, A. M. N. Lima, A. C. Oliveira, "Real-time estimation of the electric parameters of an induction machine using sinusoidal PWM voltage waveforms", IEEE Trans. Industry Appl., Vol. 36, No. 3, 2000. pp. 743-754.

[11] C. B. Jacobina, J. E. C. Filho, A. M. N. Lima, "Estimating the parameters of induction machine at standstill", IEEE Trans. Energy Conversion, Vol. 17, No.1, March 2002, pp. 85-89.

[12] S. Jafarzadeh, C. Lascu, S. Fadali, "State estimation of induction motor drives using the unscented Kalman filter", IEEE Trans. Industrial Electronics, Vol 59, 2012, pp. 4207-4216.

[13] A. Lalami, R. Wamkeue, I. Kamwa, M. Saad, J. J. Beaudoin, "Unscented Kalman filter for non-linear estimation of induction machine parameters", , IET Electric Power Applications, Vol. 6, No. 9, 2012, pp. 611-620.

[14] E. Laroche, E. Sedda, C. Durieu, "Methodological insights for online estimation of induction motor parameters", IEEE Trans. Control Syst. Technol., Vol. 16, No. 5, Sept. 2008, pp. 1021-1028.

[15] J. Stephan, M. Bodson, J. Chiasson, "Real-time estimation of the parameters and fluxes of induction motors", IEEE Trans. Industry Appl., Vol. 30, 1994, pp. 746-758.

[16] M. Cirrincione, M. Pucci, G. Cirrincione, G. A. Capolino, "A new experimental application of least-squares techniques for the estimation of the induction motor parameters" IEEE Trans. Industry Appl., Vol 39, 2003, pp. 1247-1256.

[17] M. Cirrincione, M. Pucci, G. Cirrincione, G. A. Capolino, "Constrained minimization for parameters estimation of induction motor in satured and unsatured conditions" IEEE Trans. Industrial Electronics, Vol 52, 2005, pp. 1391-1402.

[18] M. Cirrincione, M. Pucci, "Identification of an induction motor with the least-squares method", Elect. Eng. Res. Rep., No. 10, Dec. 2000, pp. 22-30.

[19] S. R. Shaw, S. B. Leeb, “Identification of induction motor parameters from transient stator current measurements”, IEEE Trans. Industrial Electronics, Vol. 46, 1999, pp. 139-149.

[20] R. Wamkeue, D. Aguglia, M. Lakehal, P. Viarouge, “Two-step method for identification of nonlinear model of induction machine”, IEEE Trans. Energy Conversion, Vol. 22, No.4, Dec. 2007, pp. 801-809

[21] J. A. de Kock, F. S. van der Merwe, H. J. Vermeulen, “Induction motor parameter estimation through an output error technique”, IEEE Trans. Energy Conversion, Vol. 9, No.1, March 1994, pp. 69-76

[22] R. Wamkeue, I. Kamwa, M. Chacha, “Unbalanced transients-based maximum likelihood identification of induction machine parameters”, IEEE Trans. Energy Conversion, Vol. 18, No.1, March 2003, pp. 33-40

[23] C. Grantham, D. J. McKinnon, “Rapid parameter determination for induction motor analysis and control”, IEEE Trans. Industry Appl., Vol 39, No. 4, 2003, pp. 1014-1020.

[24] Whei-Min Lin, Tzu-Jung Su, Rong-Ching Wu, “Parameter identification of induction machine with a starting no-load low-voltage test”, IEEE Trans. Industrial Electronics, Vol. 59, No. 1, Jan. 2012, pp. 352-360

[25] F. Corcoles, J. Pedra, M. Salichs, L. Sainz, “Analysis of the induction machine parameter identification” IEEE Trans. Energy Conversion, Vol 17, No 2, June 2002, pp. 183-190.

[26] power_AsynchronousMachineParams. The Mathworks Inc.: MATLAB Release 2012a, available at http://www.mathworks.com.

[27] J. Pedra, F. Corcoles, “Estimation of induction motor double-cage model parameters from manufacturer data”, IEEE Trans. Energy Conversion, Vol 19, No 2, June 2004, pp. 310-317

[28] J. Pedra, “On the determination of induction motor parameters from manufacturer data for electromagnetic transient programs” IEEE Trans. Power Systems, Vol. 23, No. 4, November 2008, pp. 1709-1718

[29] R. Babau, I. Boldea, T. J. E. Miller, N. Muntean, “Complete parameter identification of large induction machines from no-load acceleration-deceleration tests”, IEEE Trans. Industrial Electronics, Vol 54, No. 4, 2007, pp. 1962-1972.

[30] J. Lesenne, F. Notelet, G. Seguier, “Introduction a l´ Electrotechnique Approfondie”, Paris: Technique and Documentation, 1981.

[31] The MathWorks, Inc., Matlab 7.9 (2009b). Natick, MA: 2009.

[32] T. O’Haver, “An introduction to signal processing with applications in chemical analysis”, http://terpconnect.umd.edu/~toh/spectrum/TOC.html

[33] S.J. Miller, The method of Least Square, Brown University, RI 02912, P.P. 1-7.

[34] Paul. C. Krause, 1986, Analysis of Electric Machinery. MCGraw-Hill, Inc.

[35] A. Savitzky, M. J. E. Golay, “Smoothing and differentiation of data by simplified least square procedures”, Anal. Chem., 36, 1964, pp. 1627-1639.

10 Appendix: Publications

Parameters estimation of wound-rotor induction motors from transient measurements

Journal:	*IEEE Transactions on Energy Conversion*
Manuscript ID:	TEC-00015-2013
Manuscript Type:	Transactions
Date Submitted by the Author:	09-Jan-2013
Complete List of Authors:	Kojooyan-Jafari, Hengameh; ETSEIB, UPC, Department of Electrical Engineering Monjo, Lluis; ETSEIB, UPC, Department of Electrical Engineering Córcoles López, Felipe; ETSEIB, UPC, Department of Electrical Engineering Pedra, Joaquin; Universitat Politecnica de Catalunya, Eng. Electrica
Technical Topic Area:	Wound rotor induction machinery < Electric Machinery
Key Words:	AC motors, Parameter estimation, Transient analysis

Parameter estimation of wound-rotor induction motors from transient measurements

Hengameh Kojooyan-Jafari, Lluís Monjo, *Student Member, IEEE*, Felipe Córcoles, Joaquín Pedra, *Member, IEEE*

***Abstract*— A new method for determination of the steady-state equivalent circuit parameters of wounded induction motors using experimental data from starting transient measurements is presented. The data in the algorithm are stator currents and voltages and mechanical speed. The algorithm uses the least-square method and the motor dynamic equations in the synchronous reference frame. Moreover, an approximation of the rotor flux that improves the precision of the estimation method, as well as a detailed study of the errors of the estimation procedure, are included. Method is validated with data from starting transient measurements of a 2kW wound rotor induction motor.**

***Index Terms*—Equivalent circuits, wound rotor induction motor, starting transients.**

PARAMETER determination of induction motors is a major topic because these machines are one of the most important loads in the grid. Accuracy is necessary because of the significance of power system dynamic behavior during faults and other perturbations. Another important area is high performance ac drives, where parameter estimation is crucial for the tuning of controllers. Several approaches have been presented for induction motor parameter estimation. IEEE Std-112 [1] describes the most usual method, which is based on short-circuit and no-load test. Other methods include those based on steady state [2], frequency [3] or transient tests [4-10]. Recently, more sophisticated procedures have been presented using a transient test with an extended Kalman filter [4]. Another possibility is to formulate a least square minimization problem [5-10]. Reference [5] gives a thorough description of the least-square method and the dynamic equations in rotor reference frame and [6] uses the stator reference frame. On the other hand, to the knowledge of the authors, no studies apply the synchronous reference frame.

The main issue in this paper is to develop a method that can be easily used in a real situation. Starting transients are chosen because they are the minimal disruption of normal motor operation. Furthermore, short-circuit test cannot be used for high power machines because their high currents. The method only needs measurements of stator currents, stator voltages and mechanical speed during the starting transient.

It's main restriction, however, is that it can only be applied to the wound-rotor induction motors, modeled with the equivalent steady-state circuit in Fig. 1.

The proposed is valid for motors where the mechanical transient is decoupled from the electrical transient, i.e. the time constants of the electrical and mechanical transients are in different orders of magnitude.

This research work was supported by the Spanish Ministerio de Ciencia e Innovación under Project ENE2009-10274.

H. Kojooyan, Ll. Monjo, F. Córcoles and J. Pedra are with the Department of Electrical Engineering, ETSEIB-UPC, Av. Diagonal 647, 08028 Barcelona, Spain (e-mails: kojooyan@iiau.ac.ir, lluis.monjo@upc.edu, corcoles@ee.upc.edu, pedra@ee.upc.edu).

I. Dynamic Equations

The dynamic equations in Park variables in the synchronous reference frame are

$$\begin{aligned} v_{sd} &= (R_s + L_s p) i_{sd} - L_s \omega i_{sq} + Mp i_{rd} - M\omega i_{rq} \\ v_{sq} &= L_s \omega i_{sq} + (R_s + L_s p) i_{sq} + M\omega i_{rd} + Mp i_{rq} \\ 0 &= Mp i_{sd} - Ms\omega i_{sq} + (R_r + L_r p) i_{rd} - L_r s\omega i_{rq} \\ 0 &= Ms\omega i_{sd} + Mp i_{sq} + L_1 s\omega i_{rd} + (R_r + L_r p) i_{rq} \\ T(t) &= M \wp (i_{sq} i_{rd} - i_{sd} i_{rq}) \quad , \quad s = (\omega - \wp \omega_m)/\omega \end{aligned} \tag{1}$$

and in Ku variables in the synchronous reference frame are

$$\begin{aligned} v_s &= (R_s + L_s (p + j\omega)) i_s + M (p + j\omega) i_r \\ 0 &= M (p + js\omega) i_s + (R_r + L_r (p + js\omega)) i_r \\ T(t) &= 2\wp M \operatorname{Im}(i_s i_r^*) \quad , \quad s = (\omega - \wp \omega_m)/\omega. \end{aligned} \tag{2}$$

The relation between the coefficients of the dynamic equations and the steady-state star equivalent circuit is

$$M = X_m/\omega \quad ; \quad L_s = (X_{sd} + X_m)/\omega \quad ; \quad L_r = (X_{rd} + X_m)/\omega \tag{3}$$

where $\wp$ is the number of pair of poles, $\omega = 2\pi f$ is the synchronous speed and ω_m, is the mechanical speed. The relations between Park and Ku variables are

$$v_s = \frac{v_{sd} + jv_{sq}}{\sqrt{2}} \quad ; \quad i_s = \frac{i_{sd} + ji_{sq}}{\sqrt{2}} \quad ; \quad i_r = \frac{i_{rd} + ji_{rq}}{\sqrt{2}} \tag{4}$$

The relation between the measured currents, i_{sa}, i_{sb}, i_{sc}, (shown in Fig. 2) and the Park variables i_{sd}, i_{sq}, (shown in Fig. 4a) in the synchronous reference frame $(\theta = \omega t)$ is

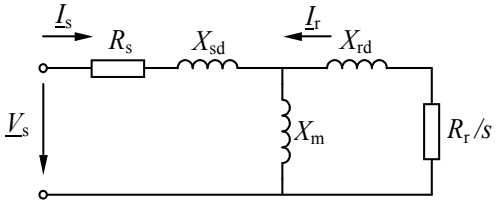

Fig. 1. Steady-state equivalent circuit for the single-cage model of the three-phase induction motor.

TABLE I
PARAMETERS OF SIMULATED MOTOR

U(V)	R_s(Ω)	X_{sd}(Ω)	X_m(Ω)	R_r(Ω)	X_{rd}(Ω)	J(kg·m^2)	P(kW)
400	2.88	3.96	88.8	2.80	3.96	1.2	2.2

$$i_{sd} = \sqrt{\frac{2}{3}}\left\{ i_{sa}\cos\theta + i_{sb}\cos\left(\theta - \frac{2\pi}{3}\right) + i_{sc}\cos\left(\theta + \frac{2\pi}{3}\right)\right\}$$
$$i_{sq} = -\sqrt{\frac{2}{3}}\left\{ i_{sa}\sin\theta + i_{sb}\sin\left(\theta - \frac{2\pi}{3}\right) + i_{sc}\sin\left(\theta + \frac{2\pi}{3}\right)\right\} \quad (5)$$

and for the voltages , v_{sa}, v_{sb}, v_{sc}, (shown in Fig. 2), it is

$$v_{sd} = \sqrt{\frac{2}{3}}\left\{ v_{sa}\cos\theta + v_{sb}\cos\left(\theta - \frac{2\pi}{3}\right) + v_{sc}\cos\left(\theta + \frac{2\pi}{3}\right)\right\}$$
$$v_{sq} = -\sqrt{\frac{2}{3}}\left\{ v_{sa}\sin\theta + v_{sb}\sin\left(\theta - \frac{2\pi}{3}\right) + v_{sc}\sin\left(\theta + \frac{2\pi}{3}\right)\right\} \quad (6)$$

where voltages, v_{sd}, v_{sq}, are constant. Fig. 3a shows the speed during the starting transient.

The objective of the work is to determine the motor parameters with equations (1) where the rotor currents must be eliminated because they are not usually measurable. To do this, the first and second derivatives of the current must be obtained. However, difficulties arise when real measurements are used due to numerical problems caused by the derivative of a noisy signal (more details are given in Section III). For this reason, the use of a smoothing algorithm becomes necessary.

II. SMOOTHING

To determine the influence of smoothing on the measured data and their derivatives, a study based on Simulink-SimPower Systems Blockset simulation was made. Table I shows the parameters of the wound-rotor induction machine simulated in a starting transient in this section (Fig. 2). These simulations provide the data of the three phase voltages and currents and the mechanical speed. Fig. 3a and Fig 4a show the mechanical speed, ω_m, and the transformed currents, i_{sd}, i_{sq}. For this study a white noise of 35dB was added to the data.

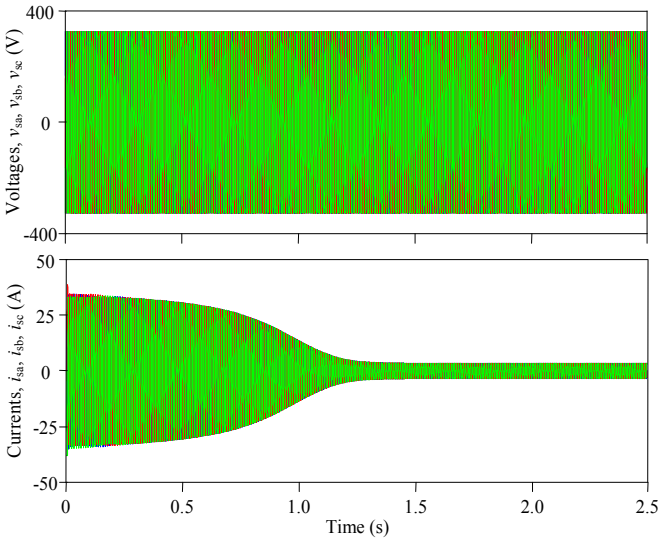

Fig. 2. Simulated currents and voltages during the starting transient of the wound rotor machine

In an attempt to filter the current, voltage and speed measurements, a smoothing function (smooth) of MATLAB based on a Savitzky-Golay filter was used [12][13]. This smoothing algorithm performs a moving average with coefficients determined by an unweighted least-square regression method and a polynomial model of a specified degree.

In this paper data obtained from simulation and measurements are smoothed with the above method considering polynomial of degrees 1 and 2 and 10% of the array data length as the smoothing window.

Ref. [14] recommends to apply the smoothing function a minimum of two times if a second derivative is calculated. Applying this recommendation, derivatives of simulated speed and noisy speed are compared for both degrees in Fig. 3b. The first and second derivatives of the simulated transformed and noised currents (for degrees 1 and 2) are provided in Fig. 4b and 4c.

As can be seen in Fig. 3 and Fig. 4, there are differences between the smoothed curves. The approximation based on polynomials of degree 2 fits the mechanical speed and transformed currents during the transient; however, in steady state smoothing amplifies the noise, invalidating the values of the derivatives. On the contrary, the polynomial of degree 1 fits the steady state and fails during the transient. As a conclusion, the smoothing of degree 2 will be used in the transient region and the smoothing of degree 1 in the steady-state region. In the next sections, a more detailed study is made to quantify the error incurred by the numerical derivatives and smoothing.

III. LEAST-SQUARE METHOD

Obtaining motor parameters from the motor dynamic equations (1) directly is not possible because of rotor currents are not generally measurable. Hence, a new set of equations with-

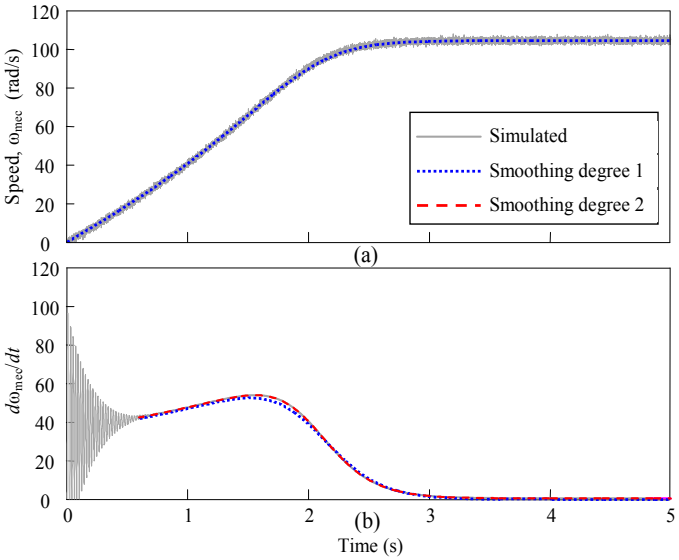

Fig. 3. (a) Noisy speed (solid line) and smoothed speed (dotted line) time evolution from simulation (b) First derivative of the simulated speed (solid line), speed smoothed with degree 1 (dotted line) and smoothed speed with degree 2 (dashed line)

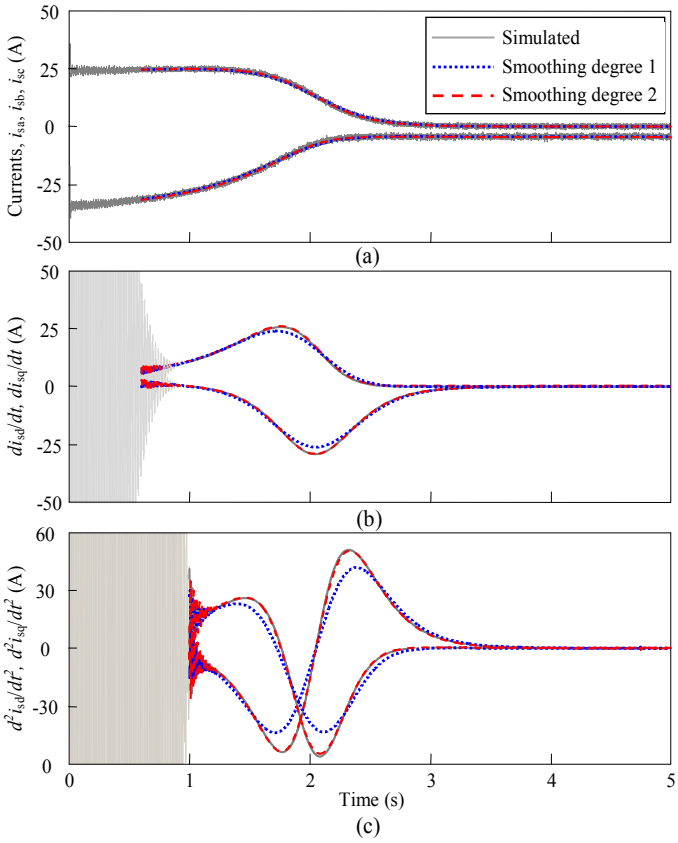

Fig. 4. (a) Currents measured (solid line) and smoothed with degree 1 (dotted line) and with degree 2 (dashed line) (b) First derivative of currents with degree 1 (dotted line) and degree 2 (dashed line) (c) second derivative currents with degree 1 (dotted line) and degree 2 (dashed line)

out rotor magnitudes becomes necessary. This new set, obtained in Appendix I, results in the following equations:

$$K_1\frac{di_{sd}}{dt}+K_2 i_{sd}-K_{31}\left(\omega-\wp\,\omega_m\right)i_{sq}-K_{32}\omega i_{sq}-$$
$$-K_4\left(\frac{dv_{sd}}{dt}-\left(\omega-\wp\,\omega_m\right)v_{sq}\right)-K_5 v_{sd}=-\frac{d^2 i_{sd}}{dt^2}+ \quad (7)$$
$$+\left(2\omega-\wp\,\omega_m\right)\frac{di_{sq}}{dt}+\omega\left(\omega-\wp\,\omega_m\right)i_{sd}+\frac{d\wp\,\omega_m}{dt}\beta\psi_{rq}$$

$$K_1\frac{di_{sq}}{dt}+K_2 i_{sq}+K_{31}\left(\omega-\wp\,\omega_m\right)i_{sd}+K_{32}\omega i_{sd}-$$
$$-K_4\left(\frac{dv_{sq}}{dt}+\left(\omega-\wp\,\omega_m\right)v_{sd}\right)-K_5 v_{sq}=-\frac{d^2 i_{sq}}{dt^2}- \quad (8)$$
$$-\left(2\omega-\wp\,\omega_m\right)\frac{di_{sd}}{dt}+\omega\left(\omega-\wp\,\omega_m\right)i_{sq}-\frac{d\wp\,\omega_m}{dt}\beta\psi_{rd}$$

where

$$\sigma=1-\frac{M^2}{L_s L_r}\;;\;\beta=\frac{M}{\sigma L_s L_r}\;;\;T_r=\frac{L_r}{R_r}\;;\;T_s=\frac{L_s}{R_s}$$
$$K_1=\frac{R_s}{\sigma L_s}+\frac{1}{\sigma T_r}\;;\;K_2=\frac{R_s}{\sigma L_s T_r}\;;\;K_{31}=\frac{1}{\sigma T_s} \quad (9)$$
$$K_{32}=\frac{1}{\sigma T_r}\;;\;K_4=\frac{1}{\sigma L_s}\;;\;K_5=\frac{1}{\sigma L_s T_r}$$

Because rotor fluxes ψ_{rd},ψ_{rq} are not measurable, a number of studies [5-10] use equations like (7) and (8) considering the terms $\left(d\wp\,\omega_m/dt\right)\beta\psi_{rq}$ and $\left(d\wp\,\omega_m/dt\right)\beta\psi_{rd}$ negligible. A contribution of this paper is to introduce an approximation of the rotor flux that improves in the estimation procedure significantly and it takes into consideration the above terms. That is the reason for the detailed justification of equations (7) and (8) in Appendix I.

Using the approximation of the rotor flux, ψ_r, described in Appendix II, the following relations are obtained

$$\beta\psi_{rd}\approx\frac{v_{sq}}{\sigma\omega L_s}-i_{sd}\;\;;\;\;\beta\psi_{rq}\approx-\frac{v_{sd}}{\sigma\omega L_s}-i_{sq} \quad (10)$$

Substituting

$$\frac{d\wp\,\omega_m}{dt}\beta\psi_{rd}\approx K_4\frac{d\wp w_m}{dt}\frac{v_{sq}}{\omega}-\frac{d\wp\,\omega_m}{dt}i_{sd}$$
$$\frac{d\wp\,\omega_m}{dt}\beta\psi_{rq}\approx -K_4\frac{d\wp w_m}{dt}\frac{v_{sd}}{\omega}-\frac{d\wp\,\omega_m}{dt}i_{sq} \quad (11)$$

in the terms of (7) and (8), we obtain a system of linear equations like

$$\begin{pmatrix}a_{d1}&a_{d2}&a_{d3}&a_{d4}&a_{d5}&a_{d6}\\a_{q1}&a_{q2}&a_{q3}&a_{q4}&a_{q5}&a_{q6}\end{pmatrix}\begin{pmatrix}K_1\\K_2\\K_{31}\\K_{32}\\K_4\\K_5\end{pmatrix}=\begin{pmatrix}b_d\\b_q\end{pmatrix} \quad (12)$$

where

$$a_{d1}=\frac{di_{sd}}{dt};a_{d2}=i_{sd};a_{d3}=-\left(\omega-\wp\,\omega_m\right)i_{sq};a_{d4}=-\omega i_{sq}$$
$$a_{d5}=-\left(\frac{dv_{sd}}{dt}-\left(\omega-\wp\,\omega_m\right)v_{sq}+\frac{1}{\omega}\frac{d\wp\,\omega_m}{dt}v_{sd}\right)$$
$$a_{d6}=-v_{sd} \quad (13)$$
$$b_d=-\frac{d^2 i_{sd}}{dt^2}+\left(2\omega-\wp\,\omega_m\right)\frac{di_{sq}}{dt}+$$
$$+\omega\left(\omega-\wp\,\omega_m\right)i_{sd}-\frac{d\wp\,\omega_m}{dt}i_{sq}$$

$$a_{q1}=\frac{di_{sq}}{dt};a_{q2}=i_{sq};a_{q3}=\left(\omega-\wp\,\omega_m\right)i_{sd};a_{q4}=\omega i_{sd}$$
$$a_{q5}=-\left(\frac{dv_{sq}}{dt}+\left(\omega-\wp\,\omega_m\right)v_{sd}-\frac{1}{\omega}\frac{d\wp\,\omega_m}{dt}v_{sq}\right)$$
$$a_{q6}=-v_{sq} \quad (14)$$
$$b_q=-\frac{d^2 i_{sq}}{dt^2}-\left(2\omega-\wp\,\omega_m\right)\frac{di_{sd}}{dt}+$$
$$+\omega\left(\omega-\wp\,\omega_m\right)i_{sq}+\frac{d\wp\,\omega_m}{dt}i_{sd}$$

Considering n points in the study, we obtain the following over determined linear system,

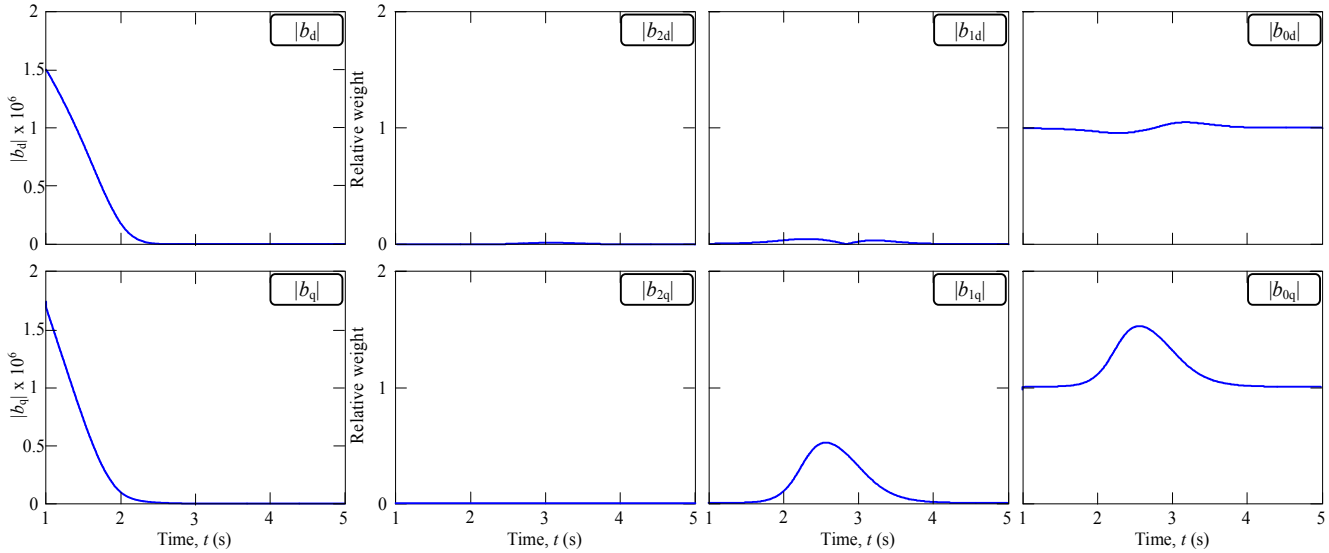

Fig. 5. Relative weight of the polynomial parts

$$\begin{pmatrix} a_{d1}^1 & a_{d2}^1 & a_{d3}^1 & a_{d4}^1 & a_{d5}^1 & a_{d6}^1 \\ a_{q1}^1 & a_{q2}^1 & a_{q3}^1 & a_{q4}^1 & a_{q5}^1 & a_{q6}^1 \\ a_{d1}^2 & a_{d2}^2 & a_{d3}^2 & a_{d4}^2 & a_{d5}^2 & a_{d6}^2 \\ a_{q1}^2 & a_{q2}^2 & a_{q3}^2 & a_{q4}^2 & a_{q5}^2 & a_{q6}^2 \\ \vdots & \vdots & \vdots & \vdots & \vdots & \vdots \\ a_{d1}^n & a_{d2}^n & a_{d3}^n & a_{d4}^n & a_{d5}^n & a_{d6}^n \\ a_{q1}^n & a_{q2}^n & a_{q3}^n & a_{q4}^n & a_{q5}^n & a_{q6}^n \end{pmatrix} \begin{pmatrix} K_1 \\ K_2 \\ K_{31} \\ K_{32} \\ K_4 \\ K_5 \end{pmatrix} = \begin{pmatrix} b_d^1 \\ b_q^1 \\ b_d^2 \\ b_q^2 \\ \vdots \\ b_d^n \\ b_q^n \end{pmatrix} \tag{15}$$

Which can be rewritten as,

$$\mathbf{Ax} = \mathbf{b} \tag{16}$$

Using the least square regression method the solution of this over determined linear system is

$$\mathbf{x} = \left(\mathbf{A}^t\mathbf{A}\right)^{-1}\mathbf{A}^t\mathbf{b} \tag{17}$$

where $\mathbf{x} = (K_1, K_2, K_{31}, K_{32}, K_4, K_5)$.

From the parameters obtained with the least-square method, (K_1, K_2, K_{31}, K_{32}, K_4, K_5), the induction motor parameters can be calculated considering the relation between parameters $L_{sd} = L_{rd}$, justified in the reference [15]. The following relations are obtained,

$$\begin{aligned} L_s = L_r = \frac{K_5}{K_{32}} \quad ; \quad \sigma = \frac{1}{K_4 L_s} \quad ; \quad M = \sqrt{(1-\sigma)L_s^2} \\ R_s = \frac{L_s}{T_s} = L_s \sigma K_{31} \quad ; \quad R_r = \frac{L_r}{T_r} = L_r \sigma K_{32} \\ L_{sd} = L_{rd} = L_s - M \end{aligned} \tag{18}$$

IV. Error Influence on b_d and b_q

To analyze the influence of the error introduced by the smoothed derivatives on coefficients b_d and b_q of equations (13) and (14), terms $|b_d|$ and $|b_q|$ are defined as

$$\begin{aligned} |b_d| &= \left| -\frac{d^2 i_{sd}}{dt^2} + (2\omega - \wp\,\omega_m)\frac{di_{sq}}{dt} + \left(\omega(\omega - \wp\,\omega_m) i_{sd} - \frac{d\wp\,\omega_m}{dt} i_{sq} \right) \right| \\ |b_q| &= \left| -\frac{d^2 i_{sq}}{dt^2} - (2\omega - \wp\,\omega_m)\frac{di_{sd}}{dt} + \left(\omega(\omega - \wp\,\omega_m) i_{sq} + \frac{d\wp\,\omega_m}{dt} i_{sd} \right) \right| \end{aligned} \tag{19}$$

and the quantities $|b_{2d}|$, $|b_{1d}|$, $|b_{0d}|$, $|b_{2q}|$, $|b_{1q}|$, $|b_{0q}|$ are defined as

$$\begin{aligned} |b_{2d}| &= \frac{\left|\frac{d^2 i_{sd}}{dt^2}\right|}{|b_d|} \quad ; \quad |b_{1d}| = \frac{\left|(2\omega - \wp\,\omega_m)\frac{di_{sq}}{dt}\right|}{|b_d|} \\ |b_{0d}| &= \frac{\left|\left(\omega(\omega - \wp\,\omega_m) i_{sd} - \frac{\wp\, d\omega_m}{dt} i_{sq}\right)\right|}{|b_d|} \\ |b_{2q}| &= \frac{\left|\frac{d^2 i_{sq}}{dt^2}\right|}{|b_q|} \quad ; \quad |b_{1q}| = \frac{\left|(2\omega - \wp\,\omega_m)\frac{di_{sd}}{dt}\right|}{|b_q|} \\ |b_{0q}| &= \frac{\left|\left(\omega(\omega - \wp\,\omega_m) i_{sq} - \frac{\wp\, d\omega_m}{dt} i_{sd}\right)\right|}{|b_q|} \end{aligned} \tag{20}$$

Fig. 5 illustrates the relative weight of each of the terms in (19). From these results, it can be concluded that the terms that have a significant influence are those corresponding to the transformed currents, i.e., b_{0d} and b_{0q}. Less important terms are those including the first derivatives, and the terms with the second derivative are negligible. The most important result from this study is that the errors introduced by the smoothing in the second derivative hardly affect the estimation procedure.

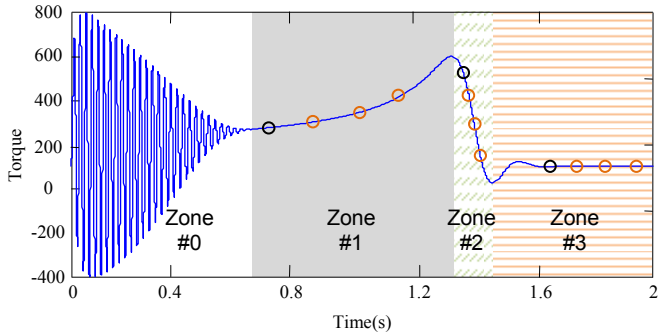

Fig. 6. Definition of different regions for the error study.

V. Error Study

In Ref. [16], the analysis of studying sensitivity of different single-cage model parameters shows that stator resistance has a small influence on the torque and current-slip curves. For this reason, the parameters of the steady-state equivalent circuit are bad indicators of the goodness of the method. An alternative is to focus the error study on magnitudes derived from the steady-state machine equations which affect the torque- and current-slip curves significally, i.e. maximum torque (Γ_m), starting torque (Γ_s), starting current (I_s) and no-load current (I_{NL}). Therefore, the definitions of the errors are

$$\varepsilon_{\Gamma m} = \left|\frac{\Gamma_{m,est} - \Gamma_{m,}}{\Gamma_m}\right| \quad ; \quad \varepsilon_{\Gamma s} = \left|\frac{\Gamma_{s,est} - \Gamma_{s,}}{\Gamma_s}\right|$$
$$\varepsilon_{Is} = \left|\frac{I_{s,est} - I_s}{I_s}\right| \quad ; \quad \varepsilon_{INL} = \left|\frac{I_{NL,est} - I_{NL}}{I_{NL}}\right| \tag{21}$$

A. Influence of Point Position

The least-square method usually works with an excess of information. That is, it uses n points to determine six parameters. In order to better comprehend how the regression method works, the influence of the position of several measurement points is studied using only three points (Minimum number to find six parameters, because each point imposes two equations).

Fig. 6 shows the torque in a starting transient. Four zones (#0, #1, #2 and #3) are delimited: #0 is the interval where the electromagnetic transients are significant, #1 includes points before the maximum torque, #2 contains points between the maximum torque and the steady state, and #3 contains points in the steady state regime. In the error study, two points are fixed and the other is moved within a range.

B. Influence of $(d\omega_m / dt)\psi_r$ Term

Fig. 7 shows the influence of the approximation on $(d\omega_m / dt)\psi_r$ described in Appendix II on the error in the estimated maximum and starting torque. In Fig. 7a the line with circles represents the error when the algorithm uses the approximation that the derivative of the speed is negligible (the usual approximation in the literature). In contrast, line with diamonds shows the error when the algorithm uses the rotor flux approximation.

In Fig. 7 the fixed points are $\omega_1 = 256$ rad/s in #1 and $\omega_2 = 314.4$ rad/s in #2. The third point varies within the range $\omega_3 = (90,317)$.

The results obtained from Fig.7 confirm that the approximation of $(d\omega_m / dt)\psi_r$ is a good improvement in the proposed algorithm.

C. Step-Size Influence

Step size affects the evaluation of the first and second derivatives, and consequently the estimation of the maximum and starting torque. Fig. 8a and 8b presents the maximum and start-

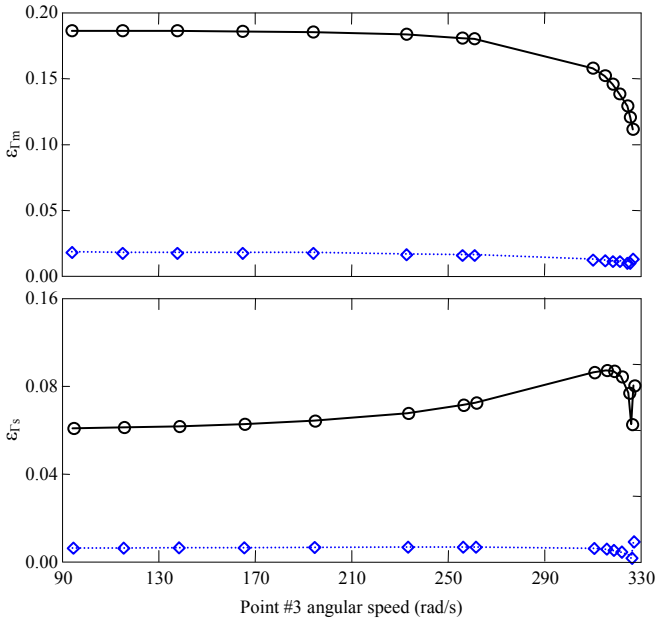

Fig. 7. Influence of the rotor flux approximation on the error in the estimated maximum and starting torques.

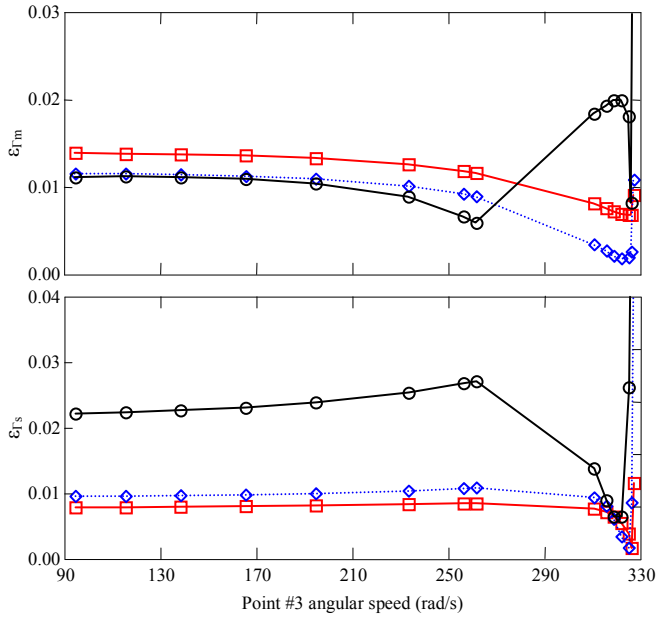

Fig. 8. Influence of the step size derivative on the error in the estimated maximum and the starting torques.

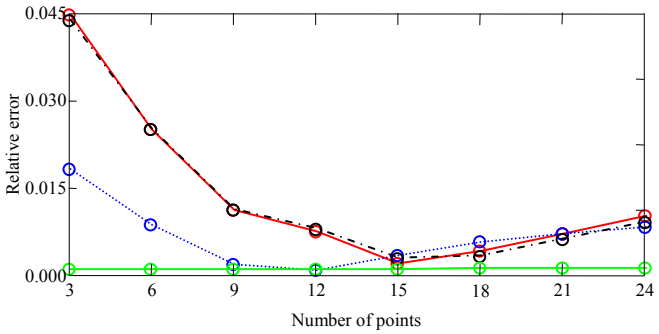

Fig. 9. Influence of equally increasing number of points in three regions on the relative error in the estimated maximum torque (solid line), the starting torque (dotted line), the starting current (dashed line) and magnetizing current (solid line).

ing torque errors respectively. The lines with squares, diamonds and circles show the error for step-size $h = 0.1$ms, $h = 1$ms and $h = 10$ms, respectively. All three cases are simulated considering $\omega_1 = 256$ rad/s in #1 and $\omega_2 = 314.4$ rad/s in #2. The third point varies within the range $\omega_3 = (90,317)$.

From the results in Fig. 8, it can be concluded that the step size for the derivatives has a little influence on the errors. This is due to the use of the synchronous reference frame, where the variables vary slowly during the mechanical transient and have constant values when steady state is reached.

D. *Influence of Number of Points*

The strategy of increasing the number of points consists in adding progressively up to seven sets of three new points, each one in different zone defined in Fig. 6. Fig. 9 shows the errors when a different number of points is considered in the estimation of the maximum torque (line with squares), starting torque (dotted line with diamonds) starting current (solid line with circles) and magnetizing current (solid line).

The analysis of the results demonstrates that taking a larger number of points give reliable results.

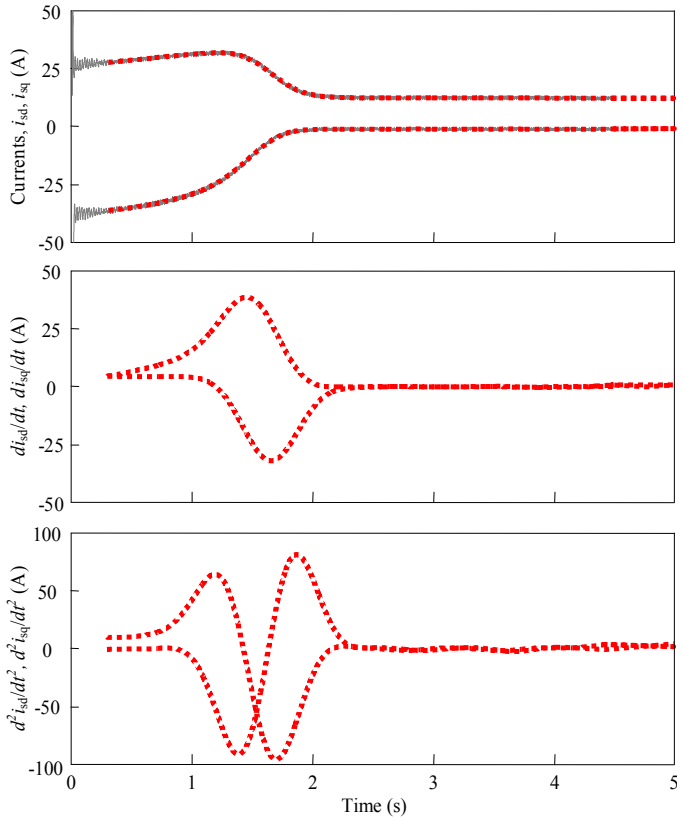

Fig. 10. (a) Measured transformed currents (solid line) and smoothed currents (dashed line) temporal evolution (b) First derivative of smoothed current (c) Second derivative of smoothed currents

VI. Transient Measurements

The method was tested with a wound rotor induction motor of rated power 2.2kW, voltage 400V and frequency 50Hz under no-load conditions.

Fig. 10a illustrates the transient currents i_{sd} and i_{sq} obtained from the measured currents i_{sa}, i_{sb}, i_{sc}, applying the Park transformation of (5) and the curves smoothed with the application in Section II with a polynomial of degree 2. Fig. 10b and 10c shows the first and second current derivatives. The transformed voltages are not plotted because they have a constant value.

Fig. 11a shows the speed evolution during the transient and Fig. 11b contains the first derivative of the speed. As a result of applying the proposed estimation method, a set of parameters was obtained and shown in Table II. The values of maximum torque, starting torque, starting current and no-load current calculated with the estimated parameters from the steady-state equivalent circuit are also included in this table.

VII. Steady-State Measurements

In order to validate the results from the above method, steady-state torque and current-slip curves were obtained with the estimated parameters of Table II. In Fig. 12, these estimated curves (in solid lines) are compared with steady-state torque and current measurements in several slip points obtained in laboratory (in circles).

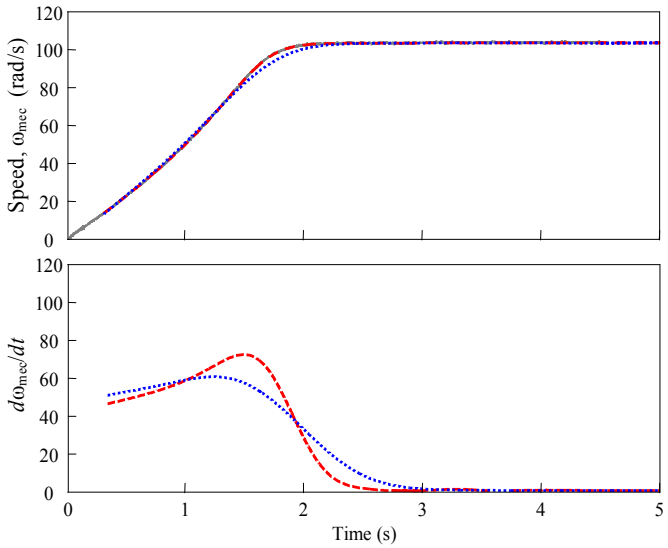

Fig. 11. (a) Speed measured (gray) and smoothed with degree 2 (dashed line) and degree 1 (dotted line) (b) first derivative smoothed with degree 1 (dotted line) and degree 2 (dashed line).

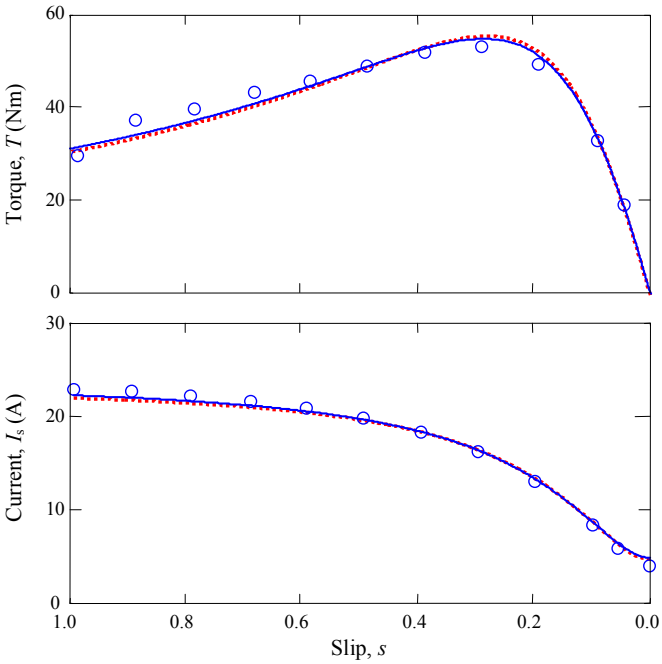

Fig. 12. Measured torque- and current – slip curves for the wound-rotor motor (circles) and estimated values with the proposed algorithm (solid line) and from steady state (dotted line).

From the steady-state measurements, a new set of parameters with the procedure described in [17] can be estimated. Table II summarizes the estimated parameters and the main characteristics of the steady-state torque and current-slip curves obtained with this alternative method. Steady-state torque and current-slip curves can be seen in Fig. 12 (in discontinuous line).

VIII. Conclusions

In this paper, a new method to estimate single-cage induction motor parameters from transient measurements is presented. The estimation procedure is based on the starting transient and uses Park variables in the synchronous reference frame because this formulation makes data filtering more reliable due to the slow variation during mechanical transients and nearly constant values in the steady state.

Furthermore, the paper contributes with an approximation of the rotor flux that improves the estimation procedure, and studies in depth the errors of the method.

The parameters estimated by the method are contrasted with torque-speed and current-speed measurements in the steady state, and good agreement is found.

TABLE II
ESTIMATED PARAMETERS IN OHMS [Ω]

Method	R_s	X_{sd}	X_m	R_r	X_{rd}
Transient	1.53	5.09	44.96	2.75	5.09
Steady-State	1.86	4.94	42.12	2.76	4.94
	T_m(Nm)	T_s(Nm)	I_s(A)	I_{NL}(A)	
Transient	55.88	30.77	22.03	4.61	
Steady-State	55.31	31.41	22.36	4.91	

IX. Appendix I

Using the induction motor dynamic equations in Ku variables the synchronous reference frame, from Eq. (2), and defining the stator and rotor fluxes as

$$\left.\begin{aligned}\psi_s &= L_s i_s + M i_r \\ \psi_r &= L_r i_r + M i_s\end{aligned}\right\} \quad \Rightarrow \quad i_r = \frac{1}{L_r}\left(\psi_r - M i_s\right) \tag{22}$$

rotor current can be eliminated and the following equations are obtained:

$$\begin{aligned} v_s &= \left(R_s + \left(L_s - \frac{M^2}{L_r}\right)(p + j\omega)\right) i_s + \frac{M}{L_r}(p + j\omega)\psi_r \\ 0 &= -\frac{R_r M}{L_r} i_s + \left(\frac{R_r}{L_r} + \left(p + j\left(\omega - \wp\,\omega_m\right)\right)\right)\psi_r \end{aligned} \tag{23}$$

These dynamic equations can be rewritten as a system of ordinary differential equations in complex variable:

$$\left.\begin{aligned}\frac{di_s}{dt} &= (-\gamma - j\omega) i_s + \left(\frac{\beta}{T_r} - j\wp\,\omega_m \beta\right)\psi_r + \frac{1}{\sigma L_s} v_s \\ \frac{d\psi_r}{dt} &= \frac{M}{T_r} i_s - \left(\frac{1}{T_r} + j\left(\omega - \wp\,\omega_m\right)\right)\psi_r\end{aligned}\right\} \tag{24}$$

where

$$\begin{aligned} \sigma &= 1 - \frac{M^2}{L_s L_r} \quad ; \quad \beta = \frac{M}{\sigma L_s L_r} \quad ; \quad T_r = \frac{L_r}{R_r} \\ \gamma &= \frac{R_s L_r^2 + R_r M^2}{L_r\left(L_s L_r - M^2\right)} = \frac{R_s}{\sigma L_s} + \frac{R_s}{L_s}\frac{M^2}{\sigma L_s L_r} \end{aligned} \tag{25}$$

The rotor flux from (24) must be eliminated because it cannot be measured. Rewriting i_s in x_1 and ψ_r in x_2,

$$\begin{aligned} \dot{x}_1 &= A x_1 + B x_2 + E v \\ \dot{x}_2 &= C x_1 + D x_2 \end{aligned} \tag{26}$$

where the derivatives are indicated with a dot. By calculating the derivative of the first equation, we obtain,

$$\ddot{x}_1 = A\dot{x}_1 + B\dot{x}_2 + \dot{B}x_2 + E\dot{v} \tag{27}$$

where coefficients A and E are constant. Using the equations

$$\begin{aligned} x_2 &= \frac{1}{B}\left(\dot{x}_1 - A x_1 - E v\right) \\ \dot{x}_2 &= C x_1 + D x_2 \end{aligned} \tag{28}$$

and replacing them in Eq. (27), we obtain,

$$\begin{aligned} \ddot{x}_1 &= A\dot{x}_1 + B\left(C x_1 + D x_2\right) + \dot{B}x_2 + E\dot{v} = \\ &= A\dot{x}_1 + B\left(C x_1 + D\frac{1}{B}\left(\dot{x}_1 - A x_1 - E v\right)\right) + \dot{B}x_2 + E\dot{v} \end{aligned} \tag{29}$$

where reordering the results, we have

$$\ddot{x}_1 = \left(A + D\right)\dot{x}_1 + \left(BC - DA\right)x_1 + \dot{B}x_2 + E\dot{v} - DEv \tag{30}$$

The literature uses the approximation $\dot{B}=0$ to eliminate x_2. This paper keeps this term and uses an approximation of x_2, which is the rotor flux ψ_r. Then, the coefficients of (30) are

$$\begin{aligned}(A+D)&=(-\gamma-j\omega)-\left(\frac{1}{T_r}+j(\omega-\wp\omega_m)\right)=\\&=-j(2\omega-\wp\omega_m)-\left(\frac{1}{T_r}+\gamma\right)=-j(2\omega-\wp\omega_m)-K_1\end{aligned}\tag{31}$$

$$\begin{aligned}(BC-DA)&=\left(\frac{\beta}{T_r}-j\wp\omega_m\beta\right)\frac{M}{T_r}+\\&+\left(\frac{1}{T_r}+j(\omega-\wp\omega_m)\right)(-\gamma-j\omega)=\frac{\beta M}{T_r^2}-j\wp\omega_m\frac{\beta M}{T_r}-\\&-\frac{\gamma}{T_r}-\frac{j\omega}{T_r}-j\gamma(\omega-\wp\omega_m)+\omega(\omega-\wp\omega_m)=\\&=\left(\frac{\beta M}{T_r^2}-\frac{\gamma}{T_r}\right)+j\wp\omega_m\left(\gamma-\frac{\beta M}{T_r}\right)-j\omega\left(\frac{1}{T_r}+\gamma\right)+\\&+\omega(\omega-\wp\omega_m)=\\&=-K_2-jK_{31}(\omega-\wp\omega_m)-j\omega K_{32}+\omega(\omega-\wp\omega_m)\end{aligned}\tag{32}$$

$$\begin{aligned}(-DE)&=\left(\frac{1}{T_r}+j(\omega-\wp\omega_m)\right)\frac{1}{\sigma L_s}=\frac{1}{\sigma L_s T_r}+\\&+\frac{j}{\sigma L_s}(\omega-\wp\omega_m)=jK_4(\omega-\wp\omega_m)+K_5\end{aligned}\tag{33}$$

$$E=\frac{1}{\sigma L_s}=K_4\quad;\quad \dot{B}=-j\wp\beta\dot{\omega}_m\tag{34}$$

Where the coefficients are defined as follows,

$$\begin{aligned}K_1&=\frac{1}{T_r}+\gamma=\frac{R_s}{\sigma L_s}+\frac{1}{\sigma T_r}=K_{31}+K_{32}\\K_2&=\frac{\gamma}{T_r}-\frac{\beta M}{T_r^2}=\frac{R_s}{\sigma L_s T_r}\quad;\quad K_4=\frac{1}{\sigma L_s}\\K_{31}&=\frac{1}{\sigma T_s}\quad;\quad K_{32}=\frac{1}{\sigma T_r}\quad;\quad K_5=\frac{1}{\sigma L_s T_r}\end{aligned}\tag{35}$$

Replacing these coefficients in equation (30), we obtain

$$\begin{aligned}\frac{d^2 i_s}{dt^2}&=\left(-j(2\omega-\wp\omega_m)-K_1\right)\frac{di_s}{dt}+\\&+\left(-K_2-jK_{31}(\omega-\wp\omega_m)-j\omega K_{32}+\omega(\omega-\wp\omega_m)\right)i_s+\\&+K_4\left(\frac{dv_s}{dt}+j(\omega-\wp\omega_m)v_s\right)+K_5 v_s-j\frac{d\wp\omega_m}{dt}\beta\psi_r\end{aligned}\tag{36}$$

Finally, reordering the terms, we obtain

$$\begin{aligned}&K_1\frac{di_s}{dt}+K_2 i_s+\left(jK_{31}(\omega-\wp\omega_m)+j\omega K_{32}\right)i_s-\\&-K_4\left(\frac{dv_s}{dt}+j(\omega-\wp\omega_m)v_s\right)-K_5 v_s=-\frac{d^2 i_s}{dt^2}-\\&-j(2\omega-\wp\omega_m)\frac{di_s}{dt}+\omega(\omega-\wp\omega_m)i_s-j\frac{d\wp\omega_m}{dt}\beta\psi_r\end{aligned}\tag{37}$$

This equation, expressed in d, q variables, results in equations (7) and (8), repeated here for clarity:

$$\begin{aligned}&K_1\frac{di_{sd}}{dt}+K_2 i_{sd}-K_{31}(\omega-\wp\omega_m)i_{sq}-K_{32}\omega i_{sq}-\\&-K_4\left(\frac{dv_{sd}}{dt}-(\omega-\wp\omega_m)v_{sq}\right)-K_5 v_{sd}=-\frac{d^2 i_{sd}}{dt^2}+\\&+(2\omega-\wp\omega_m)\frac{di_{sq}}{dt}+\omega(\omega-\wp\omega_m)i_{sd}+\frac{d\wp\omega_m}{dt}\beta\psi_{rq}\end{aligned}\tag{38}$$

$$\begin{aligned}&K_1\frac{di_{sq}}{dt}+K_2 i_{sq}+K_{31}(\omega-\wp\omega_m)i_{sd}+K_{32}\omega i_{sd}-\\&-K_4\left(\frac{dv_{sq}}{dt}+(\omega-\wp\omega_m)v_{sd}\right)-K_5 v_{sq}=-\frac{d^2 i_{sq}}{dt^2}-\\&-(2\omega-\wp\omega_m)\frac{di_{sd}}{dt}+\omega(\omega-\wp\omega_m)i_{sq}-\frac{d\wp\omega_m}{dt}\beta\psi_{rd}\end{aligned}\tag{39}$$

X. Appendix II

The rotor flux approximation is obtained from the relation between the rotor flux and stator flux:

$$\beta\psi_r=\frac{1}{\sigma L_s}\psi_s-i_s\tag{40}$$

To demonstrate this relation, the definition of β in (25) is used:

$$\beta\psi_r+i_s=\frac{M}{\sigma L_s L_r}\psi_r+i_s\tag{41}$$

and using the definition of ψ_r in (22) and σ in (25), we obtain,

$$\begin{aligned}\sigma L_s L_r(\beta\psi_r+i_s)&=M\psi_r+\sigma L_s L_r i_s=\\&=M(L_r i_r+M i_s)+(L_s L_r-M^2)i_s=\\&=L_r(L_s i_s+M i_r)=L_r\psi_s\end{aligned}\tag{42}$$

Hence,

$$\beta\psi_r+i_s=\frac{L_r}{\sigma L_s L_r}\psi_s\quad\Rightarrow\quad\beta\psi_r=\frac{1}{\sigma L_s}\psi_s-i_s\tag{43}$$

The rotor flux approximation is obtained from the voltage stator equation

$$v_s=R_s i_s+p\psi_s+j\omega\psi_s\tag{44}$$

and using the approximation for the stator flux in the steady-state, $v_s\approx j\omega\psi_s$, we obtain

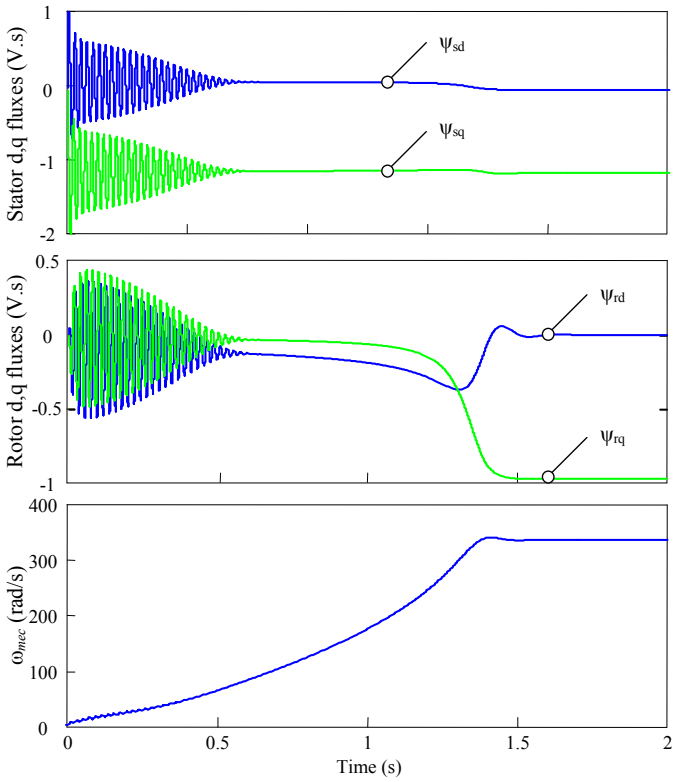

Fig. 13. (a) d and q rotor flux behavior in the starting transient (b) d and q stator flux behavior in the starting transient. (c) Motor speed evolution in the starting transient.

$$\beta\psi_r \approx \frac{v_s}{j\sigma\omega L_s} - i_s \tag{45}$$

where, separating in *d*,*q* fluxes, we have,

$$\beta\psi_{rd} \approx \frac{v_{sq}}{\sigma\omega L_s} - i_{sd} \quad ; \quad \beta\psi_{rq} \approx -\frac{v_{sd}}{\sigma\omega L_s} - i_{sq} \tag{46}$$

Fig. 13a shows the stator fluxes ψ_{sd} and ψ_{sq}. Note that when the electrical transient is finished, the stator flux value is nearly constant. On the other hand, Fig. 13b illustrates a great variability of the rotor fluxes ψ_{rd} and ψ_{rq}. In Fig. 13c we can observe that this change occurs when the mechanical speed reaches the synchronous speed.

XI. References

[1] *IEEE Standard test procedure for polyphase induction motors and generators*, IEEE Std. 112-2004, Nov. 2004.

[2] E. Laroche, M. Boutayeb, "Identification of the induction motor in sinusoidal mode", *IEEE Trans. Energy Conversion,* Vol. 25, No.1, pp. 11-19, March 2010

[3] I. Zubia, A. Zatarain, C. Alcalde, X. Ostolaza, "In situ electrical identification meted for induction wind generators", *IET Electric Power Applications*, Vol. 5, No. 7, pp. 549-557, 2011.

[4] E. Laroche, E. Sedda, C. Durieu, "Methodological insights for online estimation of induction motor parameters", *IEEE Trans. Contr. Syst. Technol.*, Vol. 16, No. 5, pp. 1021-1028, Sept. 2008.

[5] J. Stephan, M. Bodson, J. Chiasson, "Real-time estimation of the parameters and fluxes of induction motors", *IEEE Trans. Industry Appl.*, Vol. 30, pp. 746-758, 1994.

[6] S. R. Shaw, S. B. Leeb, "Identification of induction motor parameters from transient stator current measurements", *IEEE Trans. Industrial Electronics*, Vol. 46, pp. 139-149, 1999.

[7] M. Cirrincione, M. Pucci, G. Cirrincione, G. A. Capolino, "A new experimental application of least-squares techniques for the estimation of the induction motor parameters" *IEEE Trans. Industry Appl.*, Vol 39, pp. 1247-1256, 2003.

[8] M. Cirrincione, M. Pucci, G. Cirrincione, G. A. Capolino, "Constrained minimization for parameters estimation of induction motor in satured and unsatured conditions" *IEEE Trans. Industrial Electronics*, Vol 52, pp. 1391-1402, 2005.

[9] M. Cirrincione, M. Pucci, "Identification of an induction motor with the least-squares method", *Elect. Eng. Res. Rep.*, no. 10, pp. 22-30, Dec. 2000

[10] K. Wang, J. Chiasson, M. Bodson, L. M. Tolbert, "A nonlinear least-squares approach for identification of the induction motor parameters", *IEEE Trans. Autom. Control*, Vol. 50, No. 10, pp. 1622-1628, Oct. 2005.

[11] J. A. de Kock, F. S. Van der Merwe, H. J. Vermeulen, "Induction motor parameter estimation through an output error technique", *IEEE Trans. Energy Conversion,* Vol. 9, No.1, pp. 69-76, March 1994.

[12] The MathWorks, Inc., *Matlab 7.9 (2009b)*. Natick, MA: 2009.

[13] A. Savitzky, M. J. E. Golay, "Smoothing and differentiation of data by simplified least square procedures", Anal. Chem., 36, pp. 1627-1639, 1964.

[14] T. O'Haver, "An introduction to signal processing with applications in chemical analysis",http://terpconnect.umd.edu/~toh/spectrum/TOC.html

[15] F. Corcoles, J. Pedra, M. Salichs, L. Sainz, "Analysis of the induction machine parameter identification" *IEEE Trans. Energy Conversion*, Vol 17, No 2, June 2002, pp. 183-190.

[16] J. Pedra, F. Corcoles, "Estimation of induction motor double-cage model parameters from manufacturer data", *IEEE Trans. Energy Conversion,* Vol. 19, No.2, pp. 310-317, June 2004.

[17] J. Pedra, I. Candela, L. Sainz, "Modelling of squirrel-cage induction motors for electromagnetic transient programs," *IET Electric Power Appl.*, vol.3, no. 2, pp. 111-122, Mar. 2009.